DEVELOPMENT OF AN INTERPRETATION METHODOLOGY FOR LONG-TERM PRESSURE DATA FROM PERMANENT DOWNHOLE GAUGES

A DISSERTATION
SUBMITTED TO THE DEPARTMENT OF PETROLEUM ENGINEERING
AND THE COMMITTEE ON GRADUATE STUDIES
OF STANFORD UNIVERSITY
IN PARTIAL FULFILLMENT OF THE REQUIREMENTS
FOR THE DEGREE OF
DOCTOR OF PHILOSOPHY

By
Suwat Athichanagorn
June, 1999

I certify that I have read this thesis and that in my opinion it is fully adequate, in scope and in quality, as a dissertation for the degree of Doctor of Philosophy.

Dr. Roland N. Horne
(Principal Adviser)

I certify that I have read this thesis and that in my opinion it is fully adequate, in scope and in quality, as a dissertation for the degree of Doctor of Philosophy.

Dr. Khalid Aziz

I certify that I have read this thesis and that in my opinion it is fully adequate, in scope and in quality, as a dissertation for the degree of Doctor of Philosophy.

Dr. Thomas A. Hewett

Approved for the University Committee on Graduate Studies:

Acknowledgements

I would like to express my gratitude toward Professor Roland N. Horne for his constant guidance, advice, and encouragement throughout the course of the study. I would also like to thank Professor Khalid Aziz and Professor Thomas A. Hewett, who are members of the dissertation committee for their revision of the manuscript of this dissertation and suggestions.

I would like to express my great appreciation to my colleagues in the SUPRI-D research group for their suggestions towards the project, which greatly contributed to many improvements.

I would like to thank Jitendra Kikani for his valuable advice and recommendations and for obtaining field data for this study. I am also indebted to Trond Unneland, Bob Hite, and Phil Fair, who helped me in obtaining field data for this research and to Statoil, Shell, and Chevron for providing the data.

I am grateful to my parents, Somchai and Suparat Athichanagorn for their love and support for my studies.

I would also like to thank the Schlumberger Foundation and the member companies of the SUPRI-D Research Consortium for Innovation in Well Test Analysis for providing financial support for this work.

Contents

List of Tables

List of Figures

Chapter 1

Introduction

Reservoir pressure is probably the most important type of data used to monitor reservoir conditions, obtain reservoir descriptions, develop recovery schemes, and forecast reservoir performance. The changes in the reservoir pressure due to alteration of the production conditions are characteristic of reservoir properties themselves. Therefore, the reservoir properties can be inferred by matching the pressure response to a reservoir model. The inferred reservoir model can then be used for future reservoir management. For this purpose, pressure transient tests are conducted to observe the pressure response by changing well flow rates for a certain period of time.

To monitor the well conditions in real time, many recently completed wells have been equipped with permanent downhole pressure gauges. Continuous measurement of pressure enables engineers to observe ongoing changes in the well and make operating adjustments to prevent accidents and optimize recovery. From past experiences of oil field operations, the installation of permanent downhole pressure gauges has proven to be cost-effective even for the use of well monitoring alone, not to mention the additional reservoir information obtained from the analysis of pressure data.

Although the installation of permanent downhole gauges has been a phenomenon of the 1990s, their use has been discussed since much earlier. There have been many

publications on the applications and benefits of using permanently installed downhole pressure gauges. As early as the 1960s, Nestlerode (1963) introduced the use of permanent gauges for optimizing production, locating operational problems, and extracting information for well control. Weeks and Farris (1975) and Gallivan, Kilvington, and Shere (1988) discussed the installation and reliability of permanently installed pressure gauges. Gallivan, Kilvington, and Shere (1988) concluded that permanent pressure gauges have adequate resolution and reliability. Schmidt, Stright, and Forcade (1987) studied the use of a multiwell data acquisition system for permanent bottomhole pressure gauges in the Gullfaks field in the North Sea. Shepherd, Neve, and Wilson (1991) discussed the use and application of downhole pressure gauges for reservoir monitoring and extended well tests in the Balmoral Field in the United Kingdom.

Unneland and Haugland (1994) discussed the applications of permanent pressure gauges in well monitoring and reservoir management. They demonstrated the cost-effectiveness of installing permanent downhole gauges to obtain pressure information for the purpose of well control. Botto and de Ghetto(1994) reviewed the electronic and fiber-optic technology for permanent reservoir monitoring. Chalaturnyk and Moffat (1995) presented the application of permanent gauges in vertical, slanted, and horizontal wells for different recovery processes. Baker *et al.* (1995) discussed the history, instrumentation, data acquisition system, and application of permanent downhole pressure gauges.

Long-term pressure data from permanent pressure gauges could have greater value than for well monitoring alone. These data have the potential to provide more information about the reservoir than the data from traditional pressure transient tests which last for relatively small durations. An insufficient test duration may cause ambiguity in the trend of the pressure response. For example, an interpreter may be able to detect the beginning of the boundary response but not pinpoint the exact type of the boundary. The test may be matched perfectly with several different reservoir models. The analysis of a longer set of data would reduce uncertainty in the

interpretation. In addition, the long-term data may also provide an insight on how reservoir properties may change as the fluid is produced from the reservoir.

1.1 Problem Statement

Long-term data are prone to different kinds of errors than data from a short well test. In a traditional well test, the pressure response of the reservoir is measured carefully while the well undergoes flow rate changes for certain durations. The test is under a strictly controlled environment. By design, there are no other dynamic changes in the system except the flow rate alteration. In the case of long-term reservoir monitoring using permanent pressure gauges, the well and the reservoir may undergo dynamic changes throughout their lives. The well may be stimulated, worked over due to failure in the wellbore, etc. Due to these dynamic changes, the downhole pressure gauge may record invalid measurements. Abrupt changes in flowing temperature can also cause erroneous recordings. Besides physical changes in the reservoir, the permanent gauge data acquisition system itself may pose a problem. In some cases, pressure data are stored with low precision, creating superfluous outliers and noise. Sometimes, the system simply malfunctions. Therefore, one part in the analysis of long-term data is to remove outliers and noise from the data. These steps may be referred to as *outlier removal* and *denoising* processes.

The number of data collected by permanent downhole gauges is tremendous. In some cases, pressure is measured at 10-second interval for a period of several years. One year of data consists of over three million measurements. It is impossible to include the entire data in the interpretation due to limited computer resources. Therefore, it is essential to reduce the number of data to a manageable size by eliminating data that provide redundant information. This process may be referred to as *data reduction*.

In most cases of long-term monitoring, a complete record of well activities and flow rate history is not available. In general, the flow rate is not measured continuously,

and is not measured downhole. The flow rate may sometimes be measured only once a week or once a month while there are unmeasured rate changes in between. First, the times at which the flow rate changes occur have to be located. Since there is a sudden change in pressure when the flow rate alters, the issue is then to find a procedure to detect these changes in the pressure signal. This step may be referred to as *transient identification*.

After realizing where each transient begins, the unknown flow rate changes need to be estimated. Since the pressure response is a function of reservoir properties and the flow rates themselves, a procedure to determine these unknown rates from existing rate measurements, production history, and pressure data may be developed. The reconstruction of flow rate history is essential in the interpretation of pressure data. This process may be referred to as *flow history reconstruction*.

Since the long-term monitoring is under an uncontrolled environment, the pressure may not be consistent between transients for the reasons mentioned before. Aberrant pressure behaviors in some transients may lead to large uncertainties in the parameter estimates or even a wrong interpretation. To correct this, aberrant sections of the data need to be removed from the interpretation. This process may be referred to as *behavioral filtering*.

When interpreting the data, changes in reservoir properties and conditions that may occur during the long-term data collection have to be accounted for. Since the properties may not be constant, it is not accurate to interpret the entire the data all at once. Therefore, a procedure to analyze pressure response from changing reservoir properties needs to be developed. This process may be referred to as *data interpretation*.

In summary, the objectives of this study were to develop procedures to meet the following requirements:

1. To remove outliers and noise in the data.

2. To identify locations of flow rate changes from pressure response and discretize pressure into individual transients.

3. To reduce the number of pressure data to a manageable size.

4. To reconstruct a complete flow rate history from existing rate measurements, production history, and pressure data.

5. To remove aberrant transients from the analysis.

6. To be able to account for changes in reservoir parameters and conditions when interpreting the data.

1.2 Previous Work

Although permanent downhole pressure gauges have been installed in over a thousand wells worldwide, there have been only a few studies on the subject of data processing and interpretation of data obtained from this type of gauge. Most of these studies touch on a single or a couple of subjects related with long-term data. Major obstacles for a long-term analysis are inherent noise and outliers, tremendous data size, incomplete information, and lack of a dynamic analysis.

In the area of data processing, Osman and Stewart (1997) used the Butterworth digital filter method to remove noise in the data. Kikani and He (1998) presented a case in which the Butterworth digital filter fails to capture sharp features of a signal in a numerical experiment and used a wavelet analysis to denoise and detect transients in pressure data. They applied the wavelet analysis to data that are collected at high frequencies at a fixed sampling rate in the absence of outliers. In practice, pressure data may be collected at varying sampling rates at low and high frequencies depending on the system setup of the pressure acquisition system and the characteristics of pressure data themselves. Gauges in certain systems are preset to record pressure at a fixed interval while gauges in other systems are programmed to collect data only when a change in pressure is higher than a predetermined threshold. The subjects of

how to handle unevenly sampled data and how to detect outliers therefore need to be addressed.

Reducing the size of the data is another necessary step in cases in which pressure are recorded at high sampling frequencies. Horne (1995) discussed three main objectives in sampling pressure data in transient testing: (1) to capture essential features; (2) to apply approximately an equal weight to each flow regime; and (3) to reduce the total number of data. The logarithmic sampling with the restarting of logarithmic cycle when flow rate change was recommended for infinite acting responses. Horne (1995) also discussed the use of a pressure thresholding method which samples data only when a certain change is reached. The drawbacks of this method are that very noisy data tend to be included and that constant pressure responses may not be recorded at all. A threshold for the time interval may be set when using this type of sampling to avoid large gaps in the reduced version of the data.

On the subject of data interpretation, Unneland, Manin, and Kuchuk (1997) discussed the use of permanent gauge pressure and rate measurements for a simple reservoir description using decline curve analysis. By solving the rate convolution integral, the well rates at constant pressure were determined. These rates are the rates that would occur if the well were kept at a constant pressure during production. These rates were then used to compute parameters in the exponential decline. The authors reported that analysis of long-term data overcame the ambiguity associated with traditional well test analysis. This was a first major attempt to utilize long-term information to describe reservoir parameters. However, the issue of incomplete information and changing reservoir conditions were not addressed, and the reservoir model was only a very simplified one.

Cook and Beale (1983) discussed the application of a fixed-length data window in long-term processes in order to analyze data with varying behaviors. In this method, the data are cut into windows and analyzed independently in a sequential manner. This method is known as the sliding data window approach. Luo and Billings (1995) studied the use of the sliding data window for parameter estimation of nonlinear

systems. However, the sliding data window approach is not limited to independent analyses of data windows. It can be modified to account for previous events in prior windows that affect the analysis of subsequent windows. This method should be useful in analyzing long-term pressure data.

1.3 Outline of Approach

Since there are many separate issues involved in the processing and interpretation of data from permanent downhole gauges, a multistep procedure was developed here to achieve the goal of extracting information from the data. These approaches can be summarized as follows:

1. Wavelet analysis may be used to detect outliers, denoise data, and detect changes in flow rates from pressure data. Data used in the analysis may be collected at varying sampling rates.

2. Unknown and uncertain flow rates can be reconstructed during regression on pressure by parameterizing them as unknown parameters constrained to existing rate measurements and production data.

3. The variances between the regression match and the data can be used to determine which transients are inconsistent with the rest of the data. Thus, the aberrant transients are removed from the analysis.

4. To account for changes in reservoir properties/conditions, a window of data is analyzed at a time. The analysis is then moved forward in time to analyze subsequent windows of data. This type of analysis provides distributions of solutions instead of a single value for each parameter, which should be useful to reveal trends in reservoir parameters or to assess uncertainties associated with estimates of reservoir parameters.

The multistep procedure for processing and interpretation of long-term is implemented to actual field data sets to illustrate its effectiveness. Many steps in the

procedure can replace the work that is usually performed by humans while some steps still requires human intervention to review the results.

1.4 Dissertation Outline

Chapter 2 discusses the theory and applications of wavelet analysis. A brief review of wavelet applications in the petroleum literature is given and followed by the introduction of wavelet analysis in comparison to Fourier analysis. Theory of wavelet multiresolution analysis is discussed. Two types of wavelet decomposition are presented. The spline wavelet which is used throughout this study is introduced.

Chapter 3 discusses the applications of wavelet analysis in the processing of long-term pressure data. An algorithm to remove outliers from the data based on wavelet analysis is developed. A denoising procedure called *wavelet shrinkage* is discussed. Then, an algorithm to identify new transients in the pressure data is introduced and followed by the discussion of the data reduction process. Field examples are given in each data processing step.

Chapter 4 involves the use of nonlinear regression in data processing. First, the framework of nonlinear regression is reviewed. Then, a procedure to reconstruct flow rate history from available data, namely, a few known rates and production history is explained. A variance-based behavioral filtering of aberrant transients of pressure data is discussed.

Chapter 5 introduces the use of moving window analysis to interpret long-term data. Several simulated cases are studied to see how the temporal changes in reservoir properties may affect the results from nonlinear regression. Then, three actual field data sets are used to illustrate the applications of moving window analysis.

Chapter 6 summarizes the multistep procedure developed in this study. Remarks and conclusions are drawn from the implementation of the procedure to data acquired with permanent downhole pressure gauges.

Chapter 2

Wavelet Analysis

This chapter introduces the framework of wavelet analysis which is used to extract information contained in different frequencies of a signal at multiple levels of resolution. The most attractive feature of the wavelet analysis is that it is able to separate high frequency contents which represent small-scaled information from low frequency components which represent large-scaled information.

Section 2.1 gives a review of wavelet applications in petroleum engineering. Due to its capability to analyze data at multiple levels of resolution, wavelet analysis is particularly useful in upscaling and approximation applications. An overview of how the wavelet analysis is used in this study is also included.

The frameworks of Fourier and wavelet analyses are introduced in Section 2.2. to familiarize the readers with frequency analysis. The extraction of low and high frequency contents from a signal is discussed. The simplest form of wavelets is presented, followed by a short discussion of a few other types of wavelet families.

Section 2.3 introduces the theory of multiresolution analysis which approximates functions and signals at multiple levels of scale. The scaling function used to correlate the approximated signals across scales is defined. The computation of the difference of information contents between approximations at two successive scales by the wavelet is discussed. The evaluation of the approximated and detail signals at

different resolutions using low-pass and high-pass filters is presented.

Section 2.4 presents an algorithm called the pyramidal algorithm to compute the approximated and detail signals for multiple levels of resolution using orthonormal wavelet bases. A procedure to reconstruct the original signal from the approximated and detail signals at coarser scales is also given.

Section 2.5 discusses another algorithm called the *à trous* algorithm, which is used to decompose a signal into approximated and detail components using nonorthonormal wavelet bases. The advantage of the *à trous* algorithm over the pyramidal algorithm in our type of applications is discussed. Signal reconstruction using the *à trous* algorithm is also presented.

Section 2.6 introduces the spline wavelets, which are suitable for singularity detection using the concept of wavelet modulus maxima. Demonstration of how wavelet modulus maxima can be used to determine break points in a signal is given in this section.

2.1 Wavelets in Petroleum Engineering

Wavelet analysis has a wide range of applications in data analysis such as signal processing, image analysis, data compression, statistical analysis, etc.. In the past few years, wavelet analysis has appeared several times in the petroleum literature in different applications such as in data denoising, upscaling of reservoir properties, and solving partial differential equation governing fluid flow in reservoirs.

The most common use of wavelet analysis in petroleum engineering has been for upscaling applications. Panda, Mosher, and Chopra (1996) applied the multiresolution framework of the wavelet analysis to denoise and upscale permeability data. At approximately the same time, Chu, Schatzinger, and Tham (1996) used wavelet analysis to upscale permeability in a two-phase flow problem. Two-phase properties such as capillary pressures, phase saturations, and phase permeability were also upscaled

but with other techniques such as arithmetic-weighted average. The results of permeability upscaling were verified by comparing production performance and water cut at the production well from the original fine-grid simulation and the upscaled coarse-grid simulation. Nielson and Espedal (1996) also used the wavelet multiresolution analysis to upscale permeability fields. Jansen and Kelkar (1998) later expanded the wavelet upscaling technique to upscale reservoir properties in three dimensions.

Beside upscaling, Moridis, Tygel, and Correa (1996) used the wavelet transforms to solve for the solution of Buckley-Leverett equation. Their solutions closely match the analytical solutions, outperforming the finite difference solutions. Later, Jansen and Kelkar (1997) applied wavelet multiresolution analysis to decompose production data into detail and smooth components and used the detail component to analyze relationships between wells. A similar approach was used by Sullera and Horne (1999) to determine breakthrough relationships between injectors and producers in geothermal reservoirs.

Kikani and He (1998) provided an overview of how to use wavelet analysis to process pressure transient data. They used the wavelet analysis to denoise data and detect transients. They showed that the standard denoising algorithm proposed by Donoho and Johnstone (1994) works well with pressure transient data. The wavelet maxima proposed by Mallat and Hwang (1992) was used to detect transients. However, much work still needed to be done in order to implement the detection algorithm to different characteristics of field data.

In this work, the wavelet analysis is used as a tool to develop algorithms to remove outliers, suppress noise, and detect the beginning of new transients for long-term pressure data. Based on the capability of the wavelet analysis to separate detail information from large-scaled information at multiple levels of resolution, the detail components of data (outliers, noise, and the changes of pressure at the beginnings of new transients) can be investigated.

2.2 Fourier Transform and Wavelet Transform

In general, an event or physical process can be described either in the time domain as $f(t)$ or in the frequency domain as $f(\omega)$ (Press *et al.*, 1995). Many types of data analysis such as data compression, noise filtering, change detection, etc. are performed in the frequency domain by extracting information contained in different frequencies. The Fourier transform is a useful tool in determining the frequency contents of a process $f(t)$:

$$\hat{f}(\omega) = (Ff)(\omega) = \frac{1}{\sqrt{2\pi}} \int_{-\infty}^{\infty} f(t) e^{-i\omega t} dt. \tag{2.1}$$

The original process $f(t)$ can be reconstructed from the frequency components $\hat{f}(\omega)$ by the inverse Fourier transform, defined as

$$f(t) = \frac{1}{\sqrt{2\pi}} \int_{-\infty}^{\infty} \hat{f}(\omega) e^{-i\omega t} d\omega. \tag{2.2}$$

The Fourier transform is generally suitable for analyzing a process whose frequency content does not change over time. Since the Fourier transform includes all information in the time domain, it can only provide the average information of the frequency content. In order to determine time-localized information in the frequency domain, Gabor (1946) introduced a windowed Fourier transform:

$$(F^{window} f)(\omega, b) = \int_{-\infty}^{\infty} f(t) g(t-b) e^{-i\omega t} dt. \tag{2.3}$$

The windowing function, $g(t)$, can be any compactly supported function. (A compactly supported function is a function that exists within a given range of t and becomes zero everywhere else.) The translations $g(t-b)$ of the function $g(t)$ ensure that the transform includes only the information around the center of the time of interest ($t = b$).

In addition to achieving the goal of extracting time-localized information of a

process, a similar framework can be used for inverse windowed Fourier transform for frequency-localized information. Therefore, the Gabor transform can be used to extract both time-localized and frequency-localized information. However, the disadvantage of the windowed transform is that once a windowing function is chosen, the size of the window is fixed. A nonstationary process may consist of both abrupt changes (high frequency content) and gradual changes (low frequency content) requiring different window sizes. A narrow window should be used to analyze high frequency content while a wider window is preferred for low frequency phenomena.

The wavelet transform, on the other hand, can utilize different window sizes accordingly to capture information in various frequency contents in addition to providing both time-localized and frequency-localized information. The wavelet theorem was first formally introduced by Grossmann and Morlet (1984) independently from a similar theorem that was proved previously by the mathematician Calderón (1964) in the context of a convolution operator. The wavelet transform at time $t = b$ and dilation a is defined as:

$$Wf(a,b) = \frac{1}{\sqrt{a}} \int_{-\infty}^{\infty} f(t)\psi\left(\frac{t-b}{a}\right) dt. \tag{2.4}$$

The function $\psi(t)$ is called a wavelet. Generally speaking, a wavelet is a function that waves through the t-axis such that

$$\int_{-\infty}^{\infty} \psi(t)dt = 0. \tag{2.5}$$

Mathematically, the function $\psi(t)$ is called a wavelet if and only if its Fourier transform $\hat{\psi}(\omega)$ satisfies the *admissibility condition*:

$$\int_{-0}^{\infty} \frac{\left|\hat{\psi}(\omega)\right|^2}{\omega} d\omega = \int_{-\infty}^{0} \frac{\left|\hat{\psi}(\omega)\right|^2}{\omega} d\omega = C_\psi < +\infty. \tag{2.6}$$

The wavelet transforms $Wf(a,b)$ are also called *wavelet coefficients*. The dilation parameter a is equivalent to the window size in the windowed Fourier transform.

By changing the dilation parameter a, information contained in different frequencies of the data can be analyzed independently. A small value of dilation a may be used to analyze high frequency information while a larger value of a may be used to analyze a lower frequency process. At any given dilation, the information obtained from the wavelet transforms has high frequency contents when comparing to low frequency information extracted from a complementary wavelet transform which will be introduced later. Therefore, the wavelet $\psi(t)$ may be interpreted as the impulse response of a high-pass filter.

Besides the requirements shown in Eq. 2.6, wavelets are carefully constructed to have certain mathematical properties so that they can be used as basis functions to transform functions or data. Some restrictions apply when constructing a wavelet for specific types of applications. The simplest form of wavelet is the Harr wavelet, which is described by the Harr function (Harr, 1910) defined as:

$$\psi(t) = \begin{cases} 1 & 0 \leq t < 1/2 \\ -1 & 1/2 \leq t < 1 \\ 0 & otherwise. \end{cases} \tag{2.7}$$

The Harr function defined in Eq. 2.7 is called a *mother wavelet*. A family of wavelets $\frac{1}{\sqrt{a}}\psi(\frac{t-b}{a})$ can be constructed from the mother wavelet by dilations using the dilation parameter a and translations using parameter b. Fig. 2.1 displays a few members of the Harr wavelet families.

There have been several types of wavelets developed for different types of applications. In his book, Ogden (1997) reviews recent developments of wavelet families. One of the early wavelet families was introduced by Meyer (1985) and became known as the Meyer basis. Later, Battle (1987) and Lemarié (1988) independently proposed the same family of orthogonal wavelets constructed from polynomial splines. The drawback of Battle-Lemarié wavelets is that they are not compactly supported. Compactly supported wavelets are more desirable in numerical computations since they exist over a finite range on t-axis and become zero everywhere else. Chui and

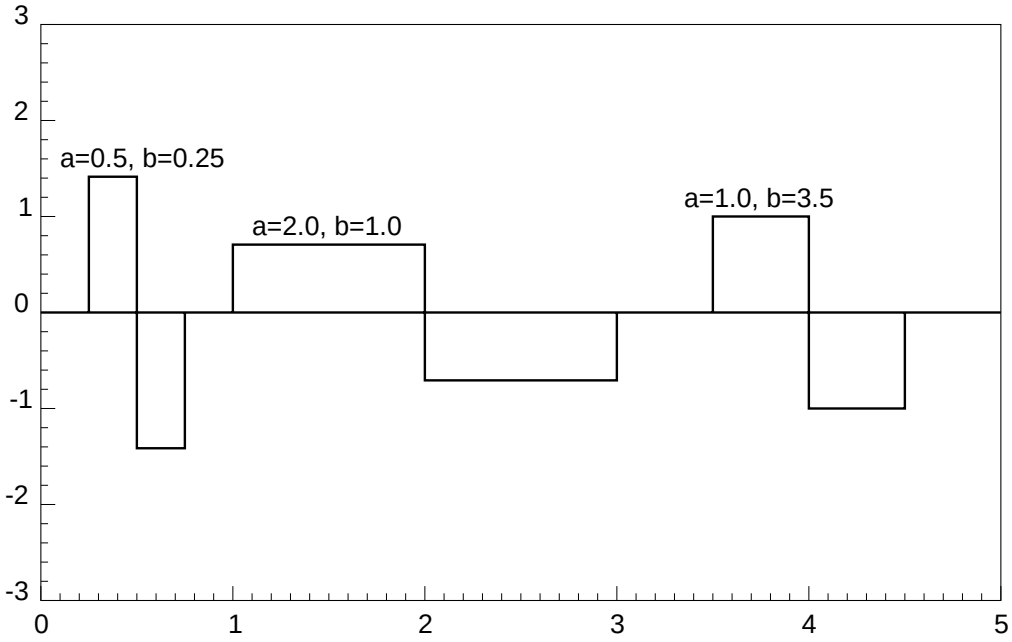

Figure 2.1: Wavelets constructed from the Harr function.

Wang (1991) later developed a new wavelet family that has compact support based on polynomial B-splines. Daubechies (1988) developed another family of compactly supported wavelets that have a wide range of applications. The Daubechies bases have become one of the most common wavelets used in practice.

To recover the function f from the wavelet transform $Wf(a,b)$, a complementary transform through the scaling function $\phi(t)$ is needed. The scaling function is a part of the wavelets as the transform moves across scales. The complementary transform is defined as:

$$Cf(a,b) = \frac{1}{\sqrt{a}} \int_{-\infty}^{\infty} f(t)\phi\left(\frac{t-b}{a}\right) dt. \tag{2.8}$$

The complementary transform $Cf(a,b)$ actually provides an approximation to the function $f(t)$ which is the low frequency content of the process $f(t)$. For this reason, the scaling function $\phi(t)$ may be interpreted as the impulse response of a low-pass

filter.

Roughly speaking, when performing a wavelet analysis, a high-pass filter is applied to the function via the wavelet transform defined in Eq. 2.4, and a low-pass filter is applied via the complementary transform defined in Eq. 2.8. This analysis is referred to as *wavelet decomposition* since the original function $f(t)$ is decomposed into two functions: a detail function which is the wavelet transform and an approximation function obtained by the complementary transform.

2.3 Multiresolution Analysis

To derive formally how the wavelet analysis can be used to extract information at different scales, we begin with the theory of multiresolution analysis (MRA) presented by Mallat (1989a, 1989b, 1989c). Relationships between the wavelet and its complementary transforms can be established through the multiresolution analysis. For convenience, the sample spacing at different resolution scales is discretized dyadically as 2^j where $j \in \mathcal{Z}$ represents the scale. As j increases, the scale becomes coarser. This implies that the resolution at scale j is finer than the resolution at scale $j+1$.

Let $f(t)$ be a signal which is measurable and has a finite energy: $f(t) \in L^2(\mathcal{R})$, where $\mathcal{R}$ denotes the set of real numbers, and $L^2(\mathcal{R})$ denotes the vector space of measurable, square-integrable one-dimensional functions $f(t)$. Let A_j be the approximation operator which approximates a signal $f(t)$ at a scale j. Then, A_j has the following properties:

1. A_j is a linear operator. Then, $A_j f(t)$, which is the approximation of the function $f(t)$ at the scale j, is not affected if the approximation operator A_j is applied again at the scale j. Therefore, A_j is a projection operator on the vector space $V_j \subset L^2(\mathcal{R})$.

2. $A_j f(t)$ is the best approximation to the function $f(t)$ among all approximations at the scale j:

$$\forall g(t) \in V_j, \qquad \|g(t) - f(t)\| \geq \|A_j f(t) - f(t)\|. \tag{2.9}$$

Thus, A_j is an orthogonal projection on the vector space V_j.

3. Since information is lost when a signal is approximated at a lower level of resolution (coarser scale), it is intuitive to see that the approximation of the signal at the scale j contains all necessary information to construct an approximation at the coarser scale $j + 1$. Therefore,

$$\forall j \in \mathcal{Z}, \qquad V_{j+1} \subset V_j. \tag{2.10}$$

4. The vector space of an approximated function at any resolution can be determined from the vector space of another approximated function by rescaling the new approximated function proportionally to its resolution level:

$$\forall j \in \mathcal{Z}, \qquad f(t) \in V_j \iff f(\frac{t}{2}) \in V_{j+1}. \tag{2.11}$$

5. The approximation $A_j f(t)$ may be characterized by 2^{-j} observations per unit length. Therefore, the spacing between samples is 2^j. If the signal $f(t)$ is translated by a length proportional to the sample spacing, then the approximation $A_j f(t)$ is also translated by the same amount. Let us characterize the translation properties for the scale $j = 0$ in particular. These properties at other scales can be derived using the scaling relationship expressed in Eq. 2.11.

   (a) The signal may be characterized discretely if there exists an isomorphism I from V_1 onto $I^2(\mathcal{Z})$ where $I^2(\mathcal{Z})$ is the vector space of square-summable integer sequences:

$$I^2(\mathcal{Z}) = \left\{ (\alpha_i)_{i \in \mathcal{Z}} : \sum_{i=-\infty}^{+\infty} |\alpha_i|^2 < \infty \right\}. \tag{2.12}$$

(b) The translation approximation may be described as:

$$\forall k \in \mathcal{Z}, \qquad A_1 f_k(t) = A_1 f(t-k) \tag{2.13}$$

where

$$f_k(t) = f(t-k). \tag{2.14}$$

(c) The translation of the samples may be described as:

$$I(A_1 f(t)) = (\alpha_i)_{i\in\mathcal{Z}} \iff I(A_1 f_k(t)) = (\alpha_{i-k})_{i\in\mathcal{Z}}. \tag{2.15}$$

In short, these properties can be written as:

$$\forall (j,k) \in \mathcal{Z}^2, \quad f(t) \in V_j \iff f(t-k) \in V_j. \tag{2.16}$$

6. Since a certain amount of information about $f(t)$ is lost when the resolution of the approximation of $f(t)$ becomes coarser, the approximation contains increasingly less information and converges to zero as the scale approaches $+\infty$. This property can be described as:

$$\lim_{j\to\infty} V_j = \bigcap_{j=-\infty}^{+\infty} V_j = \{0\}. \tag{2.17}$$

On the other hand, the approximation becomes more and more complete and converges to the original signal as the scale decreases to $-\infty$. This can be written:

$$\lim_{j\to-\infty} V_j = \bigcup_{j=-\infty}^{+\infty} V_j \quad \text{is dense in} \quad L^2(\mathcal{R}). \tag{2.18}$$

Any set of vector spaces $\{V_j\}_{j\in\mathcal{Z}}$ that satisfies properties 2.9-2.18 is called a *multiresolution approximation* of $L^2(\mathcal{R})$. The approximation $A_j f(t)$ of a signal $f(t)$ is called the *approximated signal*. Since the approximation operator A_j is an

orthogonal projection on the vector space V_j, an orthonormal basis of V_j has to be determined in order to characterize the operator A_j numerically. The following theorem is used to define this orthonormal basis.

Theorem 1: (Mallat, 1989a) Let $\{V_j\}_{j\in\mathcal{Z}}$ be a multiresolution approximation of $L^2(\mathcal{R})$. There exists a unique function $\phi(t) \in L^2(\mathcal{R})$, called a *scaling function*, such that $\phi_{j,k}(t) = \frac{1}{\sqrt{2^j}}\phi\left(\frac{t-2^j k}{2^j}\right)$. The family $\{\phi_{j,k}(t)\}_{k\in\mathcal{Z}}$ is an orthonormal basis of $\{V_j\}_{j\in\mathcal{Z}}$.

The proof of this theorem can be found in Mallat (1989a, 1998). Theorem 1 shows that an orthonormal basis of any V_j can be constructed by dilating a function $\phi(t)$ with a coefficient 2^j and translating the function on a grid in which the spacing is proportional to 2^j. For every multiresolution approximation $(V_j)_{j\in\mathcal{Z}}$, there exists a unique scaling function $\phi(t)$ that satisfies Theorem 1.

The orthogonal projection $A_j f(t)$ on V_j can be expressed as a linear combination of the orthonormal basis defined in Theorem 1.

$$A_j f(t) = \sum_{k=-\infty}^{+\infty} \langle f(u), \phi_{j,k}(u)\rangle \ \phi_{j,k}(t). \tag{2.19}$$

where the inner product between two functions is defined as:

$$\langle f(u), g(u)\rangle = \int_{-\infty}^{+\infty} f(u)g(u)du. \tag{2.20}$$

From Theorem 1, we can derive that $\frac{1}{\sqrt{2}}\phi\left(\frac{t}{2}\right) \in V_1$ and that $\{\phi(t-k)\}_{k\in\mathcal{Z}}$ is an orthonormal basis of V_0. From Eq. 2.10, we know that $V_1 \subset V_0$. Therefore, $\frac{1}{\sqrt{2}}\phi\left(\frac{t}{2}\right)$ can be written as a linear combination of the members of the family $\{\phi(t-k)\}_{k\in\mathcal{Z}}$ as follows:

$$\frac{1}{\sqrt{2}}\phi\left(\frac{t}{2}\right) = \sum_{k=-\infty}^{+\infty} h(k)\phi(t-k) \tag{2.21}$$

where

$$h(k) = \langle \frac{1}{\sqrt{2}}\phi\left(\frac{t}{2}\right), \phi(t-k)\rangle. \tag{2.22}$$

The sequence $h(k)$ can be interpreted as a discrete filter. In particular, it is called a *low-pass filter* since the scaling functions defined in Theorem 1 are used to build approximations of a function $f(t)$.

At an arbitrary scale j, $\frac{1}{\sqrt{2^j}}\phi\left(\frac{t}{2^j}\right) \in V_j \subset V_{j-1}$, and $\{\frac{1}{\sqrt{2^{j-1}}}\phi\left(\frac{t-2^{j-1}k}{2^{j-1}}\right)\}_{k\in\mathcal{Z}}$ is an orthonormal basis of V_{j-1}. Therefore,

$$\frac{1}{\sqrt{2^j}}\phi\left(\frac{t}{2^j}\right) = \sum_{k=-\infty}^{+\infty} h'(k)\frac{1}{\sqrt{2^{j-1}}}\phi\left(\frac{t-2^{j-1}k}{2^{j-1}}\right). \tag{2.23}$$

Using the change of variable $t' = 2^{-j+1}t$, we obtain

$$\frac{1}{\sqrt{2}}\phi\left(\frac{t'}{2}\right) = \sum_{k=-\infty}^{+\infty} h'(k)\phi(t'-k) \tag{2.24}$$

where

$$h'(k) = \langle \frac{1}{\sqrt{2}}\phi\left(\frac{t'}{2}\right), \phi(t'-k)\rangle. \tag{2.25}$$

Eq. 2.24 is in fact the same as Eq. 2.21. This shows that scaling functions between any two successive scales can be related to one another through the filter operations in the form of Eq. 2.21. This implies that the basis functions of all spaces $(V_j)_{j\in\mathcal{Z}}$ are related to each other across scales. Therefore, the approximation at each scale can be related through the filter operations on the scaling functions.

In the literature, sometimes Eq. 2.21 is written as:

$$\phi(t) = \sqrt{2}\sum_{k=-\infty}^{+\infty} h''(k)\phi(2t-k) \tag{2.26}$$

where $h''(k)$ now is defined as:

$$h''(k) = \langle \phi(t), \sqrt{2}\phi(2t-k) \rangle. \tag{2.27}$$

Mallat (1989a) further shows that the difference of information available at two successive scales $j-1$ and j can be computed by decomposing the signal using a wavelet orthonormal basis. The difference of information between the approximations of a function $f(t)$ at the scales $j-1$ and j is called a *detail signal* at the scale j. Since the approximations at the scale $j-1$ and j are orthogonal projections on V_{j-1} and V_j, respectively, it can be shown that the detail signal at the scale j is given by the orthogonal projection of the original signal on the orthogonal complement of V_{j-1} in V_j (Mallat, 1989a). Let W_j be the orthogonal complementary vector space at the scale j. Thus,

$$W_j \perp V_j, \tag{2.28}$$

$$W_j \bigoplus V_j = V_{j-1}. \tag{2.29}$$

where $\perp$ represents orthogonality, and $\bigoplus$ represents an orthogonal sum of two subspaces.

Since the orthogonal projection of a function $f(t)$ on the vector space W_j characterize the detail signal, it may be defined as a detail operator D_j. The detail signal at the scale j is then represented by $D_j f(t)$. Therefore, the detail signal can be expressed as:

$$D_j f(t) = A_{j-1} f(t) - A_j f(t). \tag{2.30}$$

In order to characterize the detail operator D_j, an orthonormal basis of W_j needs to be determined in order to characterize the detail signal numerically. The following theorem, for which the proof can be found in Mallat (1989a, 1998) is introduced to define this orthonormal basis.

Theorem 2: (Mallat, 1989a) Let $(V_j)_{j\in\mathcal{Z}}$ be a multiresolution vector space sequence. There exists a function $\psi(t)$, called an *orthogonal wavelet*, such that $\psi_{j,k}(t) = \frac{1}{\sqrt{2^j}}\psi\left(\frac{t-2^jk}{2^j}\right)$. For any scale j, the family $\{\psi_{j,k}(t)\}_{k\in\mathcal{Z}}$ is an orthonormal basis of W_j. For all scales, $\{\psi_{j,k}(t)\}_{(j,k)\in\mathcal{Z}^2}$ is an orthonormal basis of $L^2(\mathcal{R})$.

The orthogonal projection $D_jf(t)$ on W_j can be expressed as a linear combination of the wavelet orthonormal basis defined in Theorem 2.

$$D_jf(t) = \sum_{k=-\infty}^{+\infty} \langle f(u), \psi_{j,k}(u)\rangle \ \psi_{j,k}(t). \tag{2.31}$$

Using Theorem 2, we can derive that $\frac{1}{\sqrt{2}}\psi\left(\frac{t}{2}\right) \in W_1$ and that $\{\phi(t-k)\}_{k\in\mathcal{Z}}$ is an orthonormal basis of V_0. From Eq. 2.10 and Eq. 2.28, we know that $W_1 \subset V_0$. Therefore, $\frac{1}{\sqrt{2}}\psi\left(\frac{t}{2}\right)$ can be written as a linear combination of the members of the family $\{\phi(t-k)\}_{n\in\mathcal{Z}}$ as follows:

$$\frac{1}{\sqrt{2}}\psi\left(\frac{t}{2}\right) = \sum_{k=-\infty}^{+\infty} g(k)\phi(t-k) \tag{2.32}$$

where

$$g(k) = \langle\frac{1}{\sqrt{2}}\psi\left(\frac{t}{2}\right), \phi(t-k)\rangle. \tag{2.33}$$

Similar to $h(k)$, the sequence $g(k)$ can be interpreted as a filter sequence. Since the wavelets defined in Theorem 2 are used to construct detail signals between two successive scales, $g(k)$ is called a *high-pass filter*.

At an arbitrary scale j, $\frac{1}{\sqrt{2^j}}\psi\left(\frac{t}{2^j}\right) \in W_j \subset V_{j-1}$, and $\{\frac{1}{\sqrt{2^{j-1}}}\phi\left(\frac{t-2^{j-1}k}{2^{j-1}}\right)\}_{k\in\mathcal{Z}}$ is an orthonormal basis of V_{j-1}. Therefore,

$$\frac{1}{\sqrt{2^j}}\psi\left(\frac{t}{2^j}\right) = \sum_{k=-\infty}^{+\infty} g'(k)\frac{1}{\sqrt{2^{j-1}}}\phi\left(\frac{t-2^{j-1}k}{2^{j-1}}\right). \tag{2.34}$$

Using the change of variable $t' = 2^{-j+1}t$, we get

$$\frac{1}{\sqrt{2}}\psi\left(\frac{t'}{2}\right) = \sum_{k=-\infty}^{+\infty} g'(k)\phi(t'-k) \tag{2.35}$$

where

$$g'(k) = \langle \frac{1}{\sqrt{2}}\psi\left(\frac{t'}{2}\right), \phi(t'-k)\rangle. \tag{2.36}$$

Eq. 2.35 takes the same form as Eq. 2.32. The relationship shows that wavelets are related to the scaling functions across scales through filter operations. Consequently, the detail signals are also related to approximated signals across scales.

As it appears in the wavelet literature, Eq. 2.32 is sometimes written as:

$$\psi(t) = \sqrt{2}\sum_{k=-\infty}^{+\infty} g''(k)\phi(2t-k) \tag{2.37}$$

where $g(''k)$ is defined as:

$$g''(k) = \langle \psi(t), \sqrt{2}\phi(2t-k)\rangle. \tag{2.38}$$

In summary, the wavelet multiresolution analysis provides a framework to approximate a function at different resolutions and determine the difference of information between two successive approximations. At each resolution, small-scaled information is stored in the detail signal through a high-pass filter operation, and large-scaled information is kept in the approximated signal through a low-pass filter operation. The approximations at different scales can be related through the scaling functions while the detail information can be connected through the wavelets across scales.

2.4 Pyramidal Algorithm for Signal Decomposition and Reconstruction

As seen in the previous section, the wavelet analysis is in fact a procedure to decompose a signal into approximated and detail signals at multiple levels of resolution. In this section, we discuss the computation of the approximated and detail signals utilizing their multiscale relationships through the scaling functions and the wavelets. This computation is called *signal decomposition*. After a signal is decomposed, certain types of data analysis such as noise suppression may be performed at particular scales. In this case, the decomposed signals are usually modified and put back together to reconstruct the original signal. The denoising application is discussed in detail in the next chapter. In this section, we will explain a procedure called *signal reconstruction* to reconstruct the original signal from the approximated and detail signals. In particular, the pyramidal algorithm used to decompose and reconstruct signal is discussed.

In practice, data are collected at a finite resolution. For convenience, let us normalize the sample spacing to 1. Following the notation used in the previous section, the sample spacing is equal to 2^j, where j represents the scale or level of wavelet transform. Since the original spacing is normalized to 1, the scale of the original data is 0. The scale j is sometimes called a *decomposition level*.

Using the definition of the complementary transform given in Eq. 2.8, the discrete values of approximated signal (scaling function coefficients) at level j and time k can be computed as:

$$a_{j,k} = \int_{-\infty}^{\infty} f(t)\ \phi_{j,k}(t)dt \tag{2.39}$$

$$= \langle f(t), \phi_{j,k}(t)\rangle. \tag{2.40}$$

Similarly, the discrete values of detail signal (wavelet coefficients) are computed from the definition of the wavelet transform given in Eq. 2.4:

$$d_{j,k} = \int_{-\infty}^{\infty} f(t)\ \psi_{j,k}(t)dt \tag{2.41}$$
$$= \langle f(t), \psi_{j,k}(t)\rangle. \tag{2.42}$$

Let us define

$$f(t) = \sum_{k=-\infty}^{+\infty} a_{0,k}\ \phi_{o,k}(t) \in V_0. \tag{2.43}$$

where $a_{0,k}$ are discrete original data stream. Since $\{\phi_{0,k}\}_{k\in\mathcal{Z}}$ forms an orthonormal basis,

$$a_{0,k} = \langle f(t), \phi(t-k)\rangle \tag{2.44}$$

which is the definition of the approximated signal at level 0. This means that the best approximation at level 0 is in fact the original signal itself. The detail signal, however, does not exist at level 0.

In order to determine the approximated and detail signals at higher levels of decomposition, the multiscaled relationships established in the multiresolution analysis are used. First, let us look at the computation of the approximated signals using the scaling functions. Any function $\phi_{j+1,k} \in V_{j+1} \subset V_j$ can be written as a linear combination of members of the orthonormal basis $\{\phi_{j,k}\}_{k\in\mathcal{Z}}$ of V_j:

$$\phi_{j+1,k} = \sum_{l=-\infty}^{+\infty} \langle \phi_{j+1,k}, \phi_{j,l}\rangle\ \phi_{j,l} \tag{2.45}$$

where

$$\langle \phi_{j+1,k}, \phi_{j,l}\rangle = \int_{-\infty}^{+\infty} \frac{1}{\sqrt{2^{j+1}}}\phi\left(\frac{t-2^{j+1}k}{2^{j+1}}\right)\frac{1}{\sqrt{2^j}}\phi\left(\frac{t-2^j l}{2^j}\right)dt. \tag{2.46}$$

By using the change of variable $t' = 2^{-j}t - 2k$, we have

$$\langle \phi_{j+1,k}, \phi_{j,l}\rangle = \int_{-\infty}^{+\infty} \frac{1}{\sqrt{2}}\phi\left(\frac{t'}{2}\right)\phi(t'-l+2k)dt' \tag{2.47}$$

$$= \langle \frac{1}{\sqrt{2}} \phi \left(\frac{t'}{2} \right), \phi(t' - l + 2k) \rangle \quad (2.48)$$

$$= h(l - 2k). \quad (2.49)$$

Therefore Eq. 2.45 becomes

$$\phi_{j+1,k} = \sum_{l=-\infty}^{+\infty} h(l - 2k)\ \phi_{j,l}. \quad (2.50)$$

Taking the inner products of $f(t)$ with the vectors on each side of Eq. 2.50, we obtain

$$\langle f(t), \phi_{j+1,k}(t) \rangle = \sum_{l=-\infty}^{+\infty} h(l - 2k)\ \langle f(t), \phi_{j,l}(t) \rangle. \quad (2.51)$$

Using the definition in Eq. 2.40, the scaling function coefficients are expressed as:

$$a_{j+1,k} = \sum_{l=-\infty}^{+\infty} h(l - 2k)\ a_{j,l}. \quad (2.52)$$

The definition of a discrete convolution between a discrete signal $f(l)$ and a filter $h(k)$ is

$$f * h(k) = \sum_{l=-\infty}^{+\infty} f(l)\ h(k - l). \quad (2.53)$$

Let us denote $\overline{x}(n) = x(-n)$. Eq. 2.52 then becomes:

$$a_{j+1,k} = a_j * \overline{h}(2k) \quad (2.54)$$

Eq. 2.54 shows that the approximated signal at level $j+1$ is computed by taking every other sample of the discrete convolution between a_j and $\overline{h}$. As a result, the approximated signal at level $j+1$ is subsampled by a factor of two. Starting from the discrete signal $a_{0,k}$, approximate signals at subsequent levels of decomposition can be computed.

For detail signals, the relationships between wavelets and scaling functions across scales can be used. Any $\psi_{j+1,k} \in W_{j+1} \subset V_j$ can be written as:

$$\psi_{j+1,k} = \sum_{l=-\infty}^{+\infty} \langle \psi_{j+1,k}, \phi_{j,l} \rangle \ \phi_{j,l} \tag{2.55}$$

where

$$\langle \psi_{j+1,k}, \phi_{j,l} \rangle = \int_{-\infty}^{+\infty} \frac{1}{\sqrt{2^{j+1}}} \psi \left(\frac{t - 2^{j+1}k}{2^{j+1}} \right) \frac{1}{\sqrt{2^j}} \phi \left(\frac{t - 2^j l}{2^j} \right) dt. \tag{2.56}$$

Using the change of variable $t' = 2^{-j}t - 2k$, we obtain

$$\begin{aligned} \langle \psi_{j+1,k}, \phi_{j,l} \rangle &= \int_{-\infty}^{+\infty} \frac{1}{\sqrt{2}} \psi \left(\frac{t'}{2} \right) \phi(t' - l + 2k) dt' && (2.57) \\ &= \langle \frac{1}{\sqrt{2}} \psi \left(\frac{t'}{2} \right), \phi(t' - l + 2k) \rangle && (2.58) \\ &= g(l - 2k). && (2.59) \end{aligned}$$

Therefore, Eq. 2.55 becomes

$$\psi_{j+1,k} = \sum_{l=-\infty}^{+\infty} g(l - 2k) \ \phi_{j,l}. \tag{2.60}$$

Taking inner products of $f(t)$ with both sides of Eq. 2.60, we have

$$\langle f(t), \psi_{j+1,k}(t) \rangle = \sum_{l=-\infty}^{+\infty} g(l - 2k) \ \langle f(t), \phi_{j,l}(t) \rangle. \tag{2.61}$$

Using the definition in Eq. 2.42, the wavelet coefficients are expressed as:

$$\begin{aligned} d_{j+1,k} &= \sum_{l=-\infty}^{+\infty} g(l - 2k) \ a_{j,l} && (2.62) \\ &= d_j * \overline{g}(2k). && (2.63) \end{aligned}$$

Therefore, the detail signal at level $j + 1$ can be calculated by taking every other sample of the discrete convolution between a_j and $\overline{g}$. The size of the detail signal at level $j + 1$ is reduced by half. Starting from the discrete signal $a_{0,k}$, detail signals at subsequent levels of decomposition can be determined.

Since the sample sizes of the approximated and the detail signals are decreased by a factor of two as the decomposition level increases, this computation is called the *pyramidal algorithm*. This algorithm is sometimes called the *nonredundant* algorithm due to the fact that the number of data is different at each level. Fig. 2.2 depicts a schematic diagram of the pyramidal wavelet decomposition. Fig. 2.3 shows a diagram of how signals at coarser scales are computed using the pyramidal algorithm with a filter size of three.

In order to reconstruct the approximation at level j, an orthonormal basis of V_j has to be determined. Since W_{j+1} is the orthogonal complement of V_{j+1} in V_j, the union of the bases $\{\psi_{j+1,k}\}_{k\in\mathcal{Z}}$ and $\{\phi_{j+1,k}\}_{k\in\mathcal{Z}}$ forms an orthonormal basis of V_j. Therefore, any $\phi_{j,k}$ can be written as a linear combination of this orthonormal basis:

$$\phi_{j,k} = \sum_{l=-\infty}^{+\infty} \langle \phi_{j,k}, \phi_{j+1,l} \rangle \; \phi_{j+1,l} \; + \sum_{l=-\infty}^{+\infty} \langle \phi_{j,k}, \psi_{j+1,l} \rangle \; \psi_{j+1,l} \tag{2.64}$$

where

$$\langle \phi_{j,k}, \phi_{j+1,l} \rangle = \int_{-\infty}^{+\infty} \frac{1}{\sqrt{2^j}} \phi \left(\frac{t - 2^j k}{2^j} \right) \frac{1}{\sqrt{2^{j+1}}} \phi \left(\frac{t - 2^{j+1} l}{2^{j+1}} \right) dt. \tag{2.65}$$

Using the change of variable $t' = 2^{-j}t - 2l$, we obtain

$$\begin{aligned} \langle \phi_{j,k}, \phi_{j+1,l} \rangle &= \int_{-\infty}^{+\infty} \phi(t' - k + 2l) \frac{1}{\sqrt{2}} \phi \left(\frac{t'}{2} \right) dt' && (2.66) \\ &= \langle \phi(t' - k + 2l), \frac{1}{\sqrt{2}} \phi \left(\frac{t'}{2} \right) \rangle && (2.67) \\ &= h(k - 2l). && (2.68) \end{aligned}$$

Similarly,

$$\begin{aligned} \langle \phi_{j,k}, \psi_{j+1,l} \rangle &= \langle \phi(t' - k + 2l), \frac{1}{\sqrt{2}} \psi \left(\frac{t'}{2} \right) \rangle && (2.69) \\ &= g(k - 2l). && (2.70) \end{aligned}$$

Therefore, Eq. 2.64 becomes

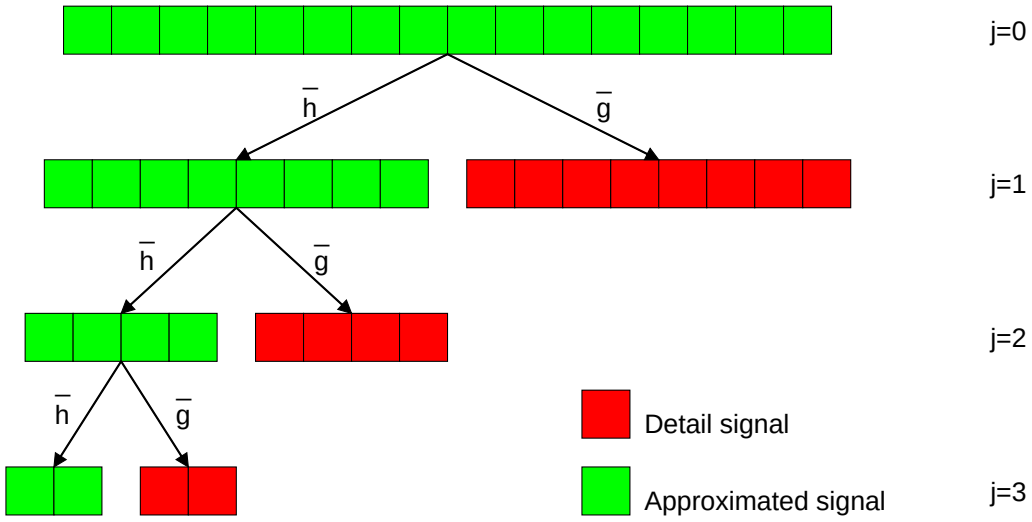

Figure 2.2: Wavelet decomposition using pyramidal algorithm.

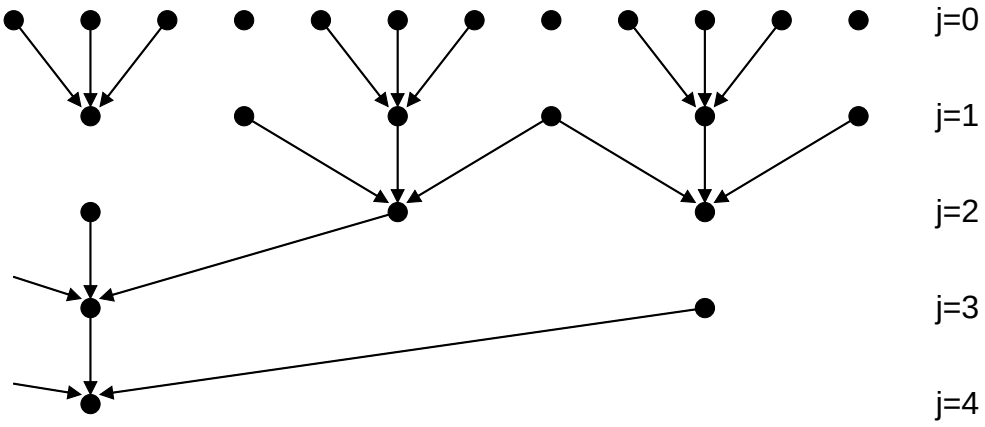

Figure 2.3: Computation of transforms using pyramidal algorithm (from Carmona *et al.*, 1998).

$$\phi_{j,k} = \sum_{l=-\infty}^{+\infty} h(k-2l)\ \phi_{j+1,l}\ + \sum_{l=-\infty}^{+\infty} g(k-2l)\ \psi_{j+1,l}. \tag{2.71}$$

Taking inner products to each side of Eq. 2.71, we have

$$\langle f(t), \phi_{j,k}(t)\rangle = \sum_{l=-\infty}^{+\infty} h(k-2l)\ \langle f(t), \phi_{j+1,l}(t)\rangle + \sum_{l=-\infty}^{+\infty} g(k-2l)\ \langle f(t), \psi_{j+1,l}(t)\rangle. \tag{2.72}$$

Therefore, the approximation signal at level j is expressed as:

$$a_{j,k} = \sum_{l=-\infty}^{+\infty} h(k-2l)a_{j+1,l} + \sum_{l=-\infty}^{+\infty} g(k-2l)d_{j+1,l}. \tag{2.73}$$

Let us denote

$$\check{x}(l) = \begin{cases} x(l) & \text{if} \quad l = 2k \\ 0 & \text{if} \quad l = 2k+1. \end{cases} \tag{2.74}$$

Therefore, Eq. 2.73 becomes

$$a_{j,k} = \check{a}_{j+1} * h(k) + \check{d}_{j+1} * g(k). \tag{2.75}$$

Eq. 2.75 shows that the approximated signal $a_{j,k}$ can be reconstructed by inserting zeros between each sample of a_{j+1} and d_{j+1} and adding together the discrete convolutions between the resulting signals and the filters h and g, respectively. Fig. 2.4 depicts a schematic diagram of the pyramidal wavelet reconstruction. Starting from any level of decomposition, approximated signals at subsequently lower levels of decomposition and the original signal can be reconstructed.

In summary, the pyramidal algorithm can be used to compute approximated and detail signals for multiple levels of resolution by subsequently convolving the approximated signal at each level with the low-pass and high-pass filters, respectively. The number of samples in each of the decomposed signals at the next coarser scale is reduced by a factor of two. This type of algorithm is very useful in signal coding, signal compression, and upscaling applications and likewise applications in which the number of data is to be reduced when a large-scaled representation is sought. The

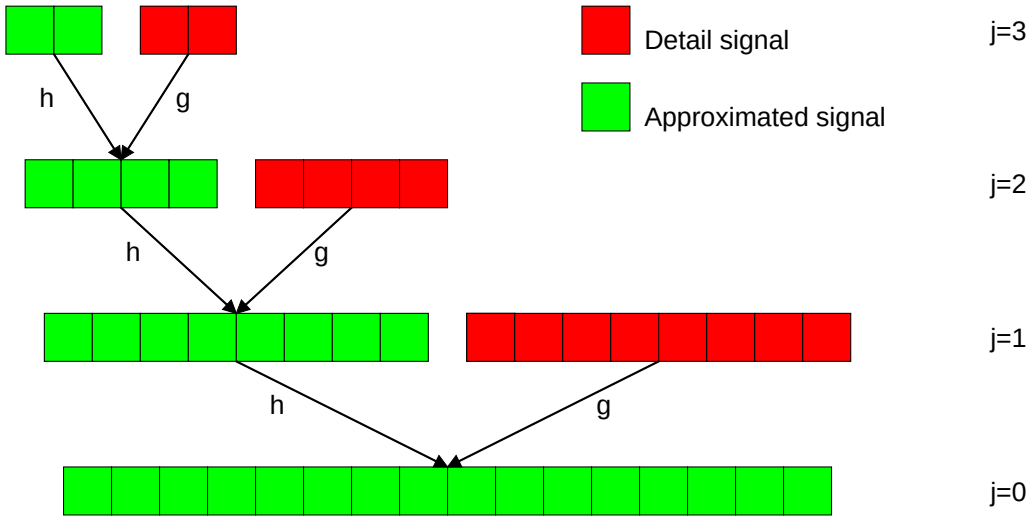

Figure 2.4: Wavelet reconstruction using pyramidal algorithm.

pyramidal algorithm is also used in certain approximation problems in which the exact locations of the approximated data and their resolution are not important.

2.5 *A Trous* Algorithm for Signal Decomposition and Reconstruction

In certain types of wavelet application such as singularity detection and nonparametric regression, it is more desirable if not essential to evaluate approximated and detail signals at the same locations across scale thus keeping the original resolution of the samples. In the pyramidal algorithm, the sample resolution becomes coarser every time a signal is decomposed. Consequently, results from any type of analysis from decomposed signals possess coarser resolutions than the original data. This phenomena is referred to as *shift-variance* because the solutions from the coarse-scaled analysis are shifted from the exact solutions in the original spacing.

In this section, we discuss a *shift-invariant* algorithm that computes the approximated and detail signals at the same spacing across scales using nonorthonormal wavelet bases. This algorithm is called the *à trous algorithm*. It was first proposed by Holschneider, Kronland-Martinet, Morlet, and Tchamitchian (1989). Shensa (1992) later studied the relationship between the *à trous* algorithm and the pyramidal algorithm and concluded that the *à trous* algorithm is in fact a nonorthonormal multiresolution algorithm for which the discrete wavelet transform is exact.

To formulate signal decomposition and reconstruction, orthonormality is not essential. We are only interested in the multiscale relationships in the form of Eq. 2.21 and Eq. 2.32 between the scaling functions and the wavelets through filter operations. In order to keep the original sampling frequency (in which $2^j = 2^0 = 1$), the wavelets are now discretized as:

$$\psi_{j,k}(t) = \frac{1}{\sqrt{2}}\psi\left(\frac{t-k}{2^j}\right), \tag{2.76}$$

and the scaling functions are discretized as:

$$\phi_{j,k}(t) = \frac{1}{\sqrt{2}}\phi\left(\frac{t-k}{2^j}\right). \tag{2.77}$$

Mallat (1998) showed that the multiresolution relationships for nonorthogonal wavelets exist in the Fourier domain as follows:

$$\hat{\phi}(\omega) = \frac{1}{\sqrt{2}}\hat{h}\left(\frac{\omega}{2}\right)\hat{\phi}\left(\frac{\omega}{2}\right), \tag{2.78}$$

and

$$\hat{\psi}(\omega) = \frac{1}{\sqrt{2}}\hat{g}\left(\frac{\omega}{2}\right)\hat{\phi}\left(\frac{\omega}{2}\right) \tag{2.79}$$

Mallat (1998) further showed that the approximated signal $a_{j+1,k}$ and detail signal $d_{j+1,k}$ can be computed using these multiscale relationships through low-pass filter h and high-pass filter g. Obviously, the filters h and g are different from h and g defined in the previous section in which the wavelets are orthogonal. For any filter sequence $x(n)$, $x_j(n)$ is denoted as the filter sequence obtained by inserting $2^j - 1$ zeros between each sample of $x(n)$. The insertion of zeros into the sequence creates holes, thus the algorithm is called the *à trous* algorithm (*trous* means holes in French). The approximated and detail signals are respectively determined by:

$$a_{j+1,k} = a_j * \overline{h}_j(k), \tag{2.80}$$

and

$$d_{j+1,k} = a_j * \overline{g}_j(k). \tag{2.81}$$

Therefore, the approximated signal at level $j+1$ can be calculated by inserting $2^j - 1$ zeros between each sample of the low-pass filter h and performing the discrete convolution between a_j and the resulting filter. The detail signal at level $j+1$ can be computed in a similar fashion using the high-pass filter g. A diagram of the *à trous* algorithm for wavelet decomposition is depicted in Fig. 2.5. The size and spacing of the original data are preserved across scales while signals at higher levels of decomposition provide information with coarser contents. Fig. 2.6 shows how the

signals at coarser scales are computed using the *à trous* algorithm with a filter size of three.

In order to reconstruct signal at lower levels of decomposition, Mallat (1998) defined the *dual scaling function* $\tilde{\phi}(t)$ and *dual wavelet* $\tilde{\psi}(t)$ using frame theory introduced by Duffin and Schaeffer (1952). For an orthonormal wavelet basis, the basis and its dual are the same. The multiscale relationships for the dual scaling function $\tilde{\phi}(t)$ and the dual wavelet $\tilde{\psi}(t)$ exist in the Fourier domain as:

$$\hat{\tilde{\phi}}(\omega) = \frac{1}{\sqrt{2}}\hat{\tilde{h}}\left(\frac{\omega}{2}\right)\hat{\tilde{\phi}}\left(\frac{\omega}{2}\right), \tag{2.82}$$

and

$$\hat{\tilde{\psi}}(\omega) = \frac{1}{\sqrt{2}}\hat{\tilde{h}}\left(\frac{\omega}{2}\right)\hat{\tilde{\phi}}\left(\frac{\omega}{2}\right) \tag{2.83}$$

where $\tilde{h}$ is called the $low{-}pass\ dual\ filter$, and $\tilde{g}$ is called the $high{-}pass\ dual\ filter$. The reconstructed signal $a_{j,k}$ are then computed as:

$$a_{j,k} = \frac{1}{2}\left(a_{j+1} * \tilde{h}_j(k) + d_{j+1} * \tilde{g}_j(k)\right). \tag{2.84}$$

Using Eq. 2.84, the approximated signal $a_{j,k}$ can be reconstructed by first inserting $2^j - 1$ zeros between each sample of the dual filters $\tilde{h}$ and $\tilde{g}$ and then adding together the discrete convolution between a_{j+1} and the resulting low-pass dual filter and the convolution between d_{j+1} and the resulting high-pass dual filter. Fig. 2.7 depicts a schematic diagram of signal reconstruction using the *à trous* algorithm. Starting from any level of decomposition, approximated signals at subsequently lower levels of decomposition and the original signal can be reconstructed over the same grid.

The *à trous* algorithm is suitable for applications in which the exact location of the wavelet decomposition is important, such as singularity detection and certain approximation problems. Since the number of data and the location of each point are preserved across scales, this algorithm is sometimes called the *redundant* algorithm.

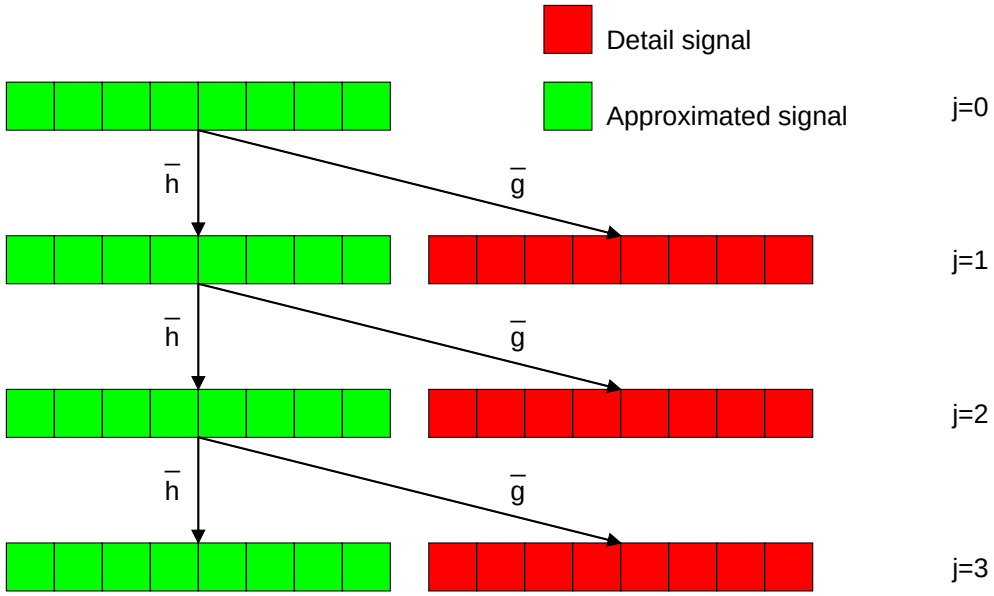

Figure 2.5: Wavelet decomposition using *à trous* algorithm.

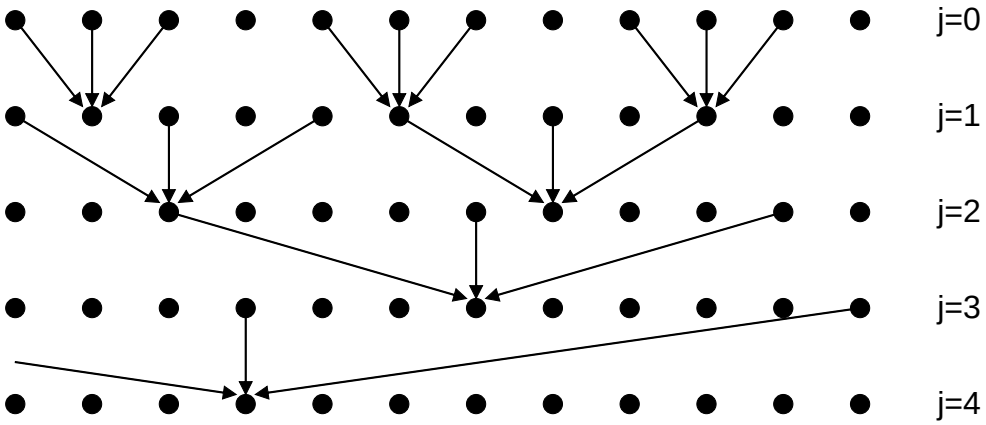

Figure 2.6: Computation of transforms using *à trous* algorithm (from Carmona *et al.*, 1998).

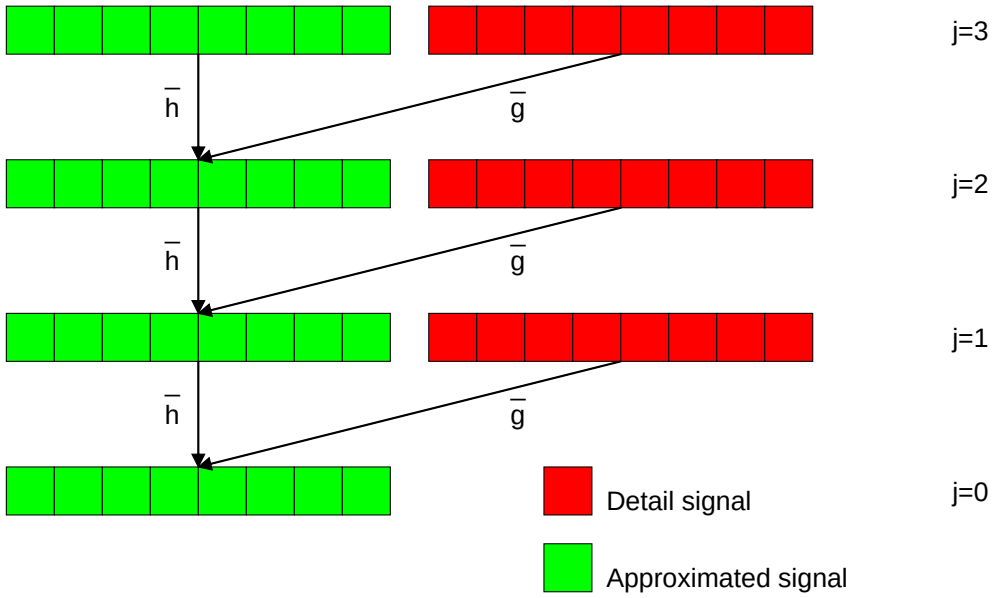

Figure 2.7: Wavelet reconstruction using *à trous* algorithm.

2.6 Spline Wavelet for Singularity Detection

Based on the Lipschitz exponent analysis which measures local regularity of functions, Mallat and Hwang (1992) and Mallat and Zhong (1992) developed a new type of nonorthogonal wavelet, a quadratic spline with compact support, suitable for detecting singularity in the data. Depicted in Fig. 2.8 is a quadratic spline wavelet given by (Gerritsen, 1996):

$$\psi(t) = \begin{cases} 2(t+1)^2 & -1 \leq t < -1/2 \\ -4t(t+1) - 2t^2 & -1/2 \leq t < 0 \\ -4t(1-t) + 2t^2 & 0 \leq t < 1/2 \\ -2(t-1)^2 & 1/2 \leq t < 1 \end{cases} \tag{2.85}$$

The filter coefficients are given by Mallat (1998) in Table 2.1. Since the spline wavelet is nonorthogonal, the *à trous* algorithm can be used to compute approximated

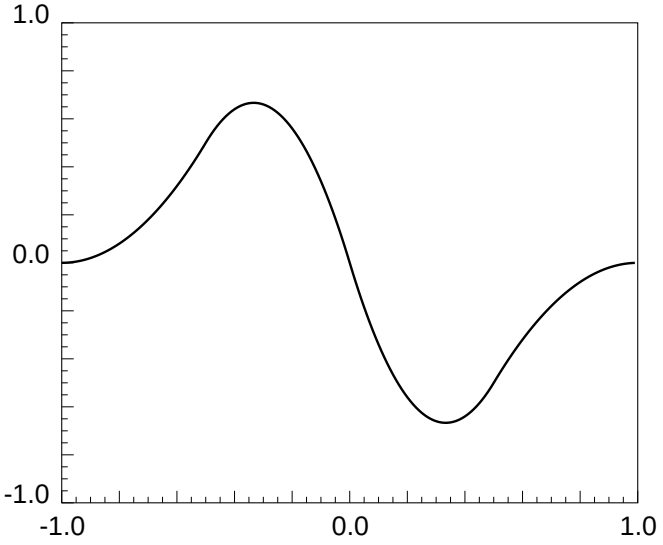

Figure 2.8: Spline wavelet (from Mallat and Hwang, 1992).

and detail signals. Thus, the data are sampled on the same grid across scales. Mallat and Zhong (1992) applied the singularity detection framework to characterize signals with edges.

Figs. 2.9 and 2.10 illustrate the results from wavelet decomposition using the spline wavelet with the *à trous* algorithm. The original data signal was passed through the low-pass and high-pass filters expressed in Table 2.1. As seen in the figures, at each

Table 2.1: Filter coefficients for the spline wavelet (from Mallat, 1998).

k	$h(k)$	$\tilde{h}(k)$	$g(k)$	$\tilde{g}(k)$
-2				-0.03125
-1	0.125	0.125		-0.21875
0	0.375	0.375	-0.5	-0.68750
1	0.375	0.375	0.5	0.68750
2	0.125	0.125		0.21875
3				0.03125

level of decomposition, the approximated signal provide information on the overall features in the original signal while the detail signal describes changes in the signal on local scales. As the level of decomposition increases, the approximated signal gives higher degrees of approximation. Similarly, the detail signal characterizes change on coarser scales with the increasing level of decomposition. This decomposition process can be performed until the desired level of coarseness is reached.

From Figs. 2.9 and 2.10, we can see that the detail signal reaches an extremum when there is a sudden change (singularity) in the original signal itself. Mallat and Hwang (1992) defined a *wavelet modulus maximum* at a scale a_0 as a point (a_0, t_0) such that $|Wf(a_0, t)| < |Wf(a_0, t_0)|$ where t belongs to the left or right neighborhood of t_0. In another word, the wavelet modulus maximum is basically the highest or lowest point in its neighborhood. The wavelet maxima can therefore be used to locate singularities in the signal. Figs. 2.11 and 2.12 depict the locations of the wavelet maxima and the values of the detail signal at the corresponding positions.

As seen in Figs. 2.11 and 2.12, the wavelet modulus maxima at different levels of decomposition provide different types of information concerning singularities. The wavelet modulus maxima at low levels of decomposition (levels 1-2) represent both signal singularities and noise singularities. In the regions where there are obvious singularities such as those in the neighborhood of $t = 14,\ t = 29,\ t = 144$, these singularities can be identified easily by the high magnitude of wavelet maxima. On the other hand, gradual singularities in the second half of the signal where $t > 144$ are mixed with noise singularities. Small values of wavelet maxima at low levels are characteristics of both noise and small changes in the data. Consequently, it is difficult to distinguish one from the other. As the signal resolution becomes coarser in levels 3-4, which are intermediate decomposition levels, the noise singularities gradually diminish revealing the gradual singularities in the second half of the signal while the obvious singularities can still be identified by the wavelet modulus maxima. At high levels of decomposition such as levels 5-6, the wavelet modulus maxima now correspond to singularities of very coarse data features. The singularities at the

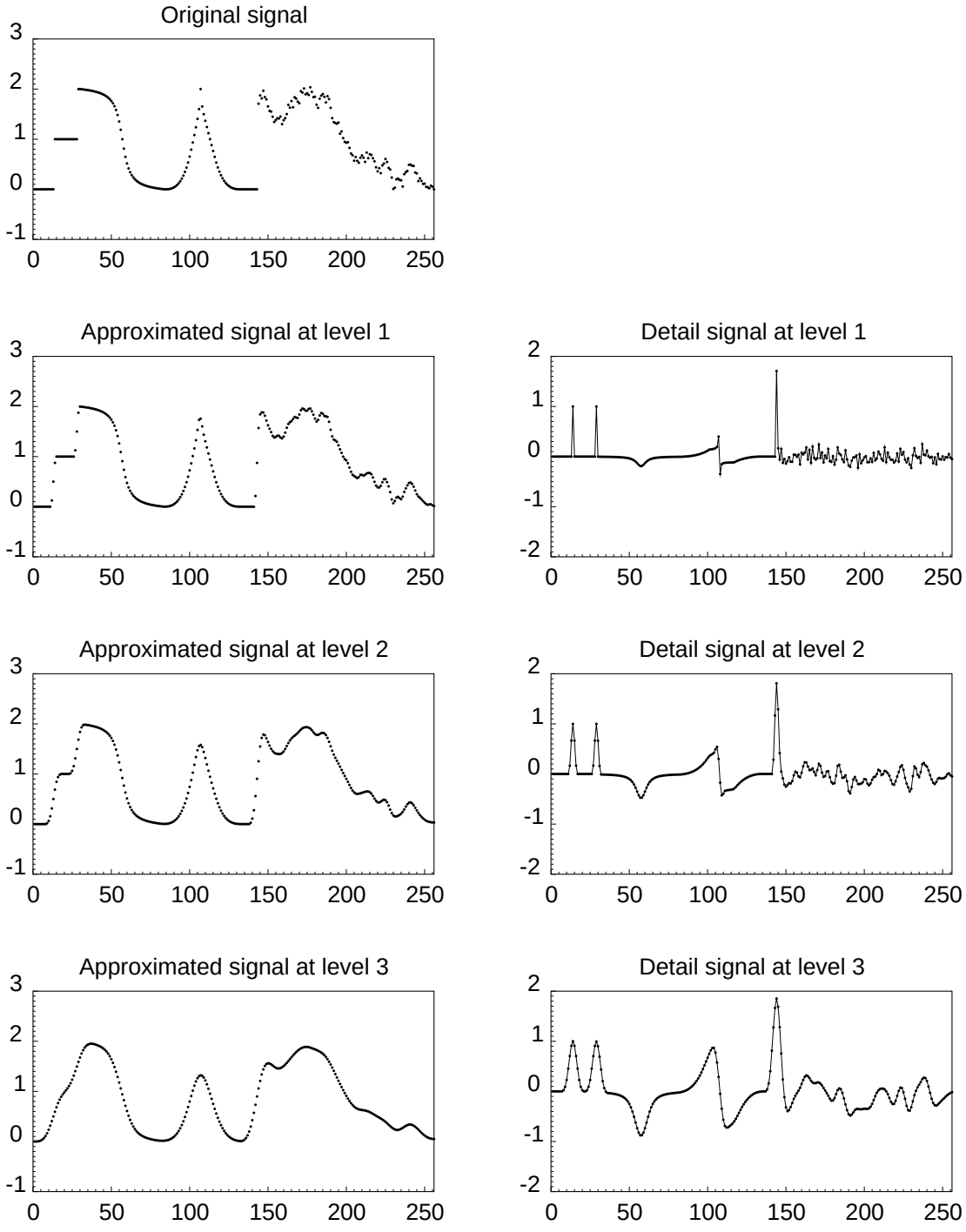

Figure 2.9: Wavelet decomposition (from Mallat and Hwang, 1992).

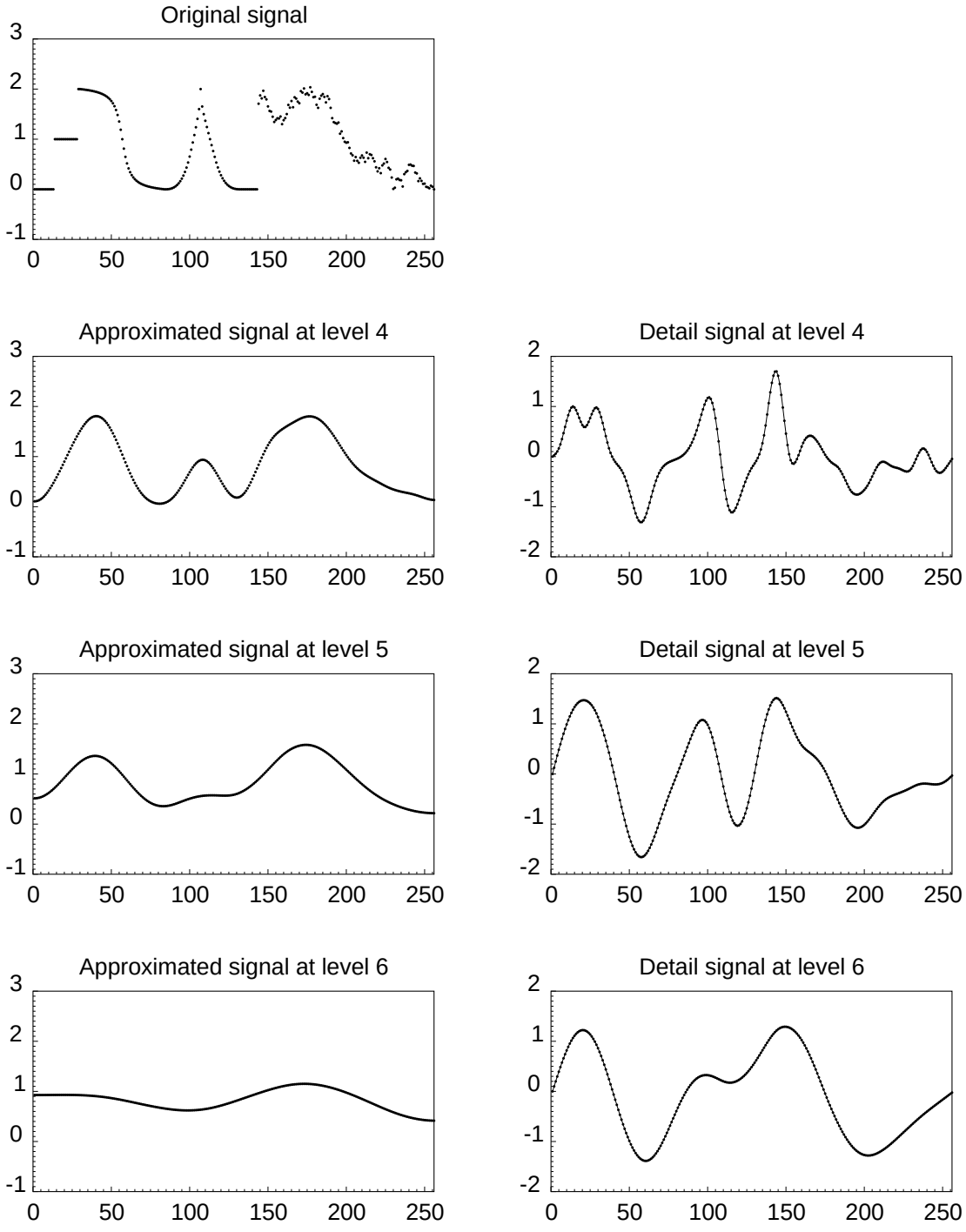

Figure 2.10: Wavelet decomposition (continued) (from Mallat and Hwang, 1992).

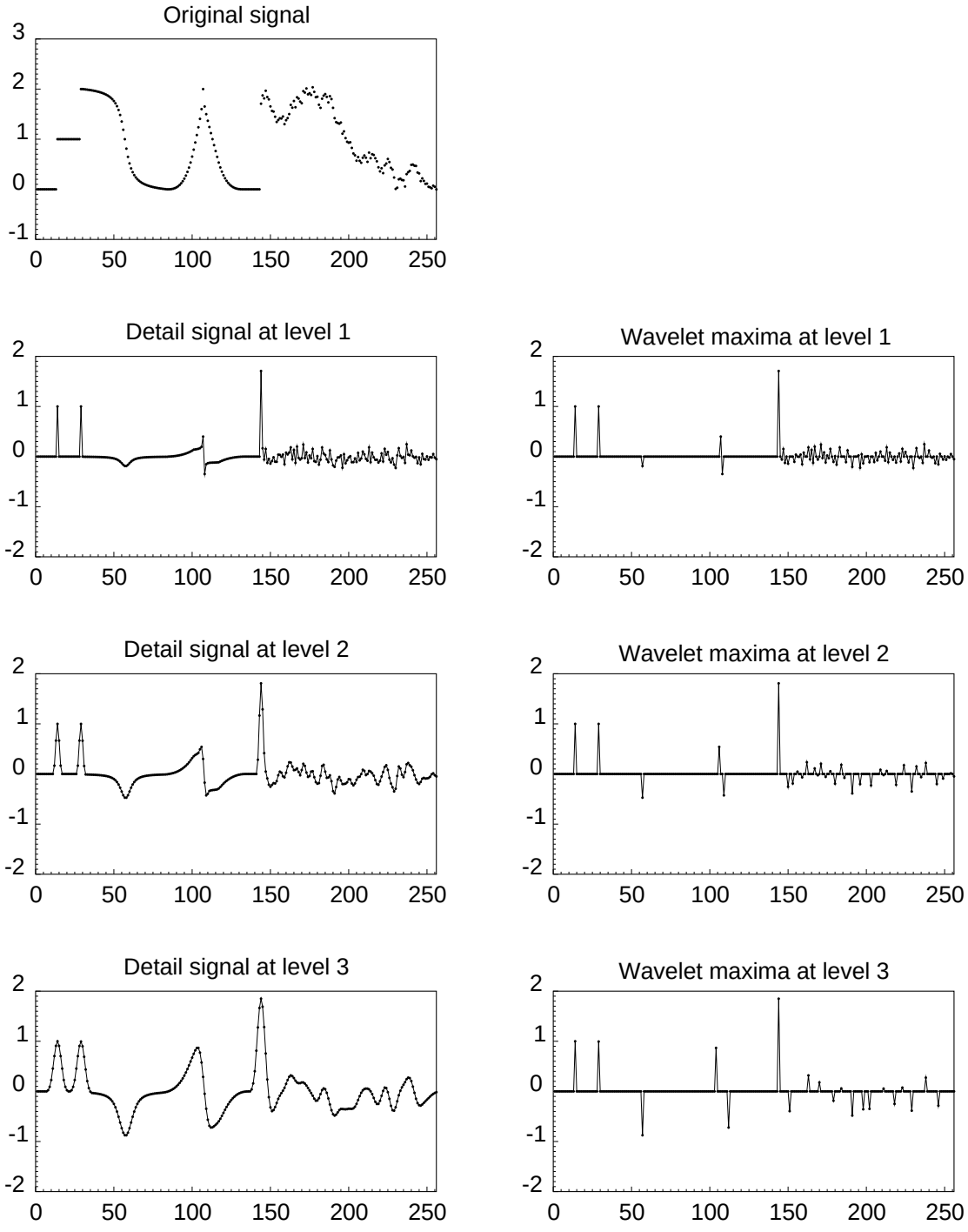

Figure 2.11: Wavelet modulus maxima (from Mallat and Hwang, 1992).

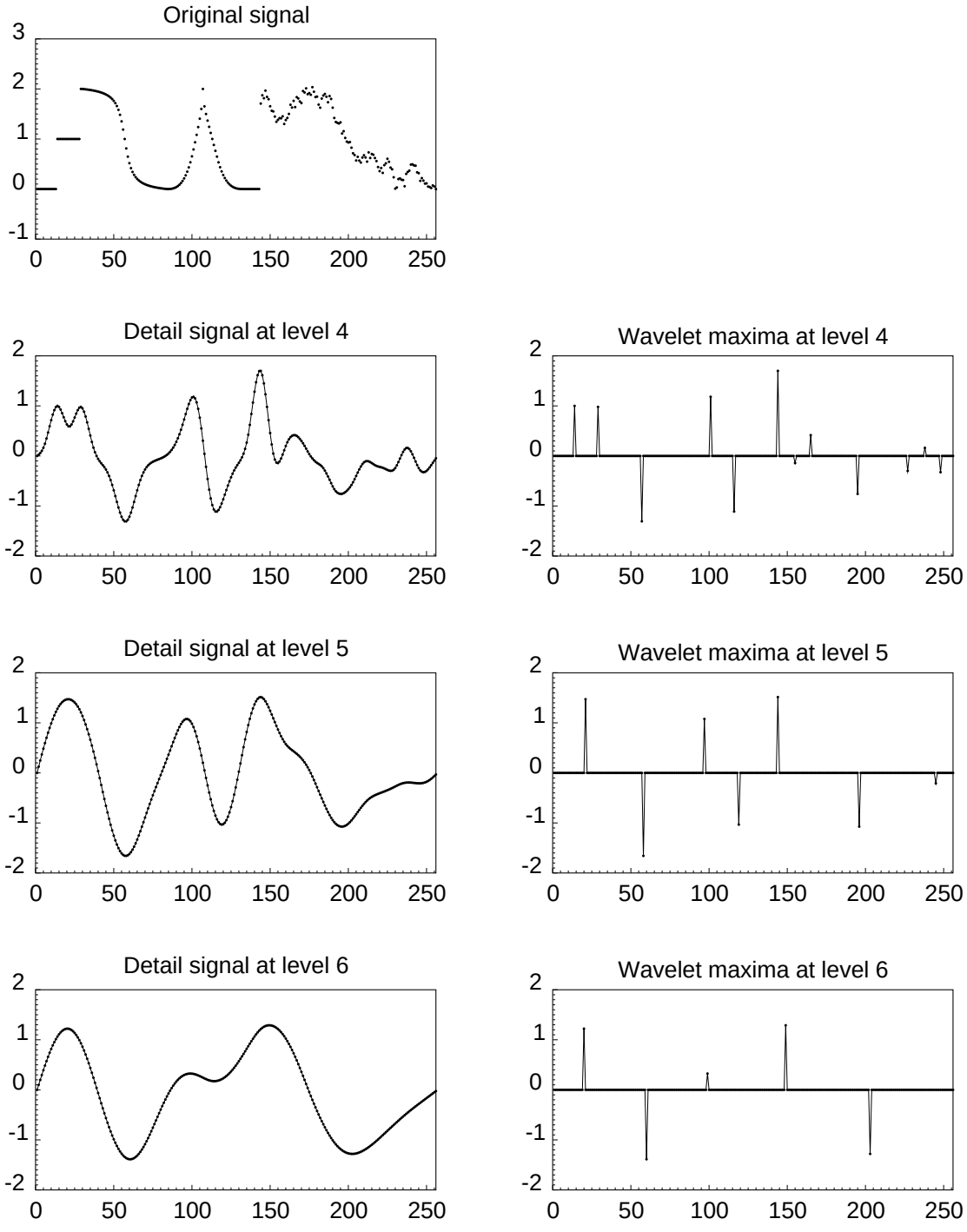

Figure 2.12: Wavelet modulus maxima (continued) (from Mallat and Hwang, 1992).

points $t = 14$ and $t = 19$ are now grouped into one singularity representing an overall upward trend in this neighborhood. In the neighborhood where $t > 144$, there is only a single singularity at level 6 representing an overall downward trend in the vicinity.

In this work, the wavelet analysis is used to: (1) detect outliers, (2) sharp pressure changes due to changes in well flow rate, and (3) suppress noise. The spline wavelet is used in all these three applications for two obvious reasons. First of all, the spline wavelet was constructed purposely to characterize signal regularity at local scale, thus it is suitable to detect outliers which represent abrupt changes in data continuity and the sharp pressure changes at new transients. The spline wavelet is also suitable for noise suppression because of its ability to characterize sharp changes and small variations and distinguish one from the other. Therefore, the sharp changes which are true data features can be preserved while suppressing noise in the signal. Another reason for using the spline wavelet, which is nonorthogonal, is that the sampling frequency in these three applications needs to be constant throughout the multiple levels of decomposition to avoid shifting in the results.

Chapter 3

Application of Wavelets to Data Processing

This chapter discusses data processing issues associated with long-term pressure data in an attempt to reduce the amount of work that needs to be performed by humans. The methods implemented here are, however, more general and not limited to the processing of pressure transient data. Many procedures can be used in other types of applications with minor or no adjustment.

Section 3.1 explains the development of an algorithm that is used to detect and remove outliers from data. The discussion of how the wavelet decomposition analysis can be used to determine outliers is presented. Two test cases of actual field data are also included to demonstrate the effectiveness of the developed algorithm.

Following the outlier analysis, Section 3.2 discusses an algorithm to suppress noise in the data. Two standard types of wavelet thresholding methods used to denoise data are examined. The development of the hybrid wavelet thresholding method is introduced. The improvement of the new method over the two existing methods is discussed. Also presented in this section are results from the implementation of the hybrid method to actual field data.

In Section 3.3, a procedure to identify the beginnings of new transients in pressure data utilizing the singularity detection algorithm from wavelet multilevel signal decomposition is discussed. The benefit of using preprocessed data, namely, denoised data, over raw data when implementing the procedure to detect new transients is illustrated. Results from three sets of field data with different appearances from different sampling schemes are shown.

Then, in Section 3.4, the issue of reducing the number of data to a manageable size is discussed. The role noise suppression plays in the data reduction process is investigated. Results from the implementation to actual field data are illustrated.

3.1 Outlier Removal

In general, pressure data collected from permanent downhole gauges contain different degrees of measurement errors. Let us first distinguish two types of measurement errors: noise and outliers. Noise is a group of data points that scatter around the trend of the overall data (true signal). They lie in the same neighborhood as the true data. Outliers, on the other hand, are data points that lie away from the trend of the data. They can be easily identified from their misalignment with the rest of the data. The difference between noise and outliers is illustrated in Figs. 3.1 and 3.2. Note that the pressure data shown in Fig. 3.1 were recorded in low precisions due to limited storage space resulting in a poor resolution in the pressure value.

There are countless reasons that lead to the occurrence of outliers and noise. The well and reservoir environments are different from the laboratory environment in which the pressure gauge is designed, built, and calibrated. Dynamic changes of reservoir conditions such as a change in temperature also contribute to fluctuations in pressure measurements. Sometimes, outliers and noise come from errors in the pressure acquisition system itself rather than the measurement system. Kikani, Fair, and Hite (1997) presented several pitfalls in the performance of pressure gauges. Often, noise is simply caused by the rounding-off of pressure measurements to save

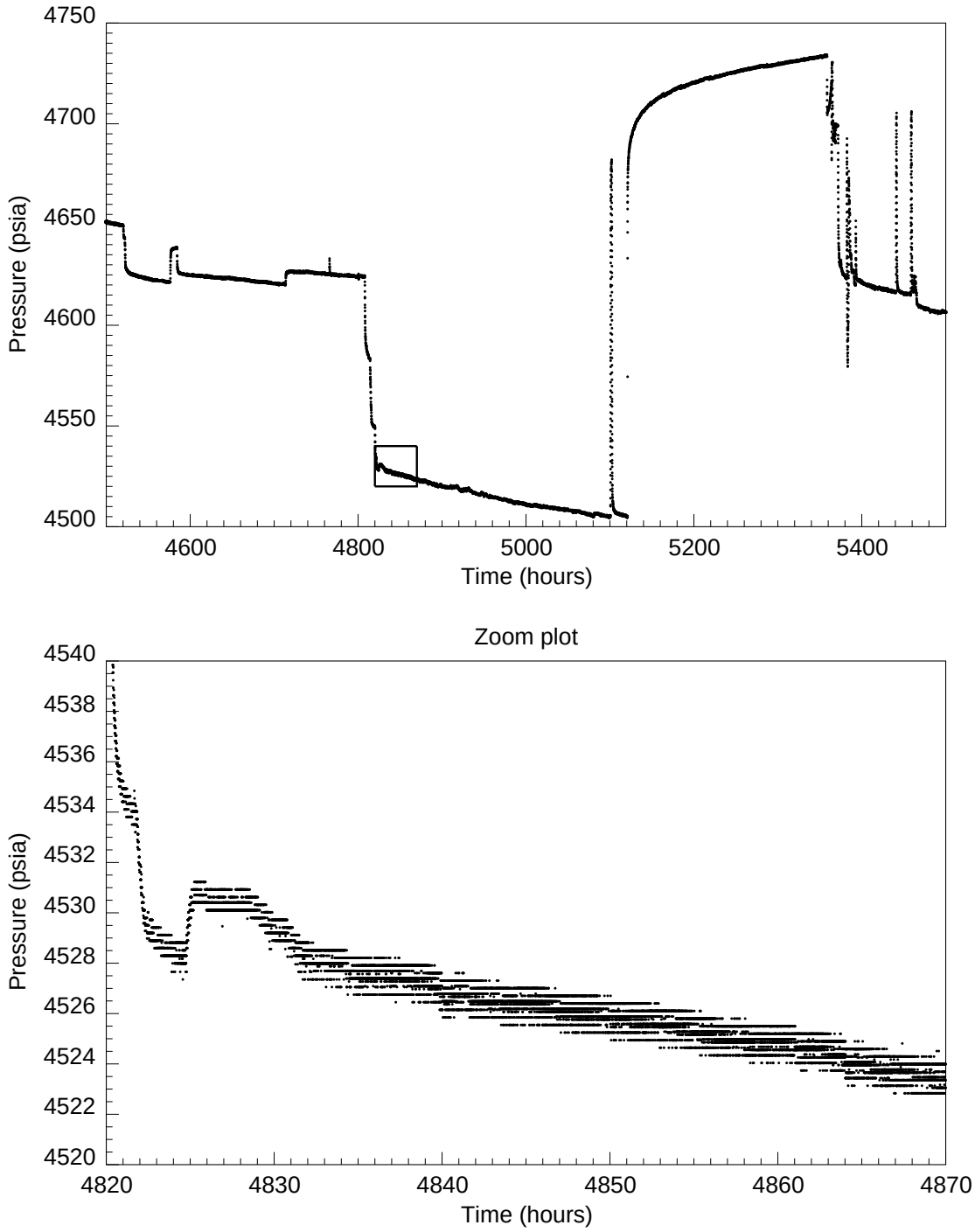

Figure 3.1: Noise in pressure measurements collected from a permanent downhole gauge.

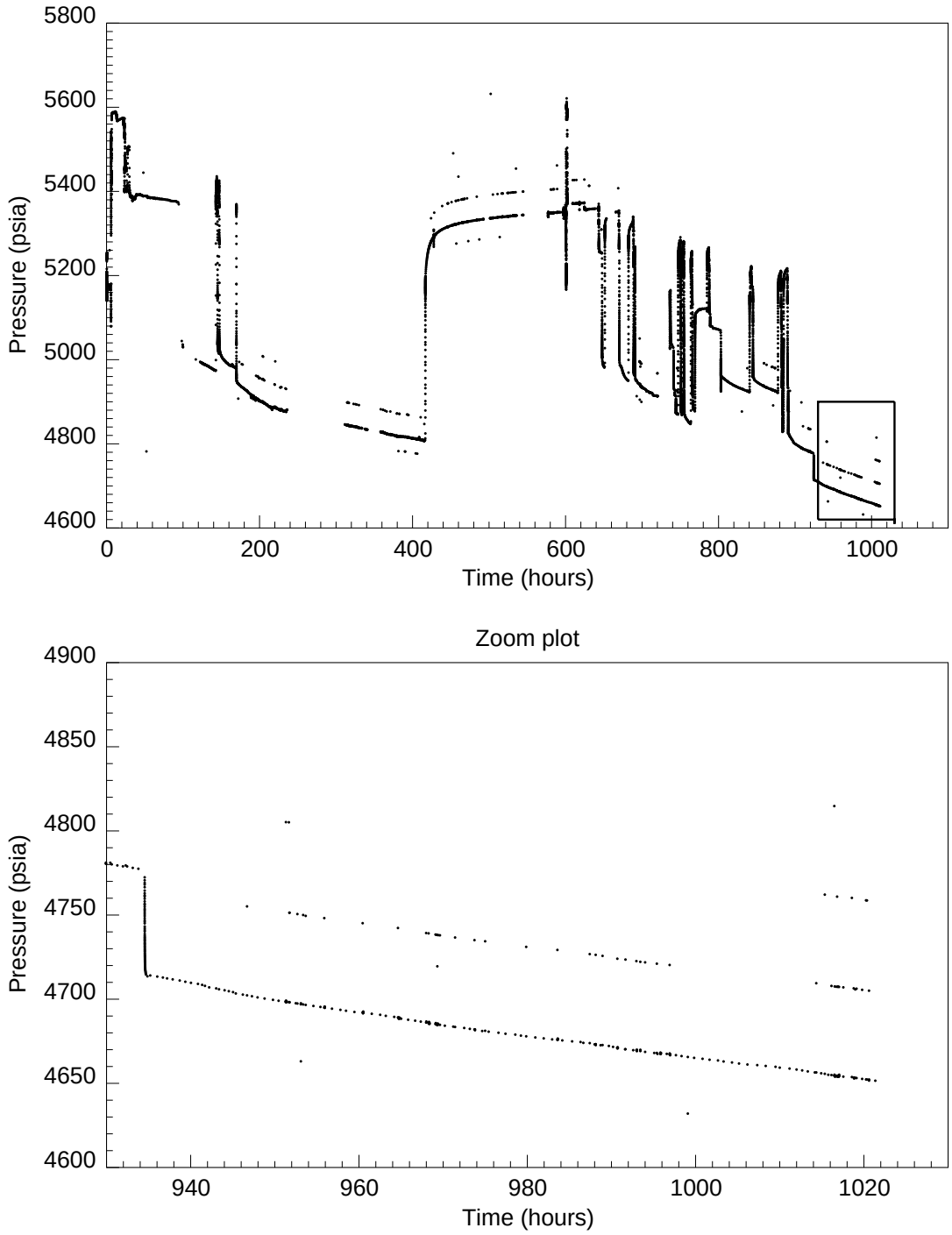

Figure 3.2: Outliers in pressure measurements collected from a permanent downhole gauge.

storage space when data are being handled. Human errors are also another source of uncertainty. Horne (1994b) also discussed sources of error associated with pressure measurement and the influence of the measurement error on the final result from well test interpretation.

The first step in data processing is to eliminate nonrepresentative data points, i.e., outliers, from the data set since they are the most obvious. Since an outlier lies away from the rest of the data, it causes discontinuities in the data stream creating two consecutive singularities. For example, an outlier that lies above the trend of the data departs from the data trend, creating the first singularity. The second singularity is a result of the sudden decrease from the outlier back to the trend of the signal. This behavior can be detected using a singularity detection framework utilizing wavelet analysis.

When implementing wavelet decomposition, the input data must be sampled uniformly. In many cases, the pressure data from permanent gauges are unevenly spaced. At first glance, it may seem desirable to interpolate between data points to obtain an evenly sampled set of data. However, interpolation from data that contain outliers may give a very bad approximation to the signal. For example, if the time gap between the point prior to the outlier and the outlier itself is several times larger than the average spacing, the interpolated points between the data point prior to the outlier and the outlier itself will establish a trend between the two points, thus, making it harder for the wavelet to see singularities in the data. The data that have been filled in might be misinterpreted as local trends in the signal instead of departures from the overall signal feature. Fig. 3.3 illustrates how data interpolation can create a microtrend from outliers embedded in a signal. Linear interpolation was applied to the data in this case. Spline or other types of interpolation would produce a similar result.

Another reason not to use interpolation when identifying outliers is simply because outliers are members of the original data not interpolated data. If interpolated data are used in the wavelet decomposition, the outliers determined by the singularity

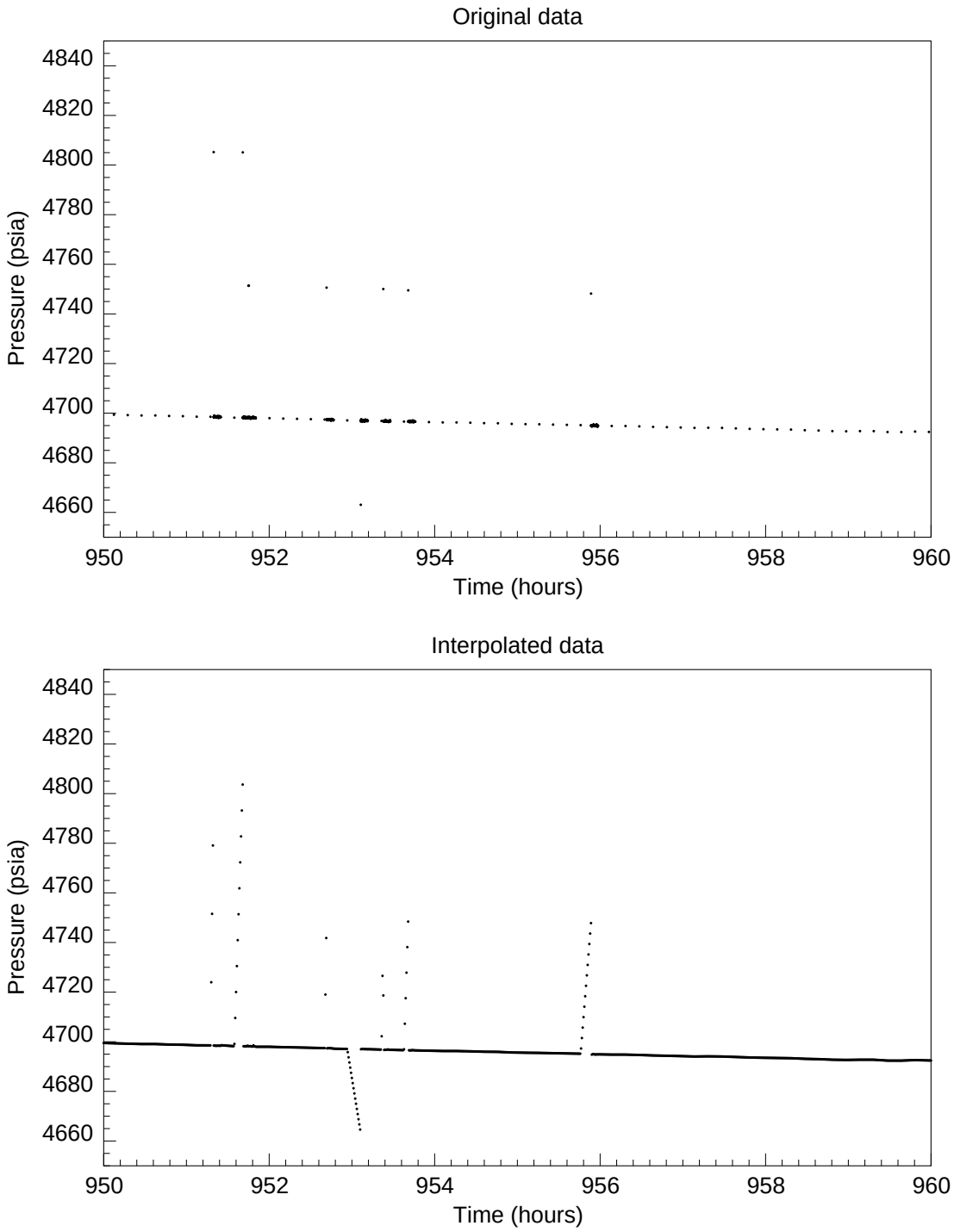

Figure 3.3: Interpolation of pressure measurements containing outliers.

detection algorithm are the interpolated points. Then, one will have to map them back to the original points to determine where the actual outliers are located. Mapping back to the original data may result in misidentifying the exact points.

For the reasons mentioned earlier, the data should be looked at as a sequence instead of as pressure versus time. The time scale should be replaced by the rank of the data collected. For example, the rank of the first data point is 1, and the rank of the second point is 2, and so on. In other words, we pretend that the spacings between data points are equal. Fig. 3.5 illustrates the new data representation using data rank for the original data from Fig. 3.4. The singularity characteristics of the outliers using rank representation are still preserved. For a uniform set of data, replacing the time scale by data rank does not change the appearance of the data as long as outliers are concerned.

Due to the nature of pressure transient data, the order of the data plays a very important role in the outlier analysis. In each transient, the magnitude of the pressure change at later times is generally lower than that of the pressure change at very early times since the response to a flow rate change becomes weaker later in the transient. A small departure of the data value from the trend at late times are easier to identify than a departure of the same magnitude at early time in which the pressure changes are large. Consequently, it is easier to identify outliers at late times than early times. The data then should be analyzed from the end back to the beginning in a reversed order. Fig. 3.6 plots the pressure data shown in Fig. 3.5 in a backward order. Results from both forward and backward algorithms are compared later in this section.

As mentioned previously, the wavelet decomposition breaks the signal down into detail and approximated signals with the detail signal representing the relative changes of the signal across scales. Therefore, abrupt changes in the signal can be identified by large magnitudes of the detail signal. When there exists an outlier, the detail signal will first change sharply in one direction, either increasing or decreasing, and then change again in the opposite direction. For example, if the outlier lies above the trend of the data, the detail signal should first increase and then decrease sharply.

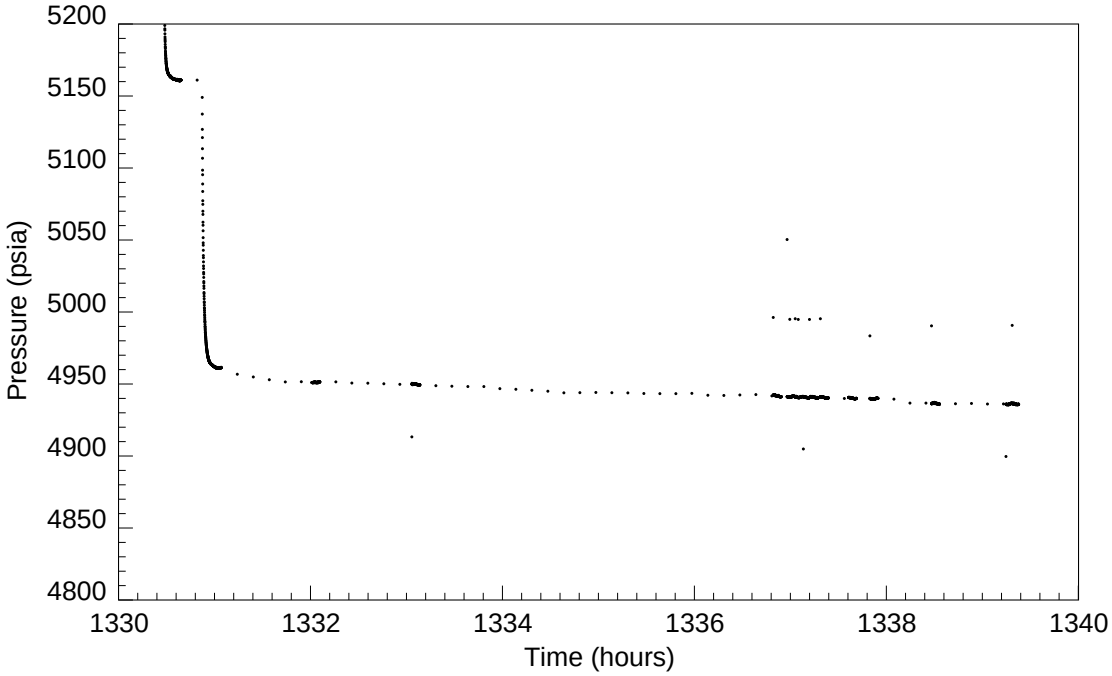

Figure 3.4: Pressure data with outliers plotted using time scale.

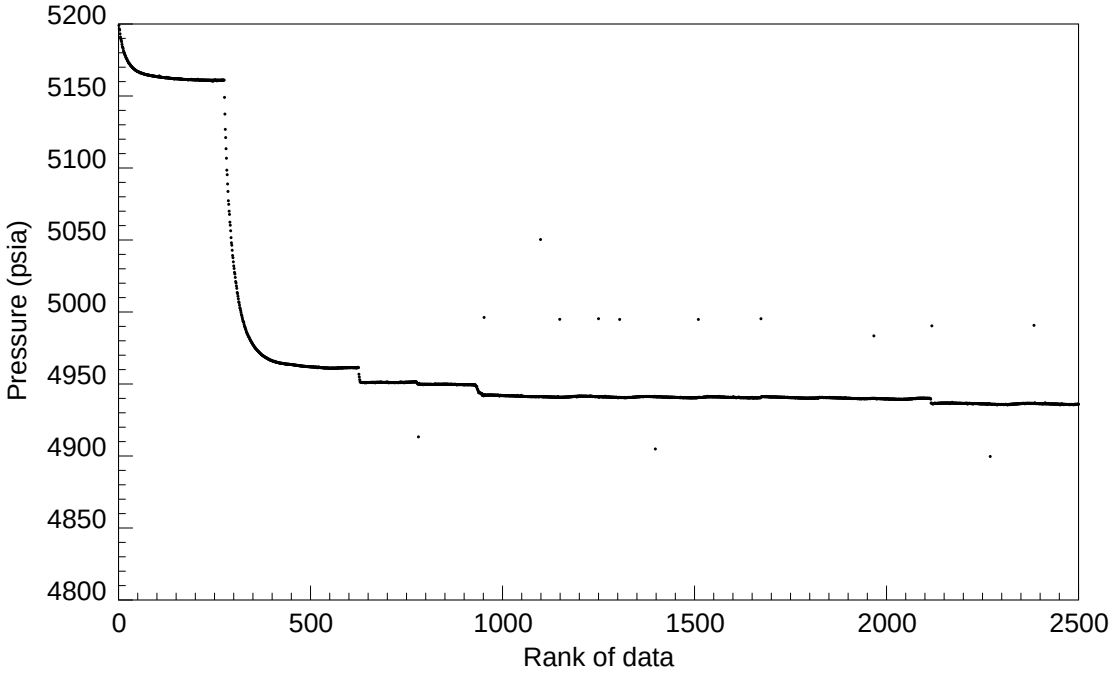

Figure 3.5: Pressure data with outliers plotted using rank of data.

Therefore, the singularities created by the outliers can be detected by screening for two large magnitudes of the detail signal with opposite signs. To illustrate the behavior of the detail signal when there are outliers in the data, the wavelet decomposition routine was applied to the data shown in Fig. 3.6. The detail signal at the first level of decomposition is shown in Fig. 3.7. As seen in the figure, the outliers can be easily identified by two consecutive peaks in opposite directions.

In order to determine which points are outliers, a threshold has to be set up for the magnitudes of detail signal. The rule of thumb in choosing a threshold is to ask oneself how far away a point lies from the general trend for that point to be considered an outlier. The magnitude of the threshold generally depends on the magnitude of changes in the pressure and/or accuracy of the measuring instruments. In general, 5 psi may be used as a threshold for outliers.

Certain parts of pressure data may be quite spurious with outliers of different magnitudes such as the data shown in Fig. 3.8. In general, it is more difficult to detect outliers from spurious data since the trend in the data is less prominent. To better see the trend in the data, the obvious outliers should be eliminated first, and the less obvious ones are eliminated iteratively. In such an implementation, the outliers whose magnitudes of the detail signal are higher than 20 psi should be removed first. Then, the threshold is reduced to 15 psi, 10 psi, and 5 psi, successively.

The iterative thresholding method was applied to actual field data. Figs. 3.8 - 3.11 show the outliers detected at threshold levels of 20 psi, 15 psi, 10 psi, and 5 psi, respectively. As seen in Fig. 3.11, the iterative method separates outliers from the data effectively. For comparison, another run was made using a single ultimate threshold of 5 psi without any iterations on the threshold. Fig. 3.12 shows the result from the noniterative method. Clearly, the iterative method outperforms the single thresholding method. In the iterative method, the outliers are gradually reduced from the most noticeable to the lesser ones.

In order to illustrate the importance of the order of data, the iterative thresholding

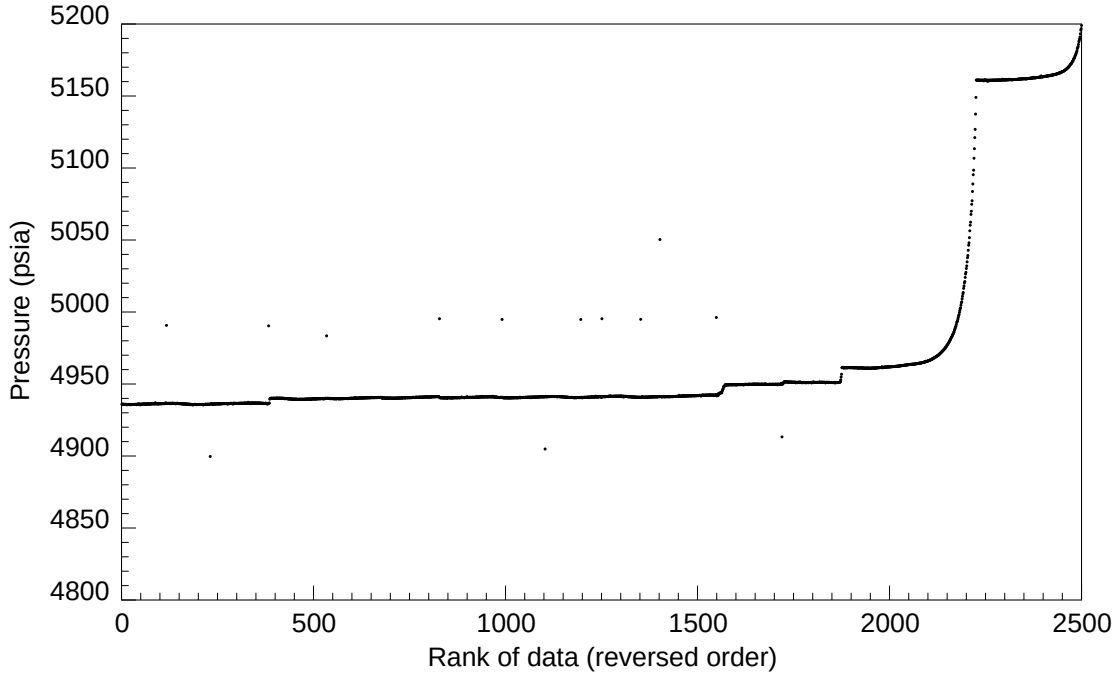

Figure 3.6: Pressure data with outliers plotted using rank of data in a reversed order.

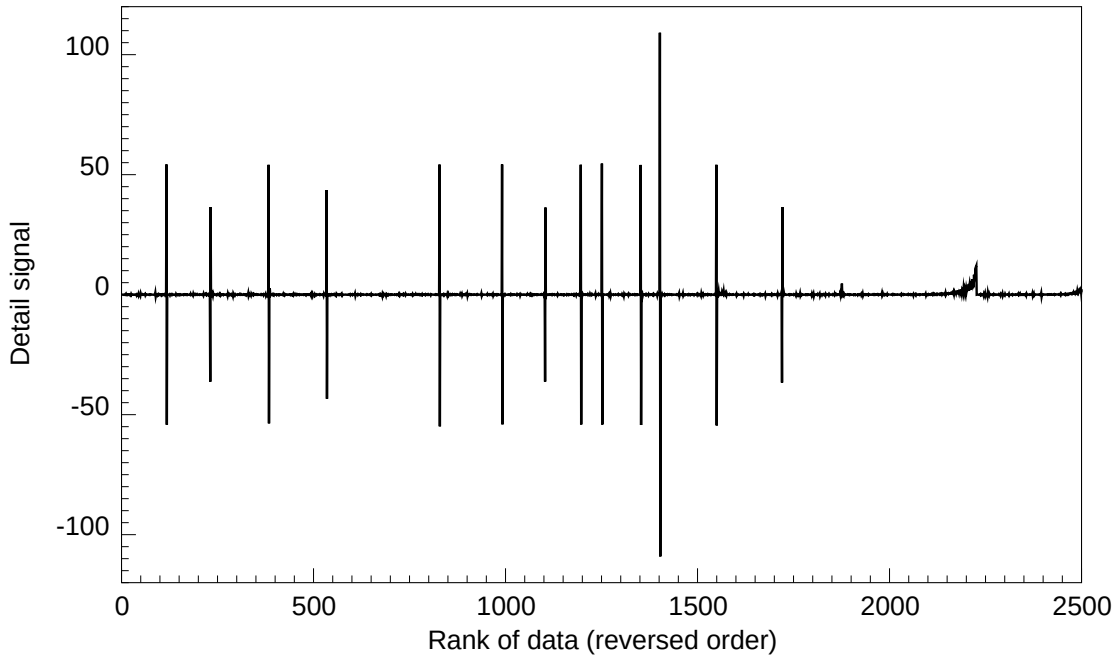

Figure 3.7: Detail signal from wavelet decomposition.

method was then applied to a data set with forward order. The final result is shown in Fig. 3.13. Comparing between Figs. 3.11 and 3.13, it is seen that reversing the order of the data helps improve the performance of the detection algorithm.

Another data set with a different outlier appearance was also used to test the robustness of the algorithm. This second set of data was collected at a much higher frequency than the first one. However, there are a few big gaps in the data due to problems in the acquisition system. The outliers in this case look more or less systematic. Generally, they lie above or below the data trend with a similar magnitude of departure. The iterative outlier removal algorithm was then implemented. Fig. 3.14 depicts the results of the outlier detection at the final iteration of 5 psi threshold. Again, the algorithm was successful in identifying outliers.

In summary, the detection algorithm developed using the wavelet decomposition framework performed well in identifying the outliers. This approach reduces considerably the tedious work that has to be carried out by humans especially when there is a tremendous amount of data to handle.

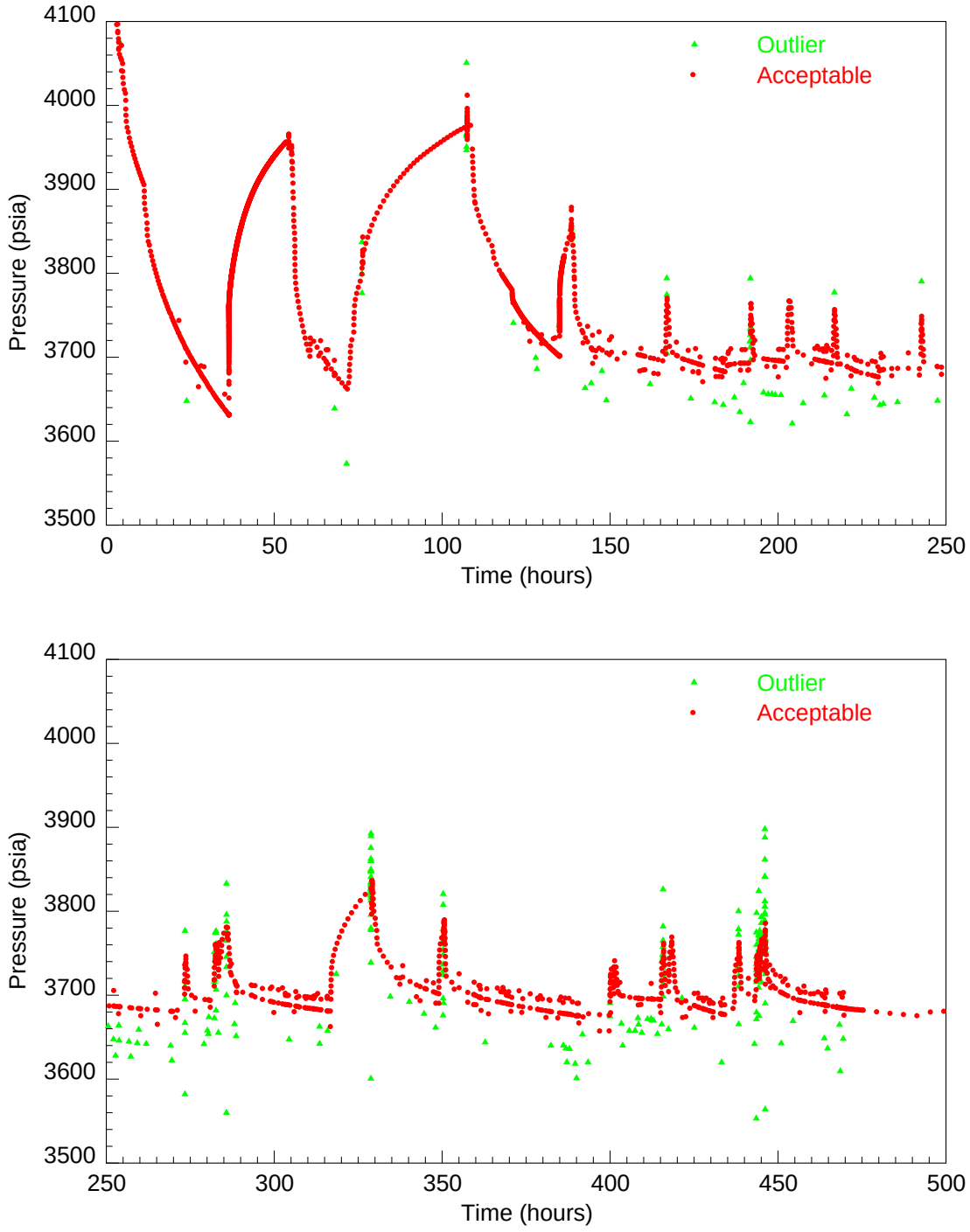

Figure 3.8: Iterative outlier detection at a threshold level of 20 psi.

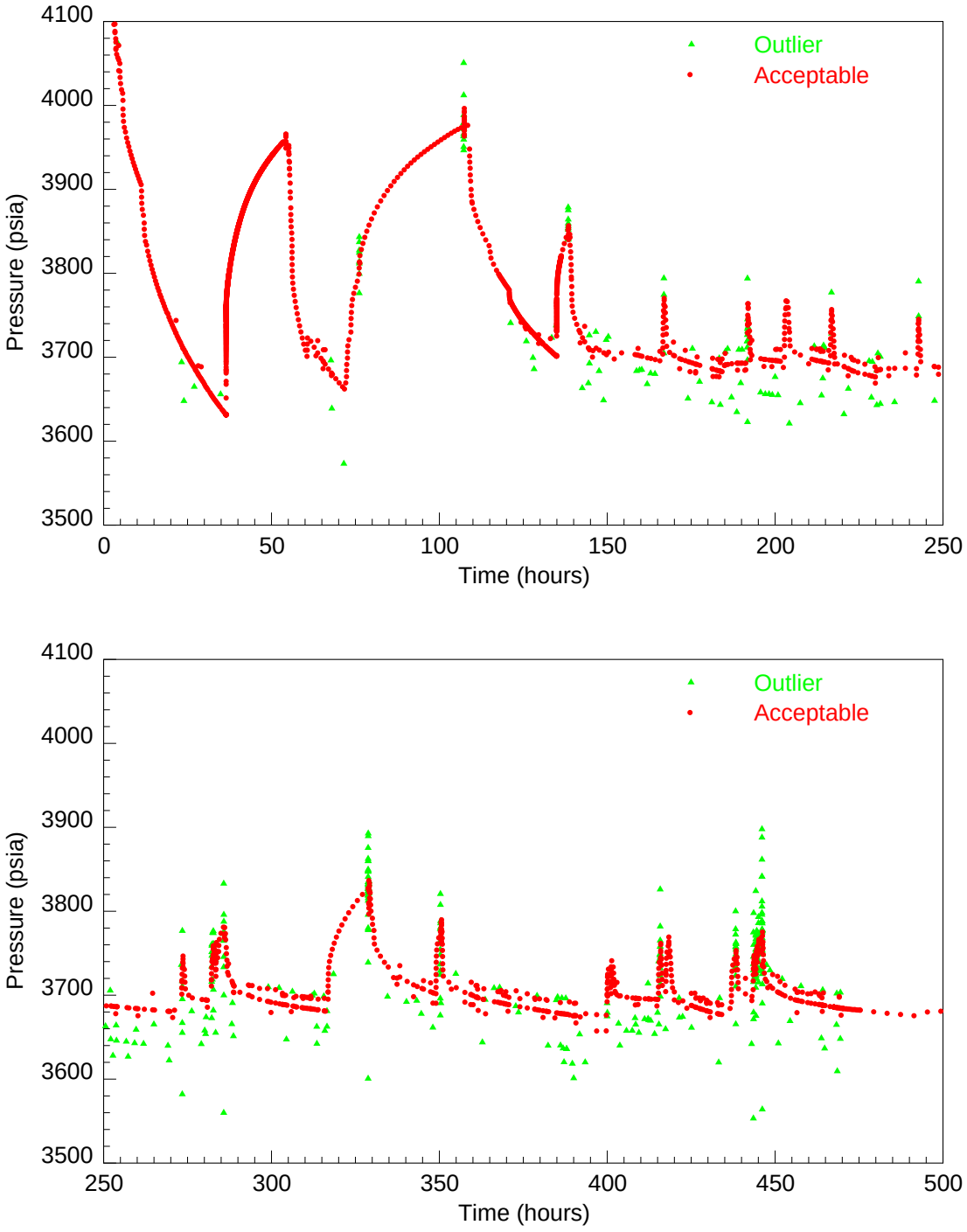

Figure 3.9: Iterative outlier detection at a threshold level of 15 psi.

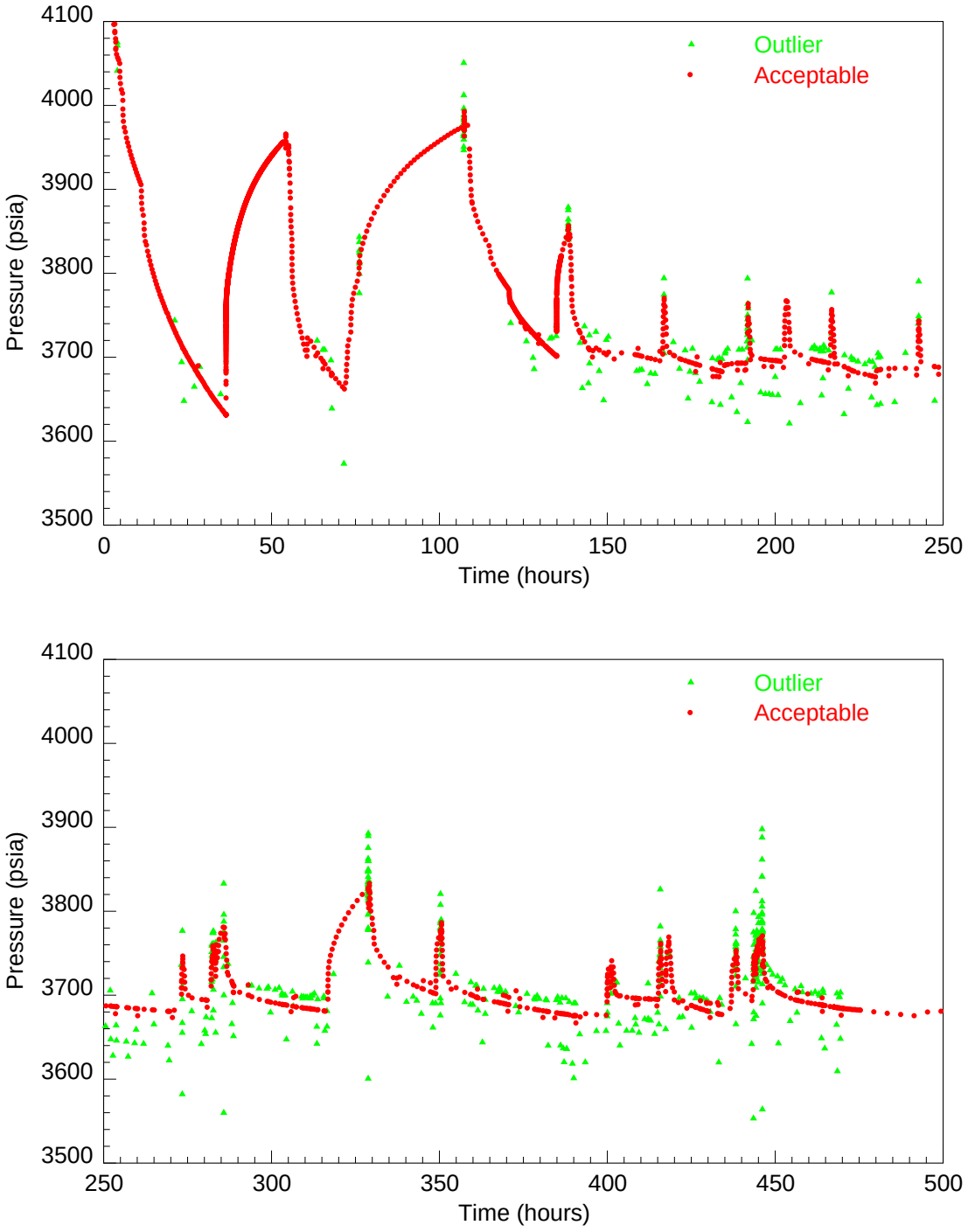

Figure 3.10: Iterative outlier detection at a threshold level of 10 psi.

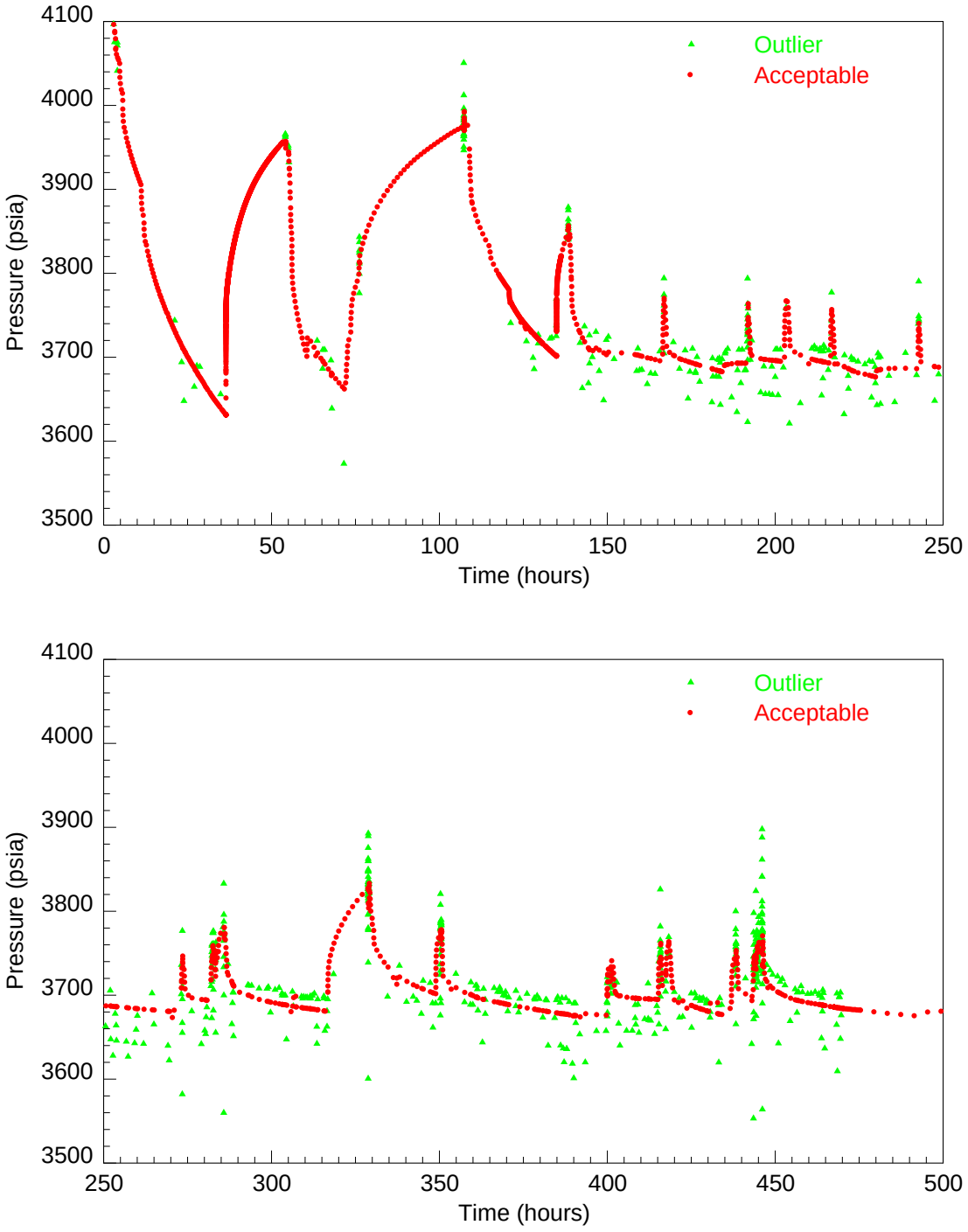

Figure 3.11: Iterative outlier detection at a threshold level of 5 psi.

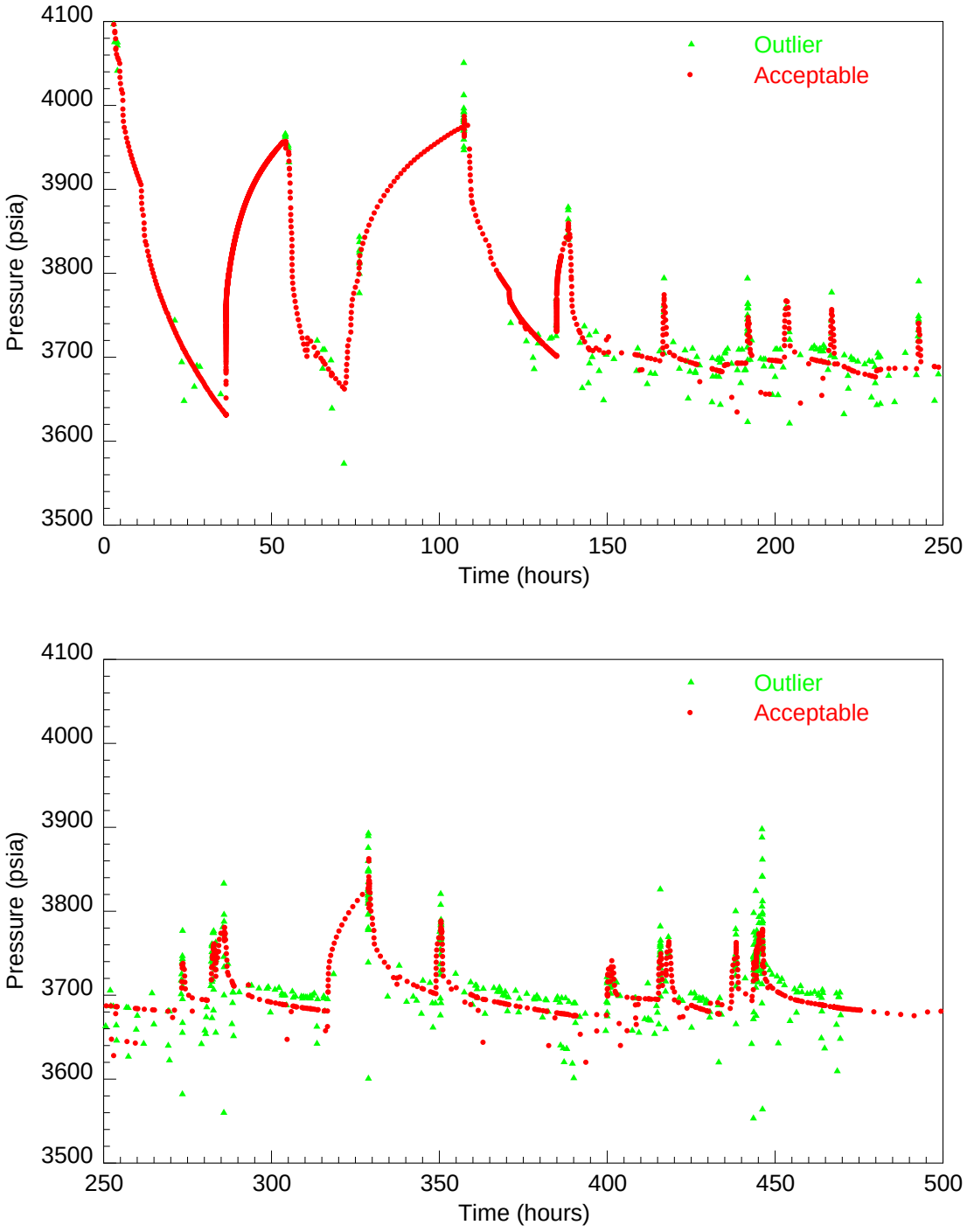

Figure 3.12: Noniterative outlier detection at a threshold level of 5 psi.

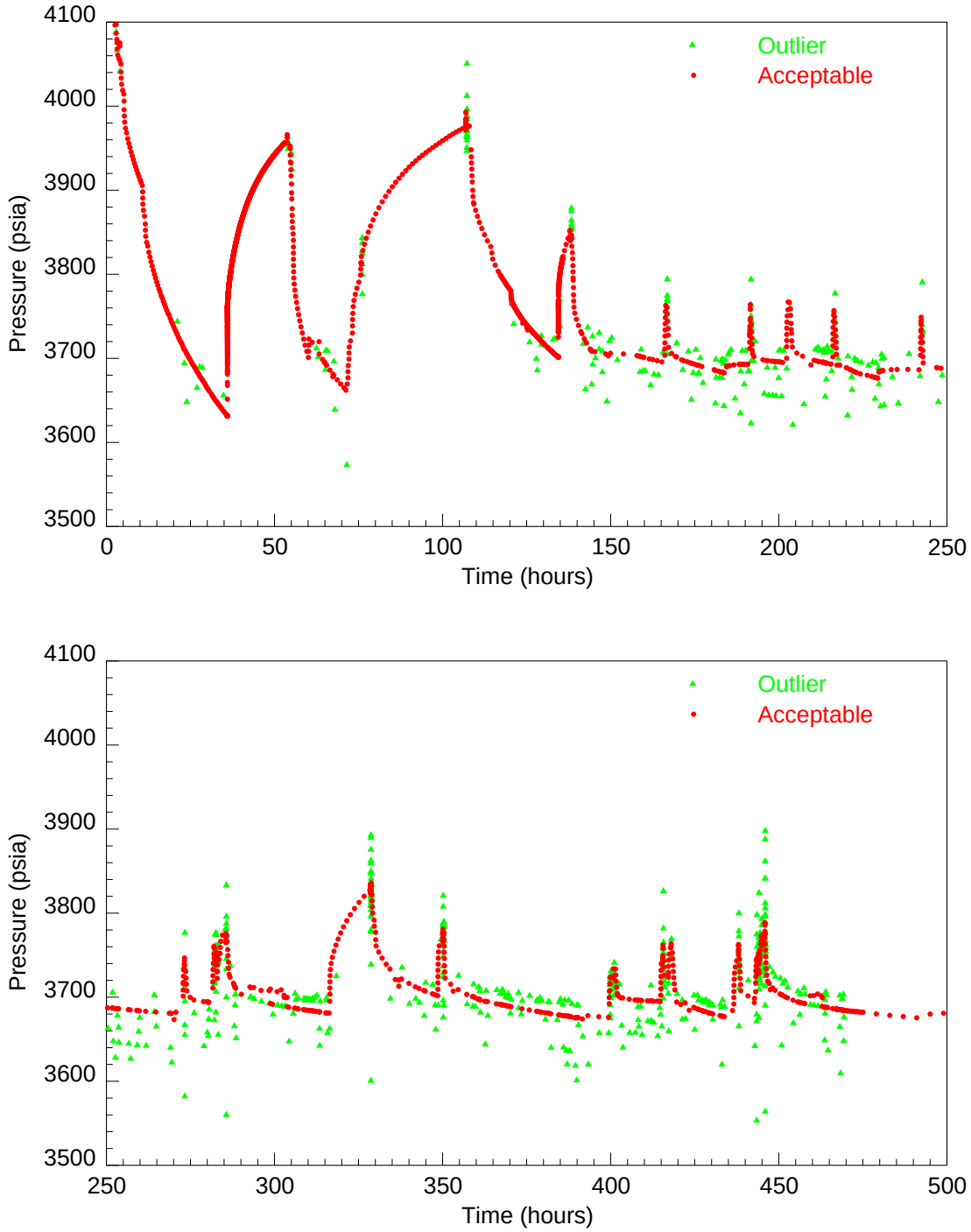

Figure 3.13: Iterative outlier detection at a threshold level of 5 psi using forward order.

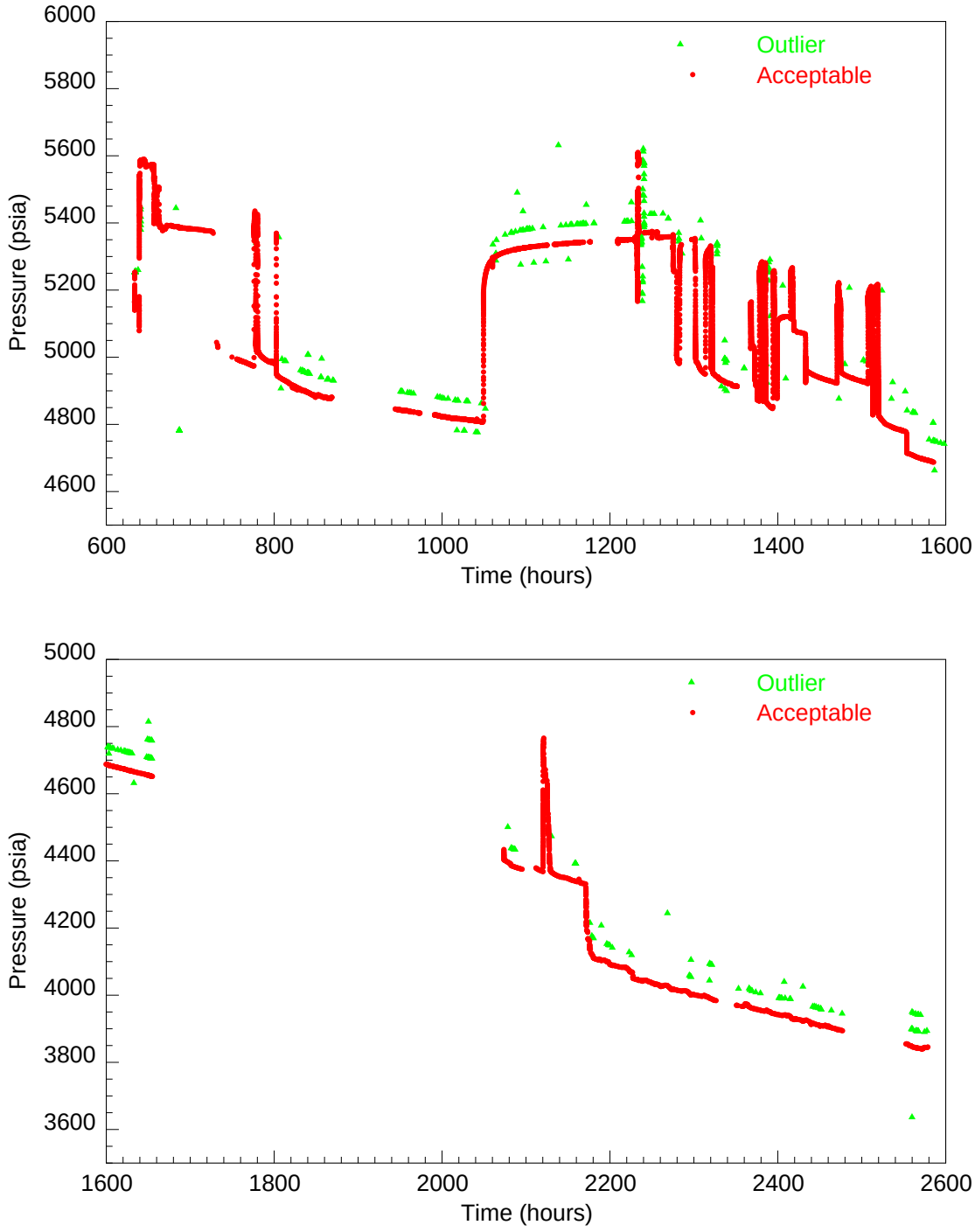

Figure 3.14: Iterative outlier detection for field data.

3.2 Denoising

In general, there is inherent noise associated with every type of measurements. Denoising is a procedure that is applied to the data to reduce the scattering and the fluctuations in data values in order to extract the most representative features from the data. When denoising is performed, the data are actually regressed in a nonparametric fashion. Let us assume that an unknown function $f(t)$ describes the behavior of a parameter of interest (such as pressure), and that $y_i = f(t_i) + \epsilon_i$ is the data measurement for the parameter, where ϵ_i is the noise associated with the data. The goal of any denoising method is to minimize the difference between the measurements y_i and the true function $f(t)$. When the function $f(t)$ is unknown, this minimization process is called a nonparametric regression.

If the function $f(t)$ is known, one can simply run a parametric regression on the data to estimate both the regression parameters and the representative features in the data. Theoretically, it is not essential nor desirable to denoise the data before running a parametric regression. One should let the regression process take care of the noise in the data by minimizing the difference between the model responses and the measurements themselves without making unnecessary data manipulation beforehand. For instance, data from typical pressure transient tests are not denoised before running a regression analysis. In general, denoising should be used when the function describing the phenomena of interest is unknown. In practice, denoising may be implemented in order to facilitate other data processing procedures such as transient identification and data reduction. Before analyzing pressure transient data, each transient which corresponds to a flow period has to be identified. The beginning of a new transient can be detected easily as a discontinuity in the pressure signal. If the data are very noisy, the noise itself may appear as a discontinuity especially at small scales causing misidentification of a new transient. The denoising procedure may be used for the sole purpose of finding better data representation by minimizing the difference between the measurements and the true signal, which is unknown at this stage. Denoising may also be used to determine representative points from a pool of noisy data when one wishes to reduce the size of the data. Sections 3.3

and 3.4 describe in detail how denoising can improve results obtained in transient identification and data reduction, respectively.

One of the most effective ways to denoise data without making prior assumptions about their behavior is the wavelet thresholding method. While most denoising methods tend to smear out sharp features in the data, the wavelet thresholding method generally preserves most of these features. Although the smearing may not be eliminated totally, the degree of smearing is reduced greatly when using the wavelet method. First, the original data signal is decomposed into detail and approximated signals. As mentioned previously, the detail signal represents the relative changes in the data across the transform scales. Therefore, noise which is small fluctuation in the data can be easily captured by fluctuations in the detail signals at low levels of decomposition. To reduce the noise level, one can simply reset the detail signals whose magnitudes are smaller than a certain threshold to zero and reconstruct the original signal using the smoother detail signals. This process is sometimes called *wavelet shrinkage* since the detail signals which are the wavelet coefficients are shrunk towards zero.

Donoho and Johnstone (1994) introduced the use of the hard thresholding method to screen for significant details in the detail signal. The criterion for this method is to replace the detail signal with zero whenever its magnitude is smaller than a preset threshold λ:

$$d_{j,k}^{hard} = \begin{cases} d_{j,k} & |d_{j,k}| > \lambda \\ 0 & otherwise \end{cases} \tag{3.1}$$

Also introduced by Donoho and Johnstone (1994), the soft thresholding criterion is similar to the one for hard thresholding. In addition to the replacement of the detail signal using the hard thresholding criterion, the magnitude of the rest of the detail signal is reduced by the threshold λ. The soft thresholding criterion can be described as follows:

$$d_{j,k}^{soft} = \begin{cases} d_{j,k} - \lambda & d_{j,k} > \lambda \\ d_{j,k} + \lambda & d_{j,k} < -\lambda \\ 0 & |d_{j,k}| \leq \lambda \end{cases} \tag{3.2}$$

Fig. 3.15 compares the hard and soft thresholding functions. The hard thresholding function is generally used in applications in which the data signal contains peak heights and discontinuities due to the sharpness of the hard thresholding function. However, this property may lead to occasional artifacts that roughen the appearance of the denoised signal (Donoho *et al.*, 1995). On the other hand, the soft thresholding function is recommended for use in applications in which smoothness of the estimates is sought since the soft thresholding function shrinks all the detail signals towards zero.

Proposed by Donoho and Johnstone (1994), a generic value called the *universal threshold* can be used as a threshold for most applications. It is computed as:

$$\lambda = \sigma\sqrt{2log(n)} \tag{3.3}$$

where n is the sample size, and σ is the noise level. The universal threshold λ can be used in both hard and soft thresholding methods. However, the authors reported that the universal threshold may not yield satisfactory results when the number of samples is small. Also, the universal threshold may not be suitable in certain applications (Donoho *et al.*, 1995).

In summary, there are three steps in the wavelet thresholding procedure:

1. Perform wavelet decomposition to obtain the detail and approximated signals.
2. Apply either hard or soft thresholding method to the detail signals to obtain new detail signals.
3. Reconstruct the data signal from the approximated and the new detail signals.

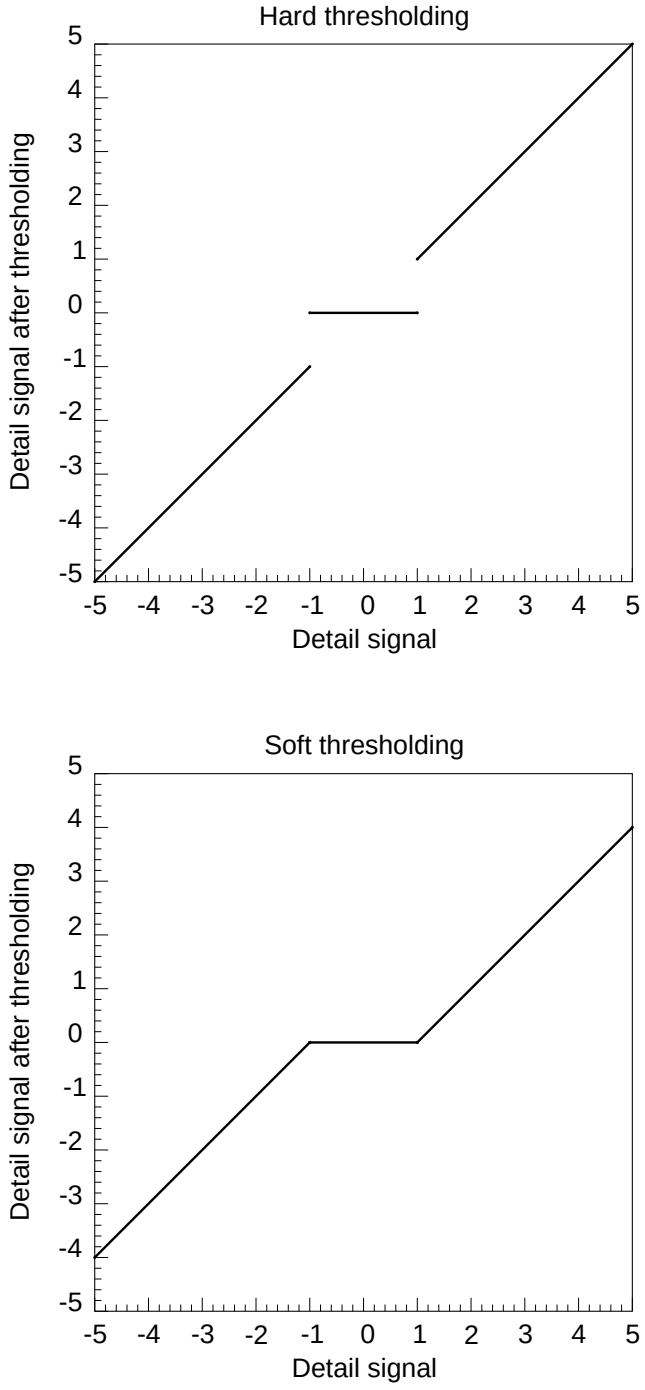

Figure 3.15: Hard and soft thresholding functions (threshold = 1).

To investigate the robustness of the hard and soft thresholding methods, a test function whose behavior follows a pressure transient response from a closed circular boundary reservoir is used. Ten thousand data points were generated evenly at 20-second interval. Normally distributed random noise with a noise level of 0.5 psi, $N(0, 0.5)$, were added to the data. Fig. 3.16 and 3.17 show the multilevel wavelet decomposition of the noisy data signal. At low levels of decomposition, the smaller-scaled information, which is the noisiness in the data, is displayed clearly in the detail signals. As the level of decomposition becomes higher, the degree of fluctuation in the detail signal becomes smaller while larger-scale information such as the increase and decrease of the pressure values at early times of a transient becomes more visible.

After decomposing the signal, the universal threshold was computed as 1.414 using Eq. 3.3. Both hard and soft thresholding methods were investigated in the first set of runs. Fig. 3.18 compares the denoised pressure signals using hard and soft thresholding methods, and Fig. 3.19 plots the differences between the original noise-free signal and the denoised signal for hard and soft thresholding methods. As seen Fig. 3.18 and Fig. 3.19, the soft thresholding method is a better smoother. However, the universal threshold is still inadequate to suppress the noise in both hard and soft thresholding methods. By looking at the detail signals at the low levels of decomposition in Fig. 3.16, one can see clearly that the magnitudes of the noise present in the detail signals for some data points are higher than the value of the universal threshold. As a result, the noise associated with these data points is not suppressed during the wavelet shrinkage process.

By observing the detail signal at the first level, a value of 2.5 was selected as a new threshold. The second set of runs was then performed using the new threshold to find a new set of estimates of the noisy signal. The results for both hard and soft thresholding methods are shown in Fig. 3.20, and the differences between the original noise-free signal and the estimates are shown in Fig. 3.21. The new estimates for both methods are considerably improved over those from the first set of runs. As depicted in Fig. 3.21, the hard thresholding method outperforms the soft thresholding method

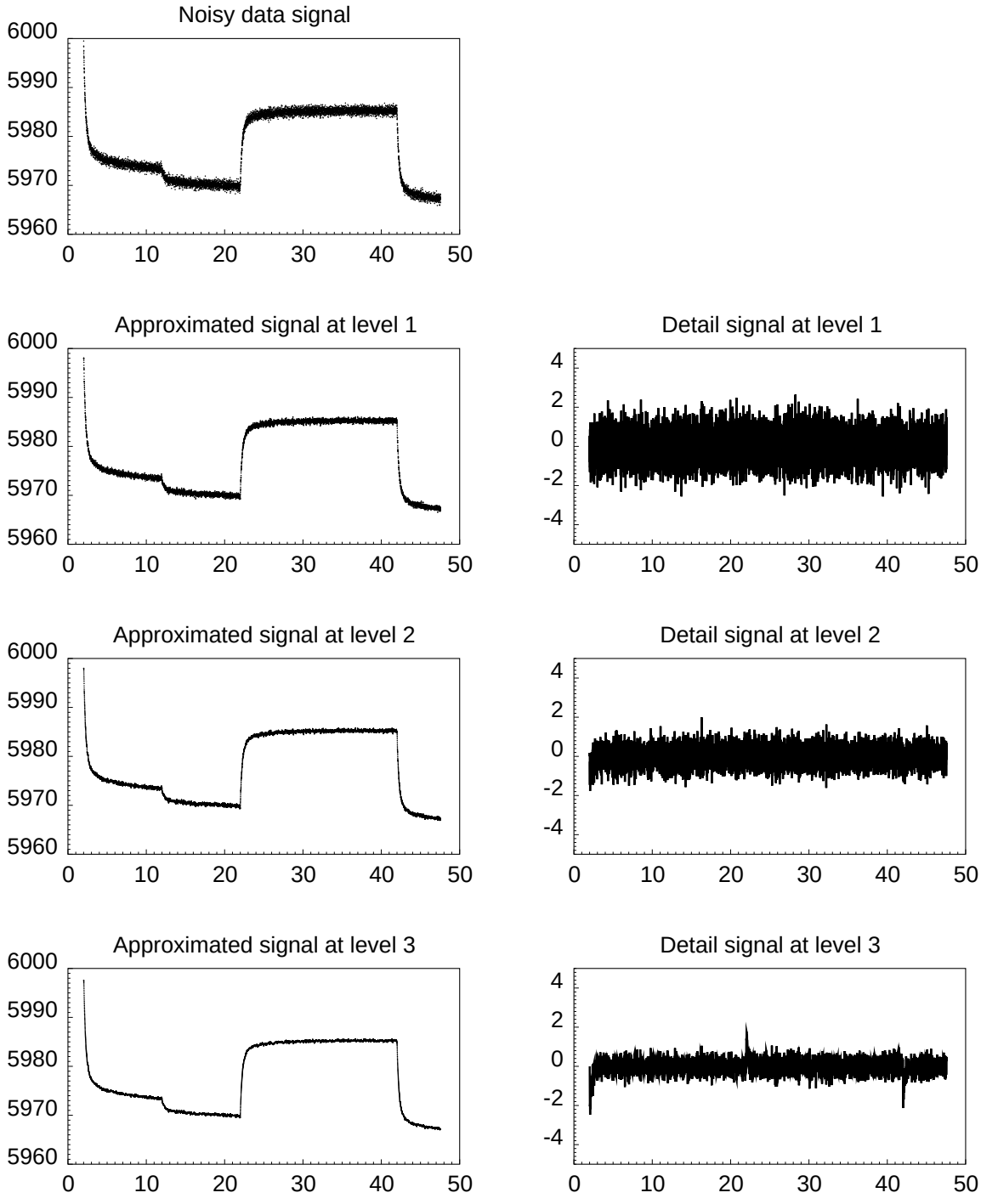

Figure 3.16: Wavelet decomposition of a noisy test function.

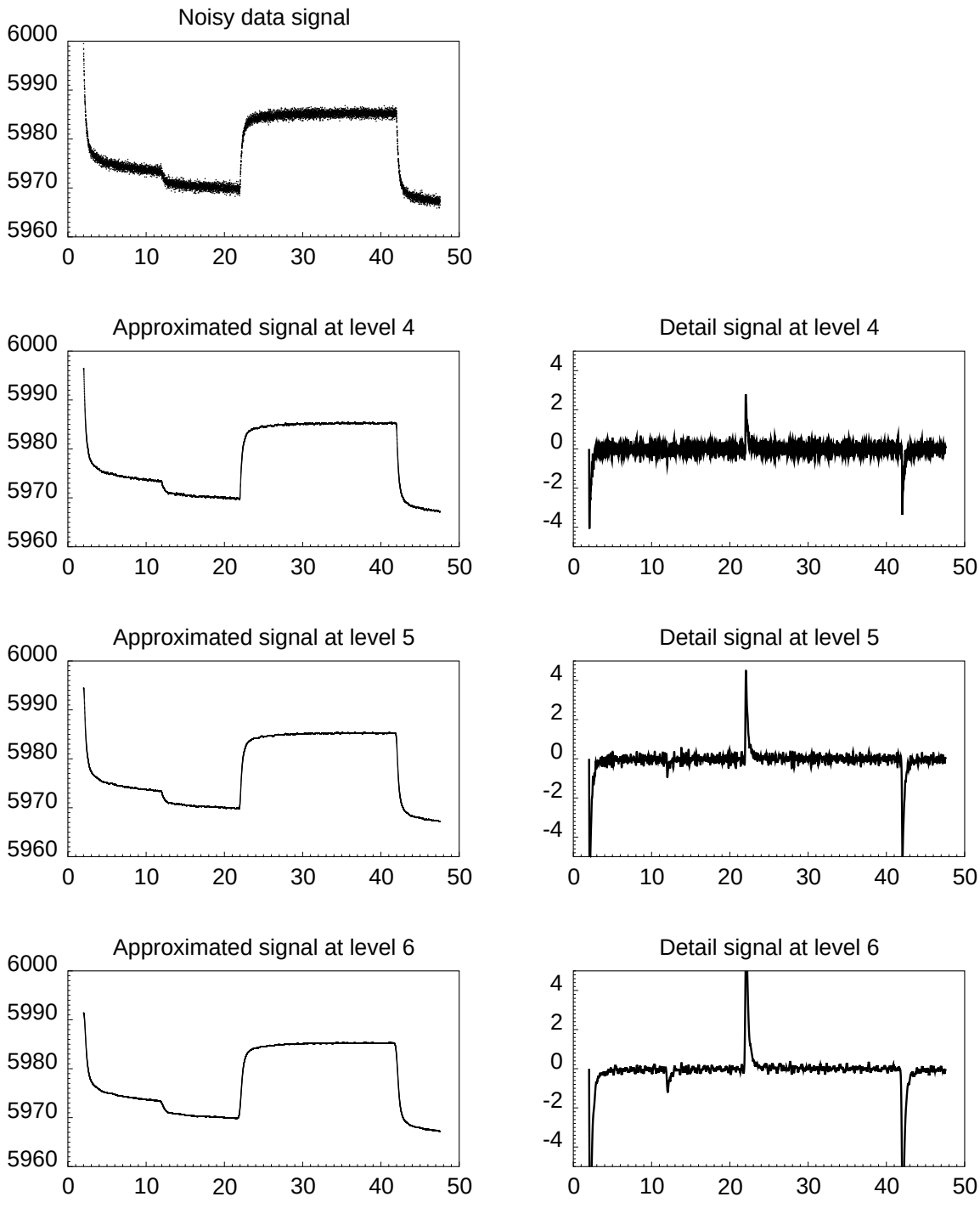

Figure 3.17: Wavelet decomposition of a noisy test function (continued).

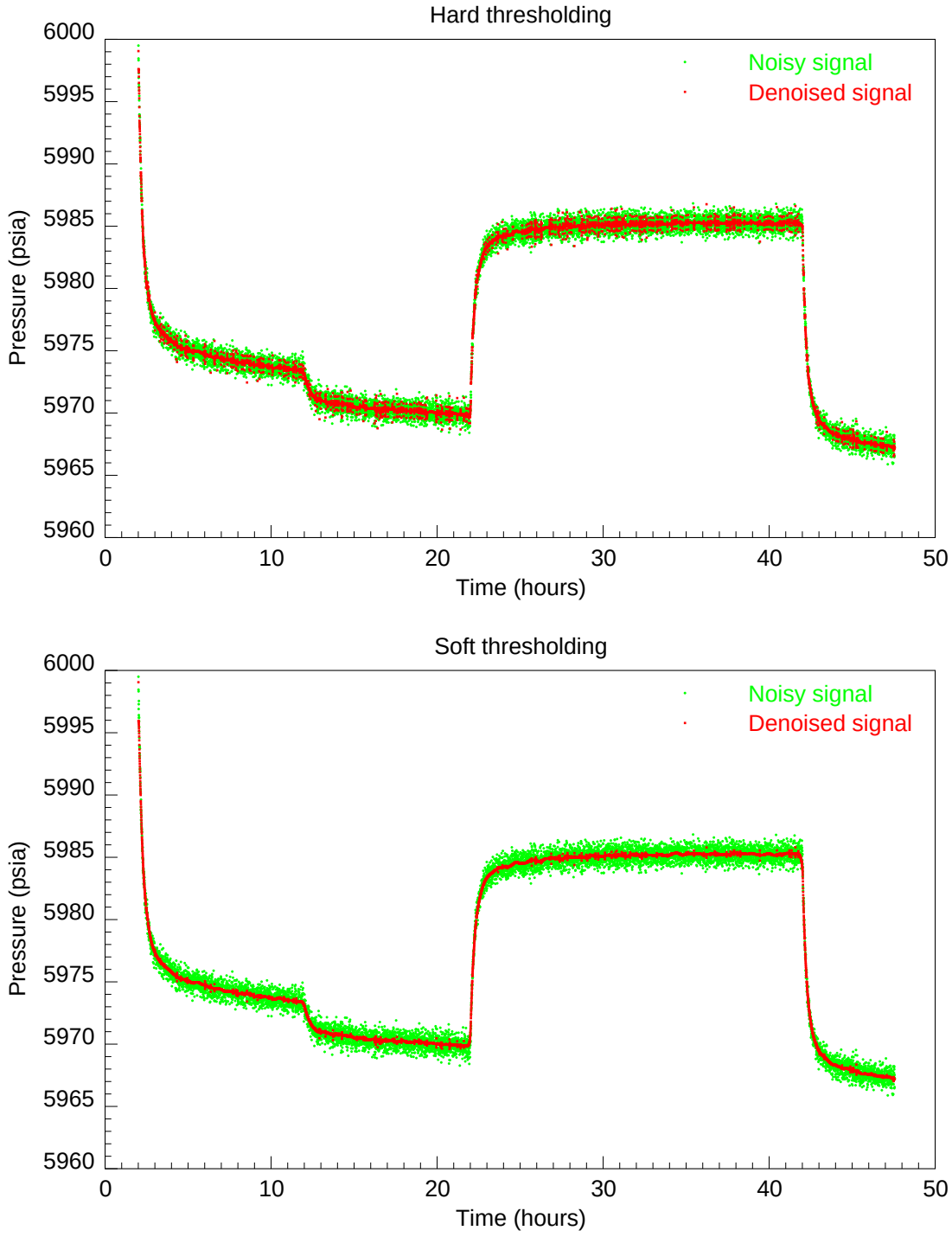

Figure 3.18: Data denoising using hard and soft thresholding methods (universal threshold).

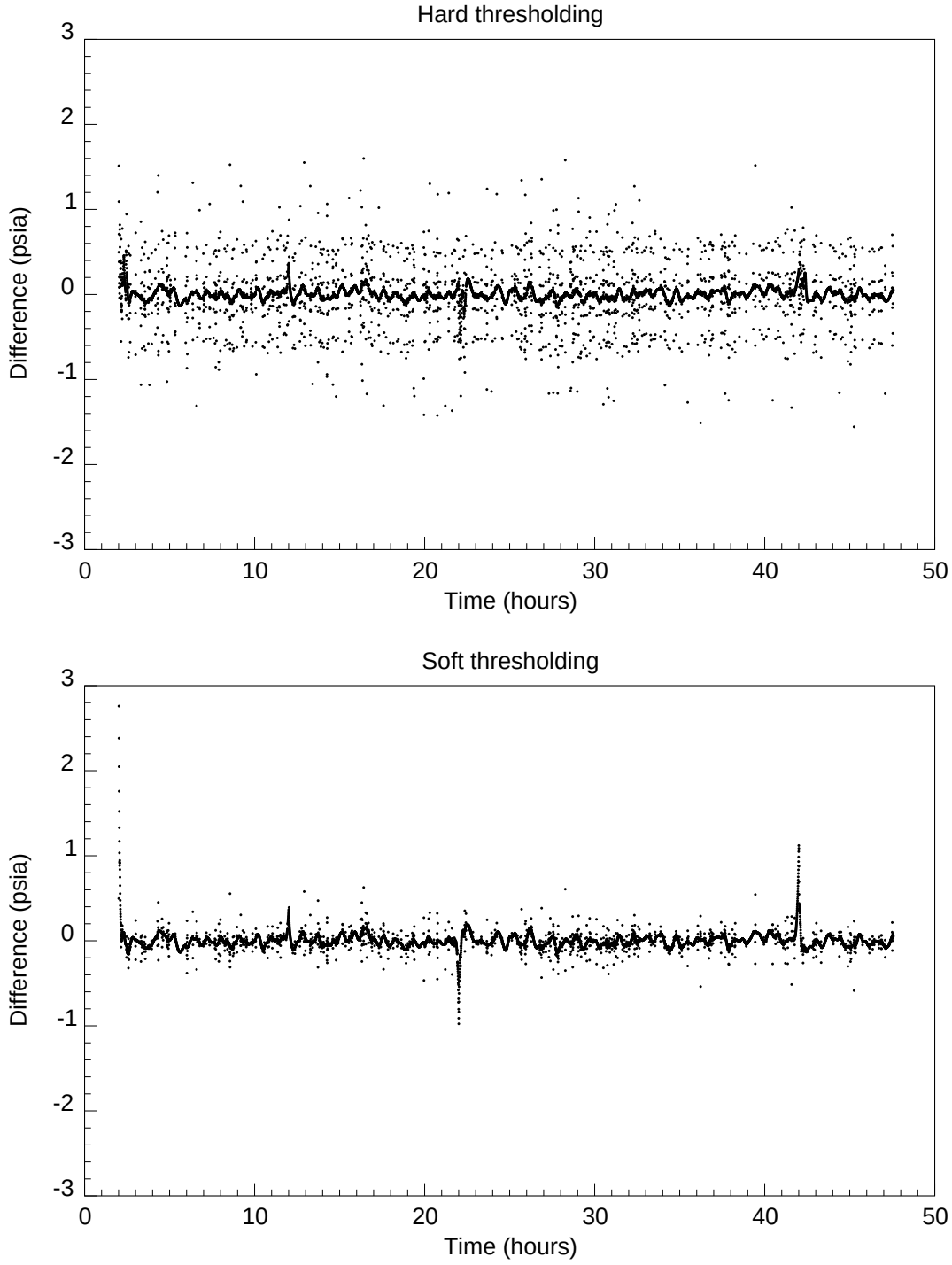

Figure 3.19: Difference between the denoised pressure and the test function for hard and soft thresholding methods (universal threshold).

around the vicinity of discontinuities in the signal. However, the hard thresholding method is still unable to suppress a few noisy points in the continuous regions of the data while the soft thresholding method can. Raising the threshold value in the hard thresholding is a possible alternative to suppress these few noisy points. But the drawback of using a high threshold value is that the sharp features in the signal are smeared off due to the high degree of suppression.

Recognizing the benefit of the hard thresholding method in preserving signal sharpness and the advantage of the soft thresholding method in smoothing noisy features, a hybrid criterion between two thresholding methods was developed. In the *hybrid* thresholding method, the soft thresholding criterion is used in the more or less continuous data regions, and the hard thresholding criterion is applied to the data located in the vicinities of the discontinuities. The locations of the discontinuities can found by checking whether the detail signals at higher levels of decomposition exceed the noise threshold (see Figs. 3.16 and 3.17). In general, it is sufficient to check only the level of decomposition in which the detail signal corresponding to feature changes exceeds the detail signal of the noise. In this work, level 5 was used. Mathematically, the hybrid thresholding criterion can be written as:

$$d_{j,k}^{hybrid} = \begin{cases} d_{j,k} & |d_{j,k}| > \lambda \;\; and \;\; |d_{l,k}| > \lambda \\ d_{j,k} - \lambda & d_{j,k} > \lambda \;\; and \;\; |d_{l,k}| < \lambda \\ d_{j,k} + \lambda & d_{j,k} < -\lambda \;\; and \;\; |d_{l,k}| < \lambda \\ 0 & |d_{j,k}| \leq \lambda \end{cases} \tag{3.4}$$

where l is the level of decomposition used to check sharp feature changes.

Results from implementing the hybrid criterion are shown in Figs. 3.22 and 3.23. As seen in the figures, the advantages of the hard and soft thresholding are combined in this method (see Figs. 3.20 and 3.21 for comparison). The noisy points left by the hard thresholding method now disappear, and at the same time the differences between the denoised pressure and the original noise-free signal around the vicinities of the discontinuities are minimal. The estimates in the early part of the data are

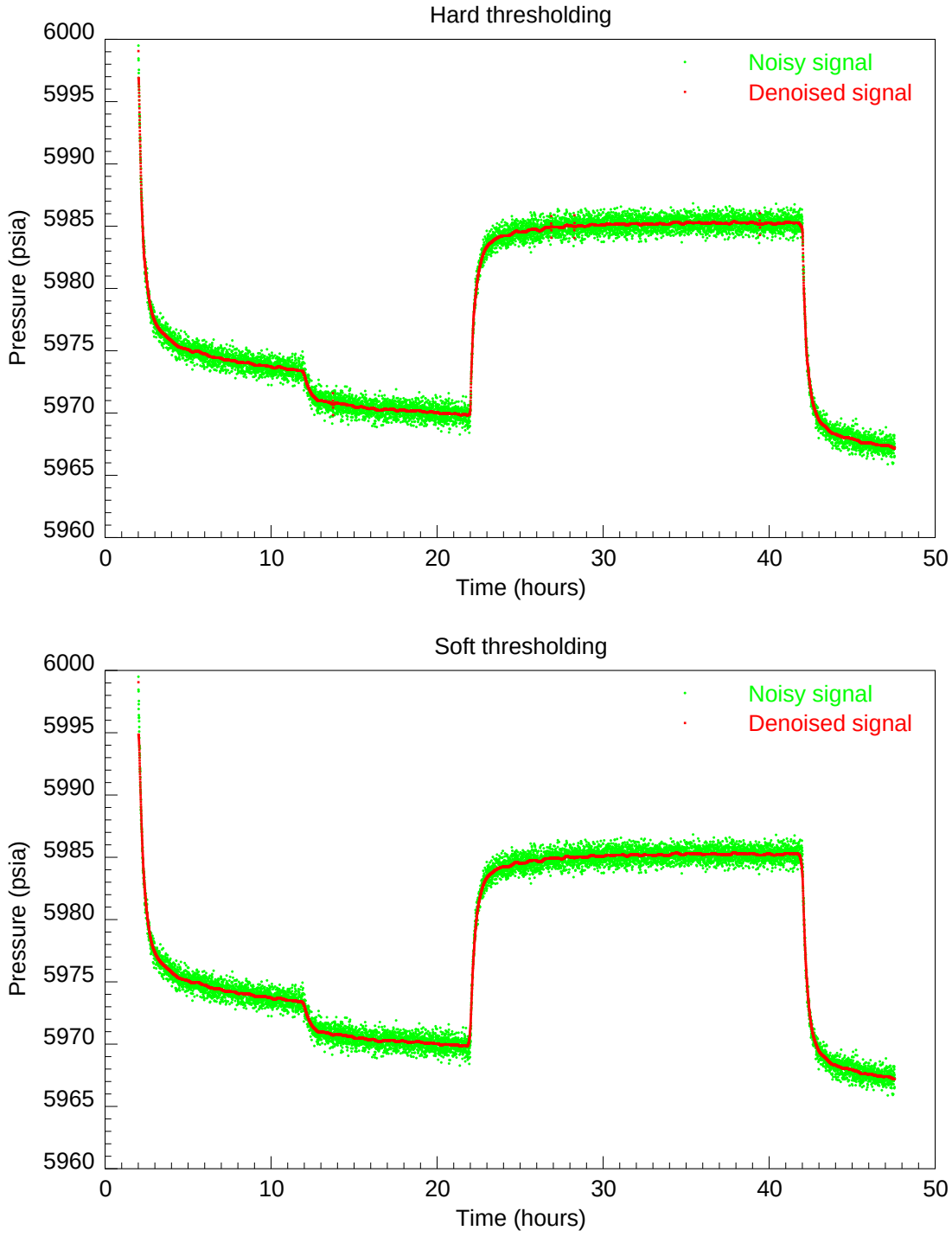

Figure 3.20: Data denoising using hard and soft thresholding methods (threshold = 2.5).

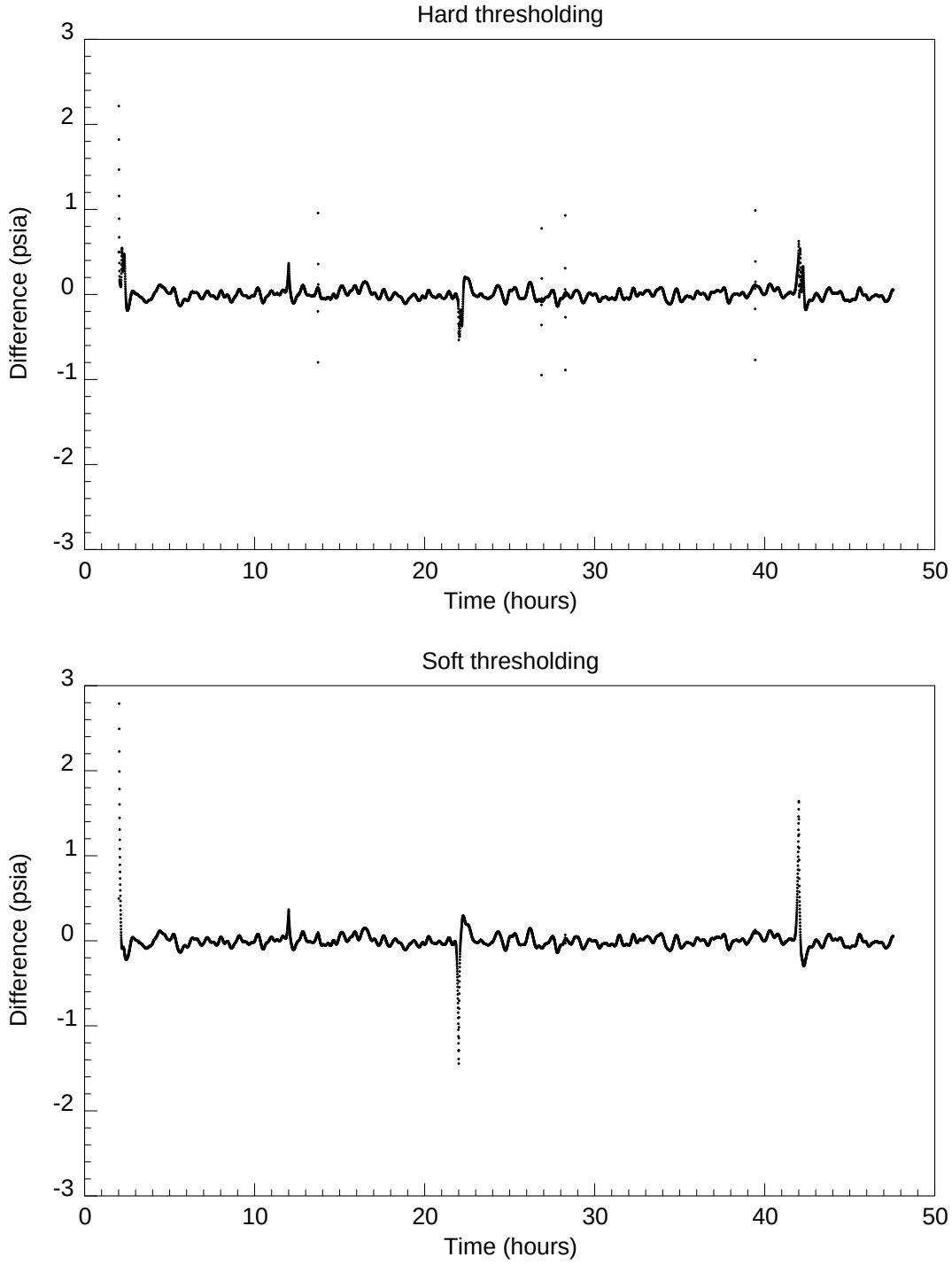

Figure 3.21: Difference between the denoised pressure and the test function for hard and soft thresholding methods (threshold = 2.5).

still poor but consistent with previous results from the hard thresholding method. The poor quality of these estimates is, in fact, simply a result of the end effect from the wavelet transform. By artificially introducing a few data points whose values are similar to that of the first data point, the end effect can be eliminated. Fig. 3.24 plots the difference between the denoised data and the original noise-free signal after the introduction of some artificial data points. The highest difference between the estimates and the original noise-free data is approximately at the noise level of 0.5 psi. To illustrate the effectiveness of the hybrid thresholding method, the difference between the noisy signal and the original noise-free signal is plotted in Fig. 3.25 for comparison.

In practice, the data may not be collected at a uniform interval while the wavelet decomposition requires the input to be uniformly spaced. To obtain an evenly sampled set of data, one may use a linear interpolation scheme to interpolate between data points. Other types of interpolation may not work as well as the linear interpolation method since they tend to smear out the regions where there are rapid changes. Besides this, the linear interpolation scheme is the easiest to implement.

The hybrid thresholding method was applied to actual field data which were collected at a general interval of 10 seconds. Several samples were recorded at higher intervals creating nonuniformity in the sample spacing. Fig. 3.26 displays the noisy pressure data acquired with a downhole permanent pressure gauge. The linear interpolation scheme was used to interpolate between data points to obtain data at 10-second spacing. The hybrid thresholding method was then implemented to the uniformly sampled data using a threshold value of 1.5. Figs. 3.27 and 3.28 displayed the estimates from the denoising process in close-up views. The denoising process is successful in suppressing the noise while the data features are still preserved.

In summary, the newly developed hybrid thresholding method overcomes the difficulties associated with the hard and soft thresholding methods in smoothing noisy signals and being able to preserve sharp features at the same time. The applications of data denoising in assisting other data processing procedures are illustrated in the

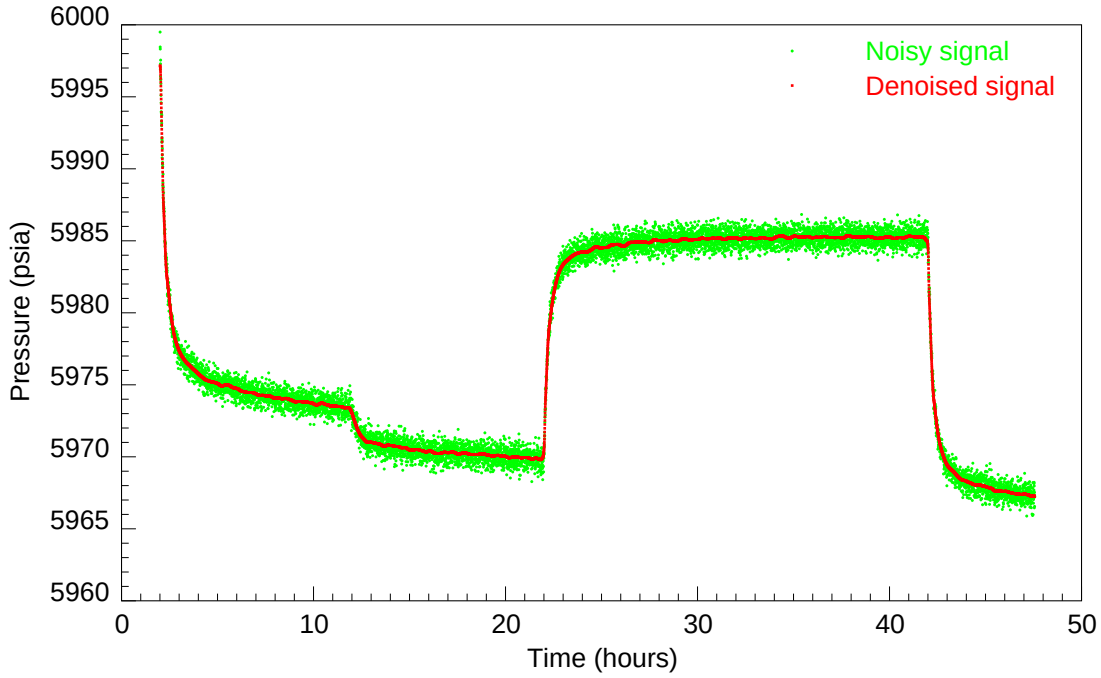

Figure 3.22: Data denoising using the hybrid thresholding method (threshold = 2.5).

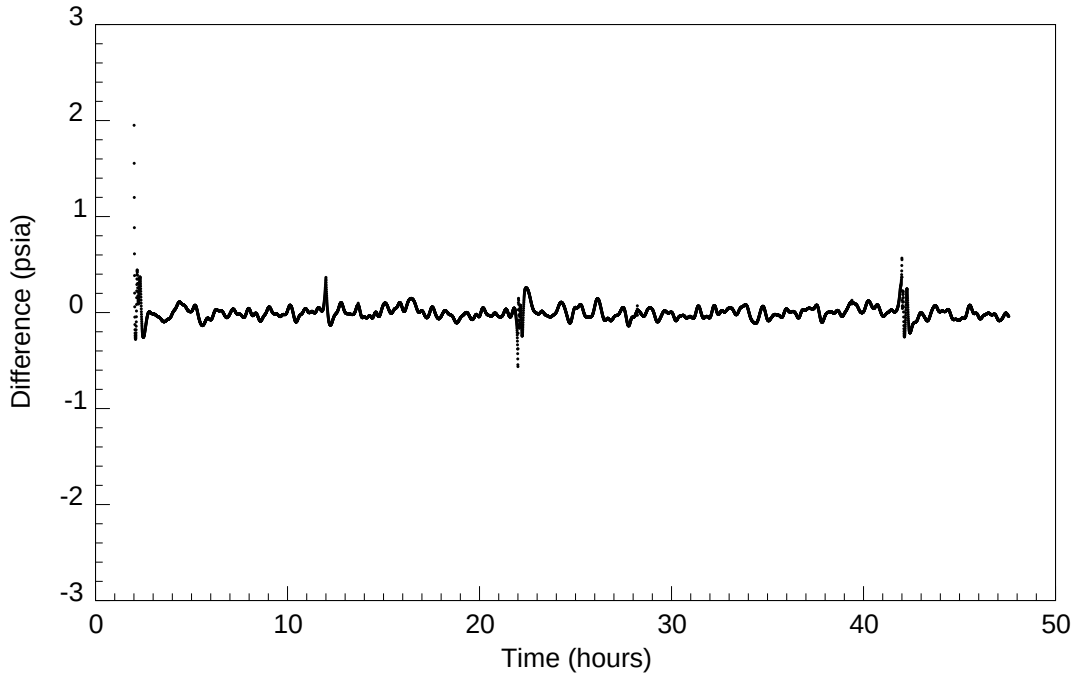

Figure 3.23: Difference between the denoised pressure and the test function for the hybrid thresholding method (threshold = 2.5).

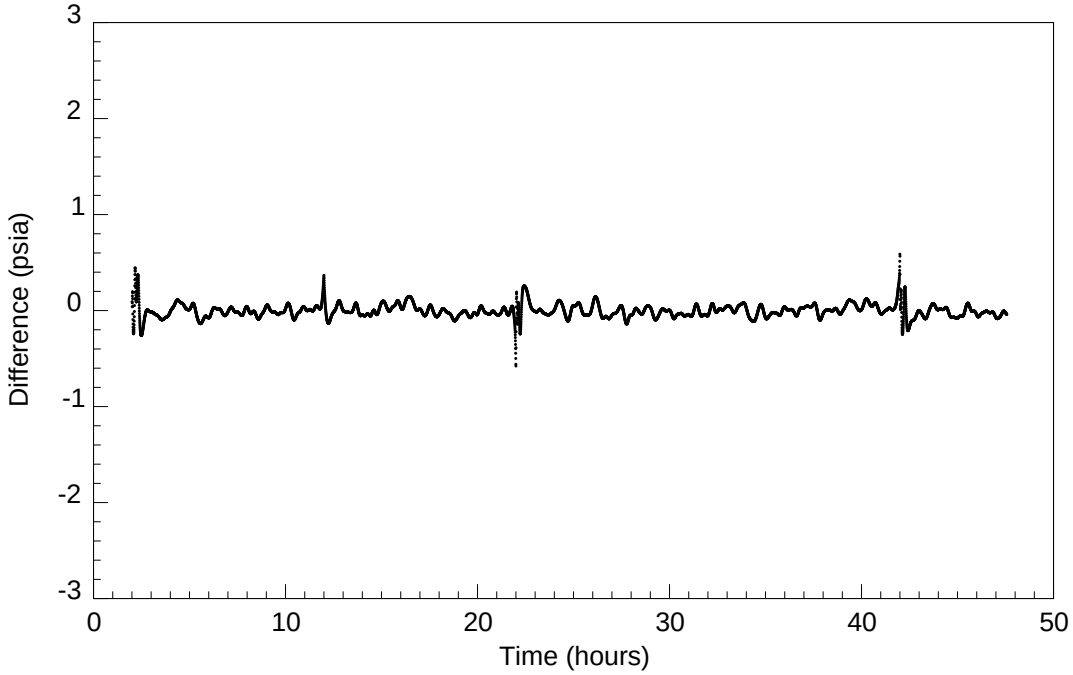

Figure 3.24: Difference between the denoised pressure and the test function for the hybrid thresholding method with no end effect (threshold = 2.5).

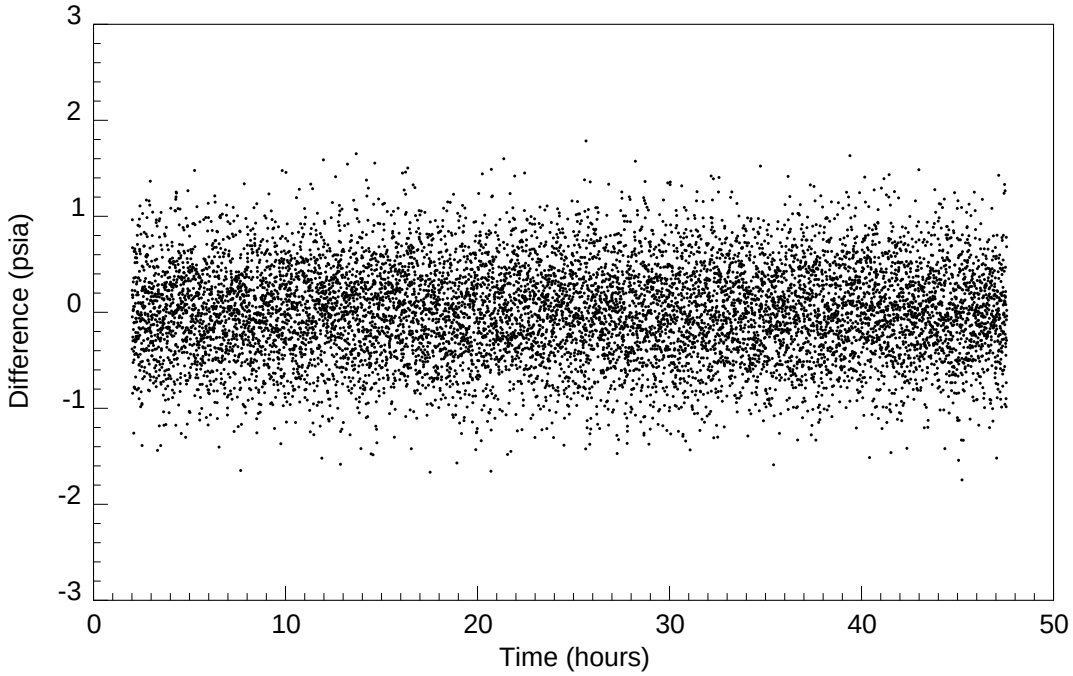

Figure 3.25: Difference between the noisy pressure and the test function.

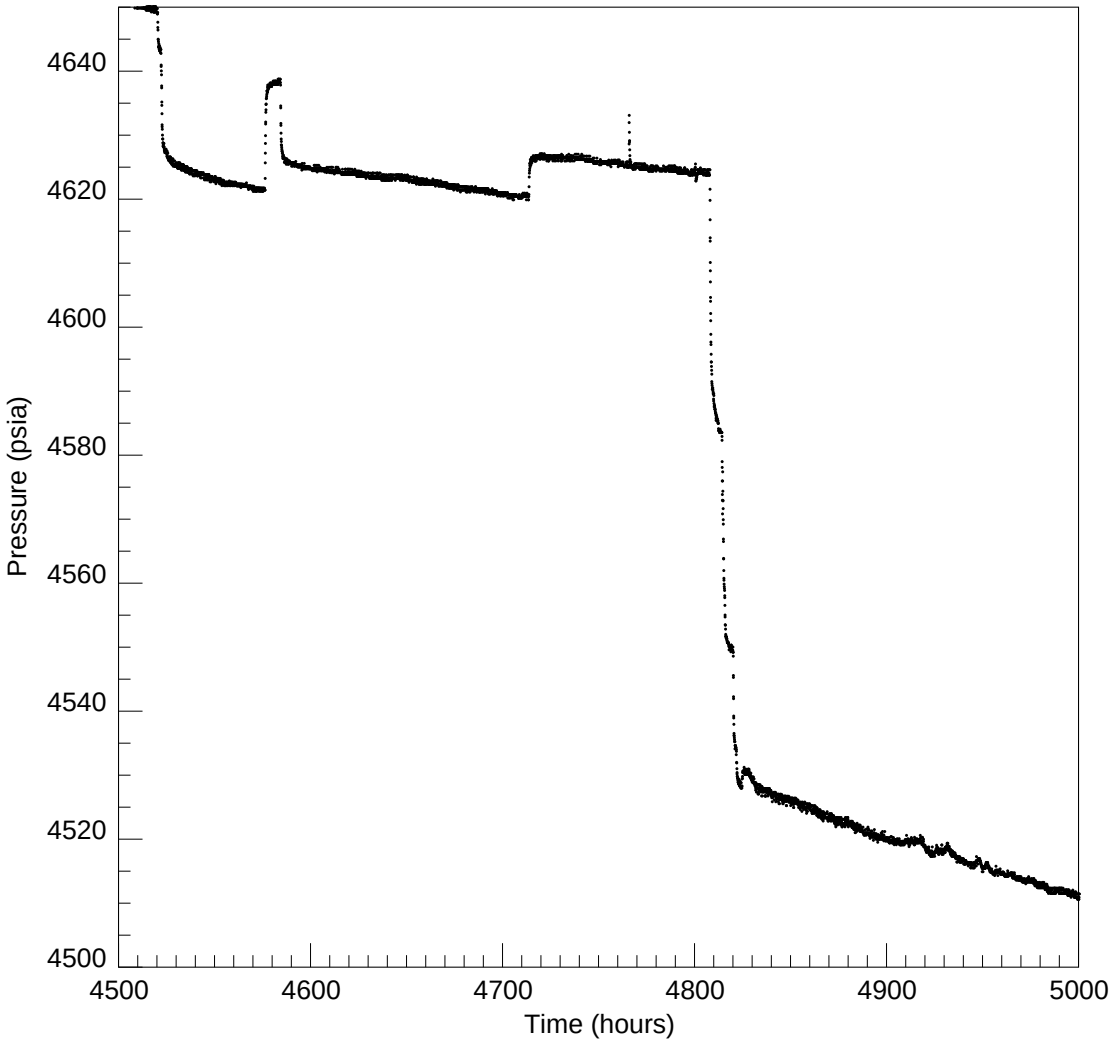

Figure 3.26: Pressure data acquired with a permanent downhole pressure gauge.

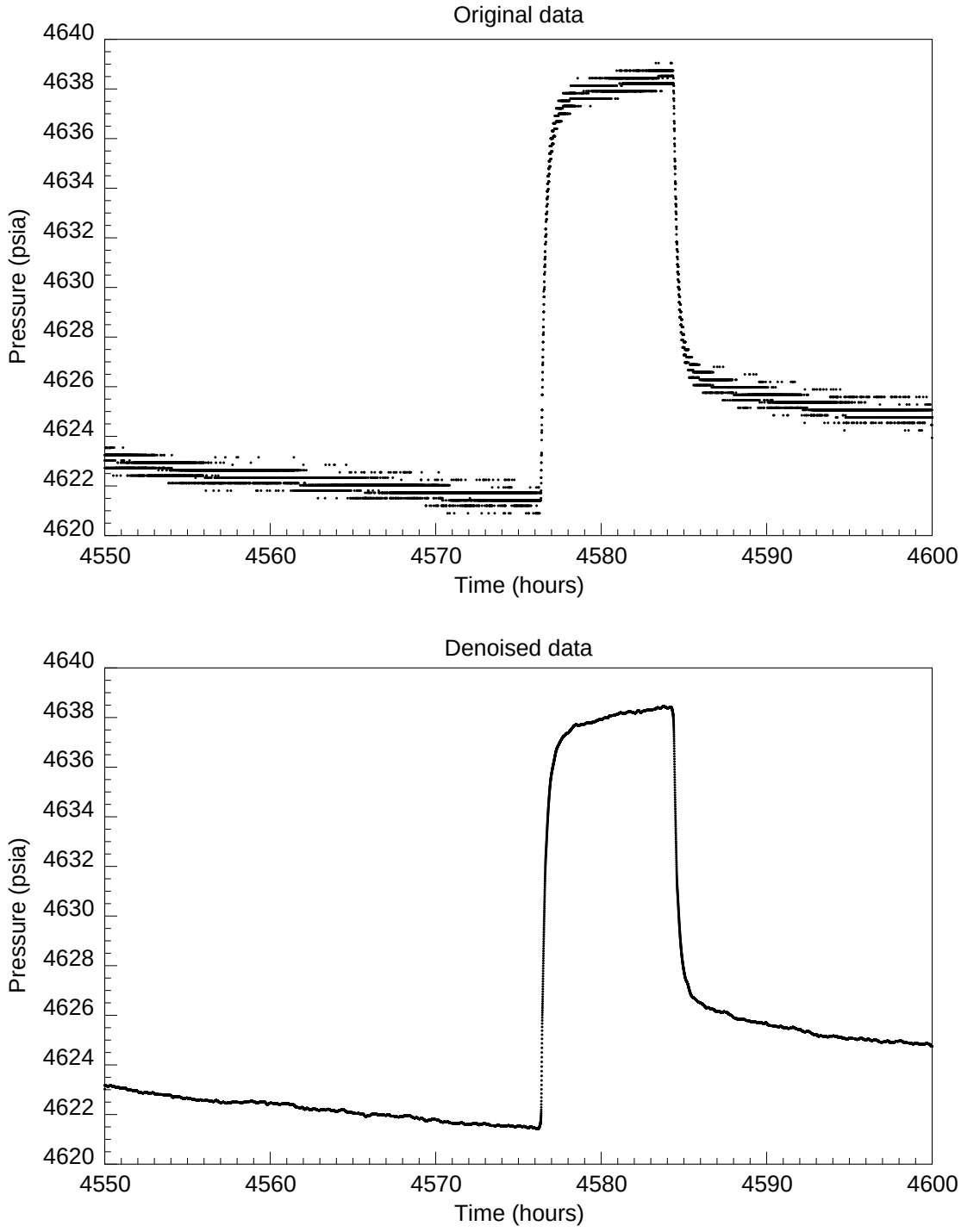

Figure 3.27: Data denoising using hybrid thresholding method (zoom plot).

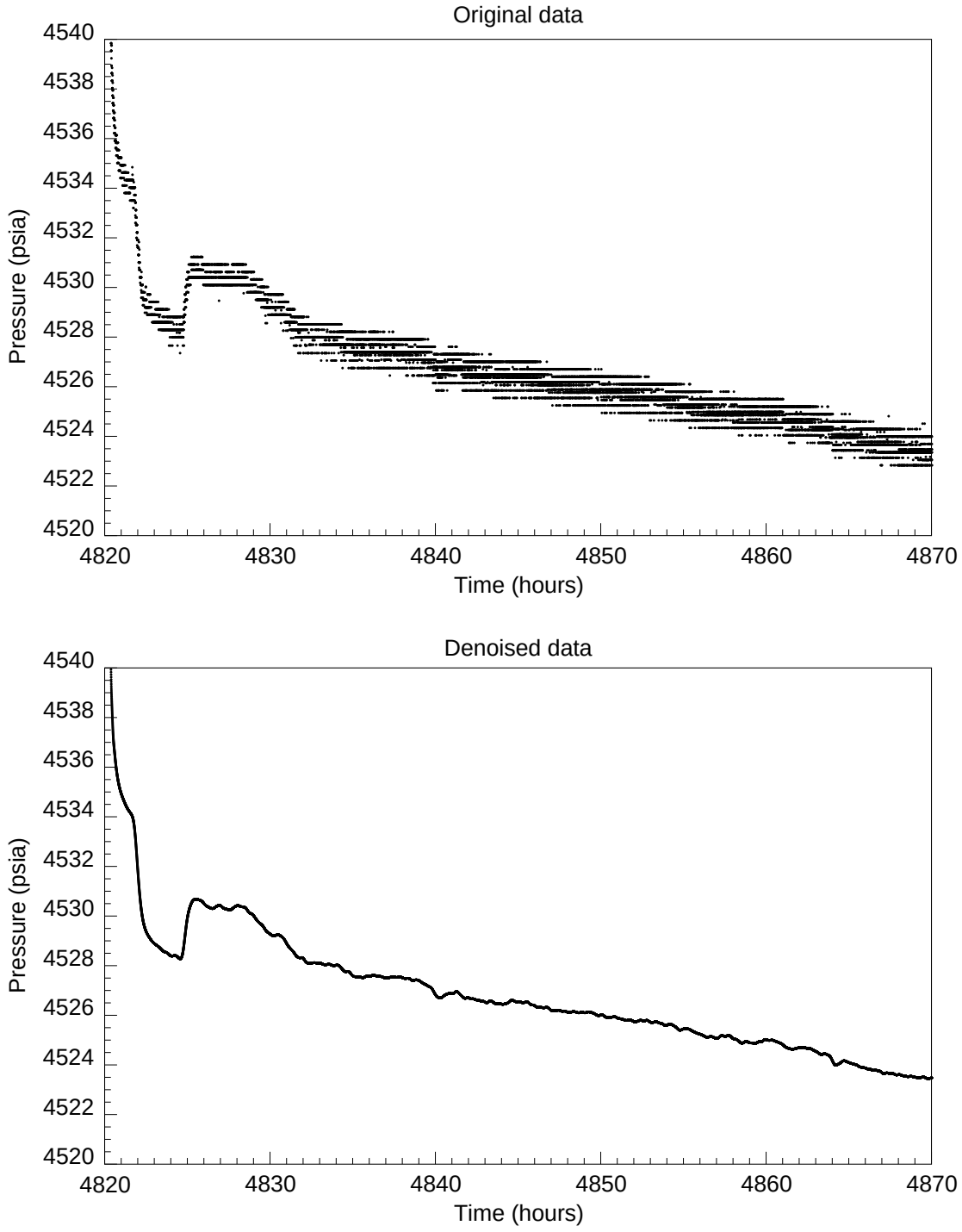

Figure 3.28: Data denoising using hybrid thresholding method (zoom plot).

next two sections. In any case, the denoising procedure should only be applied to data that are collected at high frequencies. Denoising low frequency data tends to have a smearing effect on the appearance of the data.

3.3 Transient Identification

In most cases, a complete record of times at which the well flow rate changes may not be available. Sometimes, the recorded information may contain large uncertainties due to measurement errors and other reasons. Fortunately, the times at which the flow rate changes can be determined by identifying the sudden changes in the pressure data, which can be viewed as singularities in the data. Therefore, the wavelet modulus maxima which indicate the neighborhoods of singularities can be used to determine the times at which flow rate changes.

As discussed in Section 2.6, the wavelet modulus maxima at different levels of decomposition provide different types of information. Noise singularities and signal singularities are both present at low levels of decomposition. At intermediate levels, the singularities caused by noise disappear while the signal singularities are still present. At high levels, the high degree of approximation tends to group signal singularities in the same neighborhood together as a single singularity. From these characteristics, it is seen that the beginning of a new transient should be detected at an intermediate level of decomposition.

The question is then what levels should be considered intermediate levels. An appropriate level to be used actually depends on the spacing of the data. In fact, when deciding what level should be used, we are choosing the resolution of the data. To illustrate this, let us first consider actual field data whose wavelet decompositions are shown in Figs. 3.29 and 3.30. The plot in the upper left corner in each figure shows the data in their original spacing. There are several short transients within a period of 1.5 hours. The data were generally collected at a very high frequency (one sample every 1.75 seconds). However, there are some large gaps between samples such as the one in the neighborhood of $t = 1391.65$ hours. Before applying the wavelet transform, linear interpolation was used to obtain a uniform set of data at a sampling interval of 10 seconds (0.002778 hour). As seen in the figures, the transients may be detected using the detail signal at levels 3-5. Since there is minimal noise in this case, levels 1-2 might be used as well although not recommended. The detail signals at

levels 6 and beyond are too smooth to detect all the short transients.

Now let us consider the same set of data using a new sampling interval of 36 seconds (0.01 hour). Figs. 3.31 and 3.32 display the wavelet decomposition of the signal with the new discretization. As seen in the figures, detail signals in the first three levels may be used to identify new transients. The most appropriate level is level 3. The detail signals at levels 4-6 are too smooth to capture the changes. Several short transients are grouped together at these three levels of decomposition.

In order to determine which level is the most suitable for an arbitrary spacing, the length of the shortest transient to be detected Δt_{min} first has to be chosen. The highest level at which the shortest transient can be detected is the level at which its resolution is lower than or equal to Δt_{min}. Since the dyadic wavelet decomposition is used, the resolution takes the form of 2^j, where j is the level of decomposition ($j = 0, 1, 2, ...$). Let Δt be the original spacing between data points and l be the highest level of wavelet decomposition that can be used to detect the shortest transient. The level l can be determined by solving the following constraints:

$$2^l \Delta t < \Delta t_{min} < 2^{l+1} \Delta t \tag{3.5}$$

Rewriting Eq. 3.5, one obtains:

$$l < \frac{log\left(\frac{\Delta t_{min}}{\Delta t}\right)}{log\ 2} < l + 1 \tag{3.6}$$

For the case shown in Figs. 3.29 and 3.30 in which the data spacing Δt is 0.002778 hour, the highest level l is computed as 5 using 0.1 hour as the length of the shortest transient. The resolution of data at this level is $2^5 \times 0.002778 = 0.089$ hours which is lower than Δt_{min}. Therefore, any transient that is longer than 0.089 hours can be detected. When the sample interval is 0.01 hour as is the case shown in Figs. 3.31 and 3.32, the highest level l is 3. The resolution at this level is $2^3 \times 0.01 = 0.080$ hours. Therefore, the most suitable decomposition level (which is the highest level that

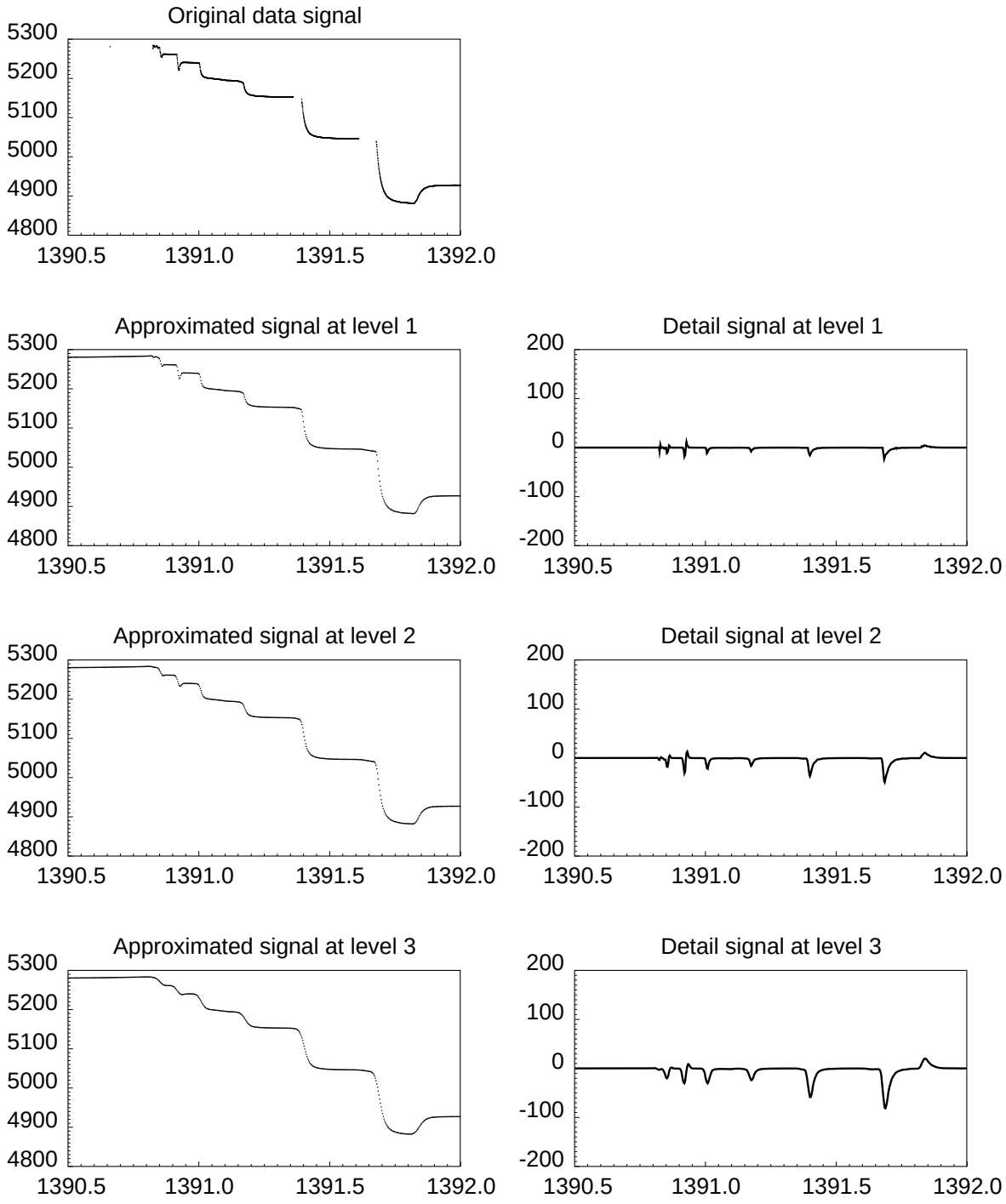

Figure 3.29: Wavelet decomposition of pressure data with short transients for $\Delta t = 0.002778$ hour.

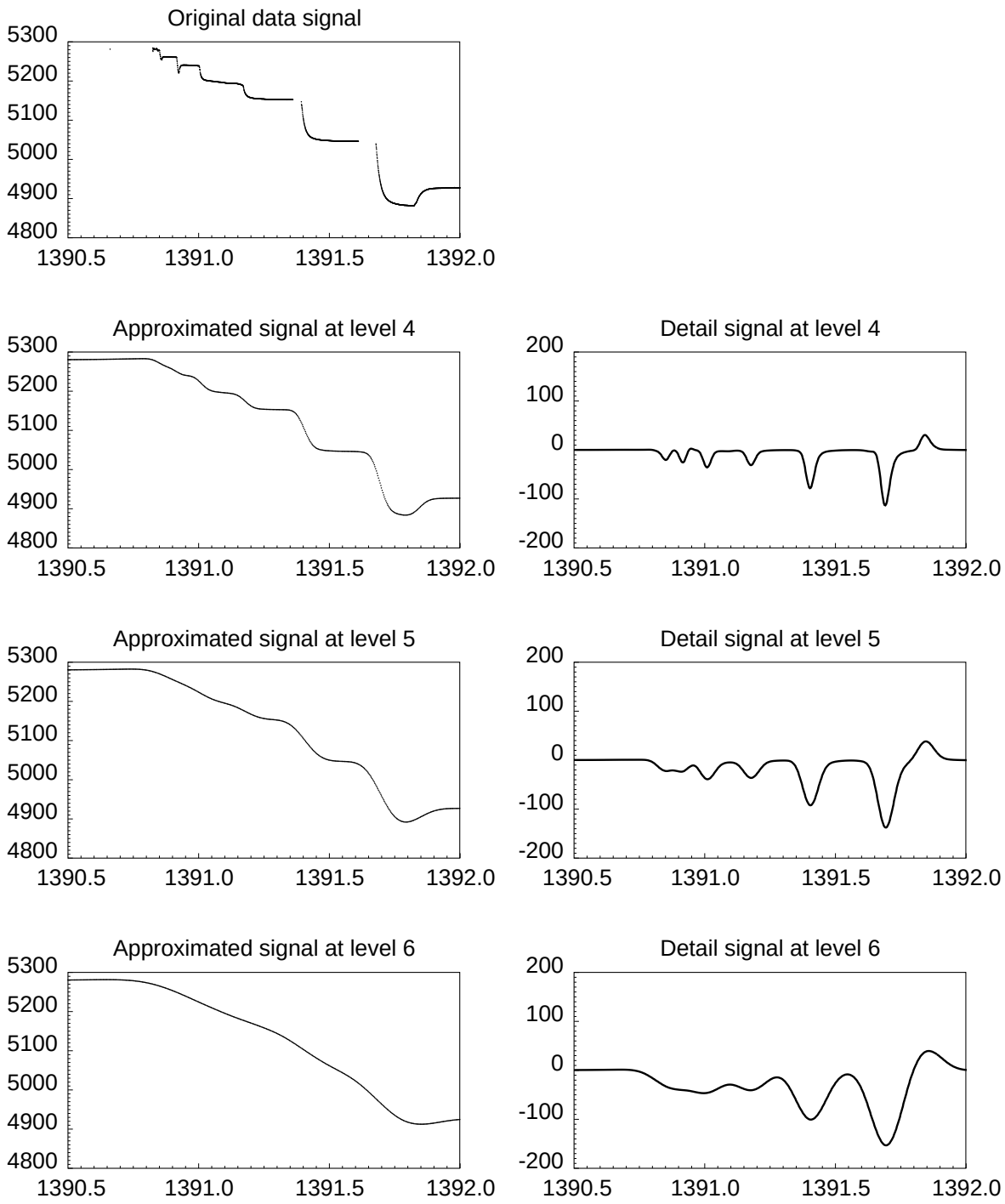

Figure 3.30: Wavelet decomposition of pressure data with short transients for $\Delta t = 0.002778$ hour (continued).

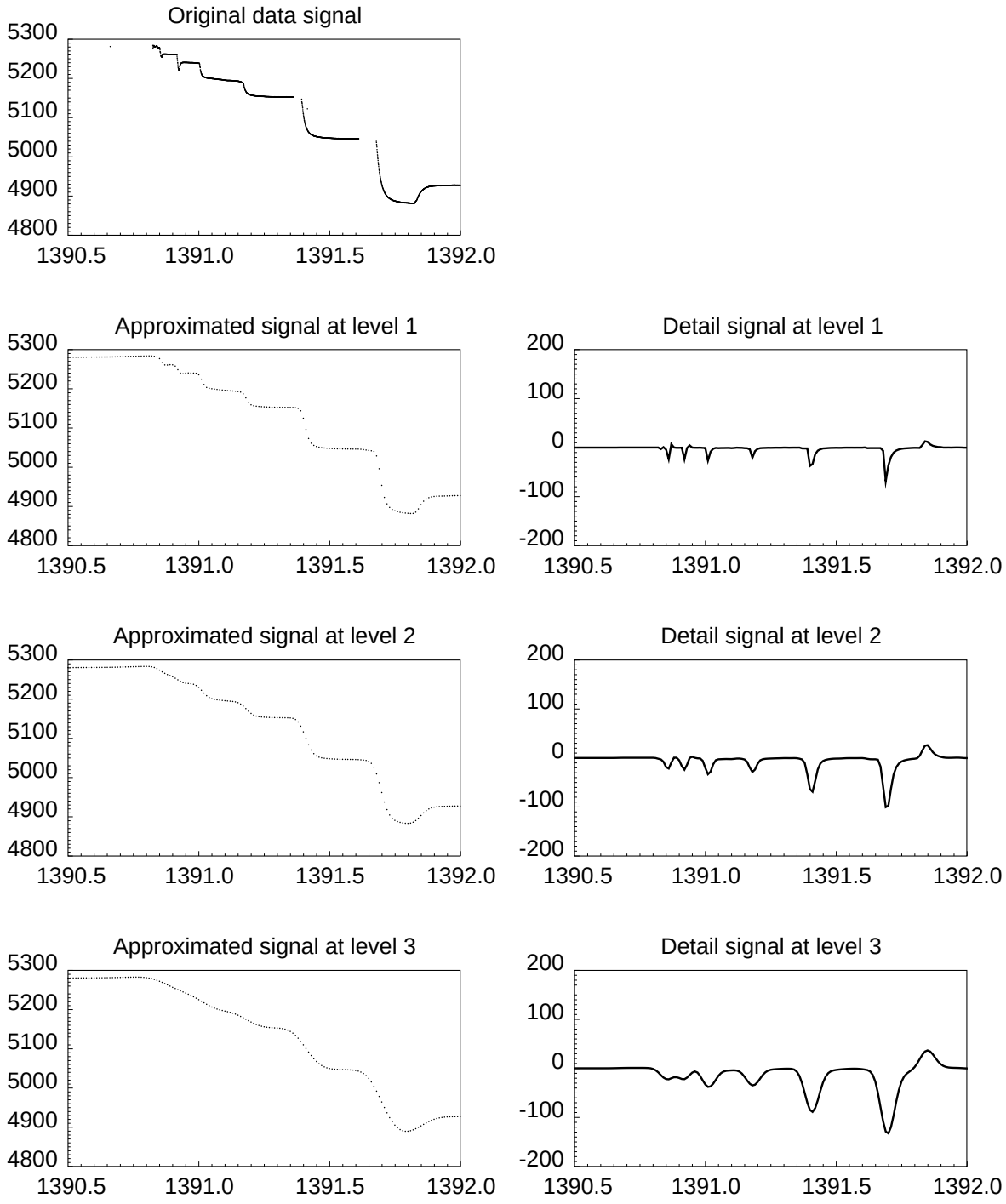

Figure 3.31: Wavelet decomposition of pressure data with short transients for $\Delta t = 0.01$ hour.

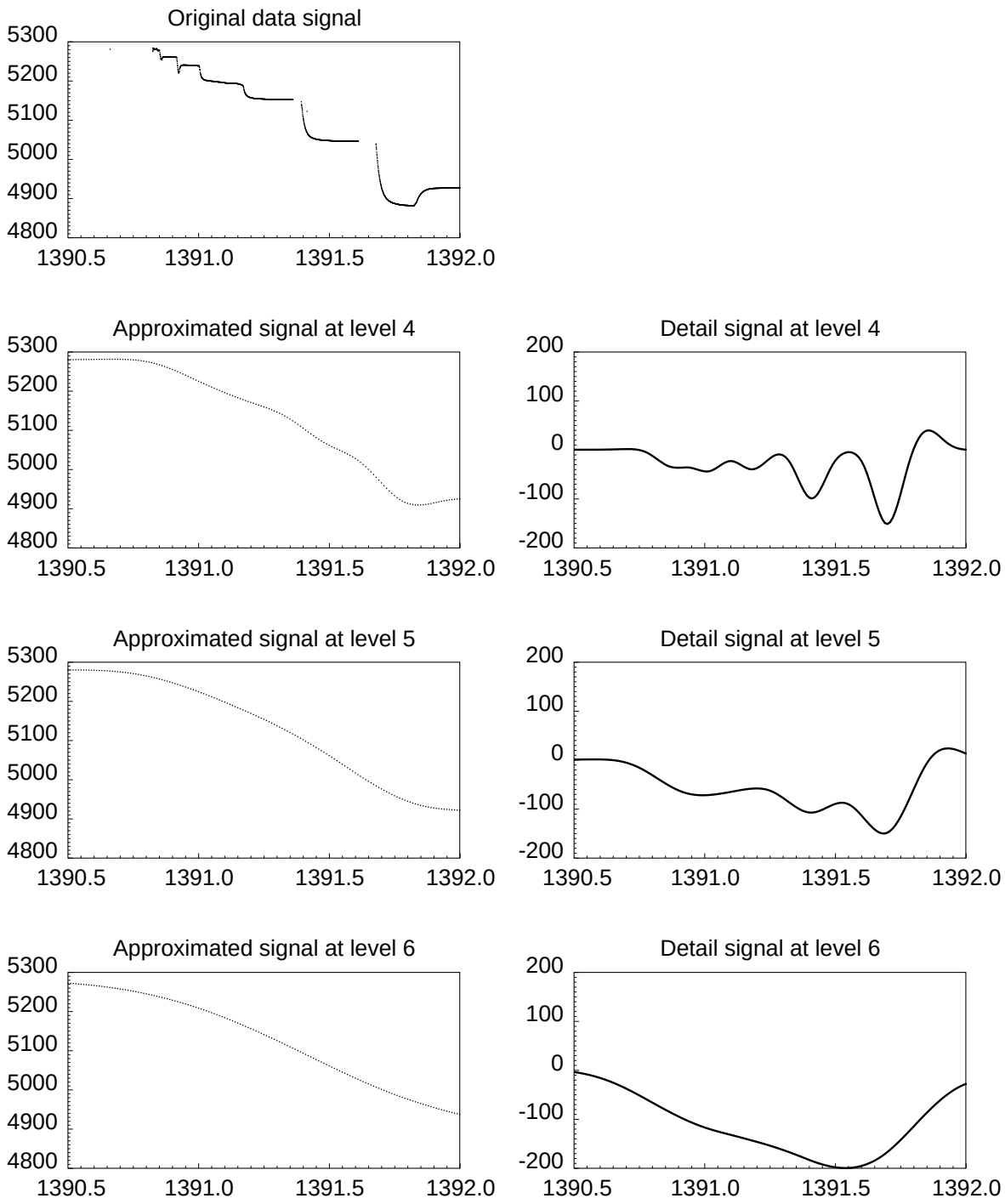

Figure 3.32: Wavelet decomposition of pressure data with short transients for $\Delta t = 0.01$ hour (continued).

the shortest transient can be detected) is different for data with different sampling frequencies.

As in detecting outliers (Section 3.1), a threshold has to be chosen for the wavelet detail signal in order to determine which change is actually a singularity. The rule of thumb in choosing the threshold is to determine how much pressure difference between two data points is considered the beginning of a new transient. The threshold then obviously depends on the spacing between the data points. Once a pressure threshold is chosen for the original data spacing, the threshold at any decomposition level j can be computed by multiplying 2^{j-1} to the threshold in the original spacing. Note that the multiplier is 2^{j-1} not 2^j because the detail signal at level j contains the high-frequency information content of the approximated signal at level $j-1$. It may be more intuitive for us to choose a threshold in terms of a rate of pressure change per unit time (slope of pressure data) instead of an absolute pressure change. However, in terms of computation, it is more efficient to use the absolute pressure threshold to avoid computing the slopes for the detail signal at the desired resolution. In this study, the pressure threshold and the slope threshold are referred to interchangeably. In order to determine small pressure changes that are responses of small variations in flow rate, the slope threshold should also be small. However, the threshold should not be too small. Otherwise, all minor variations such as noise may be misinterpreted as new transients.

After choosing a decomposition level and a slope threshold, possible locations for starting positions of new transients may be identified from wavelet modulus maxima whose detail signals are higher than the threshold. The wavelet maxima at the chosen scale only provide indications of singularities not the exact locations of singularities for two reasons. First of all, the detail signal at the chosen scale has less resolution than the original signal. Therefore, the wavelet maxima are determined at a coarser resolution rather than the original data. Secondly, a singularity at the beginning of a new transient is not necessarily an extremum, but is actually the first point that departs from a prior trend in the signal. Since the decomposition at level 1 uses the

data in their original resolution, the location of each singularity can be determined by finding the first point whose detail signal at level 1 is higher than the pressure threshold.

To make sure that the singularities detected are characteristics of new transients instead of local variations, we need to check the slope of the data in the neighborhood of singularities. First, the forward slope extending from the point of singularity needs to be higher than the slope threshold. Secondly, the absolute difference between the forward slope and the slope of the data prior to the point of singularity should be big enough to demonstrate a discontinuity in the data trend. In this study, if the difference between the two slopes is higher than half of the slope threshold, the detected point is considered a point of singularity. Each slope can be computed by running a simple straight line regression through the data in its neighborhood.

Even at the original resolution, the exact locations of flow rate change do not necessarily lie on the discretization grid. They can be determined by finding the intersection between a straight line passing through the last two points before a sudden change in pressure and another line that passes the first two points right after the point of singularity. Fig. 3.33 illustrates how the exact locations of flow rate changes are computed. Since the data are subject to noise, the computed intersection may lie outside the interval between the two middle points. If this happens, the point of singularity on the discretized grid itself may be used as the starting time for the new transient.

In summary, the detection of new transients can be performed in a multistep procedure as follows:

1. Determine which level should be used in the detection algorithm based on the desired resolution of the results.

2. Choose a slope threshold to discriminate between singularities corresponding to new transients and noise singularities.

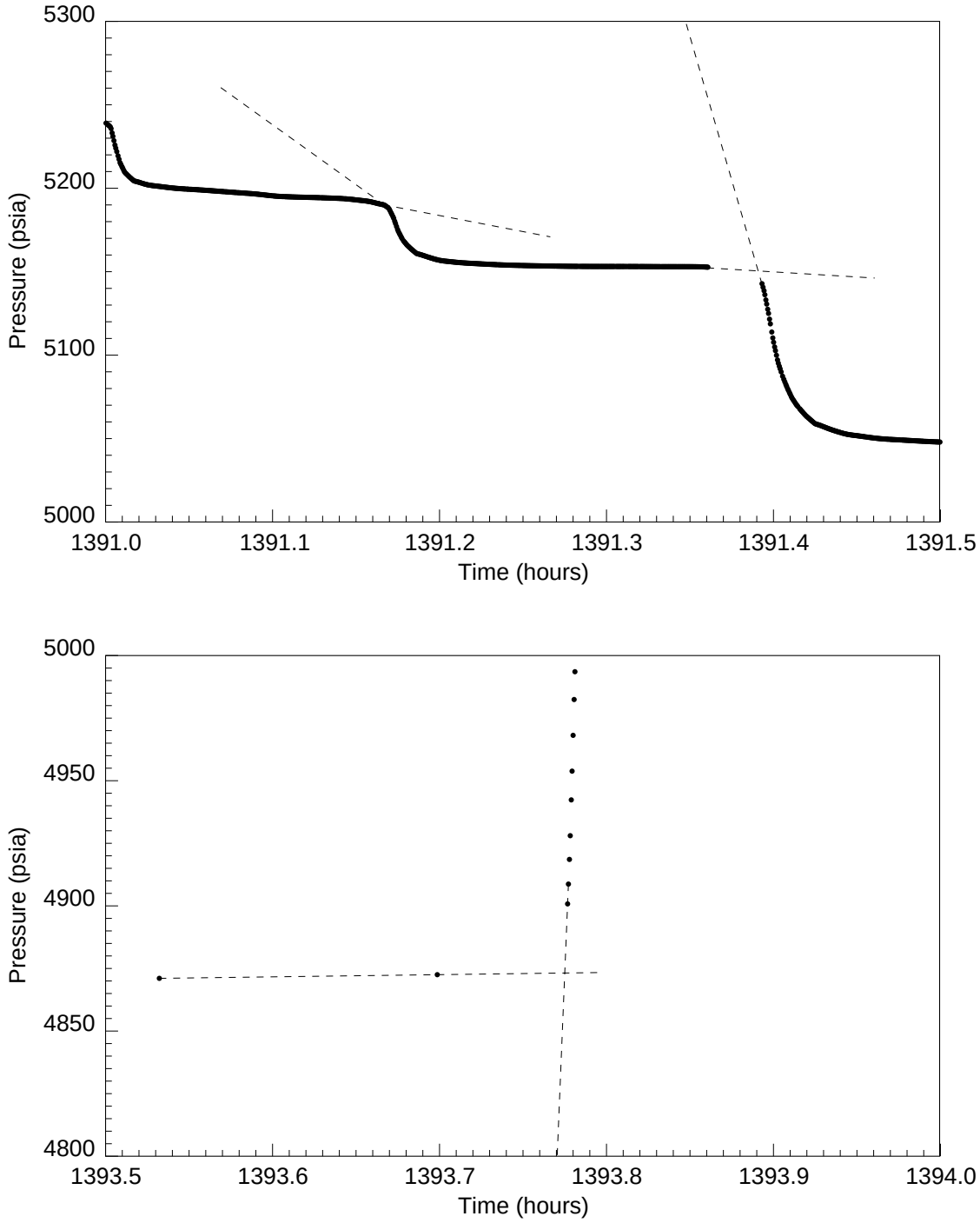

Figure 3.33: Determination of exact starting times for new transients.

3. Determine possible locations for starting positions of new transients by choosing wavelet modulus maxima whose detail signals are higher than the threshold and map the positions back to the original resolution.

4. Check whether the slope extending from the singularity point forward is higher than the slope threshold and whether it deviates from the slope of data prior to the point of singularity.

5. Determine the exact location of the beginning of a new transient by computing the intersection between a line that passes through the first two points in the new transient and another line passing through the last two points in the previous transient.

To study the effect of noise in transient detection, the algorithm was implemented to (1) original field data which are quite noisy and (2) denoised data. The spacing between data points was chosen to be 0.01 hours in both cases. The length of the shortest transient Δt_{min} was set to be 0.1 hour. Using the formula given in Eq. 3.6, the decomposition level used in the detection was computed as 3. The slope threshold was chosen to be 10 psi/hour. The resolution at this level is then $2^3 \times 0.01 = 0.08$ hours. The pressure threshold at level 3 is $10 \times 2^2 \times 0.01 = 0.4$ psi.

Figs. 3.34 and 3.35 display the multiresolution wavelet decomposition of the original noisy data, and Figs. 3.36 and 3.37 depict the wavelet decomposition of the data that were previously denoised using the hybrid thresholding method with a threshold of 1.5. As expected, the detail signals from the noisy data exhibit plenty of small fluctuations at low levels of decomposition (levels 1-4). This means that there are a lot of wavelet modulus maxima with small magnitudes. Using the detection level of 3 and the pressure threshold of 0.4, several wavelet maxima may be detected as transients in this case. The points of singularities corresponding to new transients are plotted as vertical lines in Fig. 3.38. Since the noise singularities were carried through to the decomposition level used in the detection algorithm, many of them were mistaken as signal singularities.

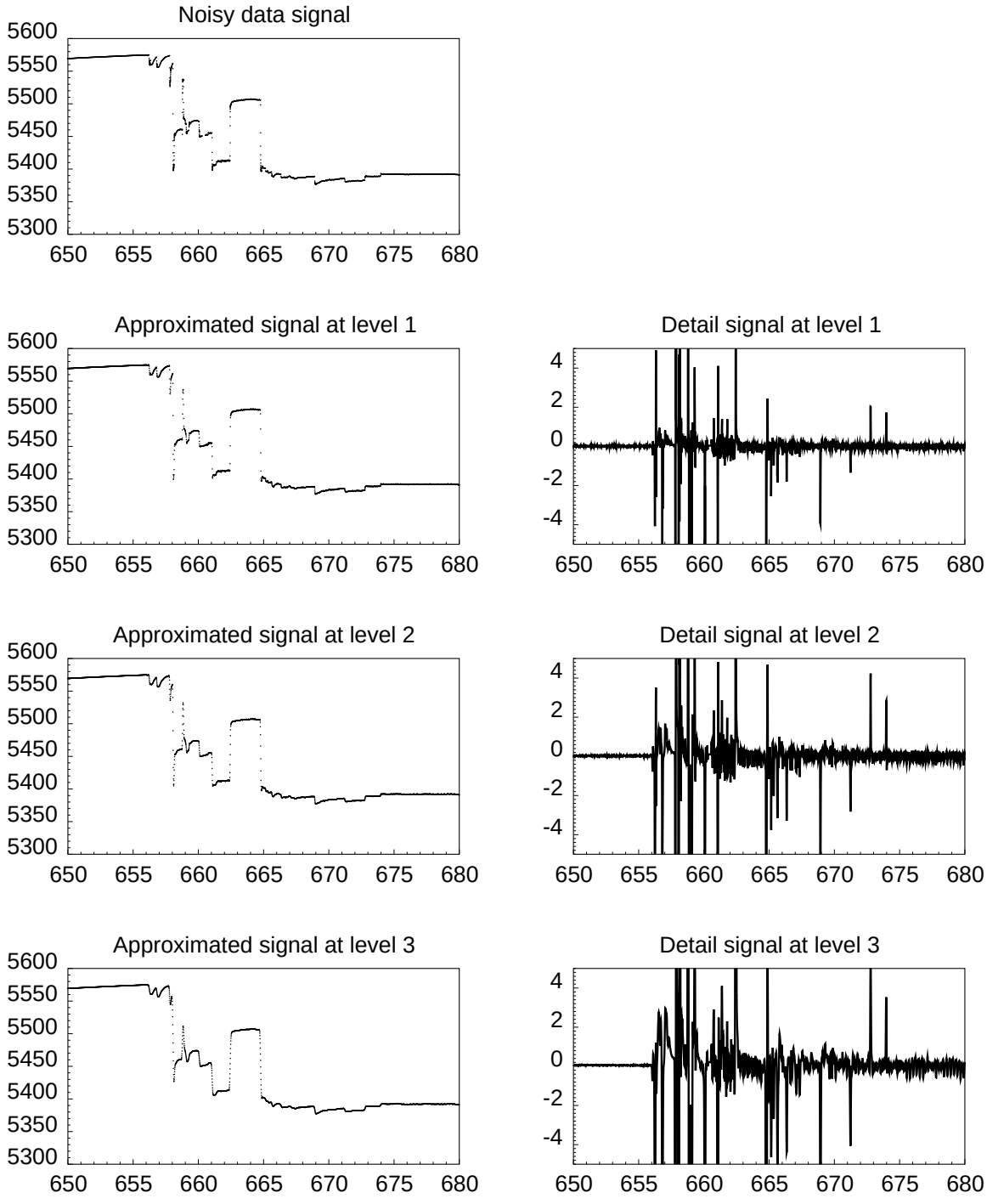

Figure 3.34: Wavelet decomposition of original pressure data.

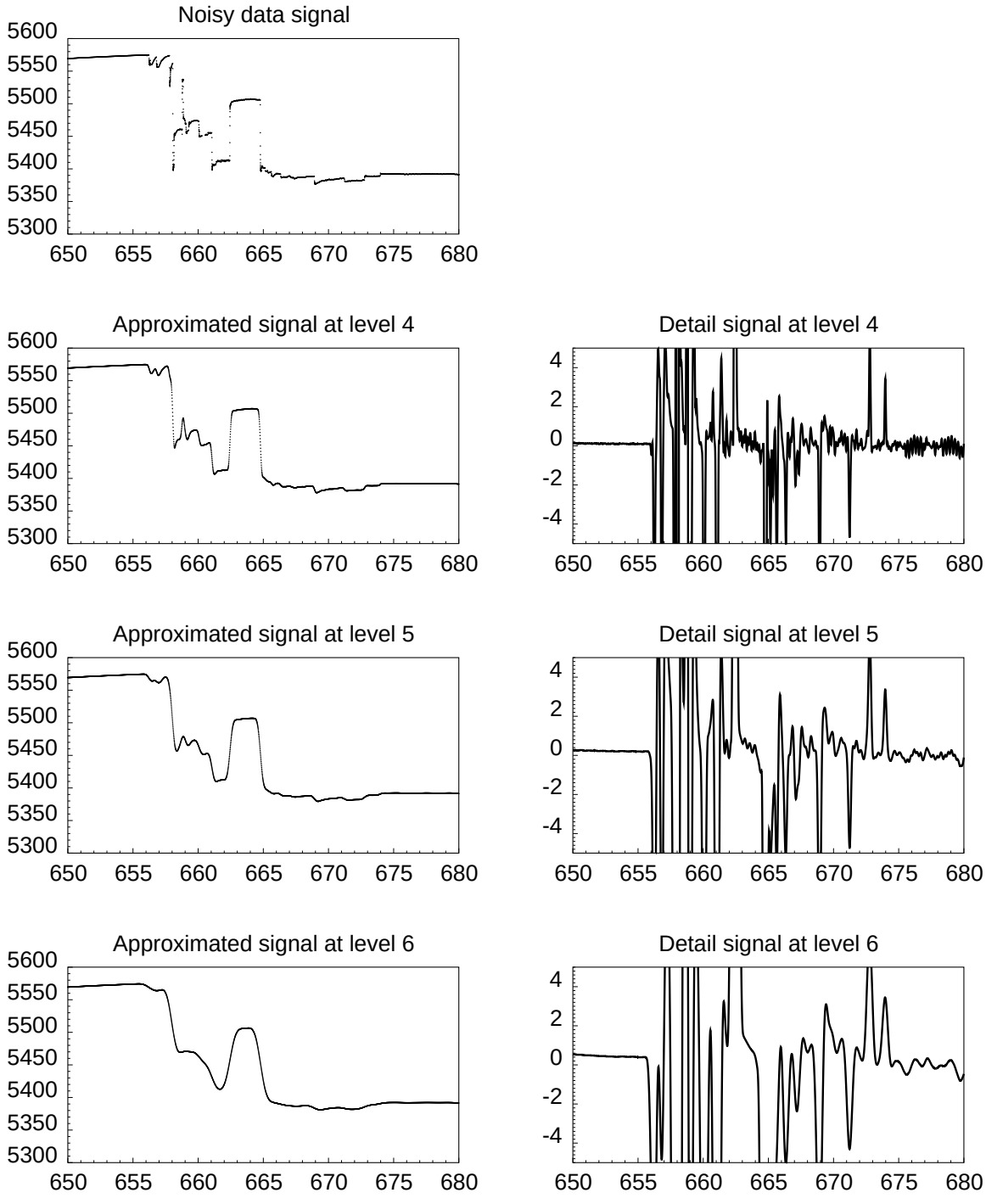

Figure 3.35: Wavelet decomposition of original pressure data (continued).

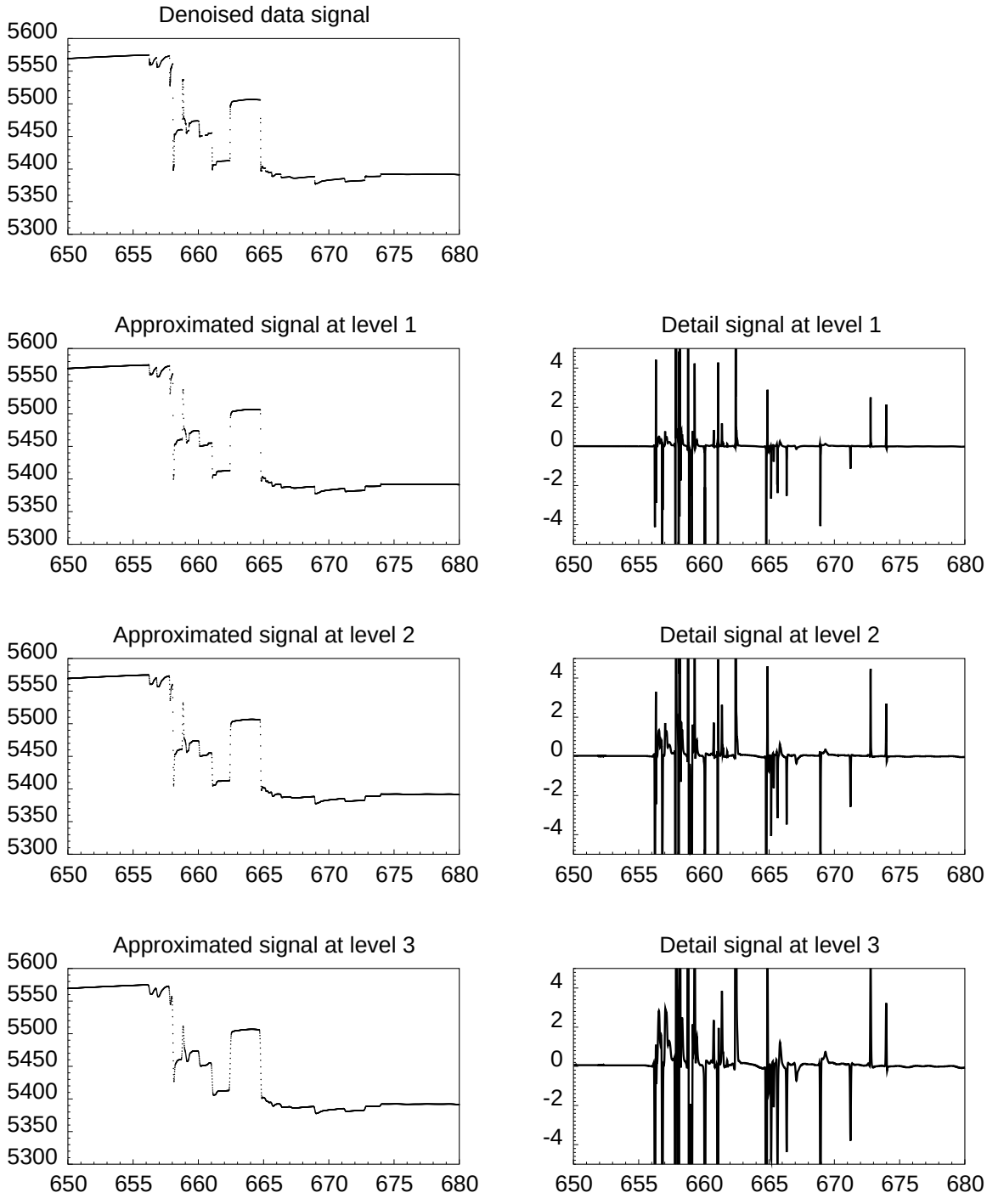

Figure 3.36: Wavelet decomposition of denoised pressure data.

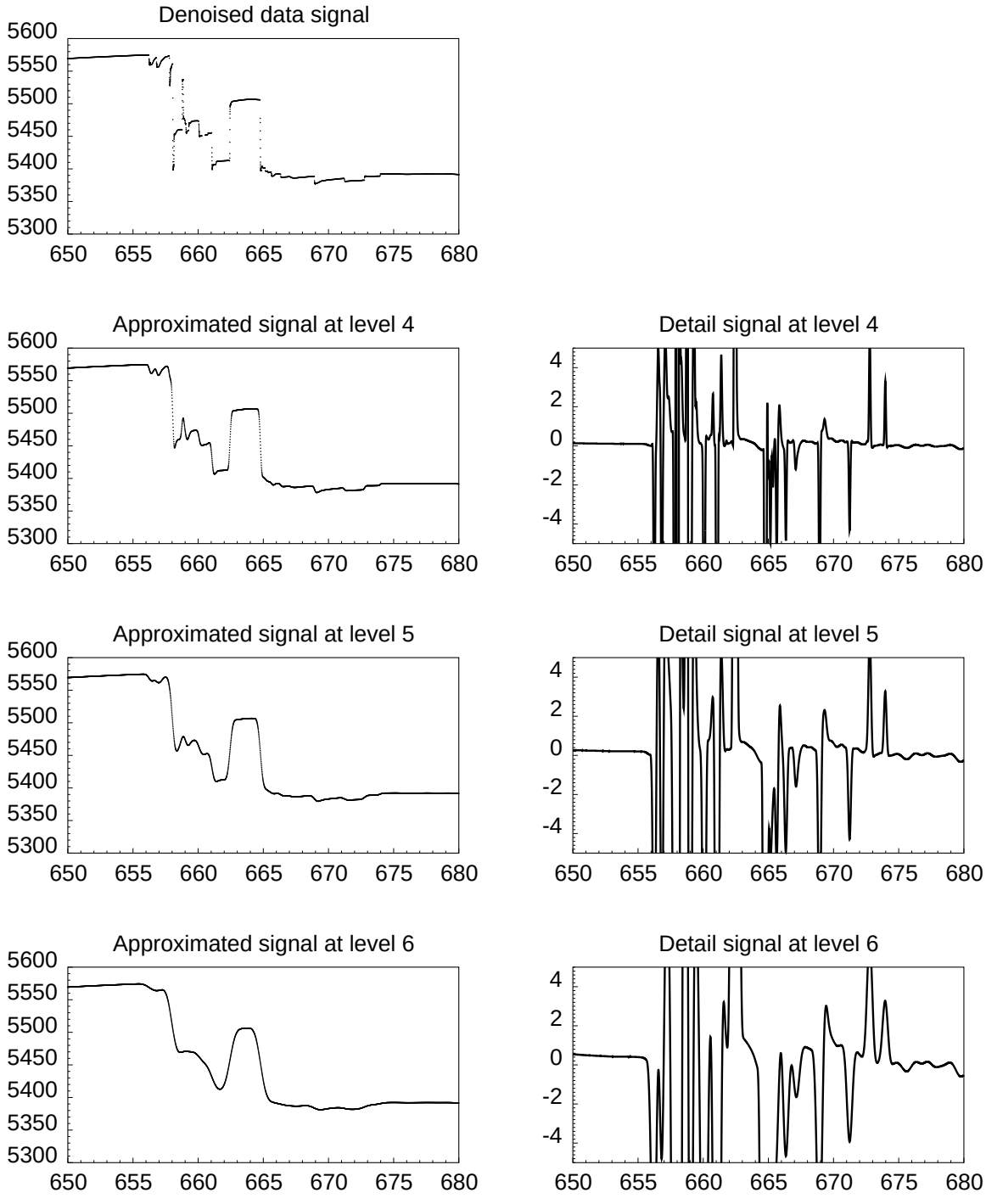

Figure 3.37: Wavelet decomposition of denoised pressure data (continued).

On the other hand, small wavelet modulus maxima corresponding to small local variations disappear when using data that were previously denoised as shown in Figs. 3.36 and 3.37. These small maxima were actually suppressed during the denoising process. Only the wavelet modulus maxima with large values which represent signal singularities were kept. Fig. 3.39 shows the break points between transients from the detection algorithm using the denoised data. Comparing Figs. 3.38 and 3.39, the denoised data provide better results than the original noisy data. Therefore, noisy data should be denoised before being used for transient identification. However, denoising may not be needed when the associated noise is minimal since denoising may smear out sharp features in the data to a certain degree.

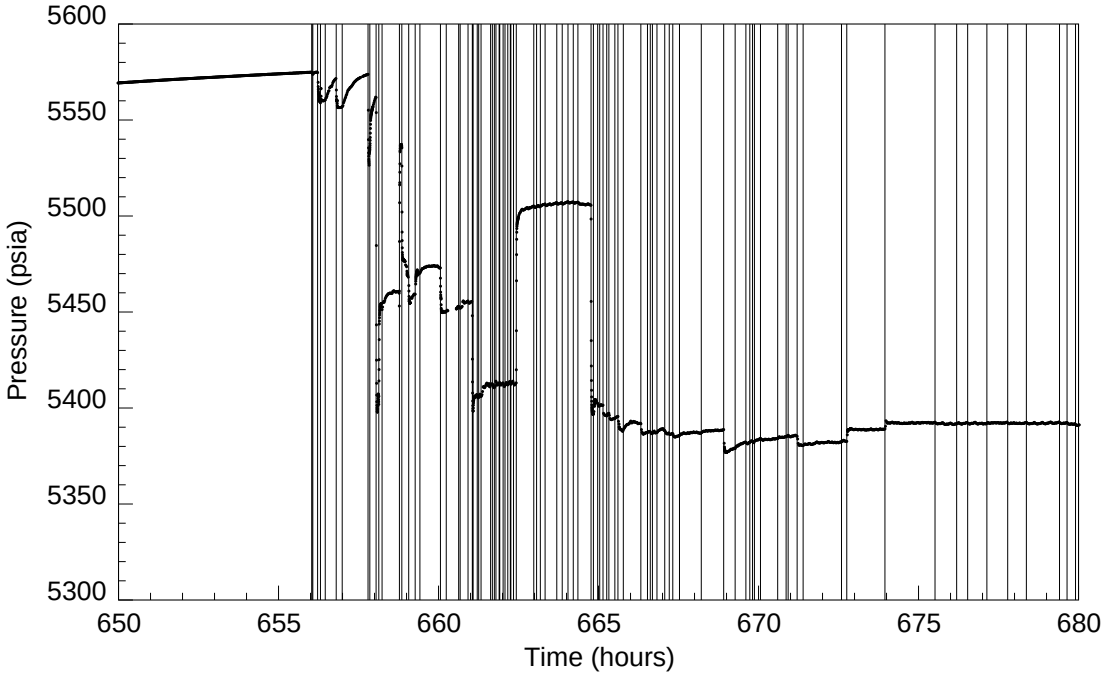

Figure 3.38: Transient identification using original data in wavelet decomposition.

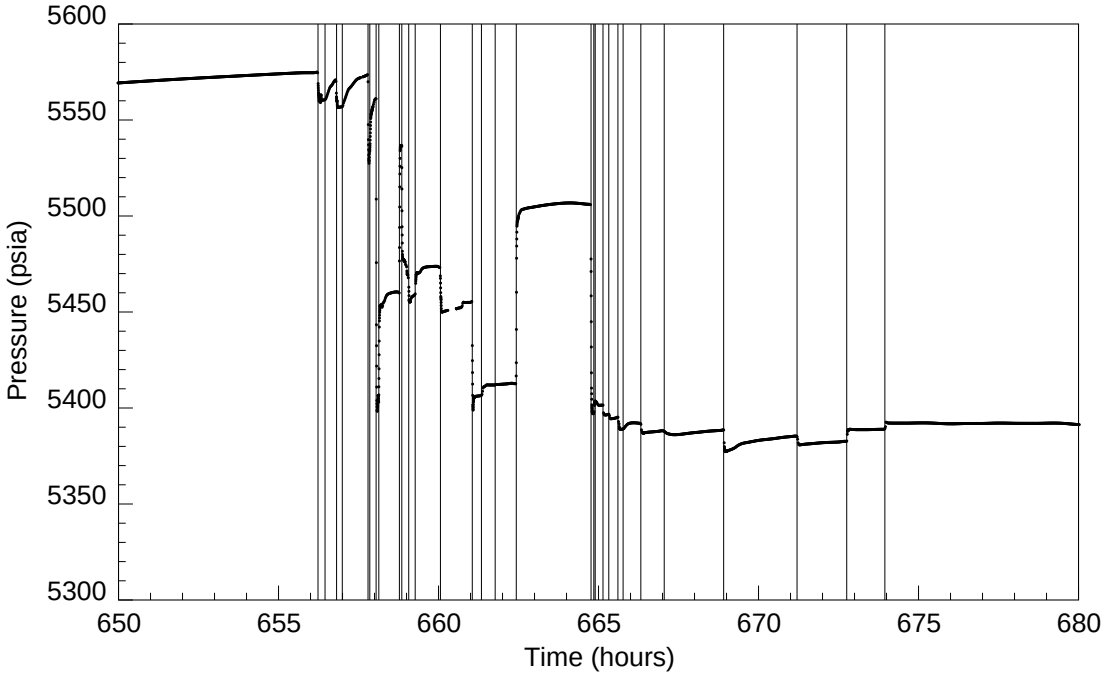

Figure 3.39: Transient identification using denoised data in wavelet decomposition.

3.3.1 Field Example 1

In this example, the data were collected from a permanent downhole pressure gauge in a newly drilled well. The pressure was recorded at variable frequencies with a minimum recording interval of 1.728 seconds (0.00048 hours) and a maximum spacing of 1.5 hours (excluding large gaps). In general, the data were collected at high frequencies when there were large changes in pressure and lower frequencies when the pressure changes became more gradual. The average time interval between measurements is approximately 30 seconds (0.008333 hour). There are a few large gaps in the data due to operational problems which prevented the gauge from registering the pressure measurements. Almost all of the transients in the data exhibit very rapid changes in the pressure value at the beginnings of new transients. There are a few series of several short transients embedded in a downward trend that seems like a single drawdown. This type of response calls for a small value of Δt_{min}. In this example, Δt_{min} was set to be 0.1 hour.

Before applying the detection algorithm, outliers were removed from the data using the procedure described in Section 3.1. Linear interpolation was then applied to the original data to obtain a new uniform sample spacing of 10 seconds (0.002778 hour). When examined closely, the data are quite noisy. Therefore, the hybrid denoising algorithm with a threshold of 1.5 was used to suppress noise in the data. The denoised data were then used in the detection algorithm with a slope threshold of 10 psi/hour.

The starting points of new transients detected from the algorithm are shown as vertical lines in Fig. 3.40. Close-up pictures of the detection of series of short transients in downward trends are illustrated in Figs. 3.41 and 3.42. As seen in the figures, the algorithm did well in detecting the singularities caused by flow rate changes. However, a few singularities caused by noise and small changes were also detected. The singularities at time $t = 45.617$ and $t = 123.796$ are actually noise singularities. Since the noise levels are quite high at these two locations, they were mistaken as signal singularities. The detections at $t = 47.023$, $t = 47.267$, and

$t = 126.678$ reflect the recognition of small changes in the pressure signal. The slopes of these changes are higher than the slope threshold of 10 psi/hour. Thus, these microtrends were misidentified as new transients.

The results from the detection algorithm revealed mostly singularities corresponding to changes in flow rates and a few singularities corresponding to unconventional behaviors in the data. The detection of the latter is, in fact, beneficial to us since it helps us determine problematic regions in the data. Before interpreting the data, the aberrance detected can be looked at closely and eliminated in advance. Therefore, results from the detection algorithm should be reviewed to screen for abnormalities in the data before being used for interpretation.

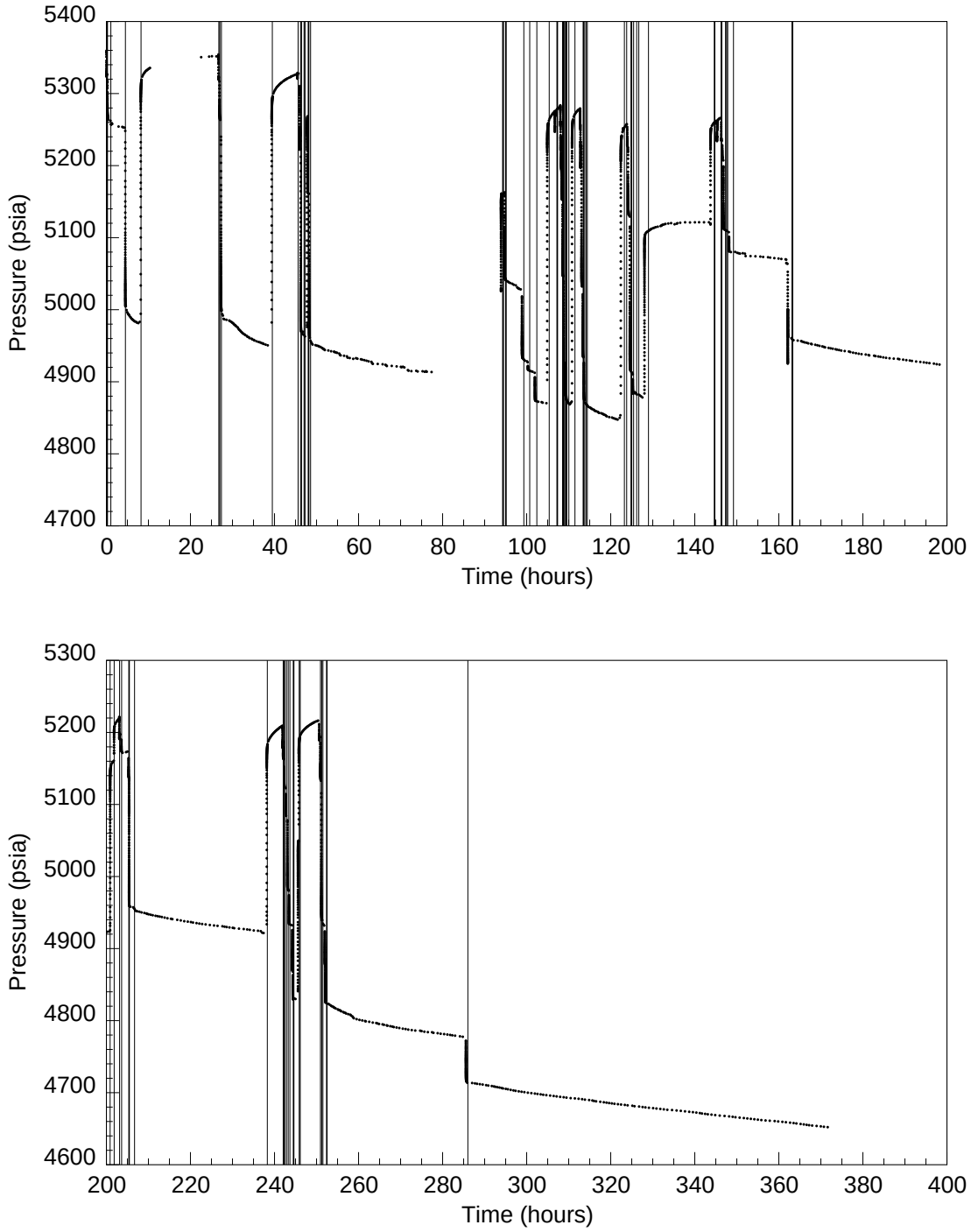

Figure 3.40: Transient identification for Example 1.

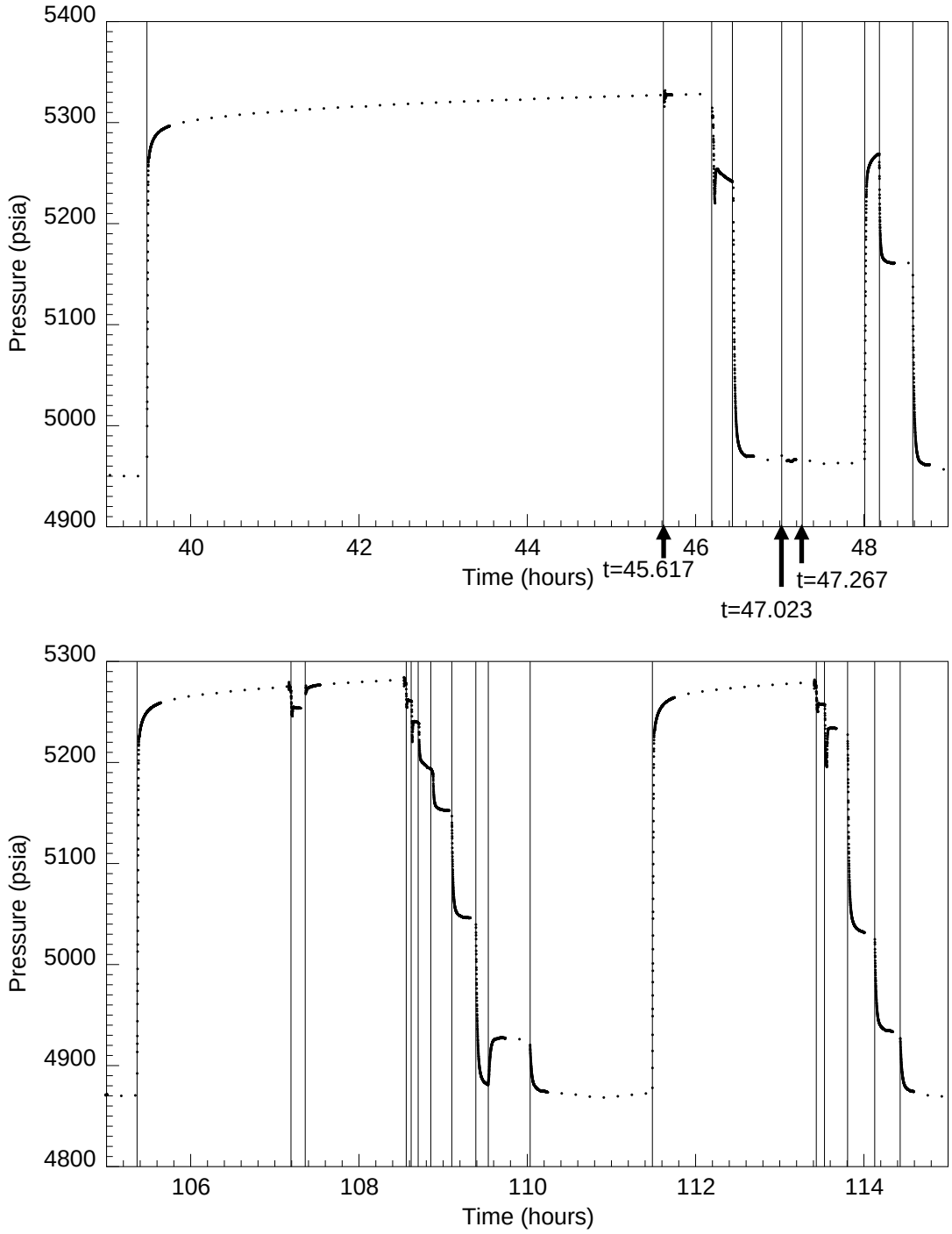

Figure 3.41: Close-up view of transient identification for Example 1.

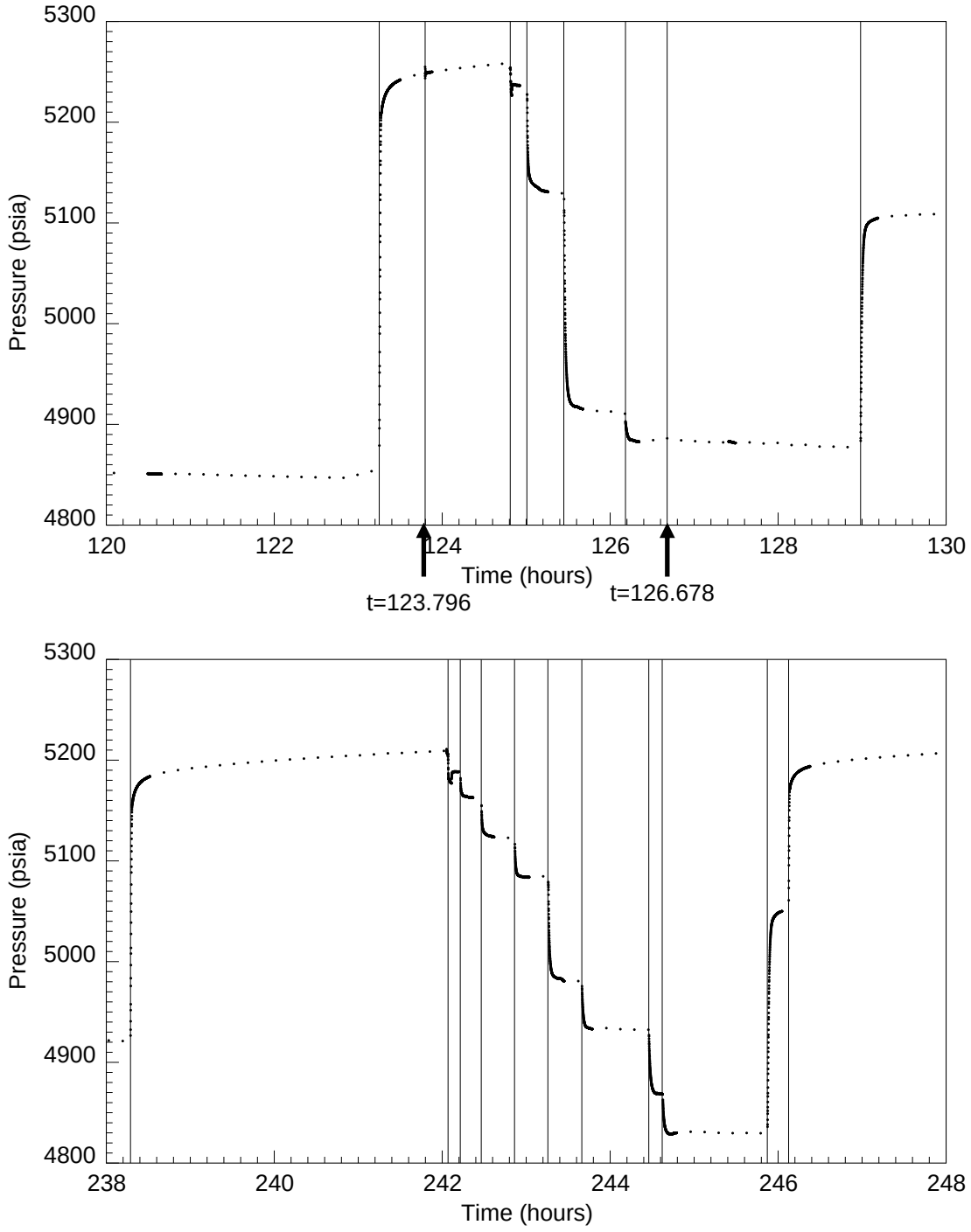

Figure 3.42: Close-up view of transient identification for Example 1.

3.3.2 Field Example 2

Most of the data in this example were collected at a uniform sampling frequency of six measurements per minute ($\Delta t = 10 seconds$). The minimum recording interval is 9 seconds (0.0025 hours), and the largest interval is 6.934 hour (excluding large gaps). As in the previous example, there are a few gaps in the measurements. The average spacing is 10.03 seconds (0.002787 hour) excluding gaps. There are a few long transients and several short ones in the data. Some of the transients have large pressure changes in the order of 200-300 psi while many exhibit minor changes in the order of 5-10 psi. Similar to the previous example, there are a few series of several short transients embedded in a downward trend that seem like a single drawdown. Again, the length of the shortest transient Δt_{min} was chosen to be 0.1 hour.

Before applying the detection algorithm, outliers were first removed from the data. Linear interpolation was then applied to the data to obtain a new uniform sample spacing of 10 seconds (0.002778 hour). The data in this example are very noisy with a noise level of 1-2 psi. Therefore, the noise in the data was suppressed using the hybrid denoising algorithm with a threshold of 1.5. Since there are some transients whose pressure changes are small, the slope threshold was chosen to be 5 psi/hour.

Figs. 3.43 and 3.44 display the results from the detection algorithm. A few close-up shots of the detection for short transients are illustrated in Figs. 3.45 and 3.46. All the major transients were detected by the algorithm. A few small changes such as the one at $t = 3400.68$ were missed (see Fig. 3.46). In fact, there exists a wavelet maximum at the position $t = 3400.68$, but the difference between the slope of the straight line extending forward from the point of singularity and the slope of the data prior to the singularity is too small. This check was imposed in order to avoid detecting small changes that are due to noise. The singularity at $t = 3394.811$ was detected at $t = 3395.112$ instead because the changes before $t = 3395.112$ are too gradual to be considered as new transients. Their slopes are less than the slope threshold. The slope becomes higher than the slope threshold at $t = 3395.112$. Therefore, the algorithm recognized the latter position as the position for the new transient.

Although there are a few misidentifications, most of the transients were properly identified, especially the important ones. The detection algorithm greatly reduces the task that otherwise would have to be performed manually even though it may still call for a certain degree of human intervention.

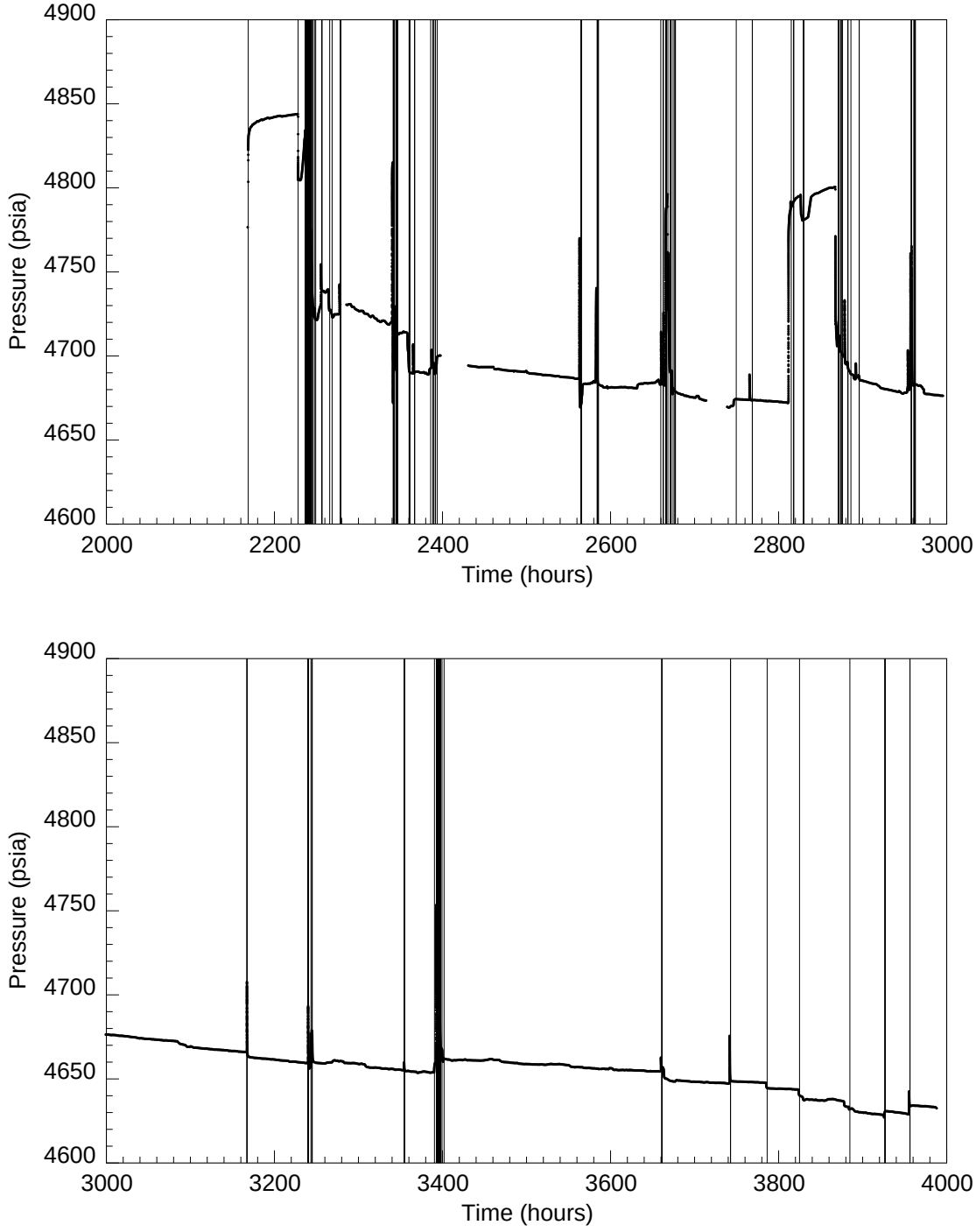

Figure 3.43: Transient identification for Example 2.

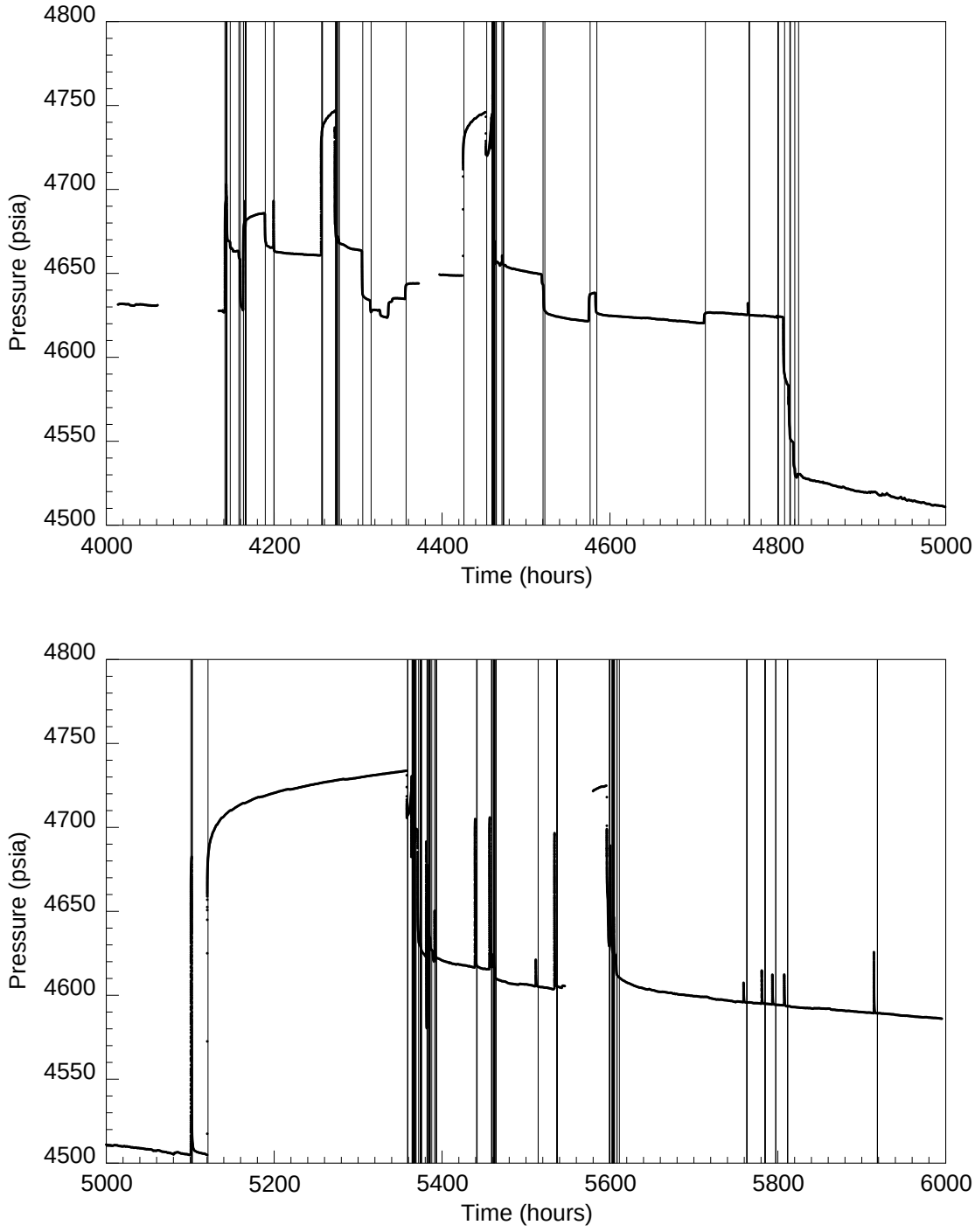

Figure 3.44: Transient identification for Example 2 (continued).

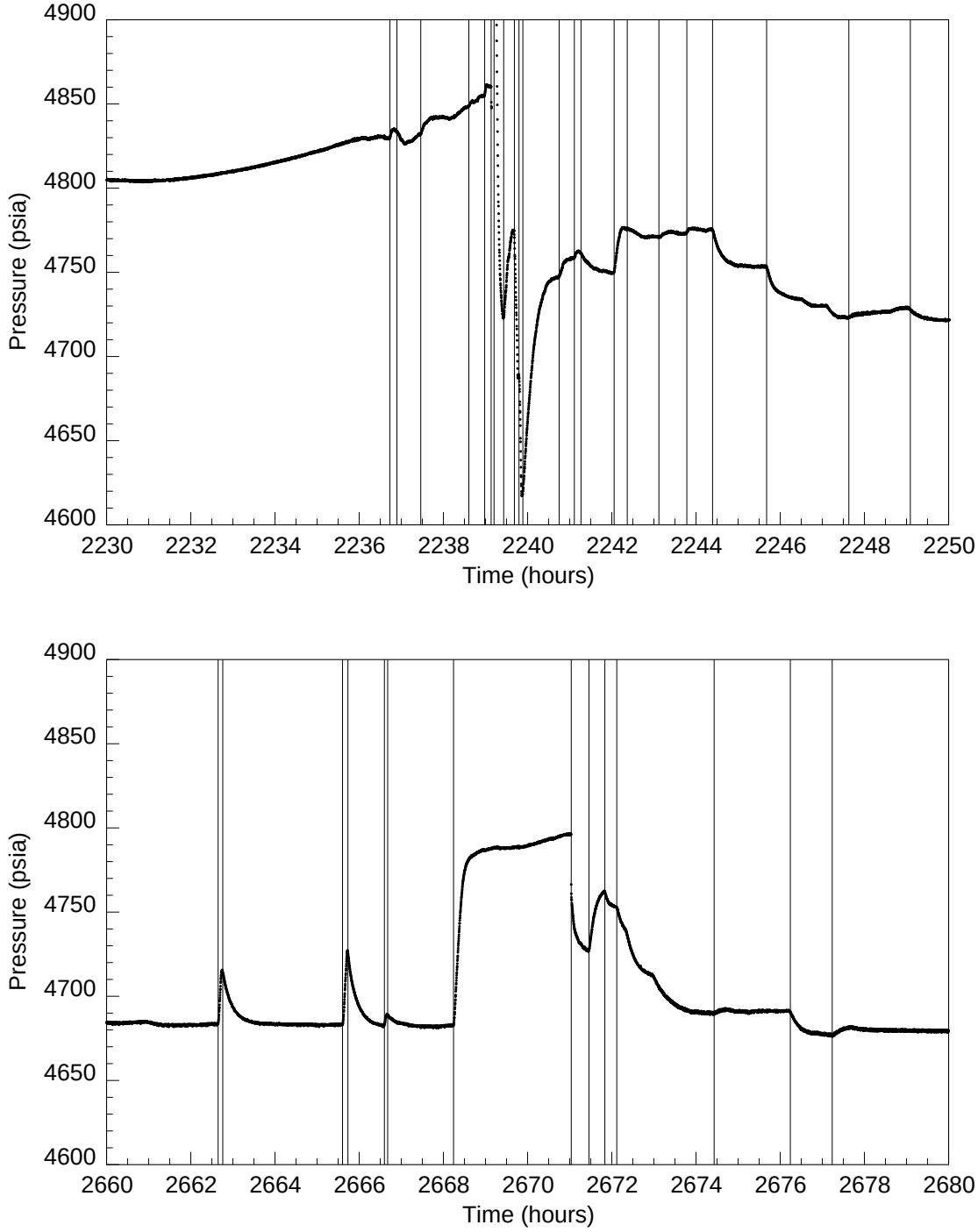

Figure 3.45: Close-up view of transient identification for Example 2.

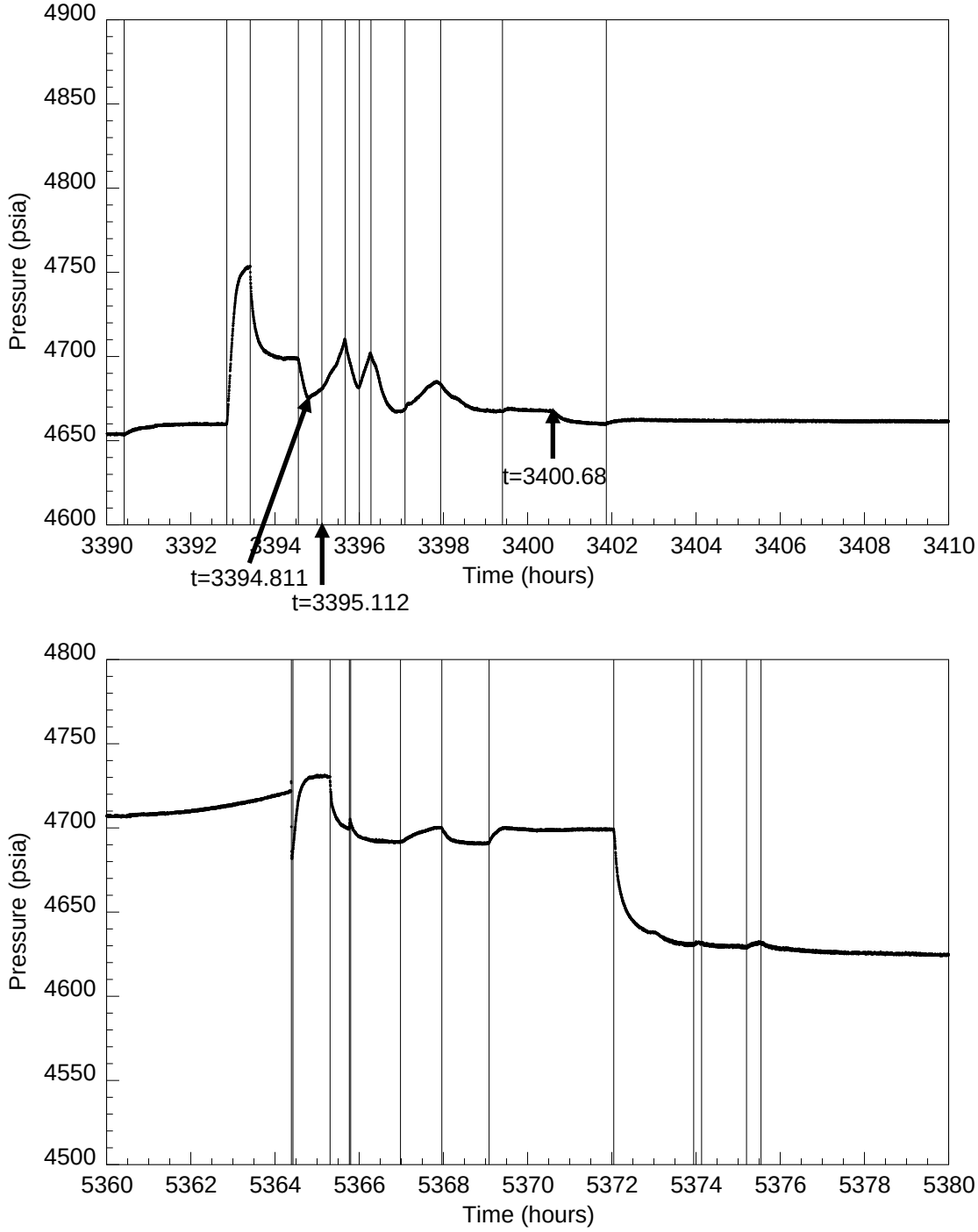

Figure 3.46: Close-up view of transient identification for Example 2.

3.3.3 Field Example 3

The data collection style in this example was quite different from the previous two. Most of the data were collected at at low sampling frequency of 4 hours between measurements. A few regions of the data were collected at higher frequency. The minimum recording interval is 1 second (0.000277 hours), and the largest interval is 4.738 hour excluding large gaps. Similar to the previous examples, there are a few gaps in the measurements due to operational problems. Some of the gaps are as large as 100 hours or more. The average spacing excluding these gaps is 0.6854 hour. At early times, most of the transients were of short and medium length. As time progressed, there were more occurrences of long transients. Similar to the previous two examples, Δt_{min} was chosen as 0.1 hour in order to detect short transients.

Outliers were first removed from the data. Linear interpolation was then applied to the data to obtain a new uniform sample spacing of 10 seconds (0.002778 hour). Although the pressure data were generally collected at a rate of one sample every 4 hours, most of the data in the regions where there were large pressure changes were collected at a medium or high frequency. Therefore, the spacing was chosen to be small. The data in this example are quite smooth. Therefore, the noise suppression algorithm was not applied to the data. As mentioned earlier, denoising may smear out sharp features in the data especially in the case of low frequency data. Since there are some transients whose pressure changes are small, the slope threshold was chosen to be 5 psi/hour.

The results from the detection algorithm are displayed in Figs. 3.47 and 3.48. Although there are more than five years of data for this well, only the first 4000 hours of data are shown. The rest of the data have similar appearances with the data shown in the two figures. All of the abrupt changes in pressure were detected by the algorithm. However, the pressure changes of smaller degree were not identified. The results from the detection algorithm in this case are in fact poorer than those in the previous two examples although similar values of the slope threshold were used. The main difference between the data in this example and the other two sets is the

sampling frequency. In this example, the transients that were not identified are the ones in which the sampling frequency is low. For instance, the spacing of the data that lie in vicinity of $t = 840$ data is 4 hours. The interpolated points between each pair of the original data are smooth. As a result, the wavelet did not see the abrupt changes in the pressure data. It is generally better to first collect data at a high sampling frequency which clearly benefits the implementation of transient identification methodology. After detecting these transients, the data can be resampled to reduce the number of data.

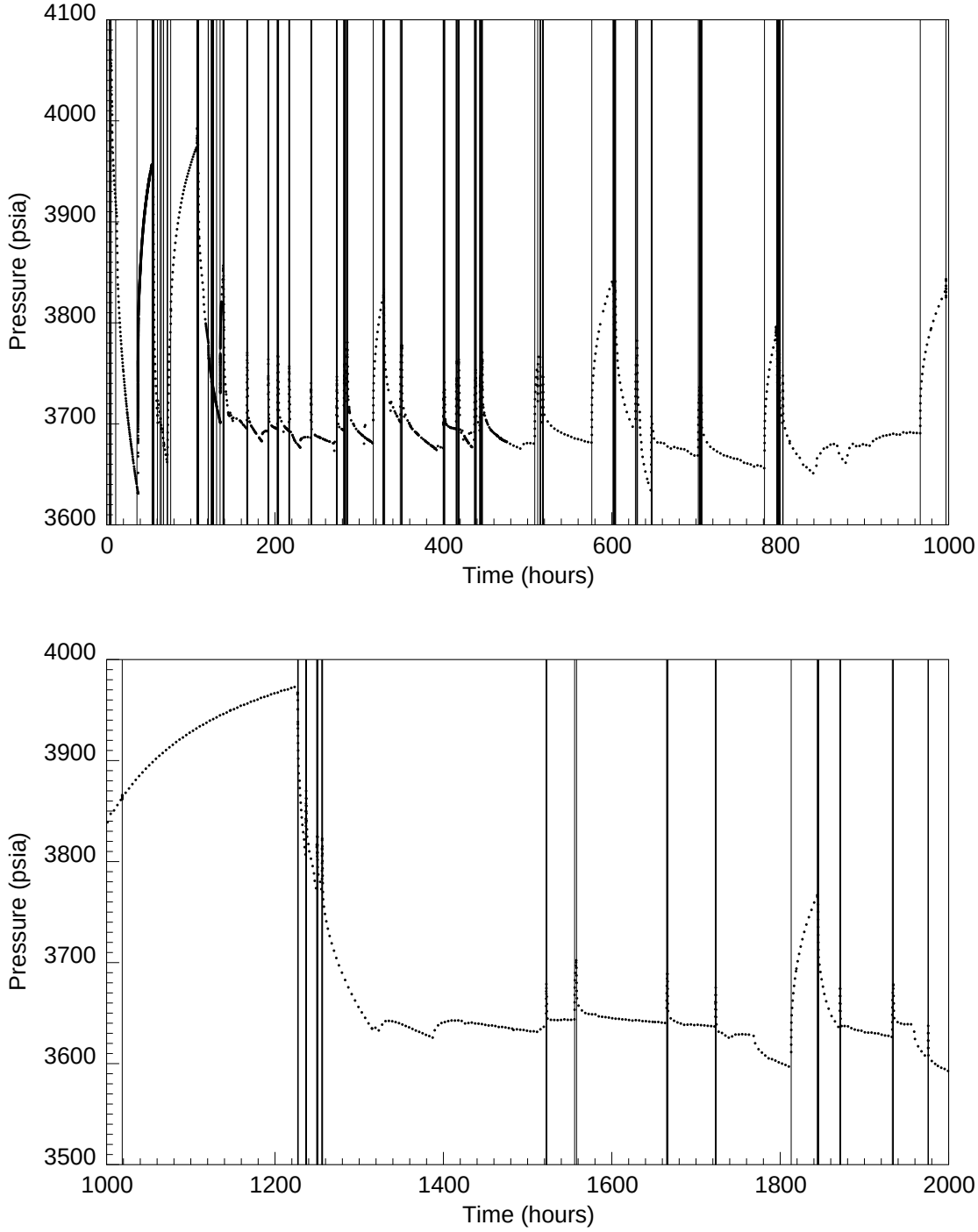

Figure 3.47: Transient identification for Example 3.

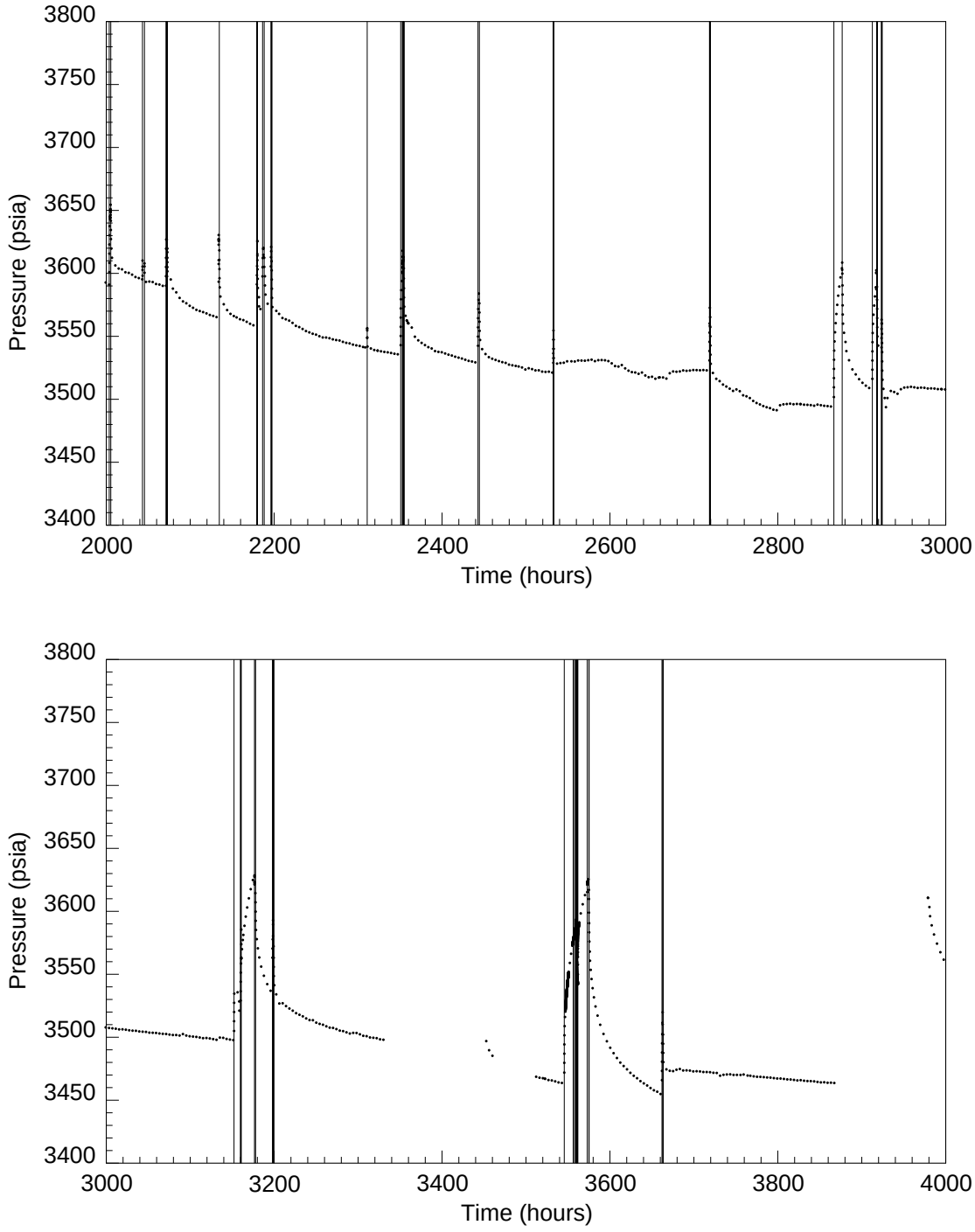

Figure 3.48: Transient identification for Example 3 (continued).

3.4 Data Reduction

Generally, the size of pressure data sets acquired with permanent pressure gauge is enormous. A gauge system with a 10-second recording interval registers more than three million data points a year. It is cumbersome even to plot the data to see a general data behavior on a graph not to mention trying to analyze them. Therefore, it is necessary to reduce the number of data to a representative set with manageable size.

One of the most widely used methods of reducing the number of data is the pressure thresholding method. In this method, the data are sampled only when a certain change in pressure is reached. However, using a threshold on pressure alone is not sufficient. In some cases, the pressure may stay constant or has minimal changes over a long period of time. The pressure threshold criterion may produce a large gap in the data. A time limit should then be imposed on the sampling space. Ultimately, the pressure should be recorded when the change in pressure is higher than a maximum preset pressure value Δp_{max} and whenever the time span between samples becomes higher than a maximum preset time threshold Δt_{max}.

For noisy data that are collected at high frequency, it may be necessary to denoise the data before undertaking the data reduction step so that it is easier to pick out representative points from the data set. Otherwise, one may not be able to reduce the size of data by much since the changes in pressure value caused by noise may exceed the pressure threshold forcing us to keep these measurements.

In order to illustrate how denoising can help reducing the size of data, the maximum-pressure-maximum-time criterion described earlier was applied to both original and denoised data shown in Fig. 3.27. The maximum value for the pressure Δp_{max} was chosen to be 0.1 psi, and the maximum time between data points Δt_{max} was set to be one hour. Fig. 3.49 displays the pressure data after the reduction process using original data and denoised data. Using the original data in the reduction process, the number of data was reduced from 18,000 to 9,387. On the other hand, the data

Table 3.1: Comparison of final data sizes using original and denoised data sets.

Pressure threshold (psi)	Original size	Final size (without denoising)	Final Size (with denoising)
0.1	1,8000	9,387	275
0.5	1,8000	3,258	99

size was reduced to 275 when using the denoised data. To reduce the data size even more, Δp_{max} was increased to 0.5 psi. The data size in each case was reduced by approximately threefold. The reduced data sizes using original and denoised data sets are tabulated in Table 3.1. Fig. 3.50 depicts the pressure data after the reduction procedure using original and denoised data sets.

In summary, the size of data can be reduced considerably while the most representative points are kept when using denoised data. As mentioned before, wavelet denoising is actually one form of a nonparametric regression. The errors between the underlying representation of the data and the measurements are minimized nonparametrically. Therefore, the denoised data are the best representation of the data. Consequently, the data left after the reduction process are much fewer than those left from the original noisy data.

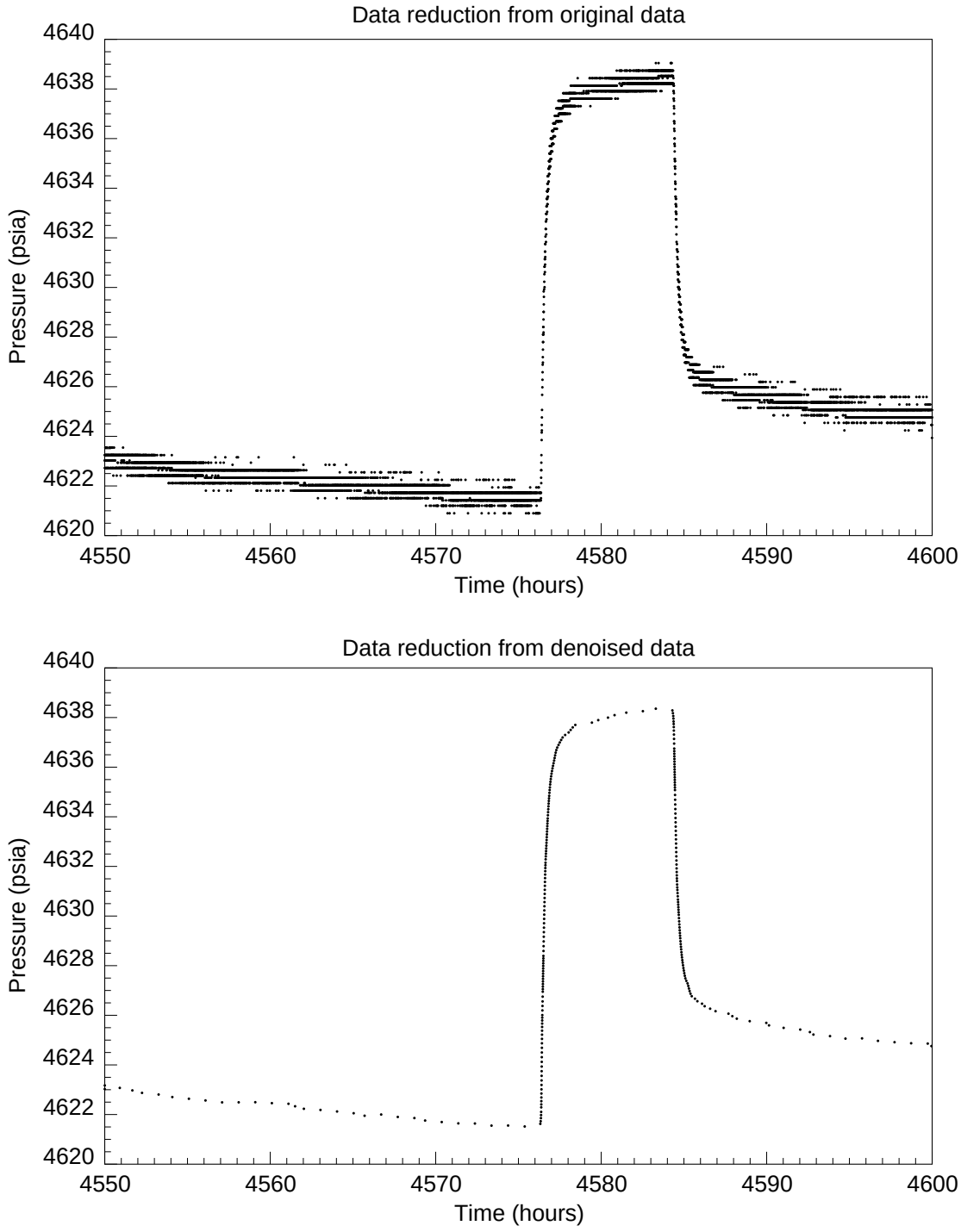

Figure 3.49: Data reduction using original data and denoise data ($\Delta p_{max} = 0.1$ psi).

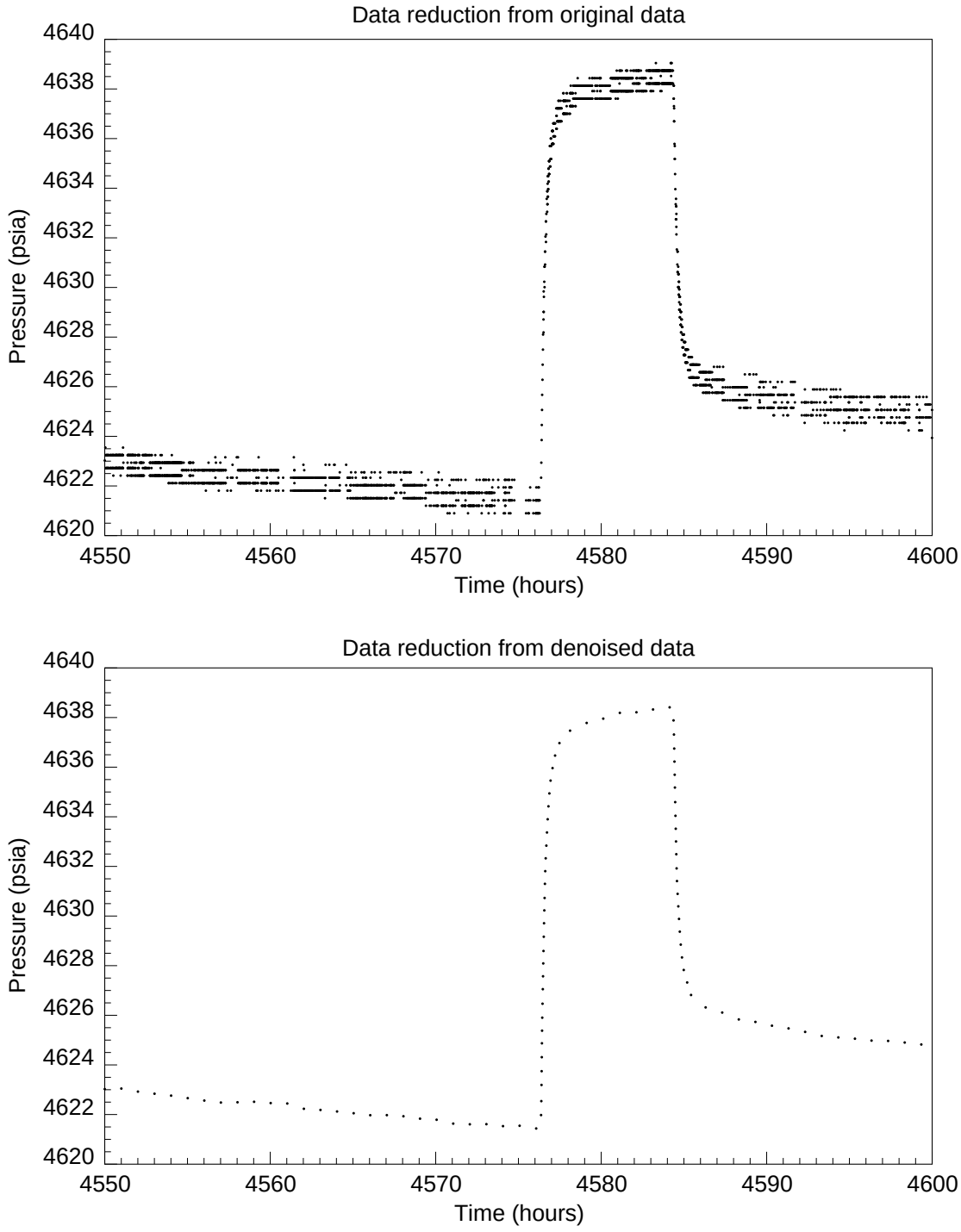

Figure 3.50: Data reduction using original data and denoise data ($\Delta p_{max} = 0.5$ psi).

Chapter 4

Rate Reconstruction and Behavioral Filtering

In practice, it is common that well flow rates are not measured continuously due to the difficulty and expense associated with the measurements. Flow rates may be measured daily, weekly, or sometimes even only once a month. The incomplete information on flow rate history is one of the factors that discourage interpreters from analyzing long-term pressure data. Fortunately, the missing flow rates can be reconstructed from the pressure history since the pressure itself is a response to flow rate alteration.

Another difficulty in analyzing long-term data comes from aberrant behaviors in the pressure data themselves. Since long-term data collection is generally unsupervised as is the case for traditional pressure transient testing, many things that happen in the reservoir and/or the wellbore can lead to strange pressure behaviors that are not characteristic of the reservoir or fluid properties. Therefore, there is a need to identify and eliminate these aberrant regions in a systematic way.

This chapter discusses the use of nonlinear regression to reconstruct flow rate history and data that are inconsistent with the rest of the transients. Section 4.1 first gives a brief review of the nonlinear regression procedure. Then, a method to

reconstruct flow rate history utilizing information from pressure responses, flow rates that are known and production history is discussed in Section 4.2. The determination of aberrant transients using the variance between the regression results and the measurements is shown in Section 4.3.

4.1 Nonlinear Regression

Nonlinear regression is a mathematical procedure used to infer model parameters by minimizing the difference between the measurement and the computed model response. The most popular approach is to use the least squares method in which the objective function to minimize is the sum of the squares of the differences between the measurements and the model response:

$$E = \sum_{i=1}^{n} \left[y_i - F\left(\boldsymbol{\theta}, x_i\right) \right]^2 \tag{4.1}$$

where

E = objective function
F = model function
$\boldsymbol{\theta}$ = unknown model parameters
x_i = dependent variable (time)
y_i = independent variable (pressure)
n = number of data.

Let us first review one of the most fundamental methods used in nonlinear regression, the Newton method. In this method, the objective function is approximated by a truncated Taylor series around the initial guesses of the unknown model parameters ($\boldsymbol{\theta}^0$):

$$\begin{aligned} E^* &= E|_{\boldsymbol{\theta}^0} + \sum_{j=1}^{m} \left(\theta_j - \theta_j^0\right) \left.\frac{\partial E}{\partial \theta_j}\right|_{\boldsymbol{\theta}^0} \\ &\quad + \frac{1}{2} \sum_{j=1}^{m} \sum_{k=1}^{m} \left(\theta_j - \theta_j^0\right) \left(\theta_k - \theta_k^0\right) \left.\frac{\partial^2 E}{\partial \theta_j \partial \theta_k}\right|_{\boldsymbol{\theta}^0} \end{aligned} \tag{4.2}$$

where

E^* = quadratic approximation of the objective function E around $\boldsymbol{\theta}^0$

m = number of unknown parameters

$$\left.\frac{\partial E}{\partial \theta_j}\right|_{\boldsymbol{\theta}^0} = -2\sum_{i=1}^{n}\left[y_i - F\left(\boldsymbol{\theta}^0, x_i\right)\right]\left.\frac{\partial F}{\partial \theta_j}\right|_{\boldsymbol{\theta}^0} \tag{4.3}$$

$$\left.\frac{\partial^2 E}{\partial \theta_j \partial \theta_k}\right|_{\boldsymbol{\theta}^0} = -2\sum_{i=1}^{n}\left[-\left.\frac{\partial F}{\partial \theta_j}\right|_{\boldsymbol{\theta}^0}\left.\frac{\partial F}{\partial \theta_k}\right|_{\boldsymbol{\theta}^0} + \left[y_i - F\left(\boldsymbol{\theta}^0, x_i\right)\right]\left.\frac{\partial^2 F}{\partial \theta_j \partial \theta_k}\right|_{\boldsymbol{\theta}^0}\right]. \tag{4.4}$$

Eq. 4.2 can be written in the matrix form as:

$$E^* = E|_{\boldsymbol{\theta}^0} + (\delta\boldsymbol{\theta})^T \mathbf{g} + \frac{1}{2}(\delta\boldsymbol{\theta})^T H\,(\delta\boldsymbol{\theta}) \tag{4.5}$$

where

$$\mathbf{g} \equiv \{g_j\} = \left\{\left.\frac{\partial E}{\partial \theta_j}\right|_{\boldsymbol{\theta}^0}\right\} \tag{4.6}$$

$$H \equiv \{h_{jk}\} = \left\{\left.\frac{\partial^2 E}{\partial \theta_j \partial \theta_k}\right|_{\boldsymbol{\theta}^0}\right\} \tag{4.7}$$

$$\delta\boldsymbol{\theta} = \boldsymbol{\theta} - \boldsymbol{\theta}^0. \tag{4.8}$$

Here, $\mathbf{g}$ is the gradient of the objective function, and H is the Hessian matrix. In order to minimize E^*, its derivatives with respect to $\delta\boldsymbol{\theta}$ have to be zero:

$$\frac{\partial E^*}{\partial(\delta\boldsymbol{\theta})} = 0. \tag{4.9}$$

From Eq. 4.5,

$$\frac{\partial E^*}{\partial(\delta\boldsymbol{\theta})} = \mathbf{g} + H\delta\boldsymbol{\theta}. \tag{4.10}$$

Combining Eq. 4.9 and Eq. 4.10, we obtain:

$$\delta\boldsymbol{\theta} = -H^{-1}\mathbf{g}. \tag{4.11}$$

The new solution for the unknown reservoir parameters can then be expressed as:

$$\boldsymbol{\theta} = \boldsymbol{\theta}^0 + \delta\boldsymbol{\theta}. \tag{4.12}$$

$\delta\boldsymbol{\theta}$ obtained by solving Eq. 4.11 is a only solution of the approximated objective function E^* around the initial guess vector ($\boldsymbol{\theta}^0$). In order to obtain the solution to the true objective function E, we need to solve for $\delta\boldsymbol{\theta}$ iterativelty until E^* is close to E; or in another word, $\boldsymbol{\theta}^0$ is approximately equal to $\boldsymbol{\theta}$.

Convergence problems may arise when using Newton method if the Hessian matrix is not positive definite. In order to ensure the positive definiteness of the Hessian, the second derivatives $\frac{\partial^2 F}{\partial\theta_j\partial\theta_k}$ are set to zero in the Gauss-Newton method. The Gauss-Newton method was implemented in the petroleum literature as early as the 1970's by Earlougher and Kersch (1972) and Dogru, Dixon, and Edgar (1977) and has become a common method used in well test interpretation.

Even after the Gauss-Newton modification of the second-order derivatives to ensure positive-definiteness, the Hessian matrix may still be ill-conditioned. Marquardt (1963) improved the matrix condition by adding a small constant to the diagonal elements of the Hessian matrix. This method is also known as the Levenberg-Marquardt method (Levenberg, 1944). When the Marquardt method is applied to the Gauss-Newton method, the algorithm is sometimes called Gauss-Marquardt. Rosa and Horne (1983) improved the convergence of the Gauss-Marquardt method by using an interpolation and extrapolation technique with a linear search and penalty functions described by Bard (1974) to limit the search space. Chang and Ershaghi (1986) used the Gauss-Marquardt method along with a direct search method to locate the neighborhood of a point where the objective function is minimum. Abbaszadeh and Kamal (1988) also used the Gauss-Marquardt method in their implementation of nonlinear regression analysis in well testing.

Instead of adding a constant to the diagonal elements of the Hessian, Greenstadt (1967) modified negative and/or small eigenvalues of the Hessian to improve the

matrix condition. Barua *et al.* (1988) implemented the Newton-Greenstadt method in well test analysis. In their comparison, the authors reported that the Gauss-Marquardt method was the most reliable but the eigenvalue modification method performs better when more than one parameter are ill-defined. A review and descriptions of several more nonlinear regression techniques can be found in Horne (1994a), Landa (1997) and Gill, Murray, and Wright (1983).

In this work, the Gauss-Marquardt method along with the interpolation and extrapolation with line search and penalty function was used. Therefore, only the model function and the first partial derivatives of the model function with respect to the unknown parameters need to be evaluated when calculating the gradient of the objective function and the Hessian. The nonlinear regression routine written by Anraku (1993) and Anraku and Horne (1995) was used as groundwork for the development of long-term regression analysis in this study.

4.2 Model Recognition

One of the most important steps in applying nonlinear regression is to select potential reservoir model(s). In general, the selection of the reservoir model is based on the shape of the derivatives of the pressure, as well as on geological and other related information. The idea of using the pressure derivative curves to identify the reservoir models was introduced by Bourdet *et al.* (1983) and later expanded by Bourdet, Ayoub, and Picard (1989). Reservoir flow regimes can be determined by investigating the shape of the derivative plot in both buildup and drawdown tests. Initial guesses of reservoir model parameters can be computed using the pressure data in the appropriate flow regimes. Table 3.1 summarizes the characteristics of the pressure derivative and the pressure change itself and additional distinguishing characteristics for different flow regimes. In practice, these characteristics should appear for a period of at least one log cycle in order to be interpreted as flow regimes. If they are shorter than one log cycle, they are probably due to noise or unrecorded flow fluctuations.

Table 4.1: Characteristics of pressure derivative for common flow regimes (from Economides, Hill, and Ehlig-Economides, 1994).

Flow regime	Pressure change slope	Pressure derivative slope	Additional distinguishing characteristic
Wellbore storage	1	1	early time pressure change and derivative are overlain
Finite conductivity vertical fracture	1/4	1/4	early time pressure change and derivative are offset by a factor of 4
Infinite conductivity vertical fracture	1/2	1/2	early time pressure change and derivative are offset by a factor of 2
Partial penetration	leveling off	-1/2	middle time after storage and before infinite acting
Infinite acting radial flow	increasing	0	middle time flat derivative
Dual porosity with pseudo-steady state interporosity flow	increasing, leveling off, increasing	0, dip, 0	middle time valley trend; duration is more than one log cycle
Dual porosity with transient interporosity flow	steepening	0, upward trend, 0	middle time slope doubles
Single sealing fault	steepening	0, upward trend, 0	late time slope doubles
Elongated reservoir	1/2	1/2	late time pressure change and derivative are offset by a factor of 2; slope of 1/2 occurs much earlier in the derivative
Pseudosteady state	1 for drawdown; 0 for buildup	1 for drawdown; steeply descending for buildup	late time drawdown pressure change and derivative are overlain; slope of 1 occurs much earlier in the derivative
Constant pressure boundary	0	steeply descending	cannot be distinguished from pseudosteady state in pressure buildup data

4.3 Flow History Reconstruction

Besides lacking complete information on flow rate history, there are also uncertainties associated with the measured flow rates. The levels of uncertainty in the measurements may vary from transient to transient due to changing conditions of the well and/or reservoir. In certain flow periods, the rate measured may not reflect the true flow rate at all. This can be seen from a discrepancy in the ratios of pressure change Δp and flow rate change Δq between transients. Since pressure change and flow rate has a linear relationship, the $\Delta p/\Delta q$ ratios should be consistent across transients (assuming constant reservoir properties) or at least be consistent for transients in the same neighborhood. The flow rates whose $\Delta p/\Delta q$ ratios are inconsistent with others may as well be regarded as unknowns. Using incorrect values of flow rates in the regression may lead to large errors in the estimates of reservoir parameters.

In order to solve the problem of incomplete flow rate history and uncertainty in flow rate measurement, the unknown flow rates themselves may be included as model parameters in a nonlinear regression model used to match the pressure response. The reservoir model function for a multiple rate test is written as:

$$p_{wf}(t) = p_i - \frac{141.2B\mu}{kh}\sum_{j=1}^{nq}(q_j - q_{j-1})\, p_D(t - t_{j-1})_D, t > t_{j-1} \tag{4.13}$$

where nq is the number of flow periods.

The definition of dimensionless pressure drop is:

$$p_D = \frac{2\pi kh\,(p_i - p_{wf})}{qB\mu}. \tag{4.14}$$

The dimensionless pressure drop is a solution (in dimensionless form) to the diffusion equation which describes pressure transient behavior in reservoirs. This solution is a function of reservoir parameters such as permeability k, skin factor S, wellbore storage coefficient C, etc., and takes various forms for different reservoir models. Solutions to many reservoir models are available in the Laplace domain.

To solve for model parameters from the regression in the Gauss-Marquart method, the model function and the first partial derivative of the model function with respect to each unknown parameter need to be evaluated. The model function can be computed from Eq. 4.13 after evaluating the dimensionless solutions p_D corresponding to that model. The derivatives can be computed by taking the first partial derivative of the pressure solution with respect to each reservoir model parameter. Since solutions to most reservoir models are available in the Laplace domain, the dimensionless pressure p_D is evaluated in the Laplace domain and inverted back to the time domain using a numerical Laplace inversion method proposed by Stehfest (1970a, 1970b) to compute the model function. Similarly, the derivatives with respect to reservoir model parameters can be computed in the Laplace domain and inverted back to the time domain (Rosa and Horne, 1983).

The derivatives of the model function with respect to reservoir parameters are model dependent, thus have to be evaluated on a model by model basis. Discussion of the computation for several reservoir models can be found in Anraku (1993). Here, only the description of the evaluation of the first partial derivative of pressure with respect to each unknown flow rate is presented. The derivatives with respect to the unknown flow rates are, on the other hand, model independent. From Eq. 4.13, the partial derivative of the model function with respect to unknown flow rate q_k can be expressed as:

$$\begin{aligned}
&\frac{\partial p_{wf}(t)}{\partial q_k} \\
&= \frac{141.2B\mu}{kh}\frac{\partial}{\partial q_k}\left[(q_k - q_{k-1})\, p_D(t-t_{k-1})_D + (q_{k+1} - q_k)\, p_D(t-t_k)_D\right] \quad (4.15)\\
&= \frac{141.2B\mu}{kh}\left(p_D(t-t_{k-1})_D - p_D(t-t_k)_D\right),\ t > t_{k-1}, k = 1, ..., kq \quad (4.16)
\end{aligned}$$

where kq is the number of unknown flow rates.

After evaluating the model function and the first partial derivatives with respect to each of the model parameters, the gradient of the objective function ($\mathbf{g}$) and the

Hessian matrix (H) can then be computed easily. The unknown model parameters, including the unknown flow rates, can then be estimated using the regression procedure described earlier.

4.3.1 Rate Reconstruction Constrained to a Few Known Rates

From Eq. 4.13, it is clear that permeability and flow rates are linearly dependent. If all the flow rates are unknown, there is a nonuniqueness in solutions due to the strong correlation between permeability and flow rates. The pressure response may be matched perfectly by several values of permeability by simply adjusting the flow rates. To avoid encountering nonuniqueness, some flow rates need to be known in order to constrain the regression match. Theoretically, if there exists at least one flow rate that is known to us with absolute certainty, the model parameters can be determined uniquely. This known flow rate is the flow rate that fixes the level of permeability and other parameters in the regression. In practice, a single known flow rate may not contribute sufficiently to the data matching process since the data prior to the known flow rate is not a function of the known rate at all and the data at times much after the known rate are only weak responses of the known rate. Therefore, data in these two regions can be matched with other values of model parameters as well. The most useful constraint scenario is to have known flow rates scattered among the unknown flow rates.

To demonstrate how a complete flow rate history can be retrieved using a few known rates as constraints, a simulated pressure response from a channel model is used in the least-squares regression to estimate the reservoir parameters and unknown flow rates. Fig. 4.1 depicts the simulated pressure response generated by a channel model with the model parameters and flow rate history shown in column 2 in Table 4.2. Most of the flow rates are assumed to be unknown in the regression. The initial guesses for the unknown reservoir parameters and unknown flow rates are shown in column 3 in Table 4.2. The parameters estimated from the regression are shown in column 4 in the same table. As shown in Table 4.2, the estimates for model parameters and unknown flow rates are very close to their true values reflecting the

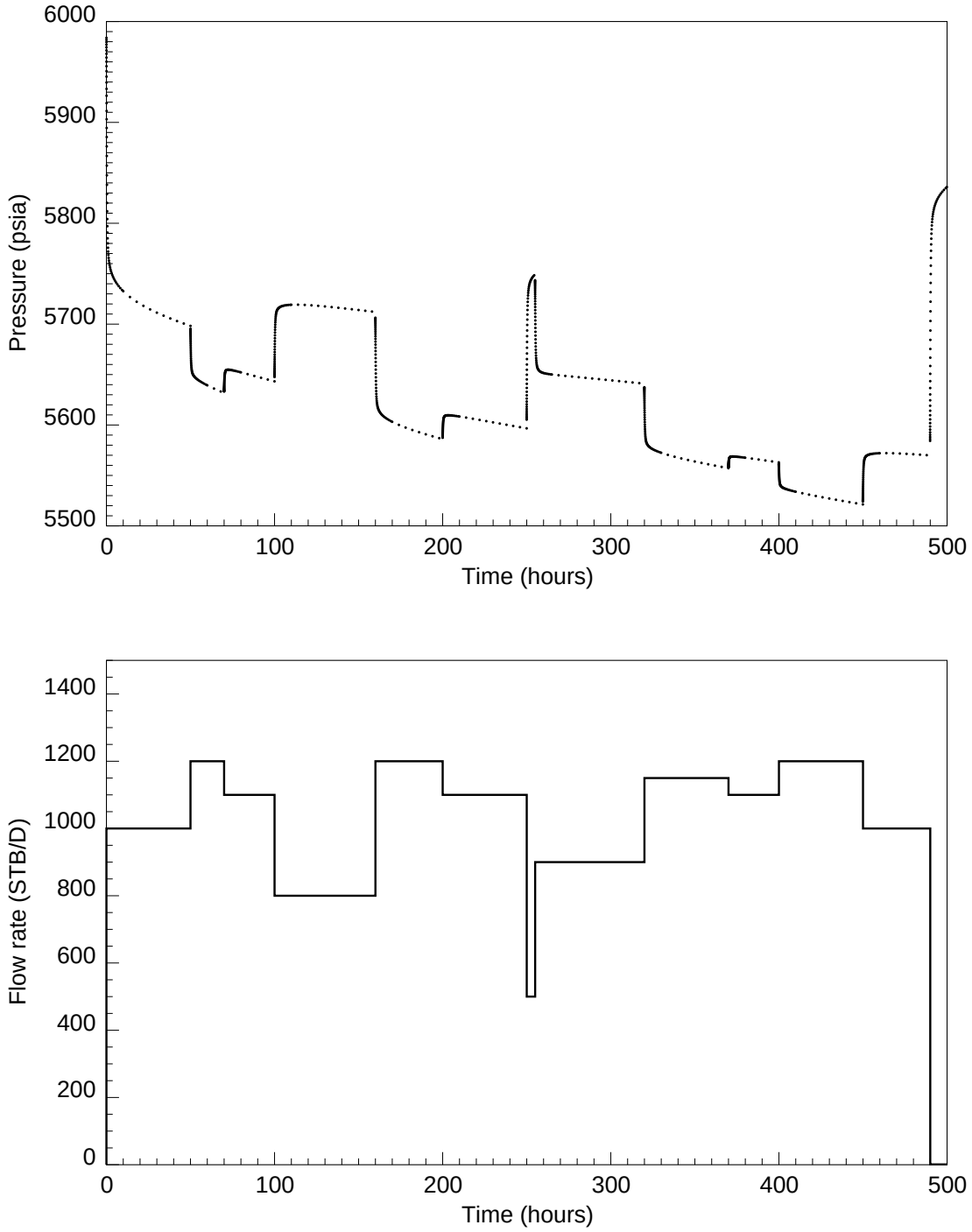

Figure 4.1: Pressure response and flow rate history for a channel model.

Table 4.2: Comparison between exact parameter values and their estimates.

Parameter	True value	Initial Guess	Estimate
Permeability (md)	100.00	50.00	100.98
Skin	3.00	-3.00	3.09
Storage (STB/psi)	0.05	0.50	0.05
r_{e_1} (ft)	500.00	400.00	500.00
r_{e_2} (ft)	1000.00	900.00	1002.86
q_1 (STB/D)	1000.00	known	known
q_2 (STB/D)	1200.00	1300.00	1199.97
q_3 (STB/D)	1100.00	1700.00	1099.96
q_4 (STB/D)	800.00	known	known
q_5 (STB/D)	1200.00	1400.00	1200.04
q_6 (STB/D)	1100.00	1000.00	1099.99
q_7 (STB/D)	500.00	700.00	499.81
q_8 (STB/D)	900.00	known	known
q_9 (STB/D)	1150.00	1000.00	1150.04
q_{10} (STB/D)	1100.00	1100.00	1100.00
q_{11} (STB/D)	1200.00	known	known
q_{12} (STB/D)	1000.00	700.00	1000.00
q_{13} (STB/D)	0.00	known	known

effectiveness of the procedure in retrieving the unknown flow rates.

This exercise was conducted using perfect pressure data and perfect values of flow rates that are known in order to prove the validity of the algorithm. The initial guesses of the flow rates are random but close to the actual values. As is often the case in nonlinear regression, initial guesses play very important roles in the convergence of the algorithm. If the initial guesses lie too far from the true solutions, the regression may converge to a wrong solution or may not converge at all. In practice, we should have good estimates of the unknown rates from the $\Delta p/\Delta q$ ratios from adjacent transients thus helping the regression converge faster and to the optimal solution.

4.3.2 Rate Reconstruction Constrained to Cumulative Production Data

Another approach to eliminate nonuniqueness in the solutions is to match the cumulative production data in addition to the pressure match. Since production data are simply the summation of fluid production in each transient, they can be used to constrain the evaluation of unknown flow rates. The objective function for nonlinear regression then becomes:

$$E = \sum_{i=1}^{n} \left[y_i - F\left(\boldsymbol{\theta}, x_i\right) \right]^2 + \sum_{i=1}^{nQ} \left[w_i - Q\left(\mathbf{q}, v_i\right) \right]^2 \tag{4.17}$$

where

v_i = time at which fluid production is recorded

w_i = production from times v_{i-1} to v_i

Q = cumulative production function

$\mathbf{q}$ = flow rates (both known and unknown)

nQ = number of production data.

The cumulative production function Q between times v_{i-1} and v_i is simply a linear combination of flow rates:

$$Q\left(v_i\right) = q_j\left(u_j - v_{i-1}\right) + q_{j+1}\left(u_{j+1} - u_j\right) + ... + q_l\left(v_i - u_{l-1}\right) \tag{4.18}$$

where

q_j = first flow rate during times v_{i-1} to v_i

u_j = time when q_j ends

q_l = last flow rate during times v_{i-1} to v_i

u_{l-1} = time when q_{l-1} starts

q_k = flow rate during time u_{k-1} to u_k, $k = j+1, j+2, ..., l-1$

Since the cumulative production function Q is only a function of flow rates, not a function of reservoir parameters, the derivatives of the cumulative production function with respect to reservoir parameters are zero. The derivatives of the cumulative production function with respect to the unknown flow rates can be expressed as:

$$\begin{aligned}
\frac{\partial Q\left(v_i\right)}{\partial q_j} &= u_j - v_{i-1} \\
\frac{\partial Q\left(v_i\right)}{\partial q_k} &= u_k - v_{k-1}, \quad k = j+1, j+2, ..., l-1 \\
\frac{\partial Q\left(v_i\right)}{\partial q_l} &= v_i - u_{l-1}
\end{aligned} \tag{4.19}$$

The same set of data as in the previous exercise was used to test the validity of this approach. In this exercise, all the flow rates are now unknown but the cumulative production data are assumed known. The cumulative production history is shown in Table 4.3. The true values and the initial guesses of the reservoir and flow rate parameters are shown in column 2 and 3 in Table 4.4, respectively. The regression was performed using the cumulative production data as constraints. The estimates of unknown parameters from the constrained regression are shown in the last column in Table 4.4. Again, the estimates of the reservoir parameters and unknown flow rates from the regression agree well with the true values. The cumulative production history was effective in constraining the regression to converge to the right solution.

The success of inferring all unknown flow rates by constraining to cumulative production history approach should not encourage engineers to stop measuring flow rates. Since this is a simulated test with perfect set of data (no noise was added), the solutions were determined with a high degree of accuracy. In practice, the flow rates are still of a great value in the interpretation. Knowing some of the flow rates, if not all, reduces uncertainty in the nonlinear regression match.

4.4 Behavioral Filtering

In long-term monitoring, the pressure data may show occasional strange behavior which does not follow the general trend. These aberrant behaviors may be caused by sudden changes in conditions and/or environment in the well and/or reservoir. The pressure gauge may record incorrect values during these sudden changes. For

Table 4.3: Cumulative production history for nonlinear regression.

Time (hours)	Cumulative production (STB)
0	0.00
96	4275.00
192	8058.33
288	12091.66
384	16329.16
480	20812.49

Table 4.4: Comparison between exact parameter values and their estimates.

Parameter	True value	Initial Guess	Estimate
Permeability (md)	100.00	50.00	100.91
Skin	3.00	-3.00	3.08
Storage (STB/psi)	0.05	0.50	0.05
r_{e_1} (ft)	500.00	400.00	490.83
r_{e_2} (ft)	1000.00	900.00	1002.52
q_1 (STB/D)	1000.00	800.00	1000.01
q_2 (STB/D)	1200.00	1300.00	1199.97
q_3 (STB/D)	1100.00	1700.00	1099.96
q_4 (STB/D)	800.00	900.00	800.00
q_5 (STB/D)	1200.00	1400.00	1200.01
q_6 (STB/D)	1100.00	1000.00	1100.02
q_7 (STB/D)	500.00	700.00	499.94
q_8 (STB/D)	900.00	800.00	899.97
q_9 (STB/D)	1150.00	1000.00	1150.02
q_{10} (STB/D)	1100.00	1300.00	1100.00
q_{11} (STB/D)	1200.00	1000.00	1200.01
q_{12} (STB/D)	1000.00	700.00	1000.00
q_{13} (STB/D)	0.00	0.00	0.10

example, if the temperature changes rapidly, the pressure gauge may record spurious information. Sometimes, these aberrant measurements may be caused by the malfunction of the pressure gauge or the pressure acquisition system themselves. In any case, these aberrant behaviors are not the true response from the reservoir; therefore, they should not be included in the interpretation. Excluding these transients from the analysis should reduce the uncertainty of the regression match and hence provide better estimates of the reservoir model parameters. The process of eliminating these aberrant transient is called *behavioral filtering*.

One measure that can be used to determine the goodness of fit of each transient is the variance between the regression match and the data. The variances of the aberrant transients are generally unusually high due to the fact that they are not well matched by the regression. To determine these aberrant transients, first the variance, which is the sum of the squares of the difference between the measurement and the model response divided by the number of data point, is calculated for each transient. The transient with the maximum variance can then be identified and excluded from the calculation of the average variance of the overall data to eliminate the influence that the most poorly fitted transient may have on the determination of the goodness of fit. Then, the variance of each transient including the one with the maximum variance is compared with the average variance. In this study, the transients whose variances are at least three times higher than the average variance are considered aberrant transients and hence excluded from the analysis. After the aberrant transients are eliminated, the regression is run again to compute new solutions. The new variances for the transients are then compared again with the new average variance. Generally, the quality of the second match is better than the previous one, i.e., the new average variance is less than the previous average variance. Using the same variance criteria, more aberrant transients may be eliminated in this second iteration. This process may be repeated until there are no more transients to eliminate.

To show how the approach works, a test case was conducted using a slightly different pressure response from the previous two cases. In this exercise, errors were

Table 4.5: Comparison between parameter estimates before and after behavioral filtering.

Parameter	Value	First estimate	Final estimate
Permeability (md)	100.00	126.38	98.93
Skin	3.00	5.14	2.91
Storage (STB/psi)	0.05	0.0555	0.0502
r_{e_1} (ft)	500.00	384.55	531.97
r_{e_2} (ft)	1000.00	1028.67	975.08

added to two transients at times 100-160 hours and 400-450 hours. The flow rate data are the same as the ones shown in Table 4.2. Most of the flow rates are not known. Cumulative production data were assumed to be unavailable in this example. The regression with the implementation of the variance test was run on the data. The first regression match to the simulated pressure is shown in Fig. 4.2. The aberration in the pressure behaviors can be seen from the unmatched model response. The parameters estimated in the first regression are shown in column 3 in Table 4.5. Due to the two aberrant transients, the estimates of the model parameters are quite poor. The variance for each individual transient and the average variance are shown in Table 4.6 for each iteration step. After eliminating the aberrant transients from the regression analysis, the quality of the match is better in the second iteration. Thus, the average variance becomes smaller. As seen in Table 4.6, the average variance reduces from 9.06 in the first iteration to 0.58 in the second iteration. At the second iteration, the variances for all the remaining transients are small. None of them is three times higher than the average variance. Therefore, the regression stops at this iteration. Fig.4.3 shows the final match from the regression to the all the transients. The estimates of model parameters from the final regression match are shown in column 4 in Table 4.5. The estimates of the final match are improved considerably over those from the original match reflecting the effectiveness of the behavioral filtering process.

Table 4.6: Variances at each iteration during behavioral filtering.

Transient	Time period	Iteration 1	Iteration 2
1	0-50	4.94	0.67
2	50-70	0.54	0.43
3	70-100	0.57	0.55
4	100-160	89.44	excluded
5	160-200	0.69	0.57
6	200-250	1.07	0.86
7	250-255	0.68	0.13
8	255-320	26.45	0.70
9	320-370	0.77	0.62
10	370-400	0.60	0.54
11	400-450	45.01	excluded
12	450-490	1.04	0.65
13	490-500	1.03	0.40
Average	0-500	9.06	0.58

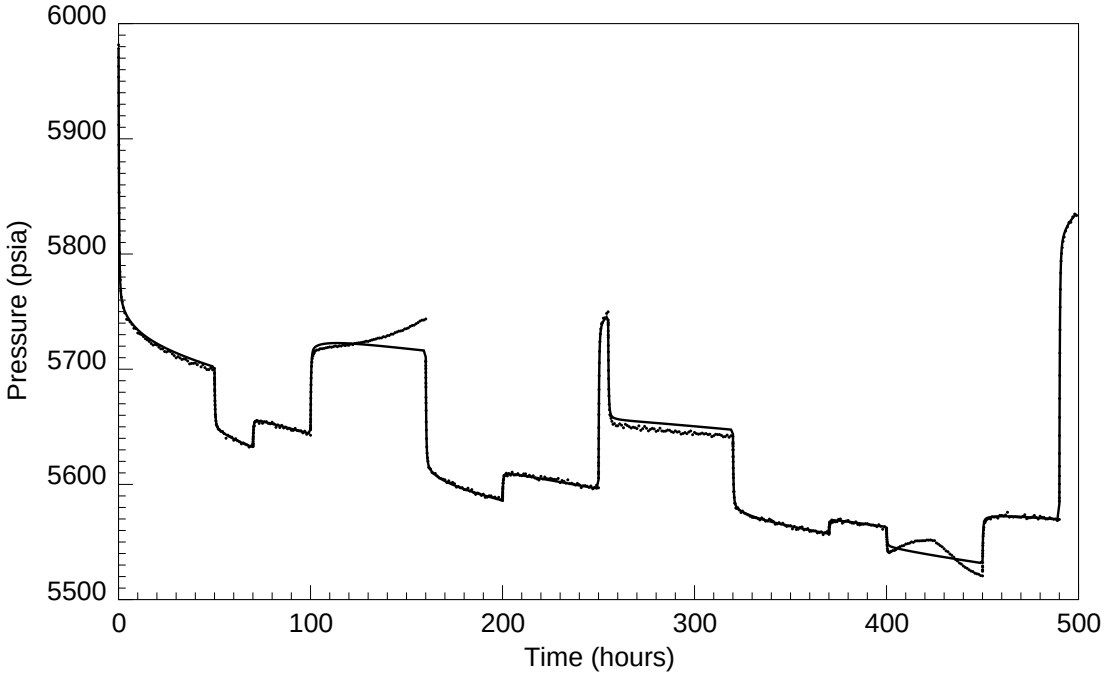

Figure 4.2: First regression match to the simulated pressure response.

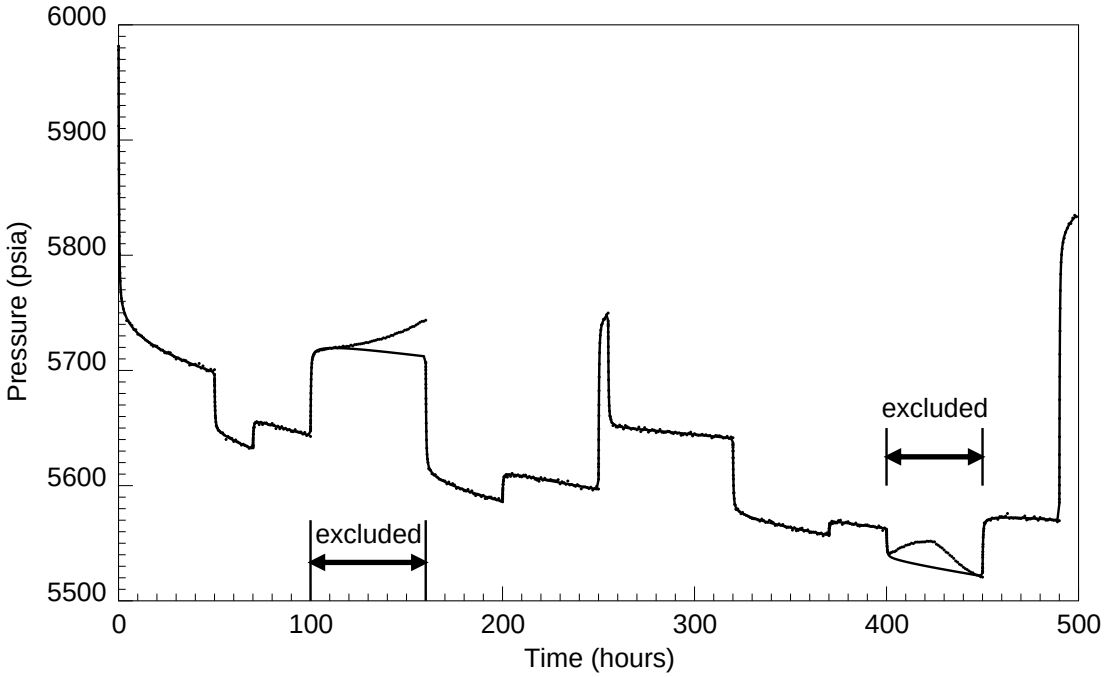

Figure 4.3: Final regression match to the simulated pressure response.

Chapter 5

Moving-Window Based Interpretation

The use of moving window analysis for a long-term analysis is introduced in this chapter. Several simulated case studies are used to study how the moving window algorithm behaves when there is a temporal change of reservoir parameter, specifically, changes in permeability and skin factor. Then, two field examples with different reservoir characteristics are analyzed. The discussion of presenting the parameter estimates in terms of possible ranges of solutions or parameter distributions is presented in these two examples.

5.1 Moving Window Analysis

As mentioned before, the reservoir properties/environment may change as the fluid is being produced from the reservoir. Due to the possibility that reservoir conditions may vary, the data should not be analyzed all at once. Sections of data should be analyzed locally to determine local values of reservoir parameters. If all the flow rates are known, each transient can be analyzed separately using local values of reservoir and fluid properties. The total pressure change in a transient can be computed by superimposing the responses due to previous flow rate changes with the response due to the current rate change. Reservoir model parameters can be determined by

matching the calculated pressure and the measurements. However, this traditional pressure transient analysis cannot be used when some of the flow rates are unknown. Each transient cannot be analyzed independently because of the unknown flow rates. A few transients need to be grouped together such that there is at least one known flow rate within the group. The known flow rates are used as constraints to reconstruct the flow rate history as described in Section 4.3 in the previous chapter. Cumulative production data can also be used to constraint the regression match in addition to the known rates.

The data in the transients that are grouped together form a window of data. Then, we can run regression with the parameterization of flow rates as unknown to concurrently determine reservoir parameters, reconstruct flow rate history, and eliminate the aberrant transients using the approach described in the previous chapter. After estimating the unknown parameters in the window, the analysis is moved forward to a new window. The starting point for the new window may lie within the span of the old window. Local unknown parameters such as unknown flow rates are updated before moving on to subsequent windows. These local unknowns are parameters that cannot be inferred with high certainty from the response in later windows. For this reason, they are estimated within the window of analysis and assumed known in subsequent windows. The steps in the moving window analysis are summarized as follows:

1. Choose a window size and translation length, i.e., the number of hours of data to be analyzed and the time length to shift the window forward.
2. Run regression on the selected data window to determine reservoir model parameters as well as unknown flow rates.
3. Eliminate the aberrant transients in the selected data window iteratively as described in Section 4.4.
4. Before moving to the next data window, update (unknown) flow rates that happen prior to the starting time of the new window.

5. Interpret data in the new window. The new window may overlap the previous one.

5.2 Temporal Change of Reservoir Parameter

In order to illustrate the use of the moving window analysis to account for temporal changes in model parameters, two sets of simulated tests were designed. The first set of examples investigates the effect of the temporal changes in permeability on the estimates of model parameters. In practice, the reservoir permeability may change during the production cycle. For instance, the permeability may be reduced due to formation compaction which is caused by the decline in reservoir pressure. The second set of experiments was designed to study the effect of the changes in the skin factor on the estimates of model parameters. In general, the skin factor may not be constant for over a long period of time. The wellbore may be exposed to a higher degree of formation damage since sand, asphalt deposits, or clay particles may plug the pores near the wellbore as the fluid flows into the well. In this case, the skin factor may be gradually increasing.

In all the examples in this section, the flow rates were assumed known for every other flow period, i.e., the first flow rate is known and the second one is unknown and so on. The well flow rate was altered every 100 hours as shown in Fig. 5.1. The reservoir and fluid properties used to generate pressure response are tabulated in Table 5.1. Data were generated without any noise or aberrant behaviors in order to exclude additional uncertainties in the parameter estimates using three different reservoir models. Each test lasts for 3000 hours. A window size of 200 hours and a translation length of 100 hours were chosen. Using this configuration, the first window starts at time $t = 0$ and ends at time $t = 200$ hours. The second window starts at time $t = 100$ hours and ends at time $t = 300$ hours. The window keeps moving in this fashion until the last window ends at time $t = 3000$ hours.

Table 5.1: Reservoir and fluid properties.

Property	Value
Porosity	0.2
Formation thickness (ft)	100
Well radius (ft)	0.35
Formation volume factor	1.2
Total compressibility (psi^{-1})	5.0e-6
Viscosity (cp)	1.5

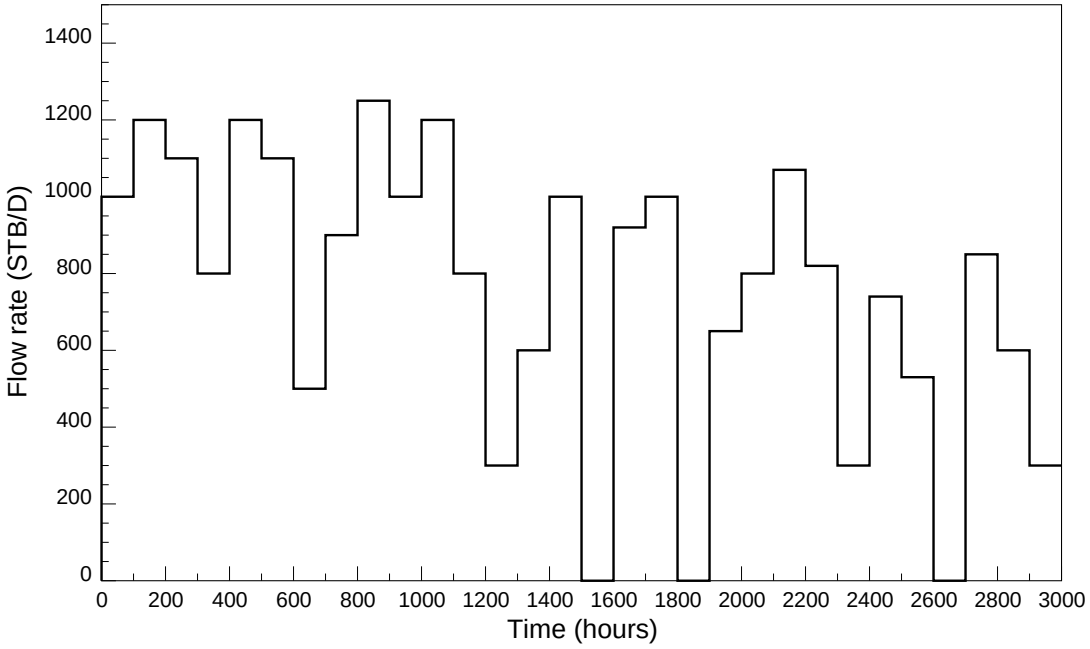

Figure 5.1: Flow rate history.

5.2.1 Case 1: Semicontinuous Changes of Permeability

This first set of examples was designed to show the use of the moving window analysis to account for changes in permeability as a function of time. In this case, the permeability decreases at a rate of 0.05 md every 10 hours in a small step function manner as shown in Fig. 5.2. Thus, there are ten small permeability changes within each 100-hour transient and twenty step changes in each 200-hour window. The initial value of permeability was chosen as 300 md. The pressure response for each 10-hour period was generated using the local value of permeability in that particular period. For example, the pressure responses due to previous and current flow rate changes at time 400-410 hours was generated using the permeability of 298.0 md, which is the permeability during times $t = 400$ and $t = 410$ (see Fig. 5.2). Three reservoir models were used as examples: infinite acting, closed circular boundary, and channel reservoirs.

Example 1A: Infinite Acting Reservoir

In the first test, we studied the effect of the changes in permeability in an infinite-acting reservoir. Although there is no infinite-acting reservoir in reality, the test can be used to study the effects of varying permeability on the estimates of reservoir model parameters. The pressure response for an infinite-acting reservoir shown in Fig. 5.3 was generated using the permeability function displayed in Fig. 5.2, skin factor of 3, wellbore storage coefficient of 0.05 STB/psi, and initial pressure of 6000.0 psi. Initial guesses for these model parameters are shown in the first row in Table 5.2. Also shown in Table 5.2 are the estimates of the model parameters from the analysis for each moving window. The initial guesses of the unknown flow rates and their estimates are tabulated in Table 5.3. Fig. 5.4 plots the permeability estimates as a function of time at the middle of each window.

Although no noise was added to the data, there is still a small degree of uncertainty associated with the estimates of permeability due to the fact that the permeability is

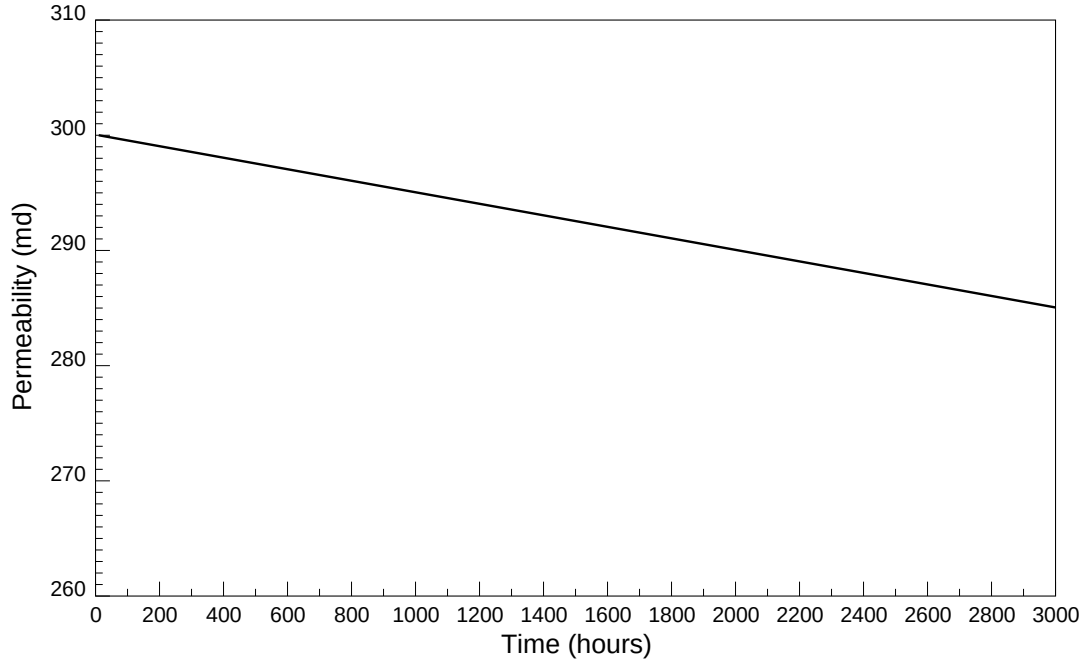

Figure 5.2: Permeability profile.

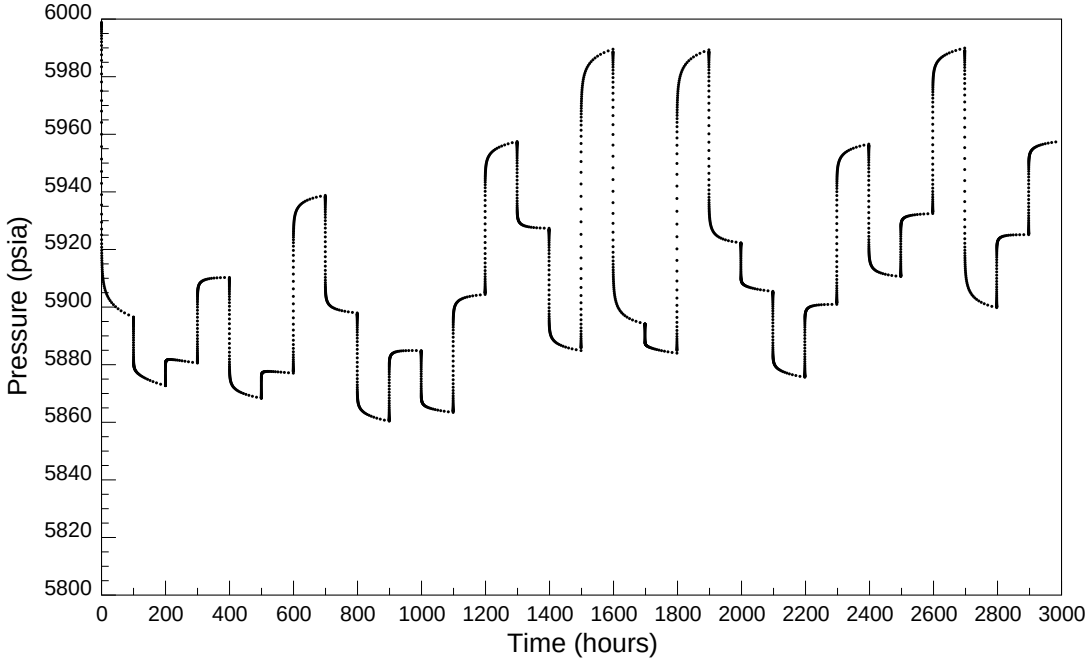

Figure 5.3: Pressure response from an infinite acting reservoir.

Table 5.2: Parameter estimates for an infinite acting reservoir.

Window	Time period	Permeability	Skin	Storage	Initial pressure
-	Initial guess	100.00	0.00	0.0010	6000.00
-	True	-	3.00	0.0500	6000.00
1	0.- 200.	297.59	2.93	0.0498	6000.02
2	100.- 300.	292.04	2.73	0.0497	6000.14
3	200.- 400.	303.10	3.08	0.0510	5999.16
4	300.- 500.	299.75	2.99	0.0500	5999.54
5	400.- 600.	290.92	2.81	0.0496	6000.77
6	500.- 700.	298.71	3.06	0.0504	5999.96
7	600.- 800.	300.68	3.03	0.0505	5998.82
8	700.- 900.	295.07	2.84	0.0503	5999.09
9	800.-1000.	287.82	2.86	0.0493	6001.68
10	900.-1100.	293.64	3.08	0.0491	6001.24
11	1000.-1200.	295.74	2.93	0.0508	5999.15
12	1100.-1300.	299.93	3.09	0.0508	5998.86
13	1200.-1400.	296.66	3.03	0.0503	5999.36
14	1300.-1500.	292.14	2.87	0.0502	5999.59
15	1400.-1600.	292.25	2.97	0.0502	6000.02
16	1500.-1700.	292.45	2.99	0.0501	6000.01
17	1600.-1800.	289.15	2.92	0.0498	6000.12
18	1700.-1900.	289.88	3.00	0.0500	6000.49
19	1800.-2000.	291.84	3.04	0.0500	5999.93
20	1900.-2100.	287.73	2.91	0.0498	6000.11
21	2000.-2200.	282.42	2.78	0.0493	6000.73
22	2100.-2300.	284.37	2.85	0.0499	6000.54
23	2200.-2400.	292.00	3.09	0.0505	5999.65
24	2300.-2500.	289.51	3.02	0.0501	5999.86
25	2400.-2600.	283.74	2.89	0.0498	6000.34
26	2500.-2700.	288.21	3.05	0.0502	6000.02
27	2600.-2800.	284.59	2.98	0.0497	6000.48
28	2700.-2900.	283.14	2.93	0.0497	6000.51
29	2800.-3000.	290.44	3.14	0.0505	5999.60

Table 5.3: Estimates of unknown flow rates for an infinite acting reservoir.

Flow period	True value	Initial guess	Final estimate
100.- 200.	1000.00	800.00	999.25
300.- 400.	1100.00	900.00	1100.73
500.- 600.	1200.00	1300.00	1198.89
700.- 800.	500.00	300.00	494.98
900.-1000.	1250.00	1050.00	1246.04
1100.-1200.	1200.00	1100.00	1202.69
1300.-1400.	300.00	100.00	297.22
1500.-1600.	1000.00	900.00	1000.90
1700.-1800.	920.00	620.00	919.25
1900.-2000.	0.00	100.00	0.01
2100.-2200.	800.00	900.00	799.92
2300.-2400.	820.00	620.00	820.65
2500.-2600.	740.00	900.00	738.82
2700.-2800.	0.00	100.00	3.61

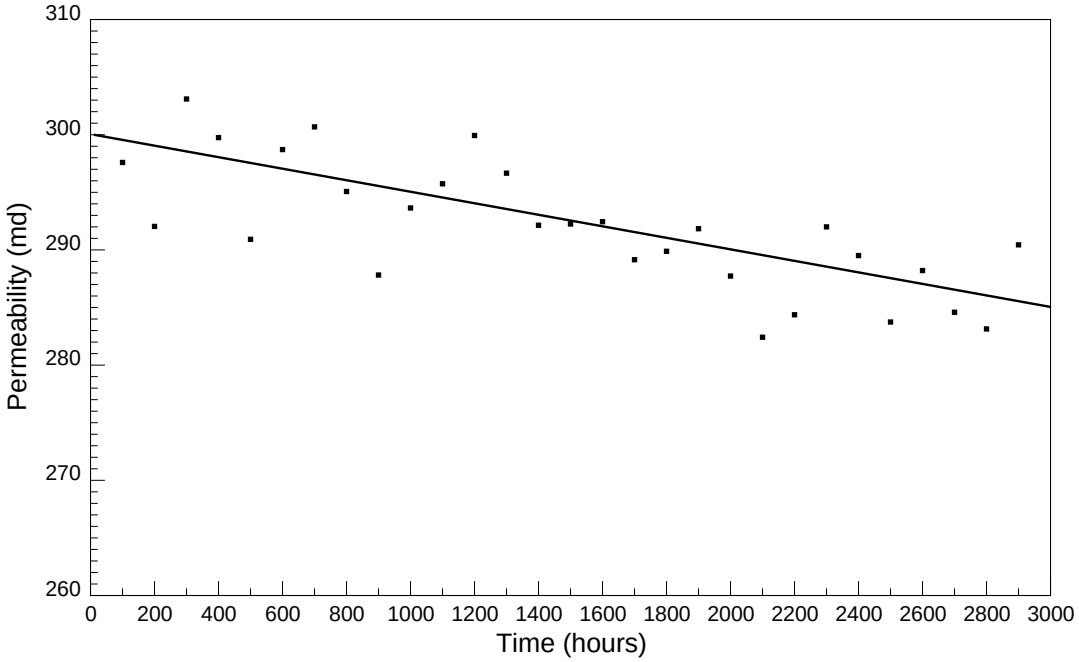

Figure 5.4: Permeability estimates for an infinite acting reservoir.

not constant. As mentioned earlier, there are twenty small step changes of permeability in each 200-hour window. The pressure data in each 10-hour period are responses to different values of permeability. The regression sees these inconsistent responses as noise in the data values. Therefore, the estimates of permeability from the regression contain a certain amount of uncertainty. Since the skin factor is strongly correlated with permeability, the skin estimates possess a similar degree of uncertainty. The estimates of wellbore storage coefficient and initial reservoir pressure are however minimally affected by the temporal changes in the permeability value. Also, the estimates for the unknown flow rates are very close to the their true values as seen in Table 5.3.

Example 1B: Closed Circular Boundary Reservoir

A second experiment was conducted using a closed circular boundary model. Fig. 5.5 shows the pressure response of a closed boundary reservoir generated by the same values of permeability, skin, wellbore storage, and initial pressure as those in the infinite acting case and a distance to the boundary of 3000 feet. Initial guesses for reservoir model parameters are shown in the first row in Table 5.4, and initial guesses for unknown flow rate parameters are shown in column 3 in Table 5.5. The estimates of reservoir parameters and the unknown flow rates from the moving window analysis are tabulated in Table 5.4 and Table 5.5, respectively. Fig. 5.6 plots the estimates of permeability as a function of time at the middle of each window.

The uncertainty associated with the estimates of permeability is much smaller than the one in the infinite acting reservoir. Although the pressure data are responses to twenty step changes in the value of permeability, the data that contribute most to the estimation of the permeability are the pressure responses that occur after the dominance of the wellbore storage effect and prior to the boundary effect. In this example, the time when the boundary is reached was estimated to be 53.6 hours. Therefore, the last 46.4 hours of data in each flow period are dominated by the boundary effect. Consequently, data in the last four step changes in each flow period

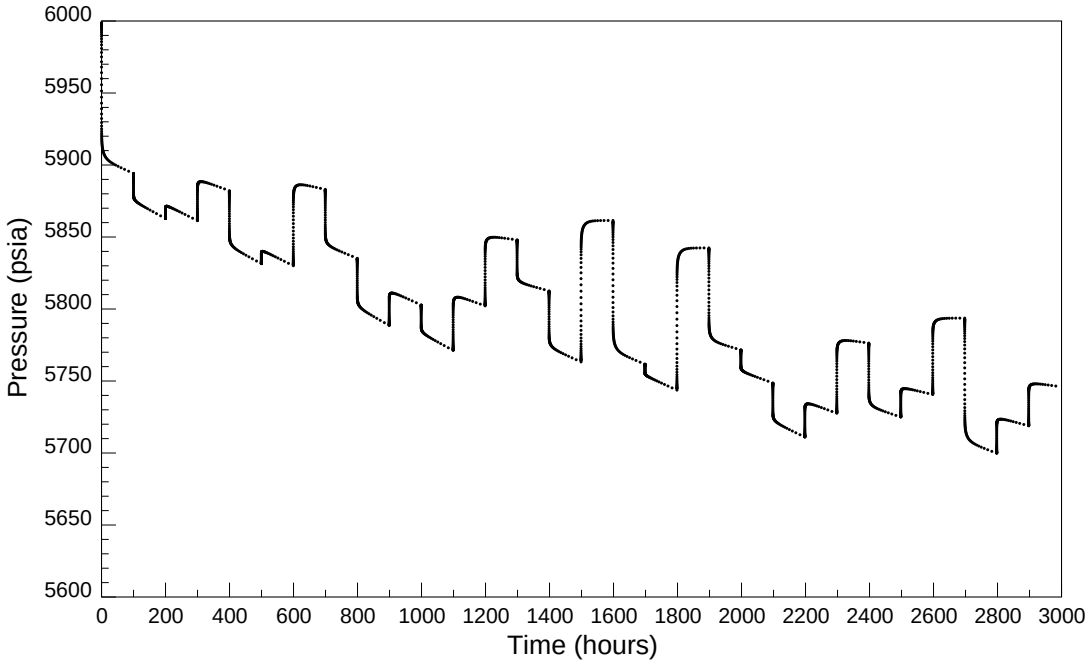

Figure 5.5: Pressure response for a closed circular boundary reservoir.

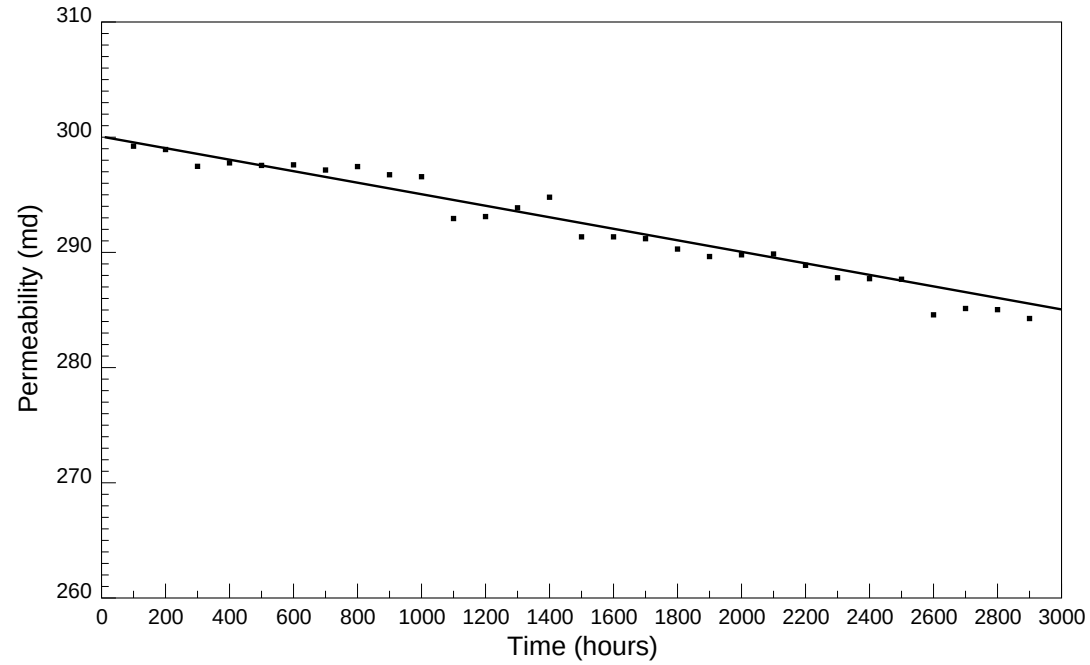

Figure 5.6: Permeability estimates for a closed circular boundary reservoir.

Table 5.4: Parameter estimates for a closed circular boundary reservoir.

Window	Time period	Permeability	Skin	Storage	r_e	Initial pressure
-	Initial guess	100.00	0.00	0.0010	1000.00	6000.00
-	True	-	3.00	0.0500	3000.00	6000.00
1	0.- 200.	299.22	2.98	0.0499	2971.13	6000.01
2	100.- 300.	298.93	2.97	0.0501	2974.71	5999.98
3	200.- 400.	297.47	2.97	0.0500	2975.50	6000.52
4	300.- 500.	297.77	2.98	0.0500	2976.62	6000.49
5	400.- 600.	297.55	2.98	0.0500	2973.99	6000.61
6	500.- 700.	297.60	2.98	0.0502	2975.57	6000.53
7	600.- 800.	297.15	2.97	0.0501	2976.21	6000.65
8	700.- 900.	297.45	2.98	0.0502	2972.12	6000.82
9	800.-1000.	296.74	2.97	0.0503	2975.41	6000.73
10	900.-1100.	296.57	2.96	0.0504	2976.82	6000.61
11	1000.-1200.	292.94	2.97	0.0498	2973.73	6002.14
12	1100.-1300.	293.11	2.98	0.0499	2975.24	6002.02
13	1200.-1400.	293.87	2.97	0.0501	2976.33	6001.70
14	1300.-1500.	294.79	3.00	0.0502	2967.41	6002.42
15	1400.-1600.	291.35	2.98	0.0499	2971.21	6002.64
16	1500.-1700.	291.35	2.98	0.0499	2979.99	6001.84
17	1600.-1800.	291.19	2.98	0.0499	2969.62	6002.82
18	1700.-1900.	290.29	2.98	0.0500	2976.25	6002.47
19	1800.-2000.	289.64	2.96	0.0499	2953.84	6004.90
20	1900.-2100.	289.79	2.98	0.0500	2969.07	6003.27
21	2000.-2200.	289.86	3.00	0.0500	2971.34	6003.14
22	2100.-2300.	288.88	2.97	0.0501	2972.64	6003.02
23	2200.-2400.	287.80	2.97	0.0500	2974.39	6003.23
24	2300.-2500.	287.72	2.97	0.0500	2974.98	6003.17
25	2400.-2600.	287.67	2.97	0.0501	2971.84	6003.59
26	2500.-2700.	284.58	2.92	0.0498	2951.65	6006.77
27	2600.-2800.	285.13	2.98	0.0498	2978.65	6003.15
28	2700.-2900.	285.03	2.97	0.0499	2969.01	6004.52
29	2800.-3000.	284.26	2.95	0.0499	2970.64	6004.36

Table 5.5: Estimates of unknown flow rates for a closed circular boundary reservoir.

Flow period	True value	Initial guess	Final estimate
100.- 200.	1000.00	800.00	999.79
300.- 400.	1100.00	900.00	1100.09
500.- 600.	1200.00	1300.00	1200.34
700.- 800.	500.00	300.00	498.07
900.-1000.	1250.00	1050.00	1251.91
1100.-1200.	1200.00	1100.00	1199.13
1300.-1400.	300.00	100.00	298.80
1500.-1600.	1000.00	900.00	998.73
1700.-1800.	920.00	620.00	919.94
1900.-2000.	0.00	100.00	0.00
2100.-2200.	800.00	900.00	799.81
2300.-2400.	820.00	620.00	820.27
2500.-2600.	740.00	900.00	740.82
2700.-2800.	0.00	100.00	1.93

do not contribute much to the estimation of the permeability. Therefore, the regression sees less uncertainty in the data as far as permeability estimation is concerned. There is also less uncertainty in the estimates for the skin factor due to the strong correlation between skin factor and permeability. Since the distance to the boundary is also correlated with permeability, there is a small amount of uncertainty associated with the estimates for the distance to the boundary. The estimates of wellbore storage coefficient, initial reservoir pressure, and unknown flow rates are again minimally affected by the changes in the permeability value.

Example 1C: Channel Reservoir

In this experiment, the effect of the temporal changes of permeability on the estimates of reservoir parameters for a channel reservoir was investigated. Shown in Fig. 5.7 is the pressure response of a channel reservoir using the same values of permeability, skin, wellbore storage and initial pressure as in the infinite acting case and distances to the boundaries of 1000 and 3000 feet. Initial guesses for reservoir model parameters and unknown flow rate parameters are shown in the first row in

Table 5.6 and the third column in Table 5.7, respectively. The estimates of reservoir parameters for each window from the moving window analysis are depicted in Table 5.6. The estimates of the unknown flow rates are tabulated in Table 5.7. Fig. 5.8 plots the estimates of permeability as a function of time at the middle of each window. The estimates of the distances to the boundaries are plotted in Figs. 5.9 and 5.10.

The level of uncertainty associated with the estimates of permeability is similar to that in Example 1B. As in the previous example, the data that contribute most to the estimation of permeability are the ones in the middle of each flow period, i.e., the measurements between the end of wellbore storage effect and the beginning of the boundary effect. Consequently, the regression sees less effect of changes in the permeability; thus, less uncertainty in the data. Again, the estimates for the skin factor are also good due to the strong correlation between skin factor and permeability. The estimates for the distance to the first boundary have small amount of uncertainty but the estimates for the further boundary are quite poor. In general, it is more difficult to estimate the second boundary than the first one since the response due to the second boundary may be marred by the response due to the first boundary. For this reason, the quality of the estimates for the further boundaries is poorer than the one for the first boundary. As in the previous two examples, the temporal change in the permeability value hardly affects the estimates for wellbore storage coefficient, initial reservoir pressure, and unknown flow rates.

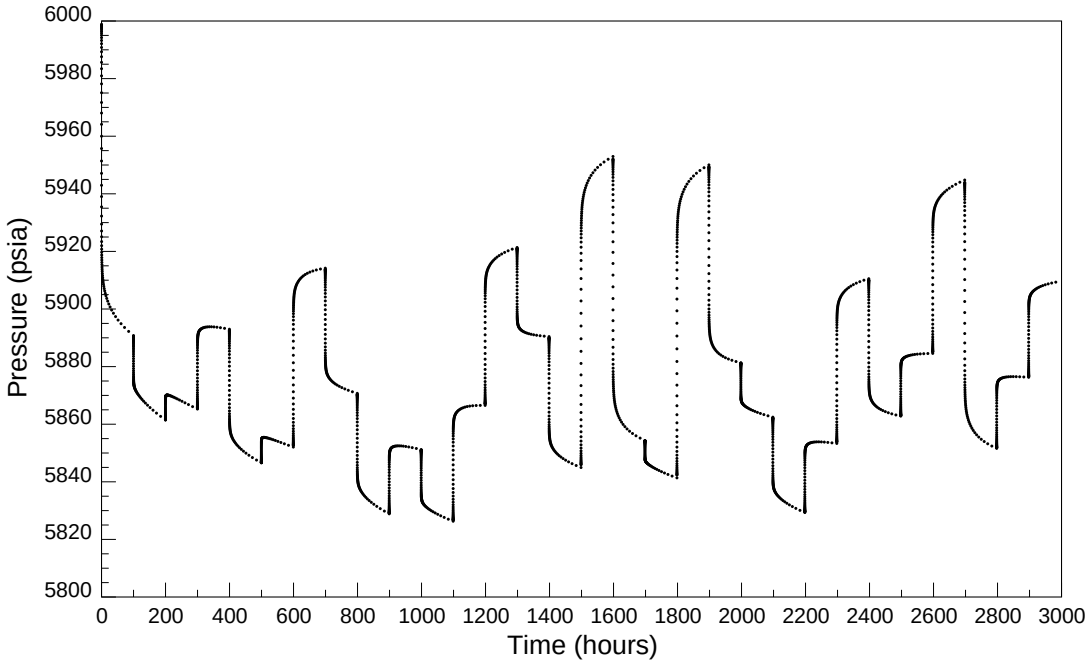

Figure 5.7: Pressure response for a channel reservoir.

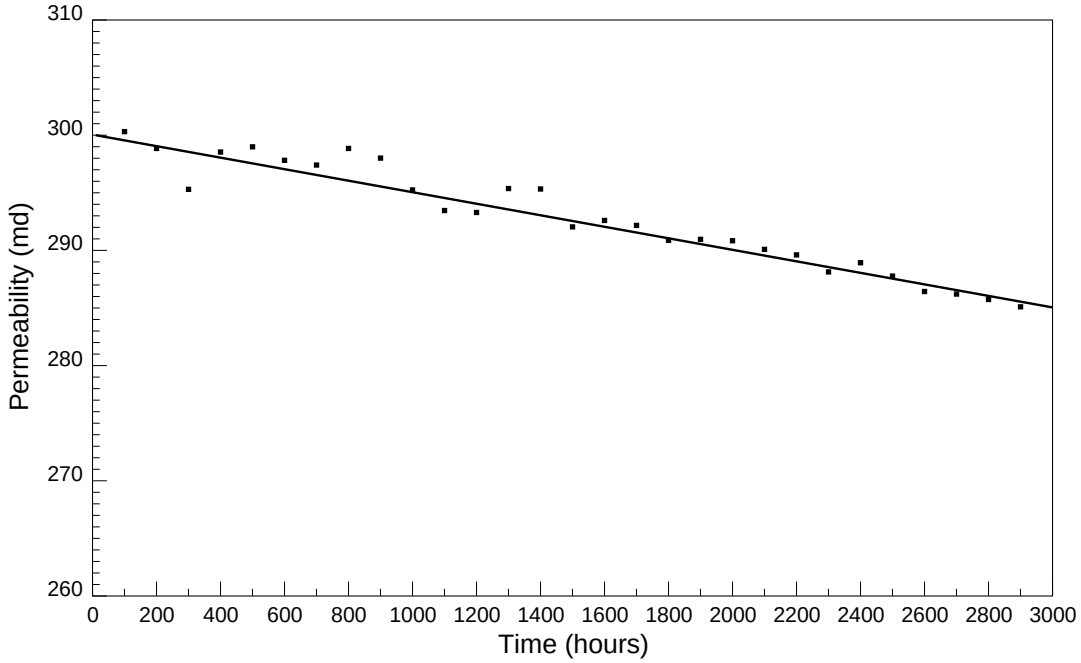

Figure 5.8: Permeability estimates for a channel reservoir.

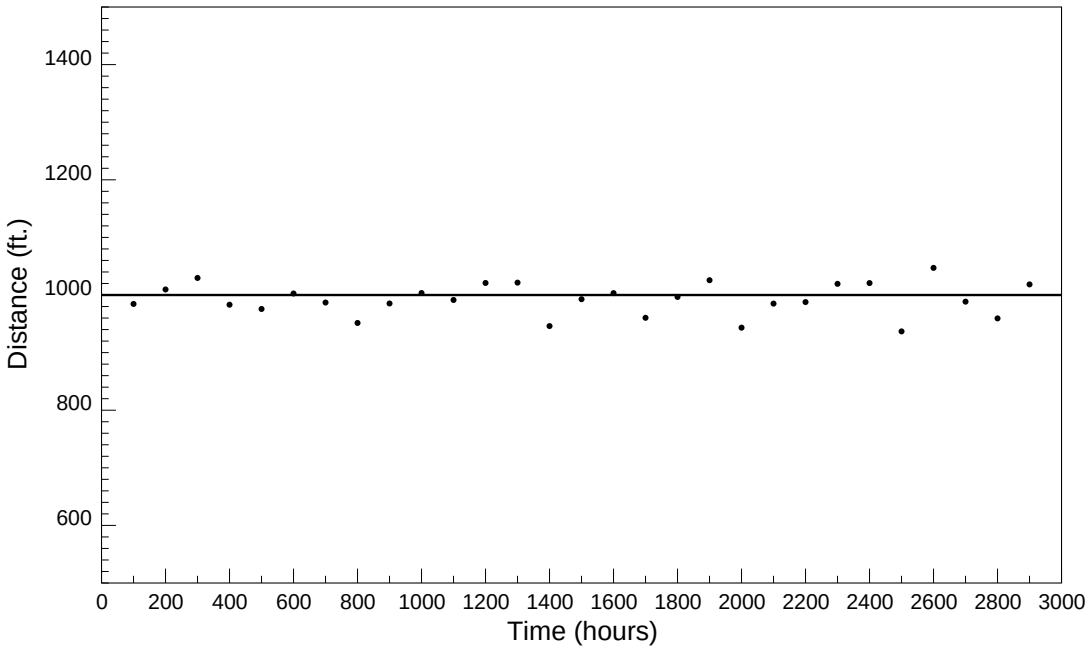

Figure 5.9: Estimate of distance to the first boundary in a channel reservoir.

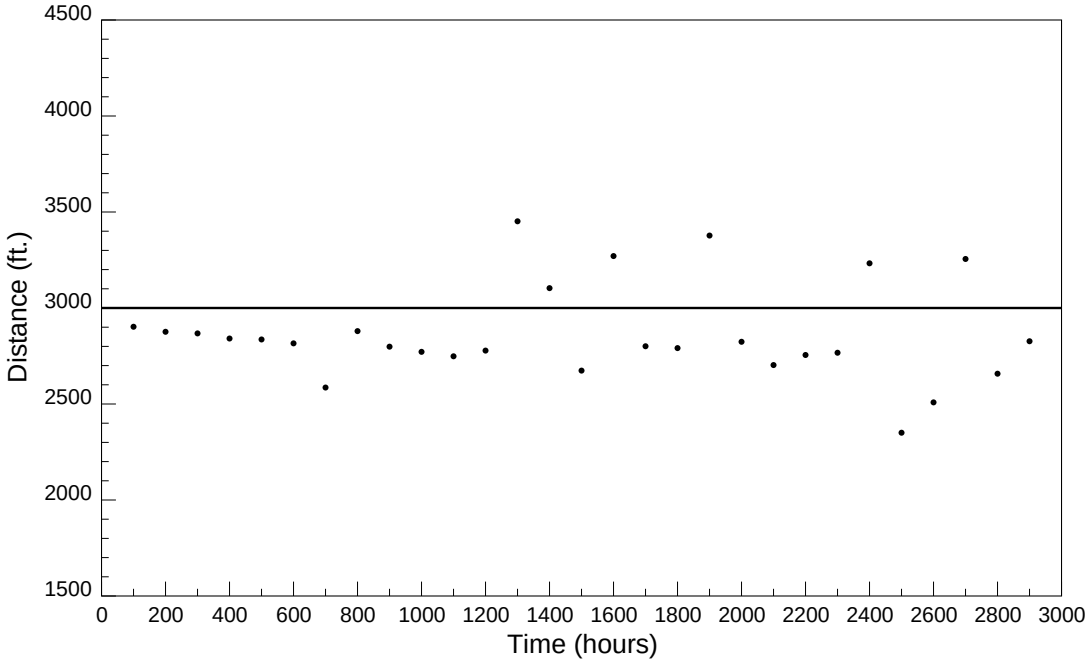

Figure 5.10: Estimate of distance to the second boundary in a channel reservoir.

Table 5.6: Parameter estimates for a channel reservoir.

Window	Time period	Permeability	Skin	Storage	r_{e1}	r_{e2}	Initial pressure
-	Initial guess	100.00	0.00	0.0010	500.00	1000.00	6000.00
True			3.00	0.0500	1000.00	3000.00	6000.00
1	0.- 200.	300.31	3.01	0.0500	984.50	2902.31	6000.00
2	100.- 300.	298.85	2.96	0.0500	1009.62	2876.10	5999.92
3	200.- 400.	295.30	2.90	0.0499	1029.61	2867.71	6000.54
4	300.- 500.	298.54	3.00	0.0500	983.16	2841.04	6000.91
5	400.- 600.	298.99	3.02	0.0501	975.76	2836.10	6000.99
6	500.- 700.	297.82	2.99	0.0502	1002.60	2815.85	6000.92
7	600.- 800.	297.41	2.98	0.0502	986.96	2585.74	6003.28
8	700.- 900.	298.85	3.02	0.0502	951.49	2879.59	6000.83
9	800.-1000.	298.01	3.01	0.0503	985.31	2798.60	6001.24
10	900.-1100.	295.25	2.92	0.0503	1003.45	2771.68	6001.59
11	1000.-1200.	293.46	2.99	0.0499	991.39	2748.47	6003.43
12	1100.-1300.	293.29	2.99	0.0499	1020.91	2778.17	6002.50
13	1200.-1400.	295.37	3.01	0.0502	1021.48	3451.58	5994.76
14	1300.-1500.	295.33	3.01	0.0502	946.07	3103.45	5999.09
15	1400.-1600.	292.04	2.99	0.0499	992.72	2673.92	6004.30
16	1500.-1700.	292.60	3.01	0.0500	1003.30	3270.52	5997.02
17	1600.-1800.	292.17	3.01	0.0500	960.43	2800.77	6002.90
18	1700.-1900.	290.87	3.00	0.0500	996.66	2791.17	6002.79
19	1800.-2000.	290.96	3.01	0.0500	1025.70	3377.36	5995.47
20	1900.-2100.	290.84	3.01	0.0500	943.29	2824.05	6002.99
21	2000.-2200.	290.09	3.02	0.0499	985.07	2702.84	6004.16
22	2100.-2300.	289.61	3.00	0.0501	987.73	2755.27	6003.38
23	2200.-2400.	288.13	2.98	0.0500	1019.40	2767.00	6003.09
24	2300.-2500.	288.93	3.00	0.0500	1020.72	3232.76	5996.51
25	2400.-2600.	287.77	2.98	0.0501	936.83	2350.41	6012.31
26	2500.-2700.	286.43	2.97	0.0501	1047.10	2508.46	6007.00
27	2600.-2800.	286.21	3.02	0.0498	988.46	3255.37	5997.17
28	2700.-2900.	285.74	3.01	0.0499	959.39	2657.80	6006.16
29	2800.-3000.	285.10	2.98	0.0500	1018.41	2826.85	6000.53

Table 5.7: Estimates of unknown flow rates for a channel reservoir.

Flow period	True value	Initial guess	Final estimate
100.- 200.	1000.00	800.00	999.77
300.- 400.	1100.00	900.00	1100.04
500.- 600.	1200.00	1300.00	1200.37
700.- 800.	500.00	300.00	497.54
900.-1000.	1250.00	1050.00	1251.93
1100.-1200.	1200.00	1100.00	1199.07
1300.-1400.	300.00	100.00	298.50
1500.-1600.	1000.00	900.00	999.08
1700.-1800.	920.00	620.00	919.89
1900.-2000.	0.00	100.00	0.00
2100.-2200.	800.00	900.00	799.92
2300.-2400.	820.00	620.00	820.22
2500.-2600.	740.00	900.00	740.63
2700.-2800.	0.00	100.00	2.55

5.2.2 Case 2: Semicontinuous Changes of Skin Factor

This set of examples was designed to illustrate the use of the moving window analysis to account for temporal changes in the skin factor. In this case, the skin increases at a rate of 0.01 every 10 hours in a small step function fashion as shown in Fig. 5.11. Similar to Case 1, there are ten small changes for the values of skin factor within each 100-hour transient and twenty step changes in each 200-hour window. The pressure response for each 10-hour period was generated using the local value of skin factor in that period. For example, the pressure responses due to previous and current flow rate changes at time 400-410 hours was generated using a skin factor of 3.4 (see Fig. 5.11). Three reservoir models were again used to investigate the effect of temporal changes in the skin factor to the estimation of reservoir model parameters.

Example 2A: Infinite Acting Reservoir

In this example, an infinite acting reservoir was used to study the effect of the changes in skin factor on the results from the regression analysis. The pressure response for an infinite acting reservoir shown in Fig. 5.12 was generated using the skin function displayed in Fig. 5.11, permeability of 300 md, wellbore storage coefficient of 0.05 STB/psi, and initial pressure of 6000.0 psi. Initial guesses for these model parameters are shown in the first row in Table 5.8. The estimates of the model parameters from the analysis for each moving window are also shown in Table 5.8. Table 5.9 displays the initial guesses of the unknown flow rates and their estimates from the regression. Fig. 5.13 plots the estimates for the skin factor as a function of time at the middle of each window.

Similar to the results in Example 1A, there is some uncertainty associated with the estimates of the skin factor due to the fact the the skin factor is not constant. Since the data in each 10-hour period are responses to different skin factors, the regression sees this inconsistency as an uncertainty in the data values. Therefore, the estimates of the skin factor from the regression also have some uncertainty. Since permeability is strongly correlated with skin factor, the permeability estimates also have a similar

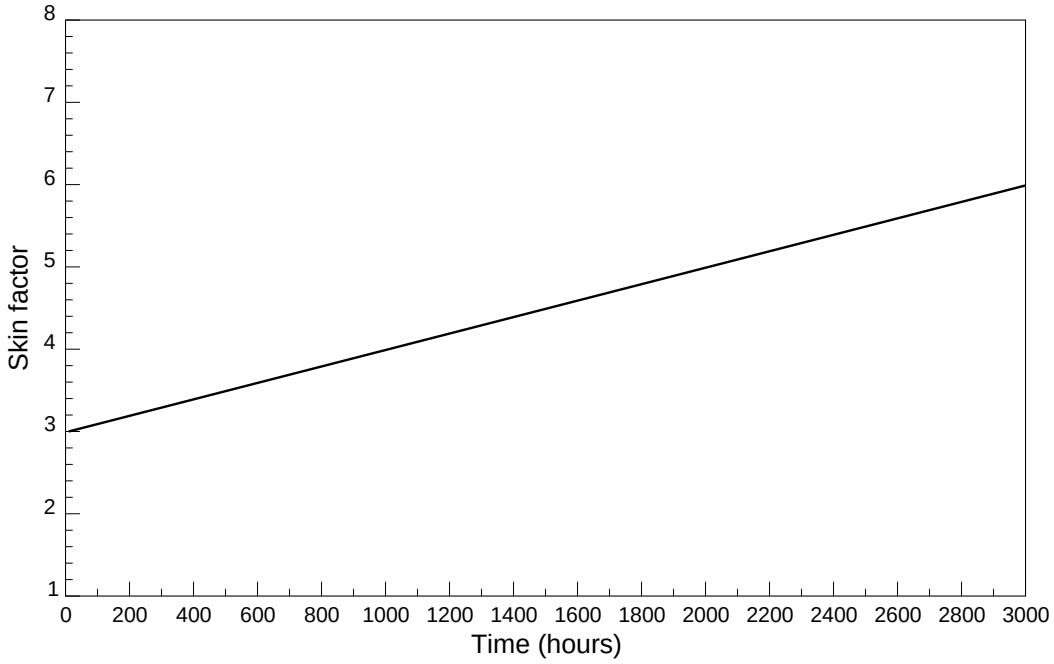

Figure 5.11: Skin Profile.

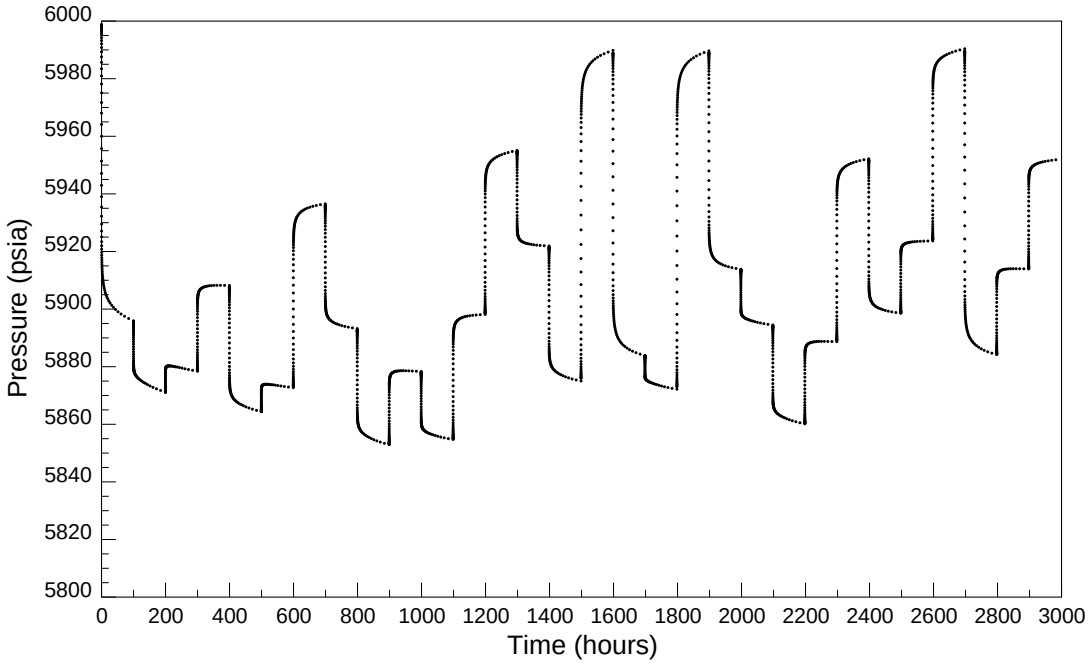

Figure 5.12: Pressure response for an infinite acting reservoir.

Table 5.8: Parameter estimates for an infinite acting reservoir.

Window	Time period	Permeability	Skin	Storage	Initial pressure
-	Initial guess	100.00	0.00	0.0010	6000.00
True		300.0		0.0500	6000.00
1	0.- 200.	287.95	2.66	0.0491	6000.09
2	100.- 300.	266.40	1.88	0.0486	6000.58
3	200.- 400.	321.37	3.63	0.0548	5996.05
4	300.- 500.	307.22	3.31	0.0502	5997.71
5	400.- 600.	268.44	2.50	0.0481	6003.61
6	500.- 700.	309.31	3.86	0.0520	5999.21
7	600.- 800.	317.86	3.74	0.0522	5994.39
8	700.- 900.	294.68	2.95	0.0515	5995.41
9	800.-1000.	265.47	3.10	0.0473	6007.31
10	900.-1100.	294.64	4.28	0.0465	6004.88
11	1000.-1200.	301.93	3.69	0.0533	5996.57
12	1100.-1300.	326.02	4.63	0.0531	5995.05
13	1200.-1400.	311.24	4.32	0.0514	5997.21
14	1300.-1500.	294.76	3.72	0.0509	5997.99
15	1400.-1600.	296.91	4.30	0.0507	6000.25
16	1500.-1700.	299.36	4.44	0.0503	6000.07
17	1600.-1800.	286.82	4.16	0.0493	6000.52
18	1700.-1900.	295.13	4.74	0.0500	6001.92
19	1800.-2000.	304.19	5.01	0.0499	5999.71
20	1900.-2100.	287.33	4.43	0.0494	6000.51
21	2000.-2200.	267.83	3.89	0.0477	6003.23
22	2100.-2300.	276.45	4.24	0.0497	6002.35
23	2200.-2400.	315.56	5.80	0.0516	5998.59
24	2300.-2500.	303.85	5.37	0.0504	5999.45
25	2400.-2600.	282.08	4.80	0.0494	6001.34
26	2500.-2700.	306.44	5.84	0.0507	5999.73
27	2600.-2800.	290.42	5.52	0.0489	6002.08
28	2700.-2900.	284.91	5.29	0.0489	6002.25
29	2800.-3000.	322.43	6.71	0.0515	5998.40

Table 5.9: Estimates of unknown flow rates for an infinite acting reservoir.

Flow period	True value	Initial guess	Final estimate
100.- 200.	1000.00	800.00	996.09
300.- 400.	1100.00	900.00	1103.65
500.- 600.	1200.00	1300.00	1195.22
700.- 800.	500.00	300.00	475.70
900.-1000.	1250.00	1050.00	1234.97
1100.-1200.	1200.00	1100.00	1211.10
1300.-1400.	300.00	100.00	287.94
1500.-1600.	1000.00	900.00	1002.79
1700.-1800.	920.00	620.00	917.01
1900.-2000.	0.00	100.00	0.22
2100.-2200.	800.00	900.00	799.55
2300.-2400.	820.00	620.00	822.64
2500.-2600.	740.00	900.00	736.74
2700.-2800.	0.00	100.00	13.35

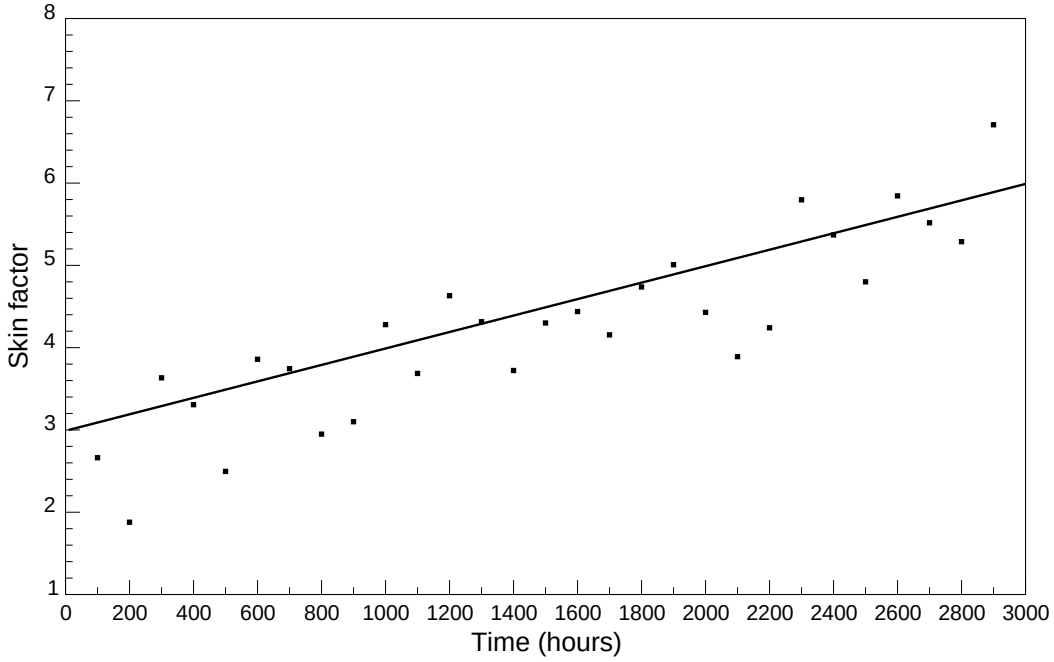

Figure 5.13: Skin estimates for an infinite acting reservoir.

degree of uncertainty. The temporal change in the skin factor has small effect on the estimates of the wellbore storage coefficient, initial reservoir pressure, and unknown flow rates. The differences between the true values and the final estimates from the regression for these parameters are larger than the differences in Example 1A because the degree of inconsistency in the pressure within a transient is higher. In other words, the magnitude of pressure change caused by the change of skin at a rate of 0.01 per 10 hours in this example is larger than the one resulted from the change of permeability at a rate of 0.05 md per 10 hours in Example 1A.

Example 2B: Closed Circular Boundary Reservoir

This example was used to study the effect of the change in skin factor on the estimates of reservoir parameters using a closed circular boundary reservoir. Fig. 5.14 displays the pressure response for a closed circular boundary reservoir using the model parameters shown in the first row in Table 5.10 and the skin function in Fig. 5.11, Initial guesses for these model parameters and the unknown flow rates used in the moving window analysis are shown in the second row in Table 5.10 and the third column of Table 5.11, respectively. Also tabulated in these two tables are the estimates for the model parameters for each window and the unknown flow rates. Plotted in Fig. 5.15 are the estimates for the skin factor as a function of time at the middle of each of the moving windows.

The degree of uncertainty associated with the estimates of the skin factor is less than in Example 2A. The increase in the certainty of the skin estimates can be explained by a similar reason to that described in Example 1B. For the infinite acting case in Example 2A, all the data after the wellbore storage period play an important role in the estimation of the skin factor. Thus, the regression is exposed to several step changes in the value of the skin factor. On the other hand, the data that contribute the most to the computation of the skin factor in this closed boundary case are the data in the middle section between wellbore storage effect and boundary effect. Hence, the regression sees less change in the skin value, which is equivalent to seeing less uncertainty in the data values. As a result, the skin estimates in this

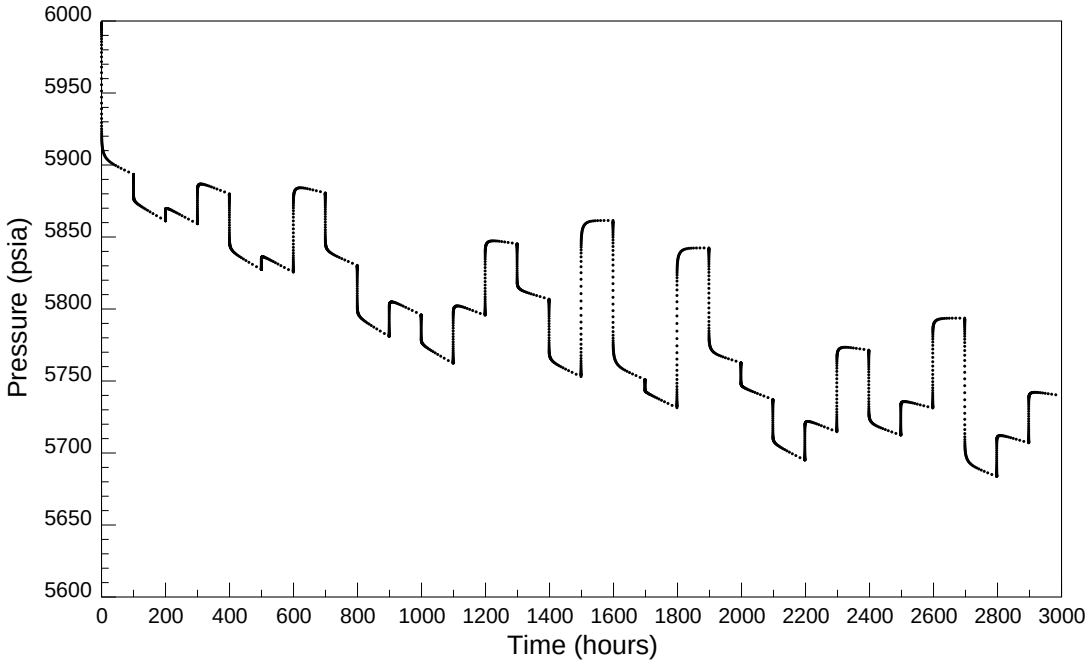

Figure 5.14: Pressure response for a closed circular boundary reservoir.

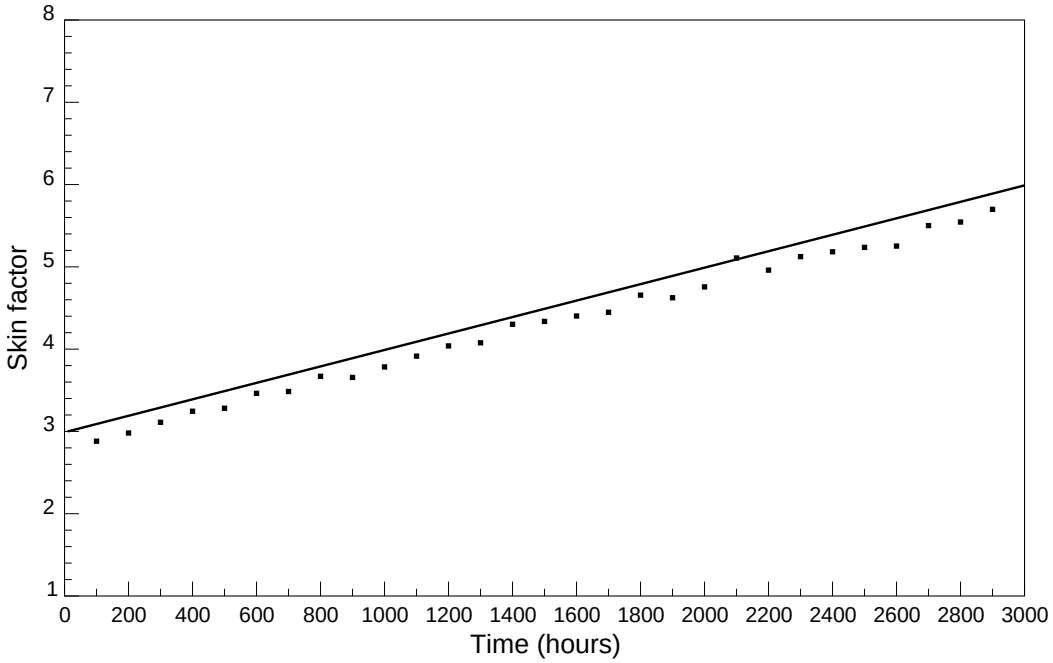

Figure 5.15: Skin estimates for a closed circular boundary reservoir.

Table 5.10: Parameter estimates for a closed circular boundary reservoir.

Window	Time period	Permeability	Skin	Storage	r_e	Initial pressure
-	Initial guess	100.00	0.00	0.0010	1000.00	6000.00
True		300.0		0.0500	3000.00	6000.00
1	0.- 200.	295.64	2.88	0.0497	2859.12	6000.03
2	100.- 300.	298.82	2.98	0.0504	2872.33	5999.75
3	200.- 400.	294.54	3.11	0.0500	2879.04	6002.68
4	300.- 500.	298.45	3.25	0.0502	2887.20	6002.35
5	400.- 600.	298.03	3.28	0.0501	2870.68	6003.16
6	500.- 700.	303.78	3.46	0.0512	2880.40	6002.39
7	600.- 800.	302.08	3.49	0.0509	2883.57	6003.06
8	700.- 900.	307.43	3.67	0.0513	2860.92	6004.09
9	800.-1000.	305.59	3.66	0.0516	2878.67	6003.47
10	900.-1100.	309.42	3.78	0.0521	2888.46	6002.62
11	1000.-1200.	291.04	3.91	0.0492	2869.84	6011.32
12	1100.-1300.	294.56	4.04	0.0496	2884.22	6009.94
13	1200.-1400.	300.47	4.08	0.0506	2889.21	6008.09
14	1300.-1500.	306.65	4.30	0.0512	2858.66	6010.82
15	1400.-1600.	293.40	4.34	0.0495	2856.18	6014.00
16	1500.-1700.	295.24	4.40	0.0498	2921.52	6007.37
17	1600.-1800.	295.65	4.45	0.0498	2859.16	6013.82
18	1700.-1900.	296.00	4.66	0.0499	2887.11	6012.34
19	1800.-2000.	294.21	4.62	0.0498	2788.54	6024.48
20	1900.-2100.	295.92	4.76	0.0498	2861.07	6015.55
21	2000.-2200.	301.33	5.11	0.0500	2865.32	6015.60
22	2100.-2300.	297.69	4.96	0.0503	2870.41	6015.02
23	2200.-2400.	296.19	5.12	0.0500	2884.34	6015.28
24	2300.-2500.	297.68	5.18	0.0502	2903.29	6012.59
25	2400.-2600.	298.61	5.24	0.0504	2868.35	6017.64
26	2500.-2700.	291.89	5.25	0.0497	2828.93	6025.48
27	2600.-2800.	292.05	5.50	0.0493	2916.58	6012.97
28	2700.-2900.	292.89	5.54	0.0494	2857.32	6022.16
29	2800.-3000.	296.06	5.70	0.0500	2884.60	6017.83

Table 5.11: Estimates of unknown flow rates for a closed circular boundary reservoir.

Flow period	True value	Initial guess	Final estimate
100.- 200.	1000.00	800.00	998.69
300.- 400.	1100.00	900.00	1100.52
500.- 600.	1200.00	1300.00	1201.94
700.- 800.	500.00	300.00	489.01
900.-1000.	1250.00	1050.00	1260.74
1100.-1200.	1200.00	1100.00	1195.45
1300.-1400.	300.00	100.00	293.42
1500.-1600.	1000.00	900.00	993.51
1700.-1800.	920.00	620.00	919.65
1900.-2000.	0.00	100.00	0.34
2100.-2200.	800.00	900.00	799.12
2300.-2400.	820.00	620.00	821.29
2500.-2600.	740.00	900.00	743.84
2700.-2800.	0.00	100.00	8.97

case are better than those in the infinite acting case. The permeability estimates also have less uncertainty due to a strong correlation between permeability and skin. Similar to Example 2A, the temporal change in the skin factor has small effect on the estimates of the wellbore storage coefficient, initial reservoir pressure, distance to the boundary, and unknown flow rates. However, the differences between the true values and the final estimates from the regression for these parameters are larger than the differences seen in Example 1B. This is simply because the degree of inconsistency created by the variation in the skin factor in this case is higher than that in Example 1B.

Example 2C: Channel Reservoir

A channel reservoir was studied in this example. Using the skin factor shown in Fig. 5.11 and the model parameters shown in the first row of Table 5.12, the pressure response for a channel reservoir was simulated as shown in Fig. 5.16. The moving window analysis was then implemented using the same configuration as all the previous examples. Initial guesses for these model parameters are shown in the

second row in Table 5.12. Shown in the third column in Table 5.13 are the initial guesses for the unknown flow rates. The final estimates from the moving window analysis for the reservoir parameters and the unknown flow rates are shown in Table 5.12 and Table 5.13, respectively. Fig. 5.17 displays the estimates of the skin factor as a function of time at the middle of each window. The estimates to the distances to the boundaries are shown in Figs. 5.18 and 5.19.

Similar to the results from the closed boundary reservoir in the previous example, the degree of uncertainty associated with the estimates of the skin factor is less than that in the infinite acting reservoir in Example 2A. Again, the data that contribute most to the estimation of the skin factor are the ones in the middle of each flow period, i.e., the measurements between the end of the wellbore storage effect and the beginning of the boundary effect. Consequently, the regression sees less step changes in the skin factor, thus, less uncertainty in the data. The permeability estimates are also better than those in Example 2A due to the strong correlation between permeability and skin. The temporal change in the skin value has similar small effect on the estimates for the wellbore storage coefficient, initial reservoir pressure, and unknown flow rates as in Example 2A. The estimates for the distances to the first and second boundaries in this case are poorer than the ones in Example 1C due to larger discrepancies in the pressure responses.

In summary, these examples show that the moving window analysis can be used to analyze data with changing trend. Although the approach might not provide perfect results in certain cases, it is better than analyzing the whole data set all at once. The method also provides us an opportunity to analyze data accounting for responses due to previous flow rate history when those flow rates are not available.

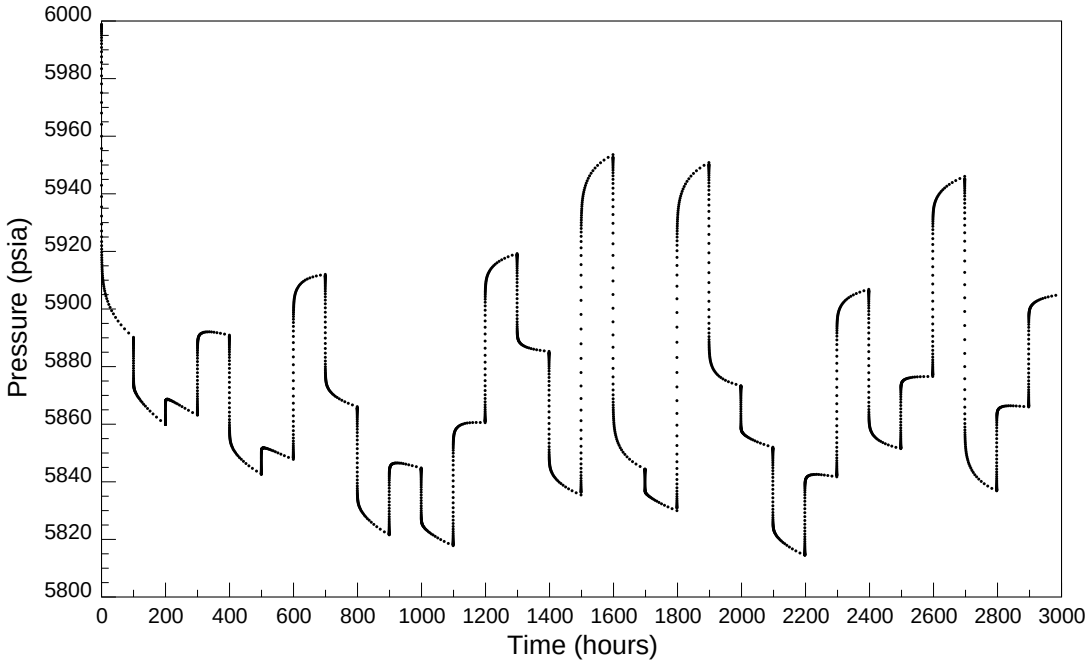

Figure 5.16: Pressure response for a channel reservoir.

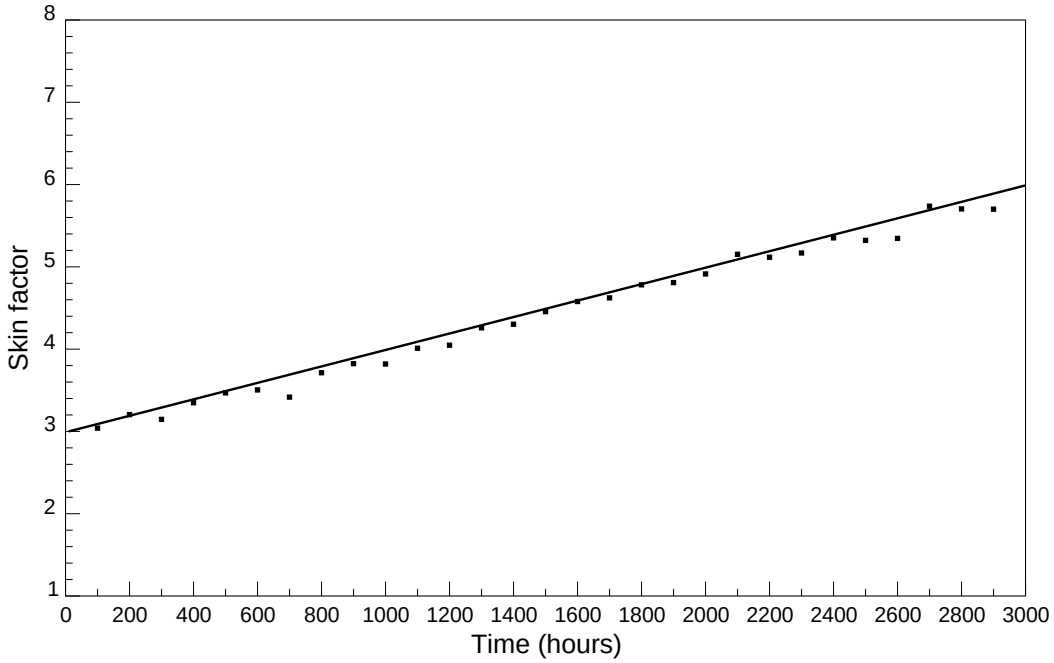

Figure 5.17: Skin estimates for a channel reservoir.

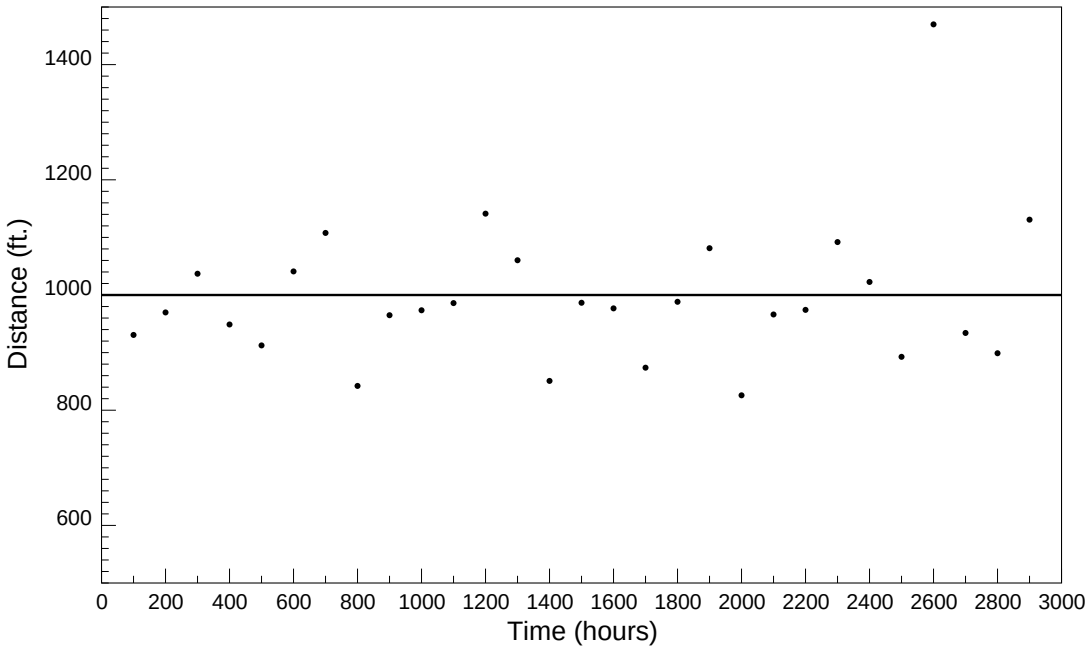

Figure 5.18: Estimate of distance to the first boundary for a channel reservoir.

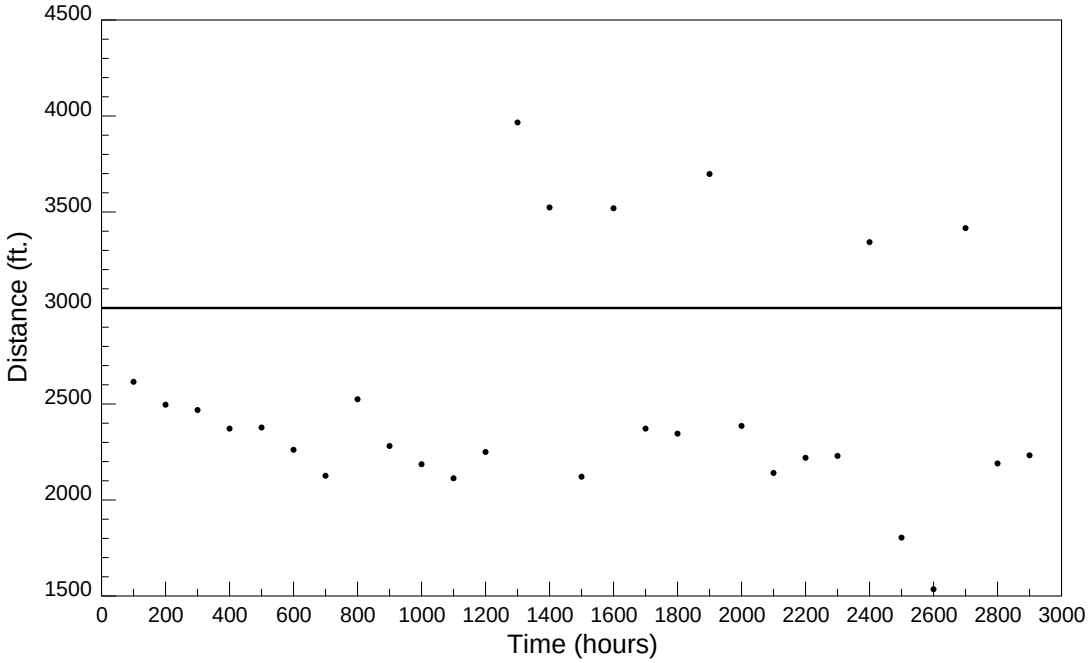

Figure 5.19: Estimate of distance to the second boundary for a channel reservoir.

Table 5.12: Parameter estimates for a channel reservoir.

Window	Time period	Permeability	Skin	Storage	r_{e1}	r_{e2}	Initial pressure
-	Initial guess	100.00	0.00	0.0010	500.00	1000.00	6000.00
True			3.00	0.0500	1000.00	3000.00	6000.00
1	0.- 200.	300.86	3.04	0.0499	930.68	2615.66	6000.00
2	100.- 300.	306.24	3.20	0.0507	969.75	2496.19	5999.43
3	200.- 400.	295.55	3.15	0.0500	1036.96	2468.75	6002.65
4	300.- 500.	301.41	3.35	0.0502	948.83	2371.83	6003.99
5	400.- 600.	303.88	3.47	0.0504	912.50	2377.50	6004.44
6	500.- 700.	304.14	3.50	0.0511	1040.96	2261.53	6003.64
7	600.- 800.	304.51	3.42	0.0513	1107.78	2126.38	6003.11
8	700.- 900.	315.18	3.71	0.0521	842.17	2524.86	6001.01
9	800.-1000.	310.40	3.82	0.0517	964.93	2281.18	6004.12
10	900.-1100.	310.07	3.82	0.0520	973.50	2186.25	6005.51
11	1000.-1200.	293.63	4.01	0.0493	985.97	2113.14	6015.20
12	1100.-1300.	294.82	4.05	0.0498	1141.25	2250.16	6008.74
13	1200.-1400.	308.19	4.26	0.0512	1060.35	3966.20	5988.32
14	1300.-1500.	310.68	4.30	0.0516	850.87	3523.56	5993.47
15	1400.-1600.	297.58	4.46	0.0498	986.54	2121.13	6013.84
16	1500.-1700.	301.07	4.58	0.0500	976.81	3519.42	5994.91
17	1600.-1800.	300.49	4.62	0.0500	873.84	2371.72	6010.49
18	1700.-1900.	299.35	4.78	0.0500	988.23	2345.58	6010.05
19	1800.-2000.	298.97	4.81	0.0498	1081.26	3697.73	5992.11
20	1900.-2100.	300.19	4.91	0.0499	825.86	2385.89	6011.88
21	2000.-2200.	302.18	5.15	0.0499	966.21	2140.90	6013.87
22	2100.-2300.	301.39	5.12	0.0503	974.21	2219.93	6012.07
23	2200.-2400.	297.43	5.17	0.0501	1091.92	2229.77	6011.31
24	2300.-2500.	302.51	5.35	0.0503	1022.67	3343.01	5994.84
25	2400.-2600.	299.29	5.32	0.0503	892.69	1804.15	6027.07
26	2500.-2700.	294.67	5.35	0.0503	1469.86	1535.15	6018.81
27	2600.-2800.	296.80	5.74	0.0493	934.12	3415.96	5997.48
28	2700.-2900.	295.85	5.70	0.0493	898.92	2190.30	6017.81
29	2800.-3000.	296.23	5.70	0.0501	1130.82	2232.83	6010.66

Table 5.13: Estimates of unknown flow rates for a channel reservoir.

Flow period	True value	Initial guess	Final estimate
100.- 200.	1000.00	800.00	998.56
300.- 400.	1100.00	900.00	1100.35
500.- 600.	1200.00	1300.00	1201.93
700.- 800.	500.00	300.00	480.36
900.-1000.	1250.00	1050.00	1260.47
1100.-1200.	1200.00	1100.00	1195.47
1300.-1400.	300.00	100.00	290.07
1500.-1600.	1000.00	900.00	995.74
1700.-1800.	920.00	620.00	919.63
1900.-2000.	0.00	100.00	0.36
2100.-2200.	800.00	900.00	799.38
2300.-2400.	820.00	620.00	821.17
2500.-2600.	740.00	900.00	742.29
2700.-2800.	0.00	100.00	11.45

5.3 Field Examples

This section illustrates the implementation of the moving window analysis to actual sets of field data. Three examples with distinguishing data appearances, reservoir fluids, and reservoir models were investigated. The pressure data in each example were collected using different criteria. Two of the data sets were generally collected at high frequencies while the other set was collected at low frequencies.

5.3.1 Field Example 1

The pressure data in this example are the same as the ones used in Field Example 1 in Section 3.3.1. Since this was a newly drilled well, there are only 375 hours of data available. To prepare the data for the moving window analysis, the raw data underwent data processing steps described in Chapter 3, i.e., outlier removal, transient identification, and data reduction. Since the pressure data were recorded at high frequencies, the denoising algorithm was applied to the data during the transient identification and data reduction steps. Before being used as input data, the results of the transient identification implementation from Section 3.3.1 were revised to get rid of misidentifications. Also, a few positions for new transients were filled in for the transients that were missed by the identification algorithm. In the data reduction step, the number of data was reduced from 41,382 to 5,184. The reduced version of data would be used in the moving window analysis.

In addition to the pressure data, flow rates and production data are needed in the analysis. In this field example, the only data available were cumulative oil production and the number of flow hours on a daily basis. These data are tabulated in Table 5.14. The flow time for day 4 (time between 61.708 and 85.708 hours) is not available due to frequent shutdowns in certain parts of the fluid gathering system. The cumulative production and the flow time were estimated roughly.

Even though the flow rates were not measured explicitly, a few flow rates can be determined from the combined information obtained from the pressure data, daily

Table 5.14: Oil cumulative production.

Time (hour)	Cumulative production (STB)	Flow time (hour)
13.708	1821	8.0
37.708	6093	10.5
61.708	12433	11.2
85.708	19399	-
109.708	23670	13.2
133.708	30615	22.0
157.708	35505	22.0
181.708	43172	24.0
205.708	49840	22.0
229.708	57650	24.0
253.708	62118	13.5
277.708	71580	24.0
301.708	81834	24.0
373.708	113788	24.0

production, and flow time. For example, we know that the transient between $t = 8.239$ and $t = 26.747$ is a build-up (see Fig. 3.40). Looking at the pressure plot alone, it is not certain that the flow rate is zero. However, we know that the number of flowing hours from $t = 0$ to $t = 13.7$ is 8 hours and that there is only one build-up between $t = 0$ to $t = 13.7$. Therefore, the well must have been shut in after $t = 8.0$. The flow rate for transient between $t = 8.239$ and $t = 26.747$ must therefore be zero. Since some of the transients are longer than 24 hours, their flow rates can also be derived from the cumulative production data. For instance, there is only one transient from $t = 205.466$ to $t = 238.288$. The oil production from $t = 205.708$ to $t = 229.708$ is $57,650 - 49,840 = 7,810$. Therefore, the flow rate for this transient is 7,810 STB/D. Using the combined information of pressure, production data, and flow time, several flow rates were determined. Table 5.15 depicts the flow rate history for the well as well as the initial guesses for the unknown rates to be used in the moving window regression analysis. As shown in the table, 11 flow rates were determined using the information on pressure, cumulative production, and flow time. The number of unknown flow rates was reduced from 84 to 73.

Table 5.15: Flow rate history and the estimates for unknown flow rates.

Time (Hours)	Value	Initial Guess	Estimate	Time (Hours)	Value	Initial Guess	Estimate
0.000	0.0	known	known	124.810	0.0	known	known
0.259	unknown	1000.0	684.0	124.828	unknown	500.0	1547.7
4.522	unknown	2500.0	2308.9	125.008	unknown	400.0	815.6
8.239	unknown	8000.0	8853.7	125.448	unknown	2000.0	3643.3
26.747	0.0	known	known	126.182	unknown	5000.0	8962.3
27.000	unknown	500.0	678.8	128.982	unknown	6000.0	9635.7
27.363	unknown	2000.0	2138.2	144.685	unknown	3000.0	4339.2
39.480	unknown	8000.0	9204.2	146.284	0.0	known	known
46.191	0.0	known	known	146.417	unknown	500.0	1055.4
46.229	unknown	2000.0	2199.1	147.311	unknown	100.0	206.4
46.437	unknown	1000.0	2101.1	147.572	unknown	500.0	1402.6
48.006	unknown	8000.0	9191.5	147.865	unknown	1000.0	1994.9
48.178	unknown	500.0	674.6	149.207	unknown	3000.0	4853.9
48.581	unknown	2500.0	3850.2	163.201	unknown	4500.0	5436.7
78.338	unknown	8000.0	9085.7	163.236	unknown	8000.0	11054.4
93.265	unknown	100.0	1506.9	163.285	unknown	5000.0	7645.2
94.265	unknown	4500.0	3256.1	200.885	unknown	8000.0	8497.3
95.138	unknown	1500.0	2977.7	201.848	unknown	1000.0	1300.2
99.317	unknown	4000.0	6531.1	203.117	0.0	known	known
100.724	unknown	5500.0	8947.2	203.143	unknown	500.0	818.5
102.419	unknown	6000.0	9220.2	203.620	unknown	400.0	817.8
105.363	unknown	8000.0	10142.3	205.328	unknown	1000.0	1493.1
107.192	0.0	known	known	205.466	unknown	1500.0	2469.5
107.361	unknown	500.0	899.7	238.288	7810.0	known	known
108.561	unknown	100.0	177.3	242.063	unknown	100.0	77.8
108.625	unknown	400.0	876.2	242.111	unknown	500.0	948.3
108.634	unknown	800.0	2257.2	242.196	unknown	400.0	510.8
108.711	unknown	500.0	1303.7	242.465	unknown	1000.0	1276.2
108.879	unknown	1500.0	2512.6	242.861	unknown	2200.0	2292.2
109.103	unknown	2000.0	3581.0	243.258	unknown	3200.0	3231.2
109.388	unknown	4000.0	6303.4	243.662	unknown	5700.0	5850.5
109.534	unknown	7500.0	10544.3	244.460	unknown	7000.0	6924.3
110.030	unknown	6500.0	9234.7	244.624	unknown	8000.0	8478.6
111.487	unknown	8000.0	10324.3	245.871	unknown	9000.0	9372.8
113.431	0.0	known	known	246.125	unknown	2000.0	3467.2

Table 5.15: Flow rate history and the estimates for unknown flow rates (continued).

Time (Hours)	Value	Initial Guess	Estimate	Time (Hours)	Value	Initial Guess	Estimate
113.451	unknown	500.0	1240.9	250.937	0.0	known	known
113.531	unknown	400.0	248.5	251.235	unknown	400.0	1688.1
113.559	unknown	1200.0	2716.0	251.517	unknown	1000.0	2935.4
113.806	unknown	800.0	912.4	252.370	unknown	7000.0	7361.0
114.128	unknown	4200.0	6685.0	252.512	unknown	7500.0	8461.0
114.431	unknown	6500.0	9101.2	286.006	unknown	9462.0	9348.1
123.250	unknown	8000.0	10338.4	374.411	10693.0	known	known

The uncertainty associated with the cumulative production data is generally larger than the uncertainty in pressure measurements. For example, a daily production of 10,000 STB of oil may contain an error in the range of 100-500 STB whereas a pressure measurement of 5,000 psi may have an error of 3-5 psi or less. Therefore, it is necessary to give less weight to the cumulative production data when matching both the pressure and cumulative production in the regression. In this example, the weight of 0.01 was applied to each of the cumulative production data.

In general, data at early times of each transient are sampled at higher frequency than data at late times (even after resampling performed in the data reduction process) due to large pressure changes at the early times. These early time data play a very important role in the regression due to their large quantity. However, most of the reservoir model parameters that we are interested in such as permeability, skin, and distances to boundaries are computed from data at middle and/or late times. Although all the data are used in the regression, the data that contribute most to the estimation of these parameters are the middle and late time data. The wellbore storage coefficient, on the other hand, is estimated primarily from the early time data. However, the storage coefficient is the least important parameter among permeability, skin, and distances to the boundaries. Thus, there is no need to put the emphasis on the matching of the early time data although there are rapid changes there. Beside being sampled at higher frequencies, the early time data also have larger

uncertainties than the late time data. The pressure gauge is more likely to register erroneous measurements during the rapid changes in the pressure at the early times whereas the more gradual changes at late times provide a more stable environment for pressure measurement. Therefore, we should put less emphasis on the early time data and increase an emphasis on the late time data. To achieve this, an arithmetic weighting scheme may be used. In this approach, the data are weighted accordingly to their spacings. For example, if the spacing between points $i-1$ and i is Δt_i , and the spacing between points i and $i+1$ is Δt_{i+1}, the weight given to point i is $(\Delta t_i + \Delta t_{i+1})/\Delta t$, where Δt is the total length of the data. This weighting scheme was implemented in the regression analysis.

A preliminary analysis of pressure derivatives of a few long transients indicates that the reservoir may be a closed boundary reservoir. Therefore, the closed circular boundary model was used in the regression analysis. To illustrate the effectiveness of the moving window analysis, two types of regression analyses were used for this set of data: moving window analysis and global analysis. In the moving window analysis, the data were divided into overlapping windows and analyzed sequentially. The number of regression steps is equal to the number of overlapping windows. In the global analysis, the entire 375 hours of data were used to run the regression in a single step.

The preliminary window width was chosen to be 100 hours, and the translation length was set to be 50 hours. In practice, the actual window widths are generally larger than the preselected value. Using a rigid window width, the window may end right in the middle of a transient. When this happens, the last transient is not appropriately analyzed. Therefore, the window should be extended to include the data until the end of the last transient. Another reason to increase the window width is to constrain the regression match by including at least one known flow rate in the window. If all the flow rates in the window are unknown, the window width is extended until a known flow rate is included as a part of the window. Similar to the window width, the translation length may also be changed such that the beginning of

Table 5.16: Parameter estimates in each window for Field Example 1.

Window	Permeability (md)	Skin	Storage (STB/psi)	Distance to boundary	Initial pressure
Initial guess	50.00	3.00	0.0100	3000.00	5360.00
1	882.30	7.08	0.0234	4717.13	5350.09
2	798.34	5.81	0.0199	5912.37	5350.36
3	826.11	4.21	0.0343	5584.66	5355.49
4	780.43	5.71	0.0176	5912.96	5351.04
5	612.25	4.32	0.0176	7039.30	5369.40
Global	827.68	6.05	0.0214	5782.20	5352.28

each window coincides with the beginning of a transient to avoid starting a window of analysis at the middle of a transient.

After choosing the preliminary window width and translation length, the moving window and global analyses were conducted. The regression matches from the moving window analysis to data in windows 1-5 are shown in Figs. 5.20 - 5.24, respectively. The regression match to the entire data in the global analysis is shown in Fig. 5.25. Only the transients that pass the variance test described in Section 4.4 are shown in these plots. The estimates for unknown rates from the moving window analysis are shown in column 4 in Table 5.15. To confirm that the model selected was an appropriate one, derivative plots of matches to transients in windows 1 and 5 are plotted in Figs. 5.26 and 5.27, respectively. The close matches to both the pressure and derivatives reassure us that the circular closed boundary model was appropriate. Although the match may be poorer at the early times in Fig. 5.27, the model selected is adequate. The storage coefficient was poorly estimate due to the smaller emphasis on the early time data resulting from the arithmetic weighting.

The estimates of reservoir model parameters from the moving window analysis are compared with the estimates from the global match in Table 5.16. The estimate for each model parameter from the global match falls within the range of the maximum and minimum estimates from the moving window analysis. For example, the

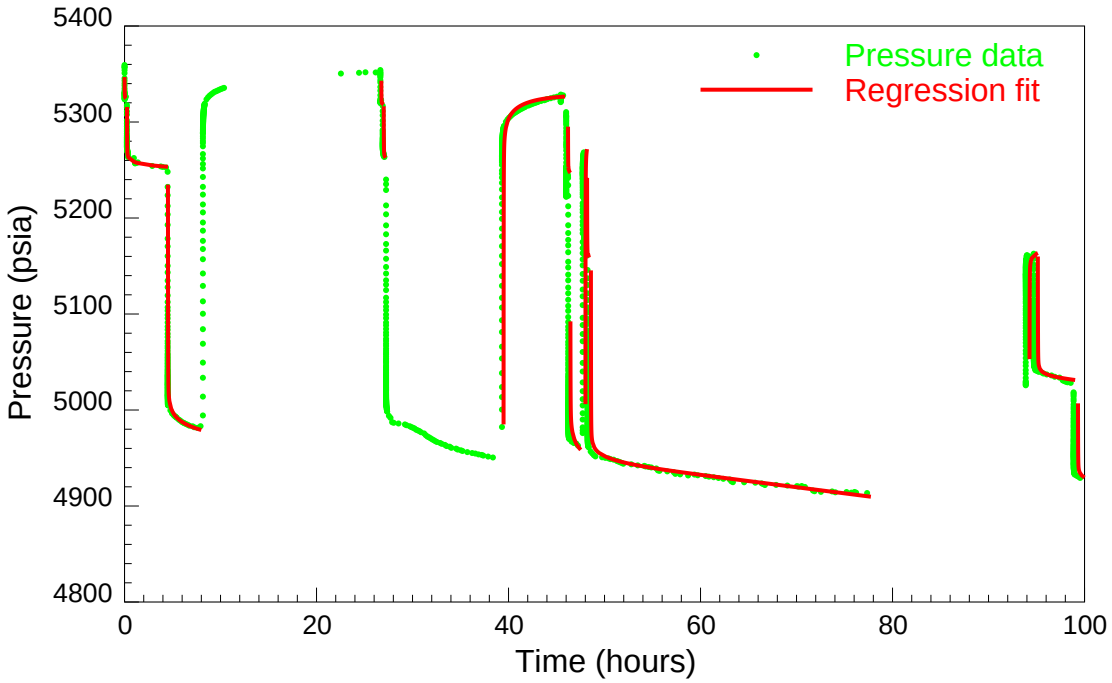

Figure 5.20: Regression match to window 1.

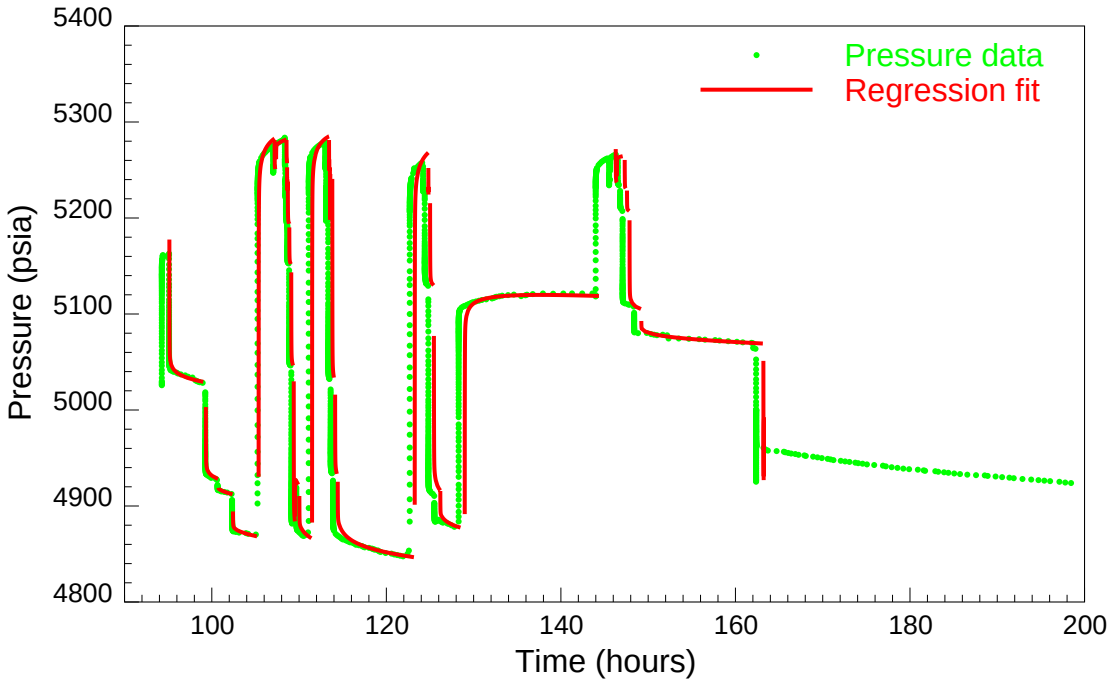

Figure 5.21: Regression match to window 2.

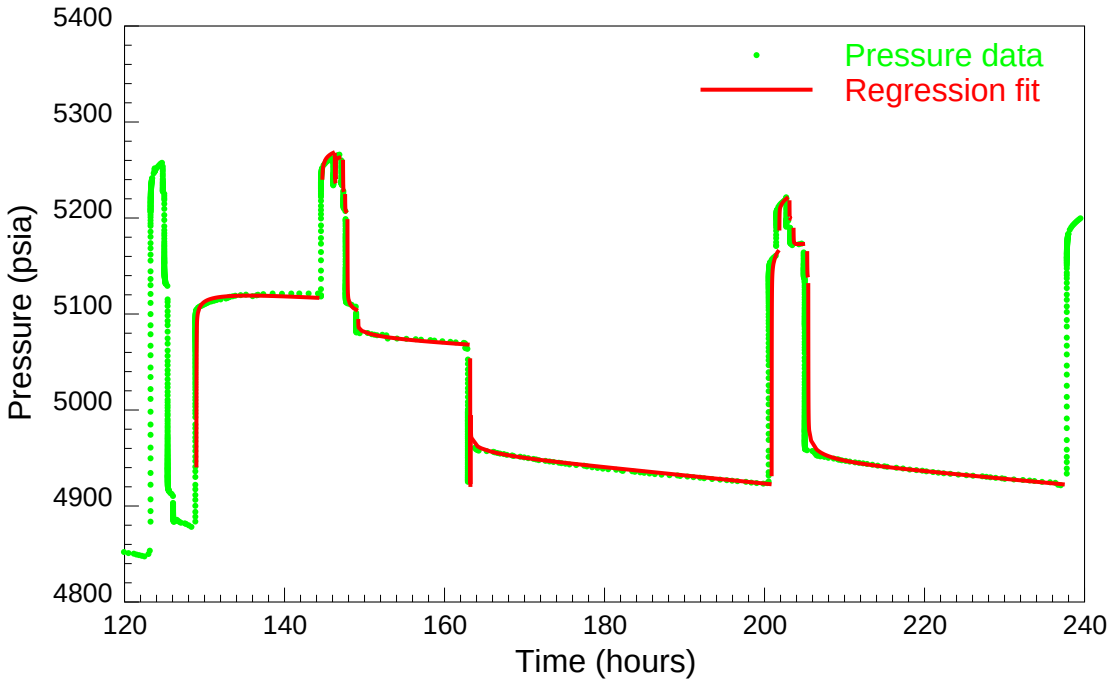

Figure 5.22: Regression match to window 3.

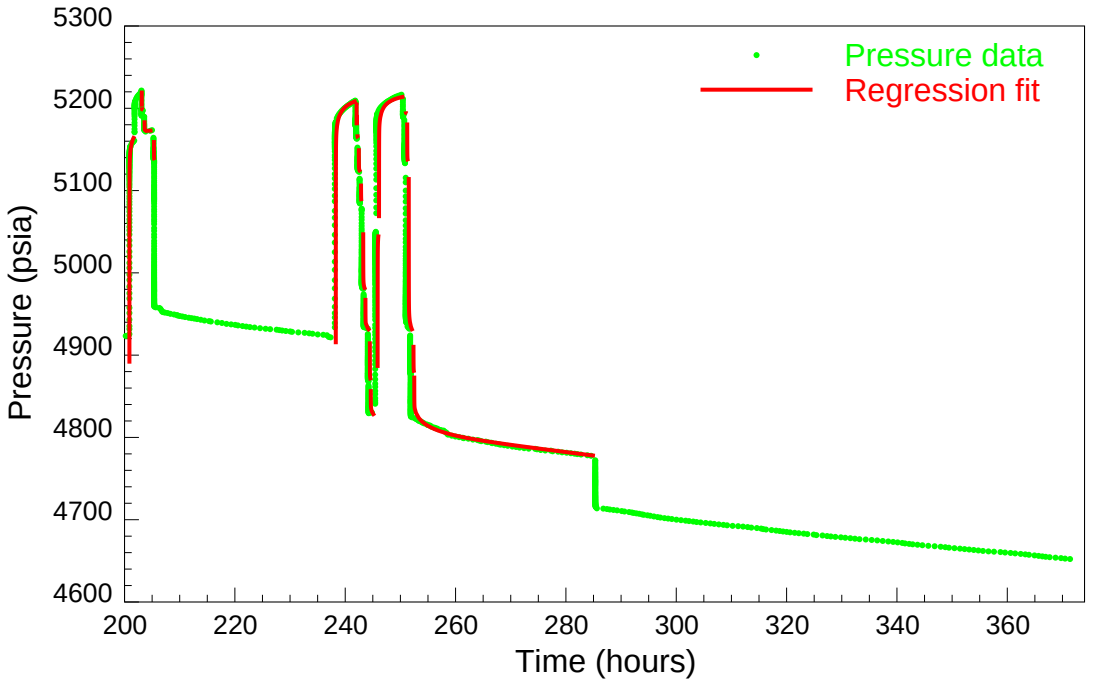

Figure 5.23: Regression match to window 4.

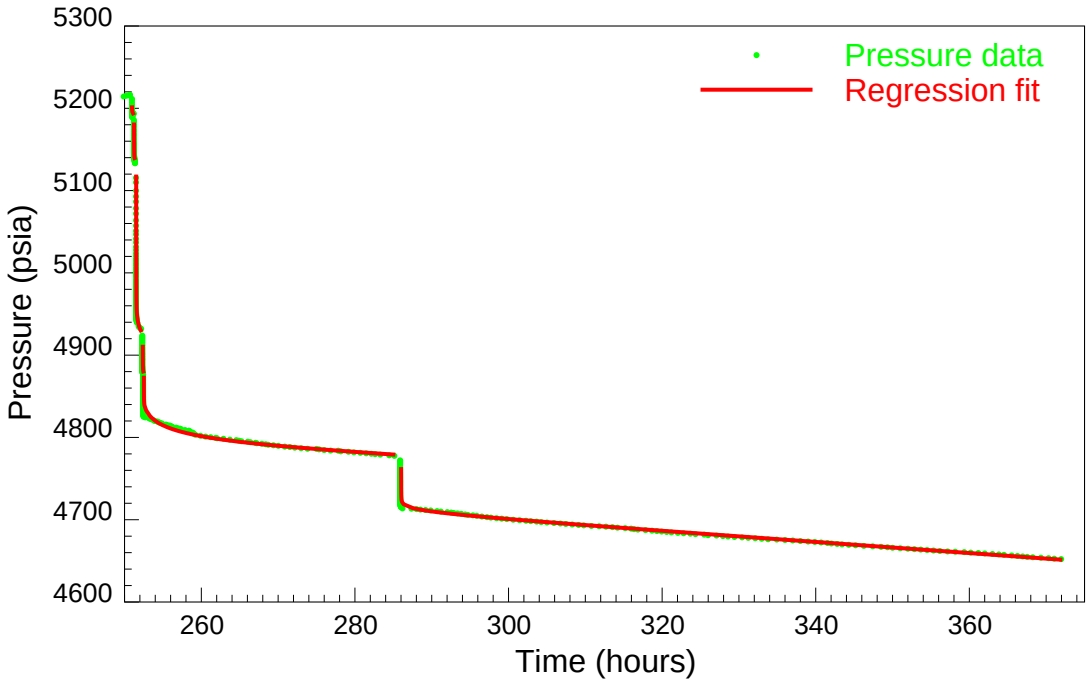

Figure 5.24: Regression match to window 5.

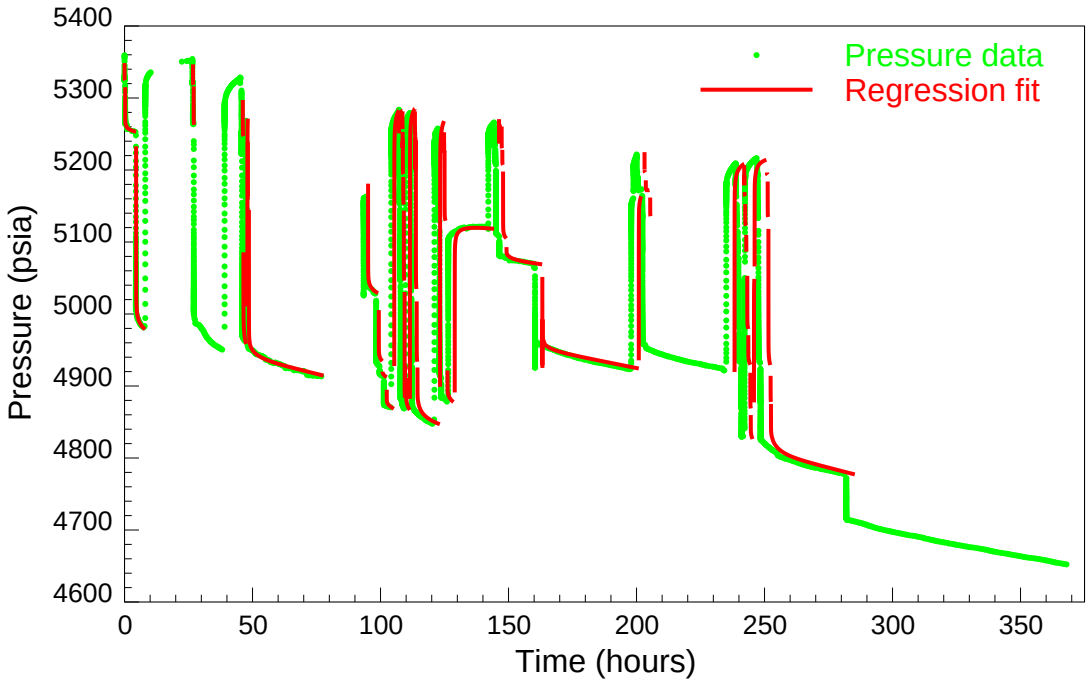

Figure 5.25: Global regression match.

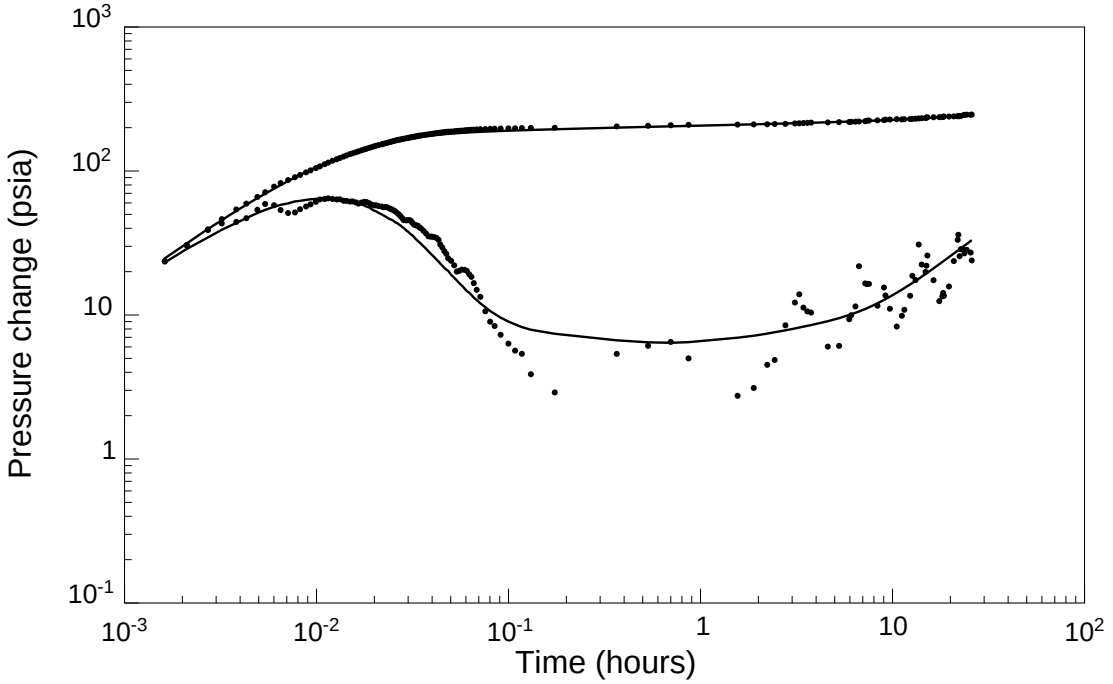

Figure 5.26: Log-log plot of regression match to a transient in window 3.

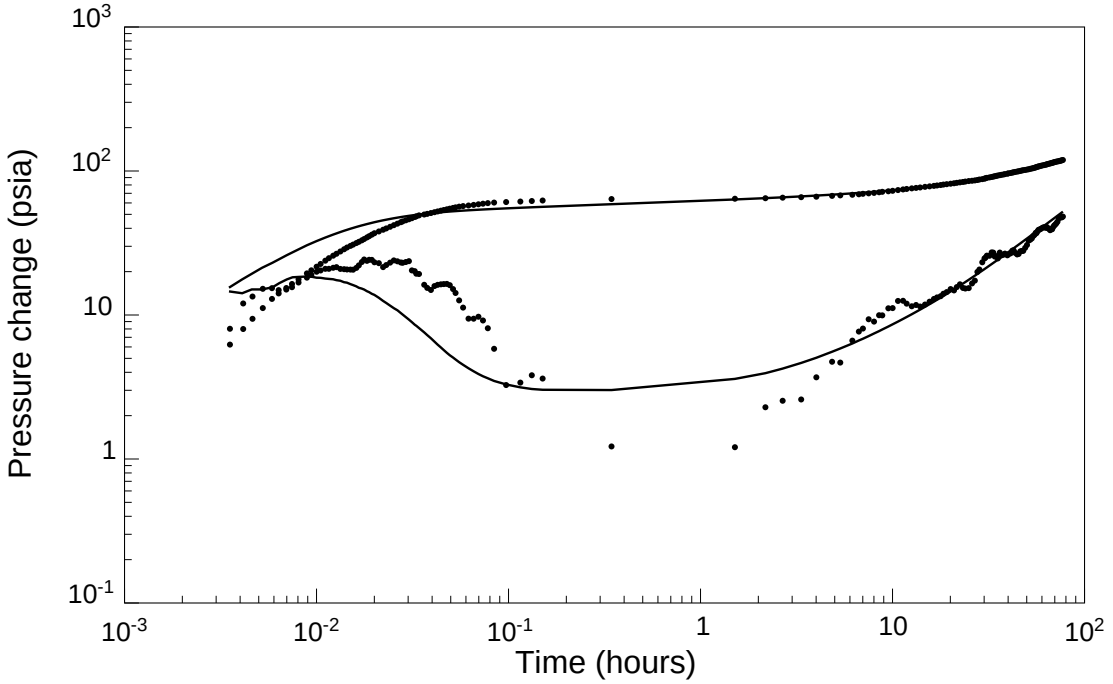

Figure 5.27: Log-log plot of regression match to a transient in window 5.

permeability estimate from the global match is 827.68 md where as the minimum and maximum estimates from the moving window are 612.25 md and 882.30 md, respectively. The global analysis matches the average overall response from the reservoir while the moving window analysis provides five snapshots of local responses, i.e., a set of temporal estimates for reservoir model parameters. If there is a trend in the estimates of parameters, there is a possibility that certain reservoir properties might be changing. If the estimates do not establish any trend, the distributions of the estimates can then be used to assess uncertainty in reservoir parameters. The estimates from each window should also be checked for consistency. If there is a set of estimates that are very different from the rest, data in that particular window should be looked at more closely and may be discarded. In any case, the data in this example are too short to see any trend or distribution since they are from a newly drilled well. However, ranges of possible values for reservoir parameters may assessed. These ranges should be useful in reservoir simulation studies, especially to history matching problems, to assess uncertainty in future fluid productions. As more data are collected, these ranges may be updated to distributions of parameter estimates.

Besides the advantage of the moving window analysis over the global analysis mentioned before, the total computational time for the moving window analysis is much less than the computational time for global match. Due to a large number of data points to match and a large number of unknowns, the global regression takes more time to compute in each iteration. In this example, there are five model parameters (k, S, C, r_e, and p_i) and a total of 73 unknown flow rates. When using the moving window approach, the number of unknown flow rates was decreased to 15-20, and the total number of data was reduced from 5184 to 500-2500 in each window. The computational time for the moving window analysis was approximately five times less than for the global analysis.

5.3.2 Field Example 2

The data used in this example are from the same set of data in Section 3.3.3. Approximately 20,050 hours (28 months) of data were collected generally at low frequencies except for a few regions in which the sampling criteria were changed such that the pressure gauge recorded the measurement at unusually high frequencies. The raw data were first screened for outliers. Due to the fact that most of the data points have large spacings, the denoising routine was not implemented to avoid smearing sharp feature changes in the data. The transient identification methodology was applied to the original data as shown in Section 3.3.3. As in Field Example 1, the transient identification results were reexamined before being used as input data in the moving window analysis. False identifications of transients were discarded, and undetected transients were added. Before performing any analysis, the data were resampled in order to reduce their redundancy. The number of data was reduced from 13,064 points to 8,487 data points. Since the data were generally collected at large spacings with a small degree of redundancy, the amount of the data left after the reduction process is not much different from the original amount.

In this example, only sparsely measured flow rates are available. There were 218 flow rate changes during the 28 months of data recording. However, only 58 flow rates were measured. This leaves us with 160 unknown flow rates. The cumulative production data were not recorded. Therefore, the constraints for the regression in this case are the measured flow rates. Since there are more than 20,000 hours of data, the width of each window can be large; was chosen to be 500 hours. However, the window width may be larger than this if there is no known flow rate within the window. The translation length for the moving window was set to be 100 hours. To begin each window at the beginning of a transient, the translation length may be larger than 100 hours.

An analysis of pressure derivative and geological information indicates that the well may be placed in a channel. Therefore, the channel reservoir model was used in

the moving window regression analysis. As in Field Example 1, the arithmetic weighting scheme was used. The reservoir model parameters estimated in each window are shown in Table 5.17. Regression matches to the pressure data for a few selected windows are shown in Figs. 5.28 - 5.31. Again, only the transients that pass the variance test are plotted in these figures. The transients that fail the test were excluded from the regression. Log-log plots of matches to long transients in windows 58 and 72 are shown in Figs. 5.32 and 5.33, respectively. A slope of 1/2 in the pressure derivatives, which is a characteristic response from a channel reservoir, is clearly present. The good matches to the pressure and derivatives confirm that the chosen model and the estimates of reservoir parameters are suitable. Due to large data spacings, there are only a few data points during the period where wellbore storage effect is dominant. As a result, we do not see an upward trend at the beginning of each derivative plot.

Fig. 5.34 shows the estimates of permeability, skin factor, wellbore storage coefficient, distances to the closest and further boundaries, and average error per data point as a function of time at the middle of each window. As seen in the figure, there are no uniform trends in the parameter estimates. Instead, the variations illustrate the uncertainties associated with the estimates. There are 74 windows of data in the analysis. As seen from the different magnitudes of average error per measurement, the estimates in each window has different degrees of uncertainties. The average error per measurement ranges from 0.32 psi to 14.7 psi. To see how the parameter estimates are distributed, they are plotted using histograms in Fig. 5.35. Also shown in Fig. 5.35 are the statistics associated with the distributions of parameter estimates. Since the estimates in certain windows are poor due to the high level of average error per measurement, only the estimates from the windows in which the average error per measurement is smaller than five psi were included in these distribution plots. Therefore, the number of the data in each of these distributions is 59 instead of 74. The average value of permeability from the estimates in 59 windows is 70.65 md, and the standard deviation of the distribution is 24.04 md. The skin is most likely to be in the range of -6.25 to -5.50 with a mean value of -5.81 with a standard deviation of 0.42. The estimate of the distance to the closest boundary is in the range of 100-600

Table 5.17: Distribution of parameter estimates.

Window	Time period	Permeability	Skin	Storage	r_{e1}	r_{e2}	Initial pressure
-	Initial guess	500.00	5.00	0.5	400	1200	4000
1	0.00- 508.48	92.17	-5.80	0.08	423	1655	4115.32
2	108.74- 628.02	180.11	-5.03	0.11	398	937	4143.51
3	216.46- 781.31	112.81	-5.32	0.13	284	1334	4184.24
4	316.58- 842.00	96.13	-5.55	0.10	334	1498	4179.57
5	418.52- 966.30	77.47	-5.80	0.09	387	2049	4149.34
6	576.20- 1226.69	90.23	-5.59	0.06	372	4771	4054.88
7	702.64- 1226.69	103.26	-5.38	0.04	329	9087	4019.94
8	803.18- 1325.92	70.17	-5.91	0.41	333	2635	4178.18
9	966.30- 1521.90	55.35	-5.81	0.13	375	3434	4196.71
10	1226.69- 1770.00	50.85	-5.64	0.05	516	8482	4181.32
11	1389.00- 1933.00	93.48	-5.72	0.06	343	3471	4037.99
12	1521.90- 2071.10	103.16	-5.71	0.06	349	5248	3986.41
13	1665.00- 2179.27	88.70	-5.82	0.07	379	2999	4073.86
14	1770.00- 2350.00	86.72	-5.81	0.08	372	2191	4141.12
15	1933.00- 2442.77	71.77	-5.71	0.15	260	2428	4194.81
16	2071.10- 2669.23	60.79	-6.12	0.27	289	2660	4194.36
17	2179.27- 2800.63	71.46	-5.94	0.17	283	2249	4193.36
18	2350.00- 2866.75	75.60	-5.82	0.40	277	2149	4192.81
19	2532.00- 3152.14	65.67	-4.76	0.09	140	4648	4193.82
20	2669.23- 3176.43	100.70	-5.05	0.12	200	6535	3930.60
21	2800.63- 3545.56	52.50	-6.20	0.42	346	2998	4192.95
22	2912.56- 3545.56	51.22	-6.21	2.84	491	2650	4193.04
23	3152.14- 3661.98	51.56	-6.28	0.64	465	2632	4193.86
24	3545.56- 4171.39	53.07	-6.17	0.13	503	4552	4052.50
25	3661.98- 4171.39	55.18	-6.40	0.09	488	2616	4166.46
26	3867.23- 4648.97	44.52	-6.23	0.06	478	7786	4076.24
27	3978.87- 4648.97	44.52	-6.23	0.06	478	7786	4076.25
28	4171.39- 4733.62	50.50	-6.22	0.06	472	5568	4052.37
29	4291.07- 4907.28	55.04	-6.15	0.05	478	2934	4164.51
30	4648.97- 5359.52	81.75	-5.76	0.09	392	2481	4113.21
31	4784.00- 5359.52	77.42	-5.60	0.13	387	2215	4187.20
32	4907.28- 5545.04	34.97	-6.37	0.11	411	7225	4188.09
33	5095.13- 5634.72	43.45	-6.56	0.25	481	3590	4177.67
34	5359.52- 6073.25	31.36	-6.53	0.25	491	5512	4196.33

Table 5.17: Distribution of parameter estimates (continued).

Window	Time period	Permeability	Skin	Storage	r_{e1}	r_{e2}	Initial pressure
35	5545.04- 6073.25	26.94	-6.79	9.73	535	6719	4197.33
36	5795.31- 6460.00	42.33	-5.54	0.18	278	7111	4179.73
37	6073.25- 7352.83	92.39	-5.53	0.12	318	2738	4023.25
38	6460.00- 7352.83	99.56	-6.45	8.94	384	2582	3960.24
39	7352.83- 8572.64	90.83	-5.66	0.08	374	2878	3993.80
40	7517.83- 8572.64	88.00	-5.79	0.14	379	2980	3984.87
41	7800.33- 8572.64	110.38	-5.39	0.08	338	2732	3959.77
42	8572.64- 9416.47	66.16	-6.85	0.27	148	4230	3990.00
43	8777.42- 9416.47	65.57	-5.98	0.19	354	4391	3965.54
44	8899.42- 9416.47	64.83	-6.05	1.46	410	4882	3919.23
45	9032.65- 9697.24	66.42	-5.92	0.08	379	3967	3988.95
46	9416.47- 9971.72	54.40	-6.01	0.09	384	2902	4196.71
47	9697.24-10393.24	59.04	-6.19	1.95	227	2974	4191.87
48	9971.72-10601.96	37.00	-6.87	0.18	163	9600	4194.10
49	10186.95-10718.17	105.48	-5.15	0.40	299	1640	4194.98
50	10393.24-10922.40	89.81	-5.54	0.56	283	2104	4088.74
51	10601.96-11108.38	76.79	-5.31	0.83	160	3477	4005.43
52	10718.17-11459.86	52.94	-5.81	0.10	541	3735	4001.15
53	10922.40-11459.86	62.85	-5.59	0.35	410	4062	3903.33
54	11108.38-11666.52	65.82	-5.46	0.05	414	3804	3905.67
55	11459.86-12338.42	56.24	-5.83	0.68	564	3981	3905.04
56	11585.71-12338.42	53.60	-5.86	0.54	542	4336	3906.76
57	11882.13-12956.72	47.61	-5.91	0.45	421	6509	3911.21
58	12338.42-12956.72	60.03	-5.12	0.33	284	5864	3905.82
59	12956.72-13680.48	58.46	-5.49	0.08	473	4381	3916.33
60	13292.56-13940.70	41.54	-6.24	0.09	553	3733	4182.78
61	13680.48-14724.14	38.02	-6.43	0.20	487	4099	4194.27
62	13940.70-14724.14	26.81	-7.13	9.26	494	5695	4185.13
63	14724.14-15753.22	35.12	-6.78	9.27	501	6621	3939.73
64	15753.22-16338.34	68.67	-6.40	0.14	304	3489	3921.02
65	15861.25-16363.87	67.87	-6.42	0.40	295	3598	3909.78
66	16153.43-16786.38	56.99	-5.81	0.06	345	3826	4028.10
67	16338.34-17237.00	54.79	-5.81	0.07	347	3621	4103.44
68	16586.29-17237.00	50.21	-5.70	0.08	514	3317	4183.44
69	16786.38-17291.27	57.02	-5.61	0.08	329	3252	4191.59

Table 5.17: Distribution of parameter estimates (continued).

Window	Time period	Permeability	Skin	Storage	r_{e1}	r_{e2}	Initial pressure
70	17237.00-18227.33	52.33	-6.05	0.47	344	3349	4188.28
71	17341.47-18227.33	56.44	-6.03	9.40	396	3153	4154.24
72	18227.33-18908.37	58.25	-5.24	0.18	265	4970	3913.66
73	18908.37-20052.32	65.36	-5.24	0.12	279	4372	3904.00
74	19247.32-20052.32	67.11	-5.62	0.14	439	3751	3903.17

feet with an average value of 372.35 feet and a standard deviation of 95.59 feet. With wider spread, the most probable estimate for the distance to the further boundary lies between 2,000 and 5,000 feet as determined by the high densities in this range. The average distance is 3,994.18 feet, and the standard deviation is 1810.00 feet.

The uncertainties in the parameter estimates are results of uncertainties in data measurements (pressure and flow rate), instability in the wellbore and reservoir, and uncertainty from the regression procedure itself. Since the data were already collected, there is nothing we can do to reduce the uncertainties caused by the measurement errors and unstable reservoir environment. The only uncertainty that can be reduced at this point is the uncertainty that originates from the regression procedure. One way of reducing the regression uncertainty is to limit the rate of change of each parameter from one window to the next by allowing each parameter to take values within a certain range. For example, the parameters may be allowed to change at most +/- 50 percent from its current values. The limit on the ranges of parameter can be imposed by adding an artificial error to the objective function when running the regression. The additional artificial error is generally a U-shape function that reaches infinity at both lower and upper limits to discourage the regression from taking values near or beyond the limits. The function that generates the additional error is called the *penalty function* (Bard, 1974).

After experimenting with several rates of allowable change, it was found that the rate of +/- 25 percent is the most effective in minimizing the variations of parameter

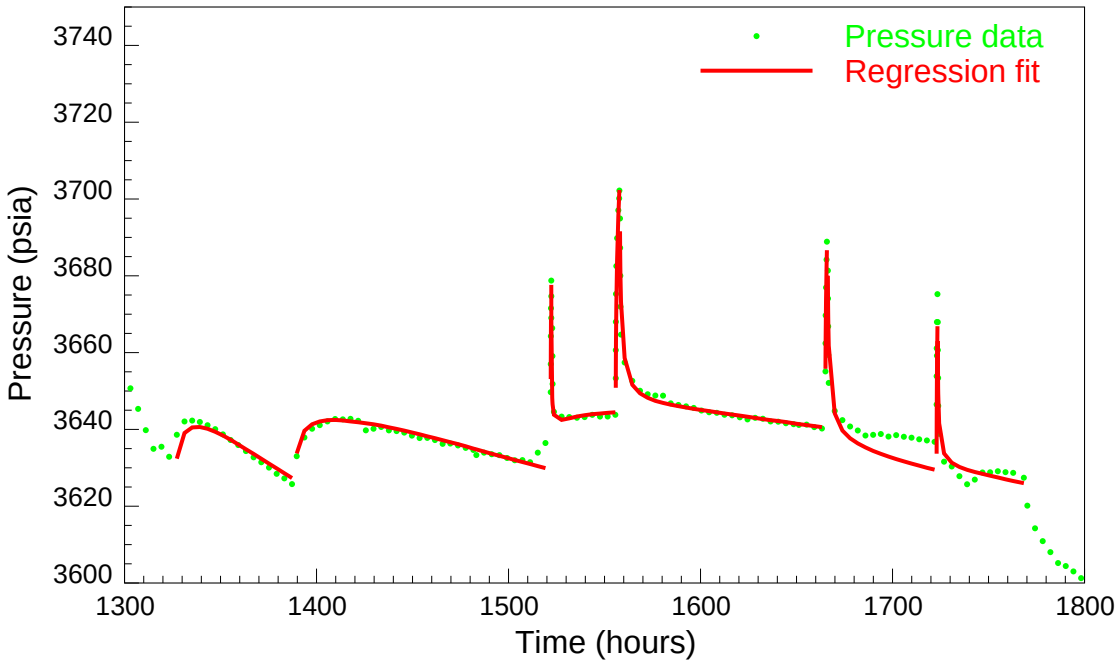

Figure 5.28: Regression match to window 10.

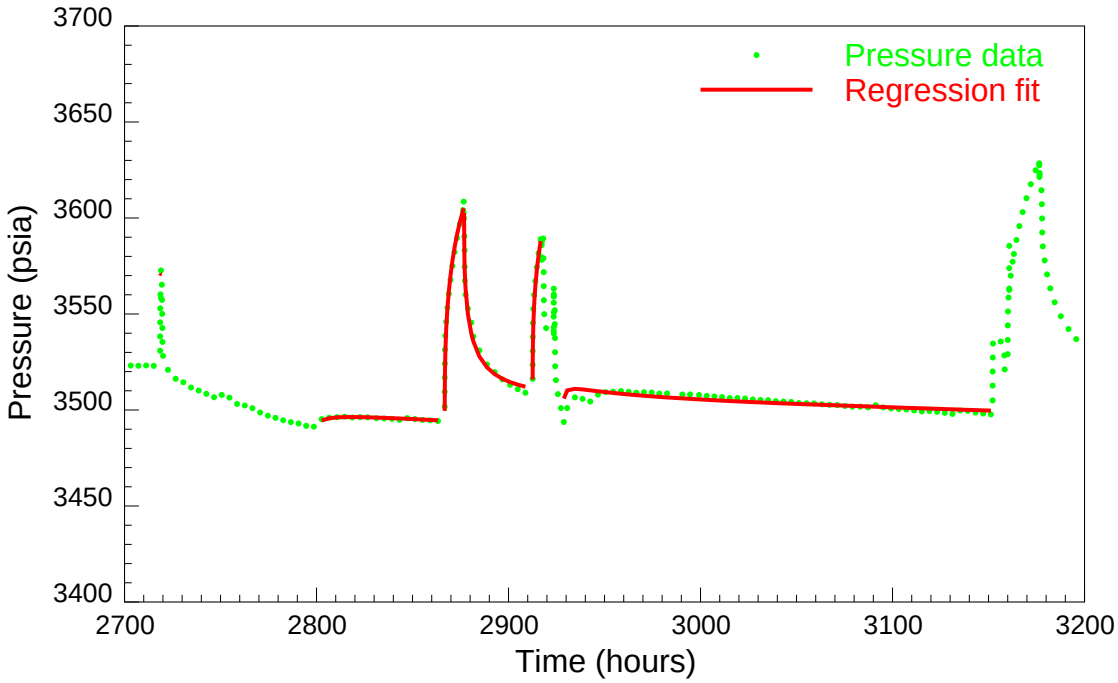

Figure 5.29: Regression match to window 20.

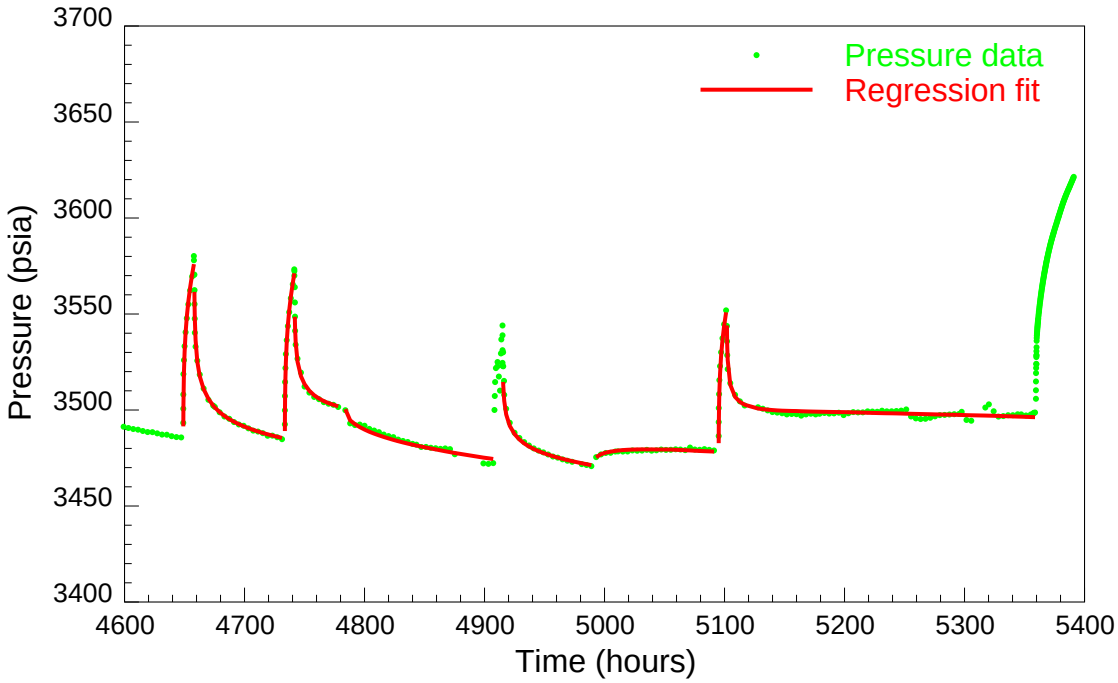

Figure 5.30: Regression match to window 30.

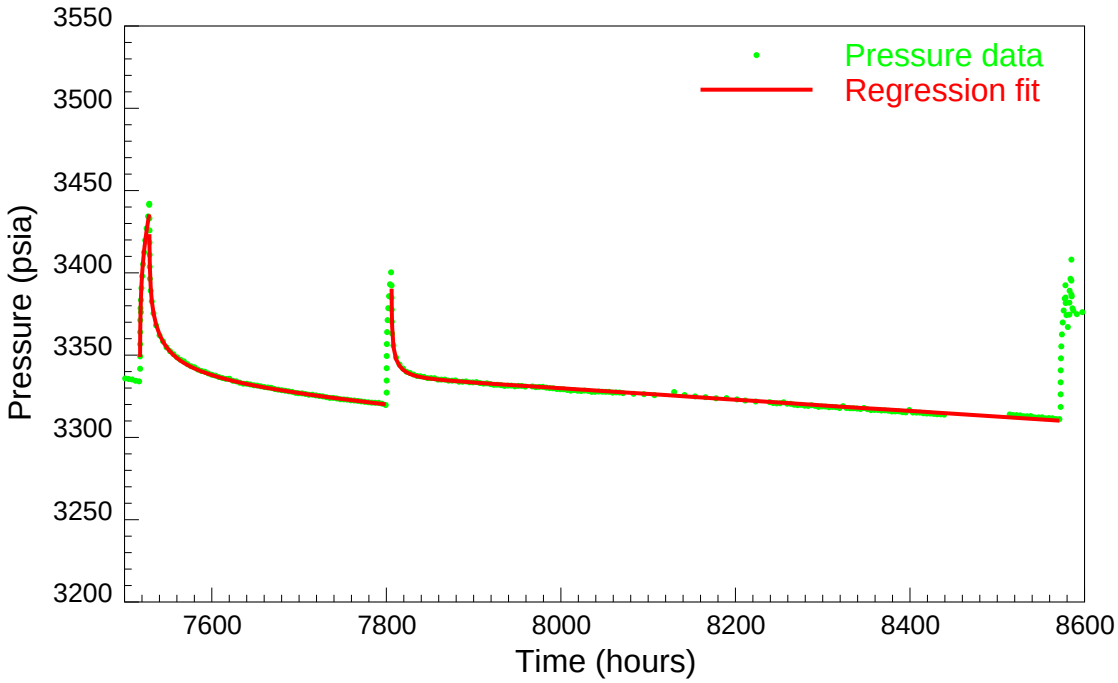

Figure 5.31: Regression match to window 40.

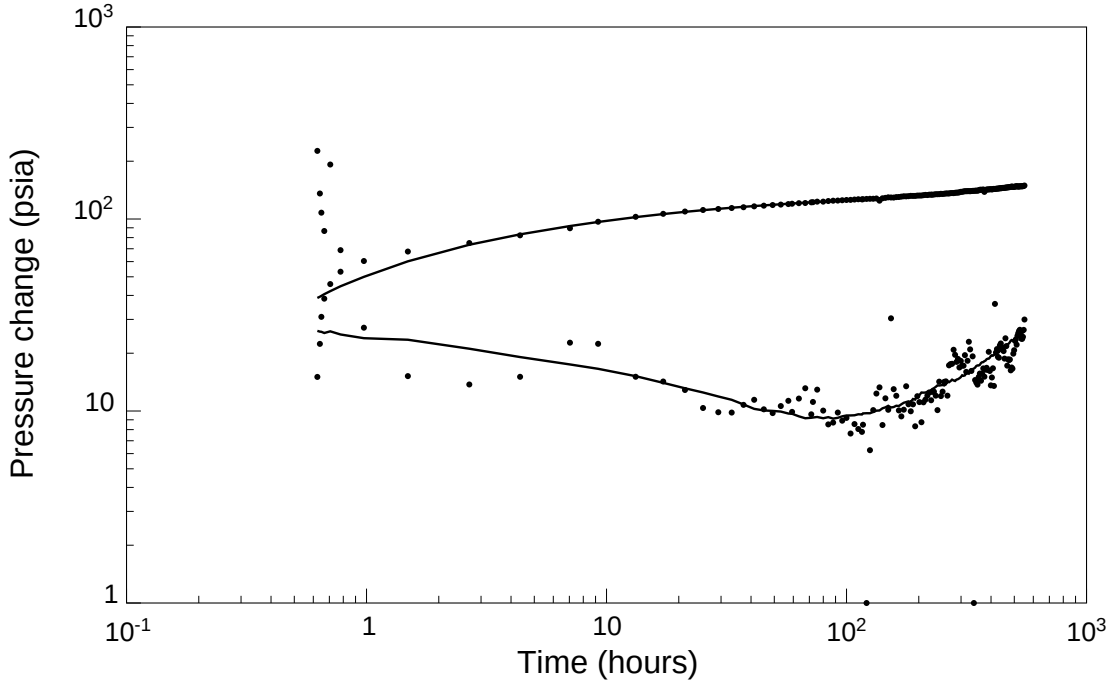

Figure 5.32: Log-log plot of regression match of a transient in window 58.

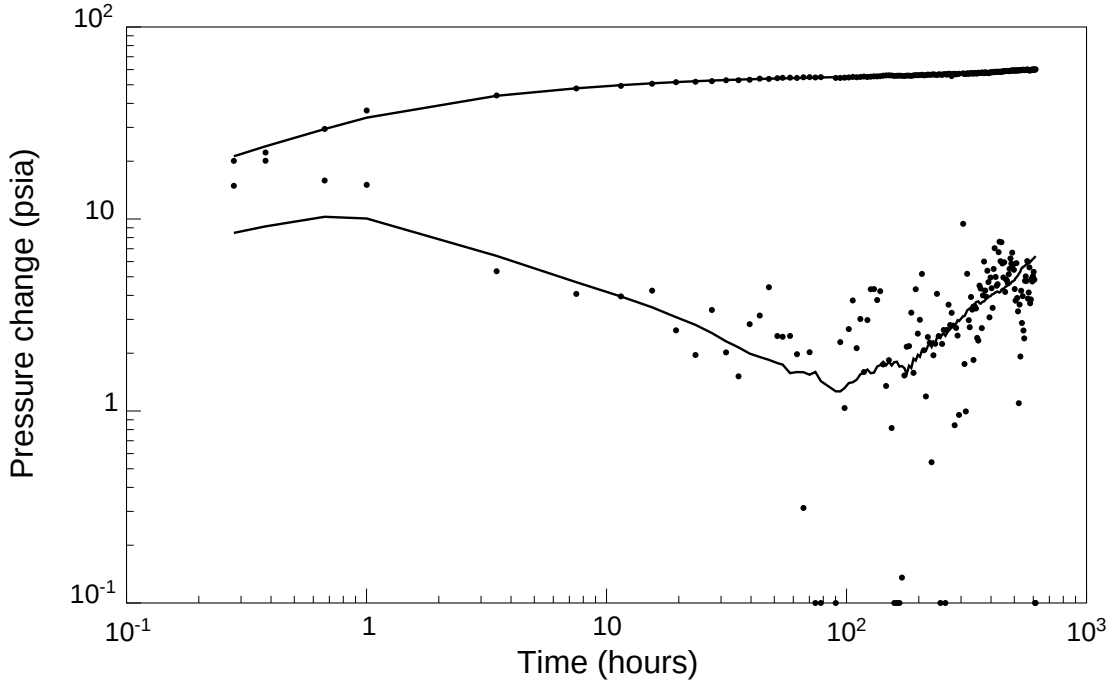

Figure 5.33: Log-log plot of regression match of a transient in window 72.

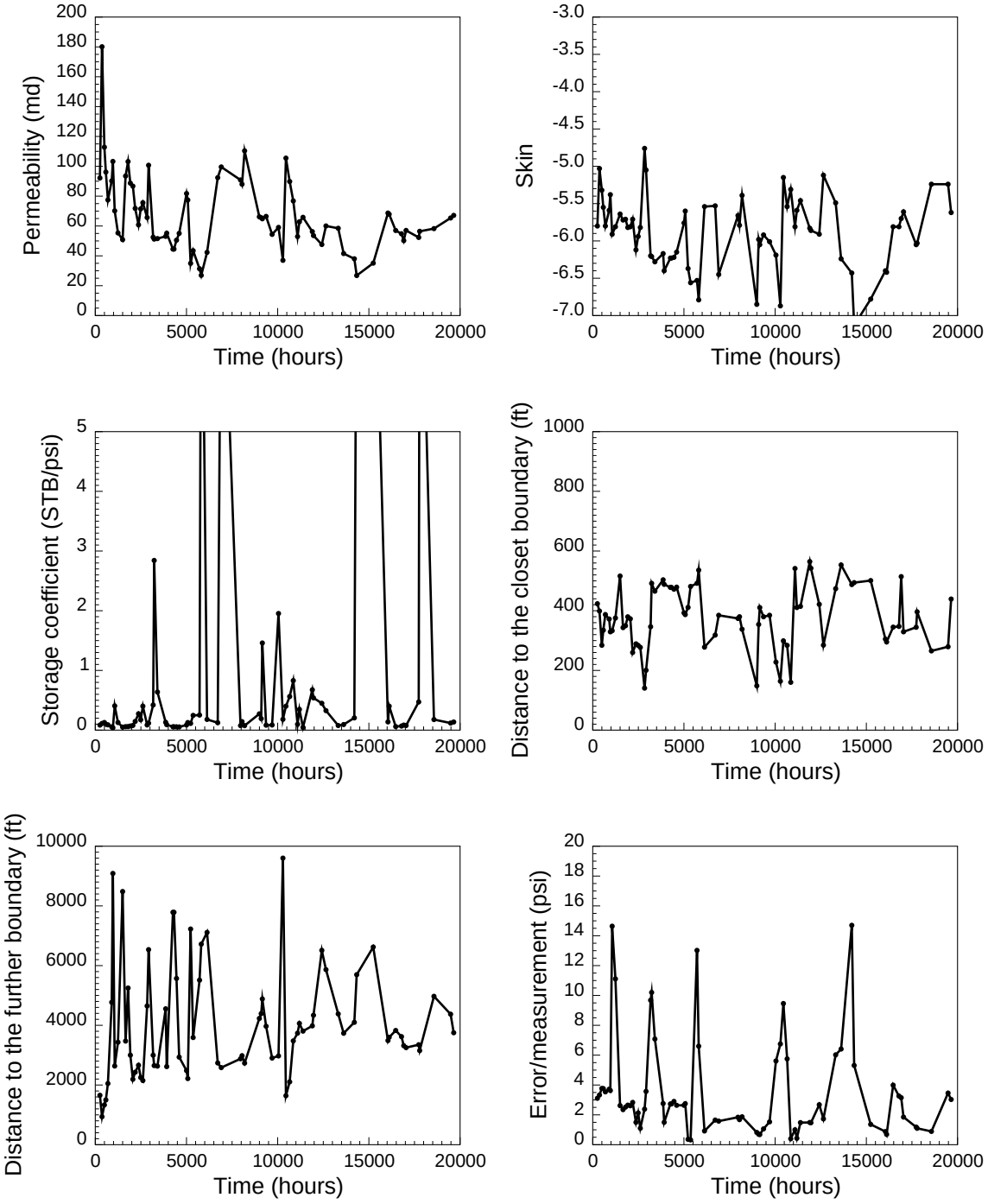

Figure 5.34: Estimates of model parameters and average error between the measurements and computed response using free search space (window width = 500 hours).

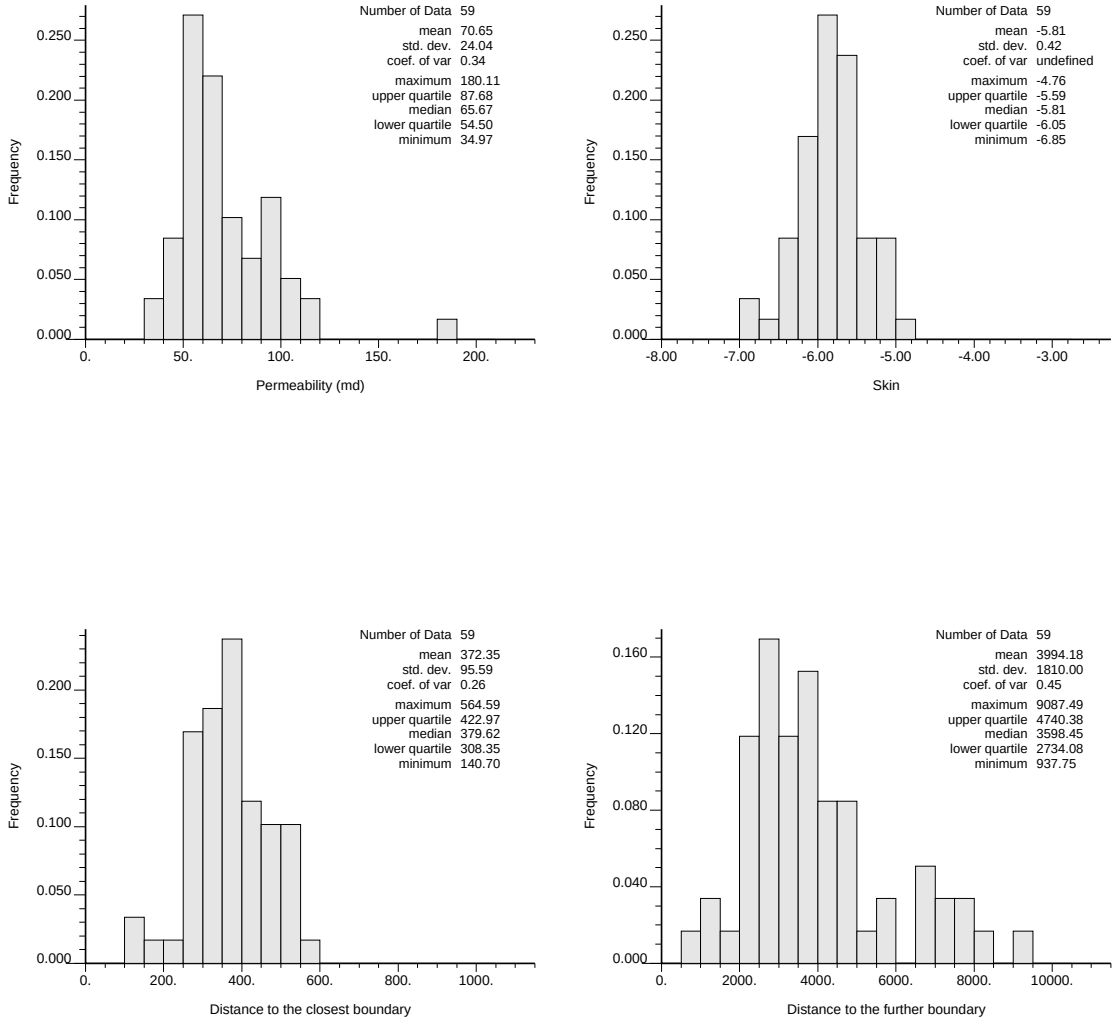

Figure 5.35: Distribution of estimates of model parameters using free search space (window width = 500 hours).

estimates while having a small effect on the average error between the measurements and computed response. The estimates of reservoir parameters and the average error between the measurements and computed response from the moving window analysis in which the parameters were allowed to change at most 25 percent from their estimates in the previous window are shown in Fig. 5.36. Since there is a limit imposed on each parameter, this implementation is referred to as a regression with *limited search space* in contrast to $free$ *search space* regression that was used previously. As seen in Fig. 5.36, the estimate for each model parameter has less variation than the estimate obtained from the regression with free search space (see Fig. 5.34 for comparison). The average error from the regression with limited search space is approximately the same as the average error from the free search space case. The small difference in the average errors between the two implementations confirms that the results from both cases are equally good. However, the results from the new implementation are better representations of actual reservoir properties as they contain less variations which are caused by uncertainties in the nonlinear regression procedure.

The distributions of parameter estimates and their statistics from the regression with limited search space are shown in Fig. 5.37. As in the previous case, the estimates from windows in which the average error per measurement is higher than five are excluded from the plots. Therefore, there are only 59 estimates in each distribution plot instead of 74. The average values of permeability, skin, distances to the closest and further boundaries are 63.18 md, -5.92, 427.80 feet, and 3,511.51 feet, respectively. In general, the distributions of the estimates in this case are narrower than those in free search space case (see Fig. 5.35 for comparison). For example, the standard deviation of the distribution of the permeability estimates is 17.02 in the limited search space case while the standard deviation of the permeability distribution in the free search space implementation is 24.04. The reduction in the spread of the distribution is a direct result of smaller variation of parameter estimates.

The distributions and statistics of the parameter estimates provide an insight into the uncertainties of the estimation of reservoir properties. They can be used to

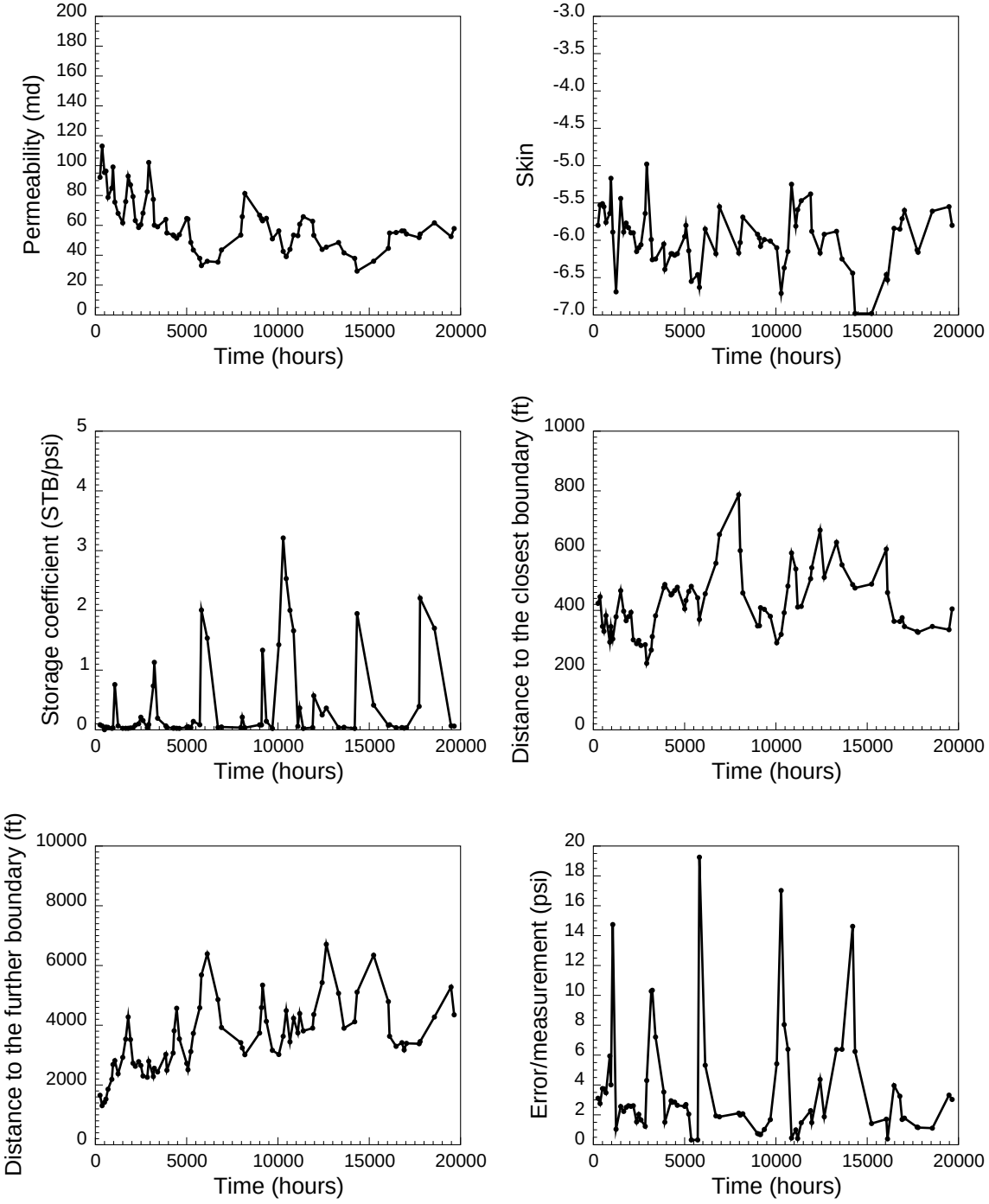

Figure 5.36: Estimates of model parameters and average error between the measurements and computed response using limited search space (window width = 500 hours).

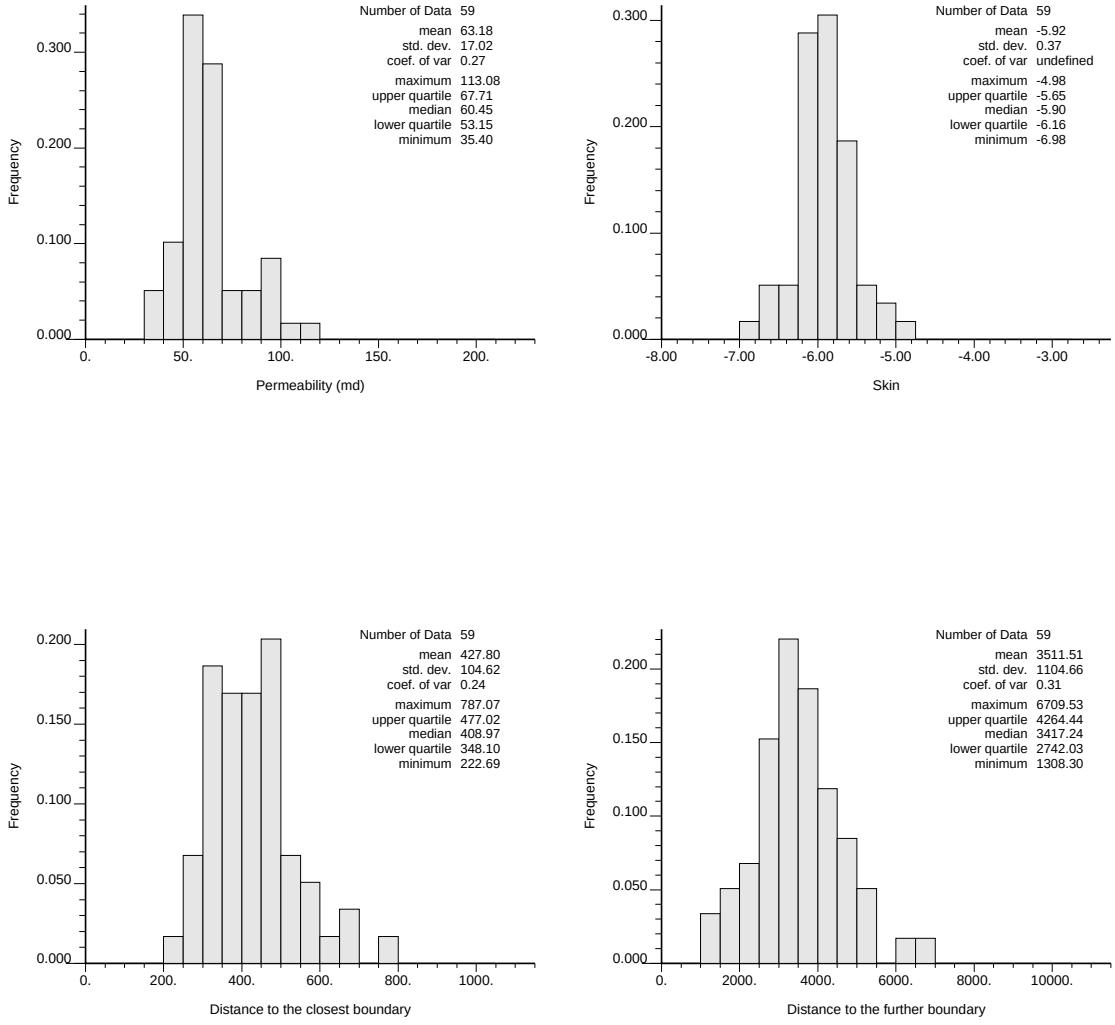

Figure 5.37: Distribution of estimates of model parameters using limited search space (window width = 500 hours).

assess uncertainties associated with results obtained from subsequent analyses such as forecasting future reservoir performance, production scheduling, economic evaluation, or any type of analysis that uses these reservoir parameters as input data. For this reason, a collection of estimates is more valuable than a single set of parameter estimates. Even though there are uncertainties associated with the estimates from the moving window analysis, results of further reservoir studies obtained by using parameter distributions are more certain than the results obtained by a single set of estimates.

To study the effect of window size on the regression results, two additional runs were conducted using a window size of 200 and 1,000 hours. The translation length was kept at the same value (100 hours). The moving window analysis with limited search space was implemented in both cases. The estimates of the reservoir model parameters and an average error between the measurements and computed response for the two runs are plotted in Figs. 5.38 and 5.40. The distributions of parameter estimates are shown in Figs. 5.39 and 5.41. Comparing among Figs. 5.36, 5.38, and 5.40, the estimates of permeability, skin, and storage coefficient appear to be a little smoother as the window becomes wider. On the other hand, the estimates for the distances to the two boundaries exhibit higher degrees of variation. The large variations in the estimation of distances to boundaries may be due to the weakness of the regression in resolving the distances to the boundaries when there are two or more boundaries. Also, data that cover over a long time span are subject to different reservoir conditions. In the moving window analysis, we assume no changes in the reservoir conditions and reservoir properties within a window (although they can be different between windows). As a result, grouping data that are collected during different reservoir conditions into the same window may introduce additional uncertainties in the regression. Therefore, the window should not be too wide. The most appropriate window size may vary for different sets of data. We may need to experiment with a few window widths to determine a suitable one. In this example, the analysis with a window size between 200-500 hours appear to provide the best results.

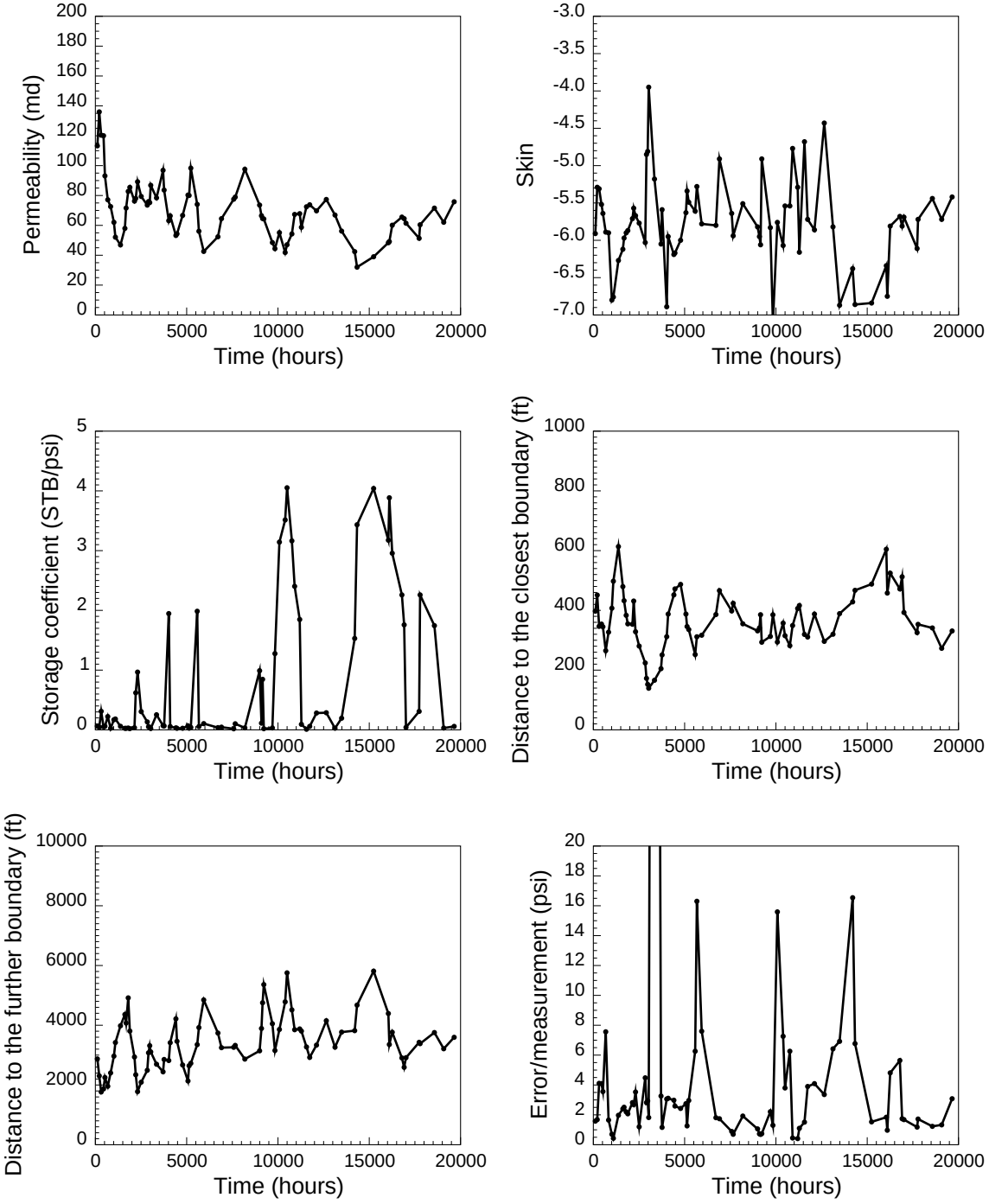

Figure 5.38: Estimates of model parameters and average error between the measurements and computed response using limited search space (window width = 200 hours).

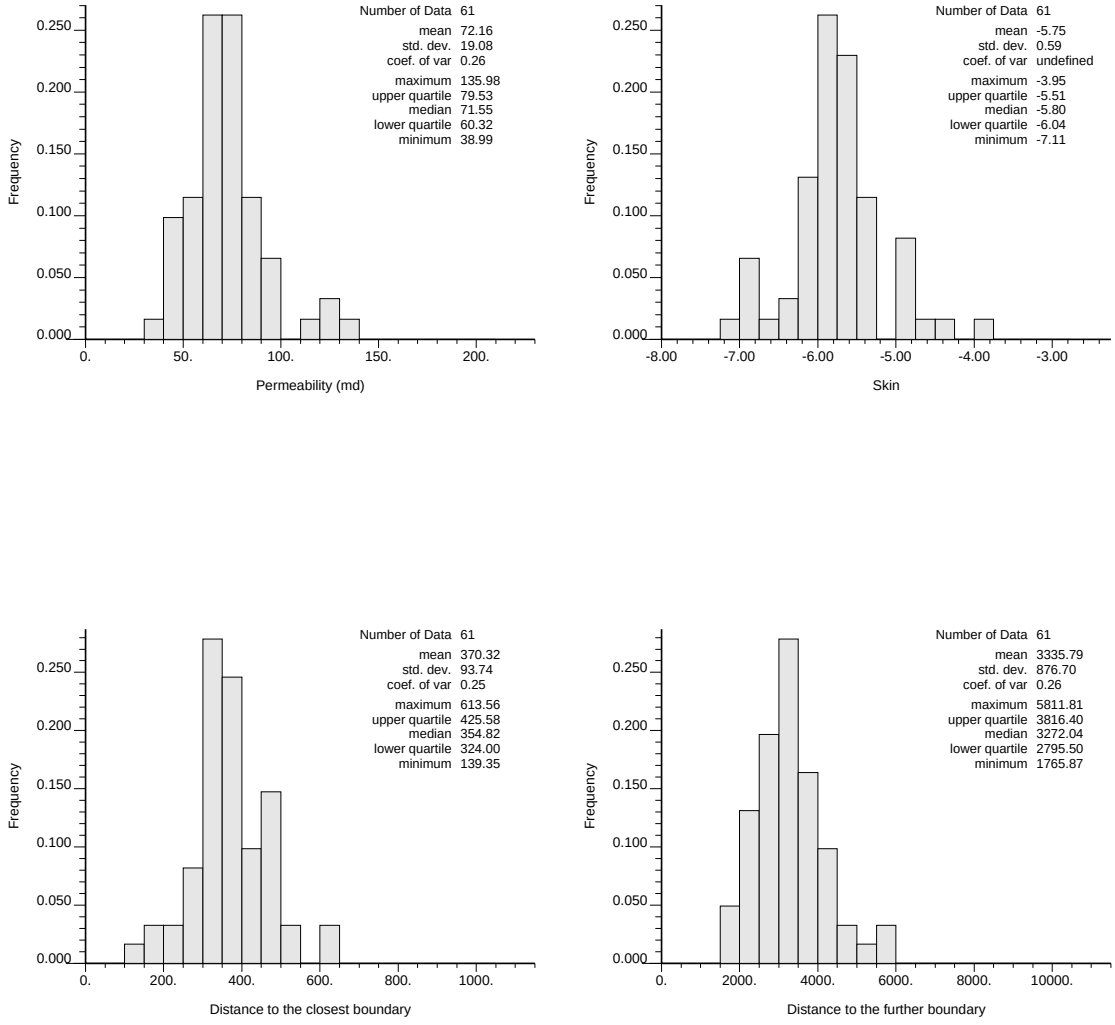

Figure 5.39: Distribution of estimates of model parameters using limited search space (window width = 200 hours).

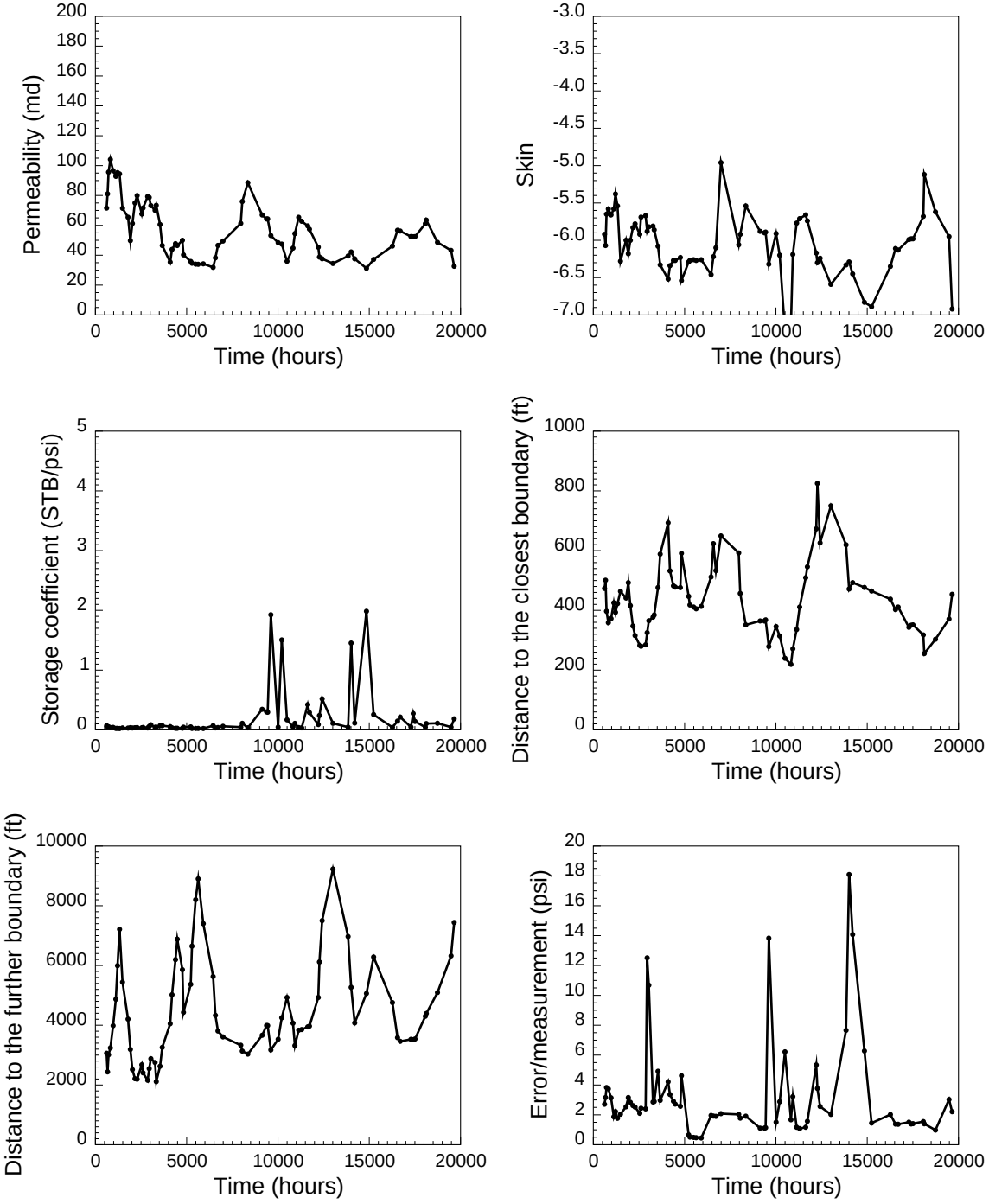

Figure 5.40: Estimates of model parameters and average error between the measurements and computed response using limited search space (window width = 1000 hours).

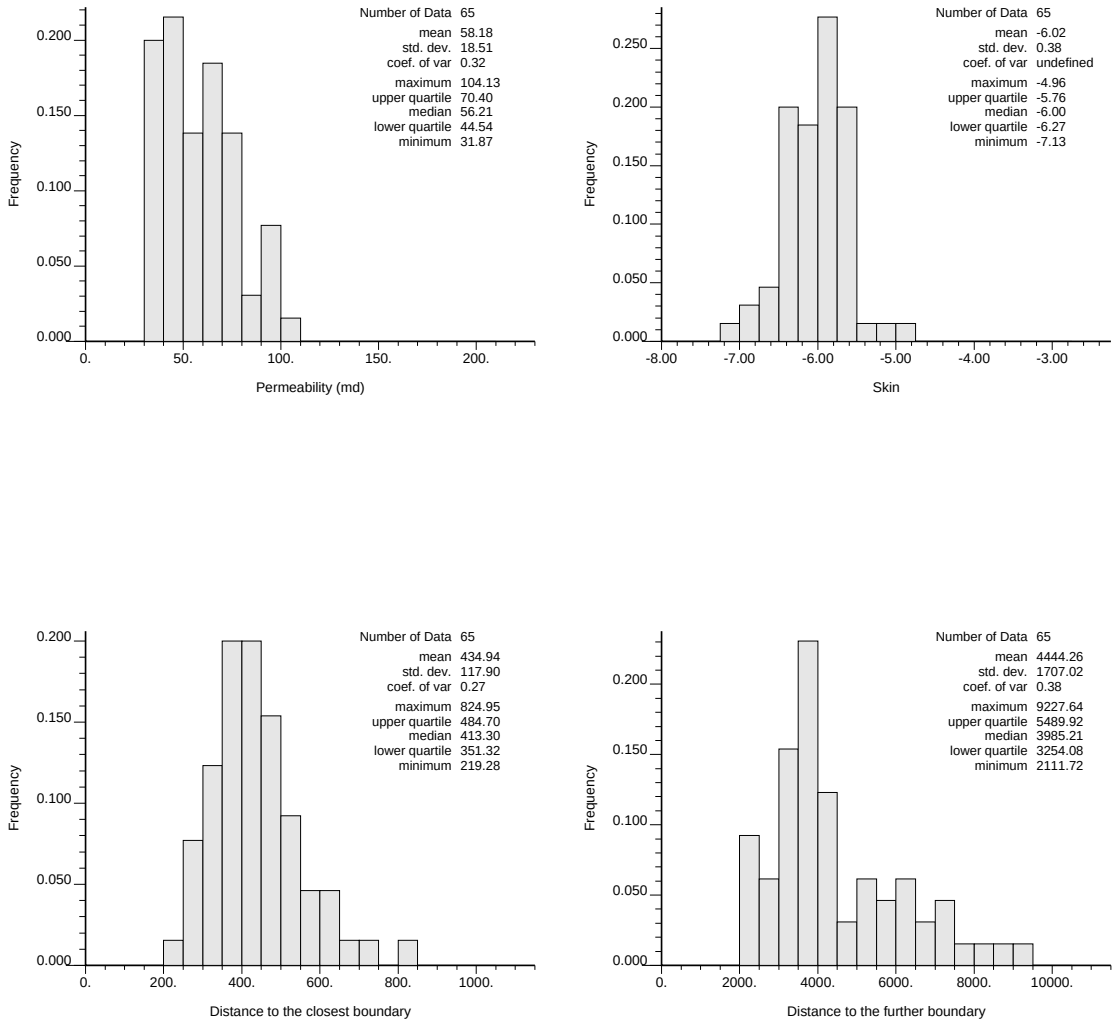

Figure 5.41: Distribution of estimates of model parameters using limited search space (window width = 1000 hours).

Two additional analyses were performed with a translation length of 50 and 200 hours using a window size of 500 hours. Figs. 5.42 and 5.43 show the estimates of reservoir parameters and an average error between the measurements and the computed response for the two analyses. The total number of moving windows increased from 74 to 102 as the translation was reduced to 50 hours. When the translation length of 200 hours was used, the number of windows was reduced to 53. It is seen from the two figures that the estimates of model parameters fluctuate more as the translation length decreases. The general trends of the parameter estimates are similar. In theory, the parameter estimates should become smoother as the translation length decreases due to a higher degree of overlapping between windows of data. The larger degree of fluctuation seen in Fig. 5.42 may be caused by the uncertainty in the nonlinear parameter estimation process. Since each of the parameter estimates is allowed to vary within 25 percent range of the estimate in the previous window, an increase in the number of window allows the parameters to change more freely. As a result, the estimates from a moving window analysis with a short translation length may have a higher degree of variations in the parameter estimates.

Another regression was conducted to compare the results obtained from the moving window analyses with the estimates in the global analysis which analyzes the entire set of data all at once. The window size in this case is 20,051 hours. This run is referred to as *Global* 1 in Table 5.18. The estimates for the model parameters from the global analysis are compared with the means of the estimates of model parameters from the moving window analyses with different window sizes in Table 5.18. With the same set of initial guesses, the global analysis did not converge to the right solutions as the average error per measurement is quite high (15.26 psi/data point). These estimates have different magnitudes from the results obtained from the moving window analyses. After resetting the initial guesses to be close to the means of the estimates obtained in the moving window cases, the global regression was able to converge to the right solutions. This case is referred to as *Global* 2 in Table 5.18. The estimates of reservoir parameters are now close to the estimates from the moving window analyses. The average error was reduced from 15.26 psi to 4.38 psi per data

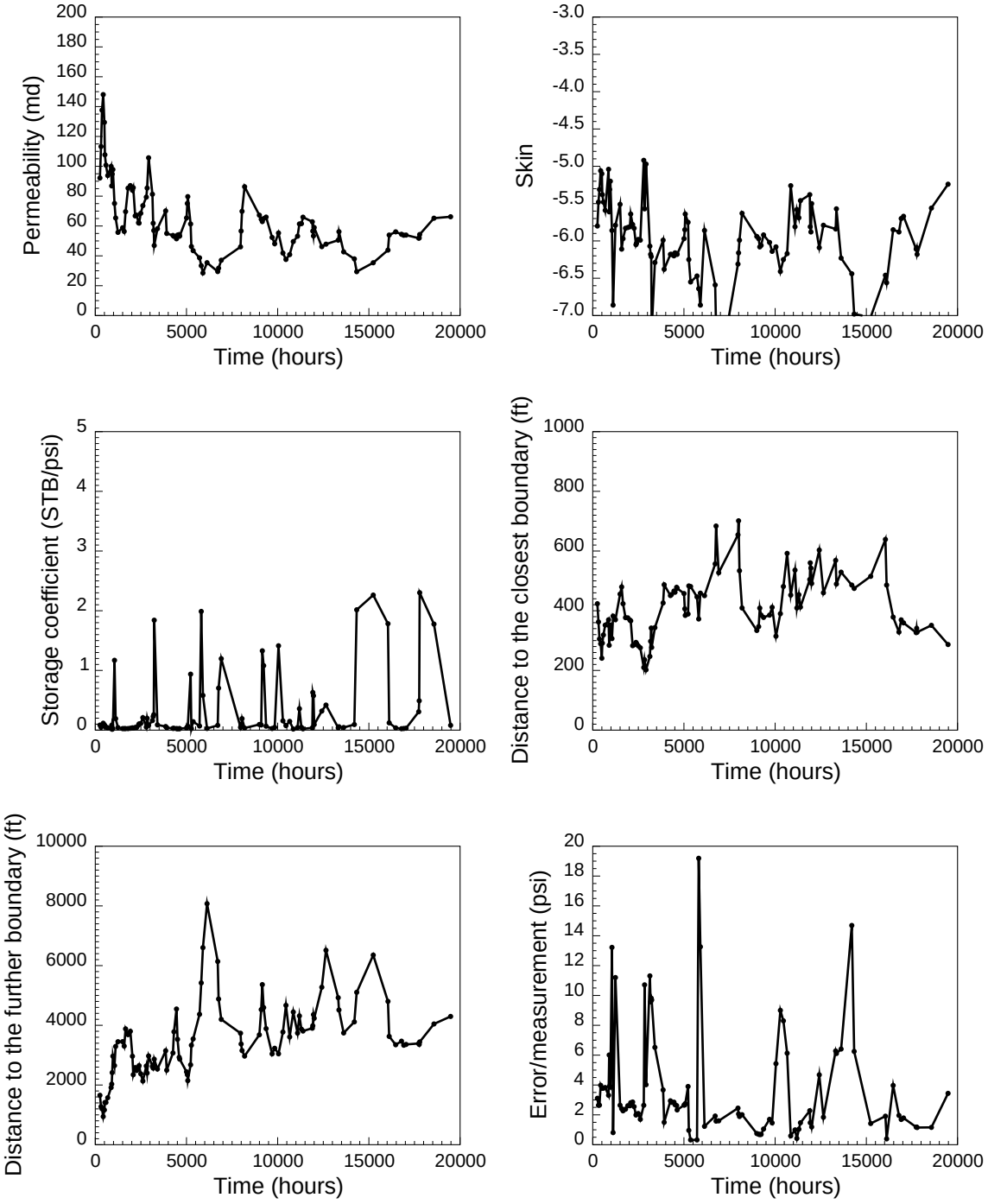

Figure 5.42: Estimates of model parameters and average error between the measurements and computed response (translation length = 50 hours).

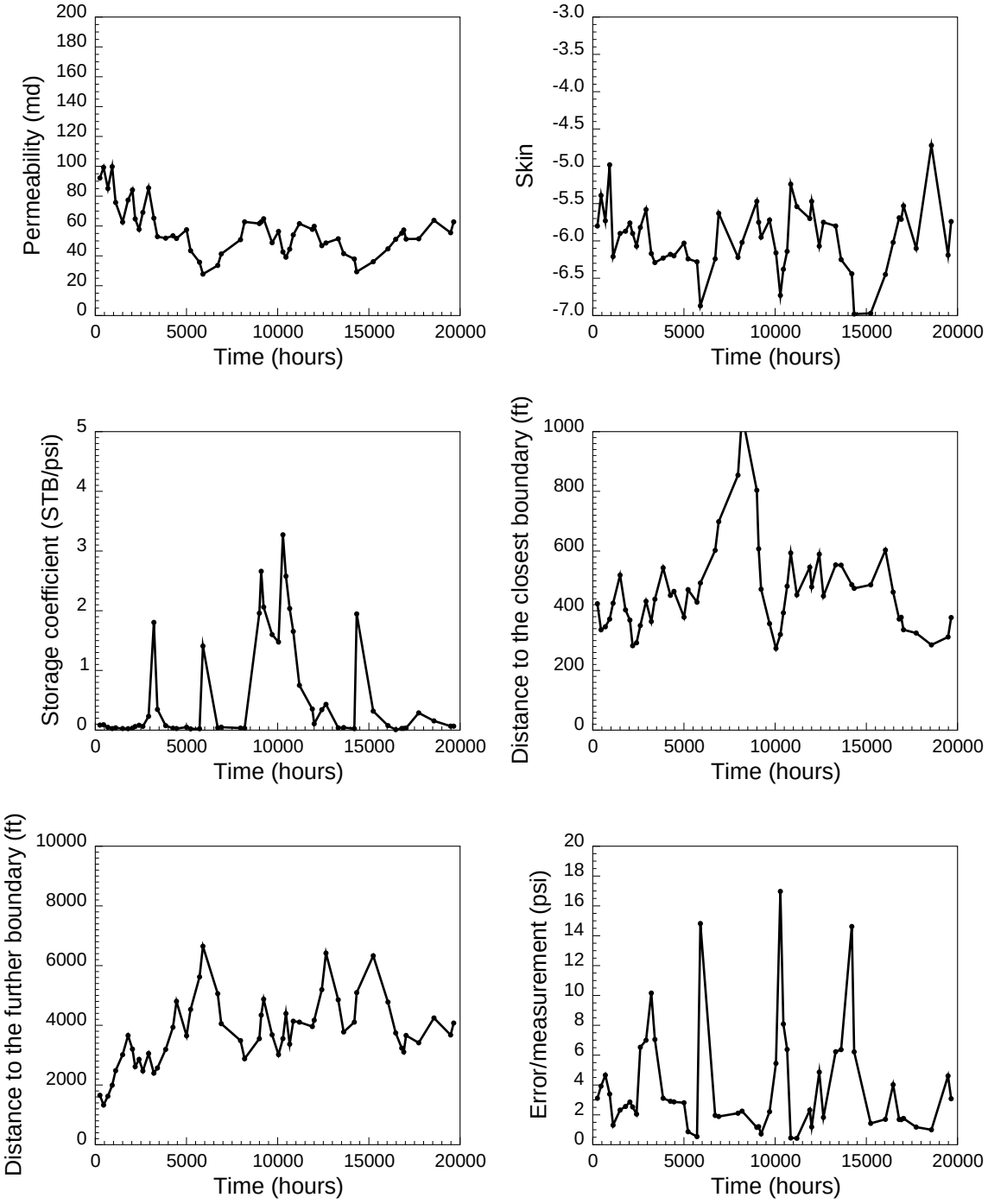

Figure 5.43: Estimates of model parameters and average error between the measurements and computed response (translation length = 200 hours).

Table 5.18: Comparison between the means of parameter estimates from moving analyses and the estimates from the global analysis.

Window size	Permeability	Skin	r_{e1}	r_{e2}	Average error
200	72.16	-5.75	370.32	3335.79	2.14
500	63.18	-5.92	427.80	3511.51	2.10
1000	58.18	-6.02	434.94	4444.26	2.17
Global 1	423.35	14.61	285.54	1063.57	15.26
Global 2	65.08	-5.90	389.72	2426.56	4.38

point. In any case, the average error is still quite high when compared to those from the moving window analyses due to unresolved inconsistencies between transients over a long period of time. The computed response from the global regression averages through the overall data instead of fitting the data locally as it is the case in the moving window analyses. Therefore, a regression match to each individual section may not be as good as the one in the moving window analyses.

In terms of computational efficiency, the moving window analyses took less time to analyze the data. The total CPU time for each moving window analysis was approximately 30 minutes on a 275 MHz DEC Alpha machine whereas it took about 120 minutes of CPU time to perform a global analysis. There are six reservoir model parameters (k, S, C, r_{e1}, r_{e2}, and p_i) and 160 unknown flow rates for this set of data. The total number of data is 8,487 points. In the moving window analysis, there are approximately 2-20 unknown flow rates and 200-1500 data points in each individual window depending on the lengths of transients and actual window lengths. Analyzing a small set of data with a small number of unknowns in a sliding window fashion reduces the total computational time by approximately a factor of four. Since data are divided into windows, the moving window analysis requires less computer memory to perform the regression.

In summary, three main advantages of using the moving window analysis over the global analysis are: (1) the moving window analysis provides distributions of estimates for reservoir model parameters instead of a single set of estimates, (2) the

time spent to perform the window analysis is shorter, and (3) the analysis requires a smaller amount of computer memory.

5.3.3 Field Example 3

The data used in this example are from a gas condensate reservoir. Most of the data were collected at a uniform sampling interval of 10 seconds. However, there are some large gaps present in the data. There are approximately 18,640 hours (26 months) of data accounting for more than six million data points. The raw data were first screened for outliers and denoised before undergoing transient identification and data reduction processes. The transient identification results were reexamined before being used as input data in the moving window analysis. During the data reduction step, the data size was reduced to 74,139 data points. Since the data were generally collected at a very high frequency, the data size was reduced by almost one hundred folds.

In this example, cumulative production data are available on a daily basis. As mentioned in Section 5.3.1, some flow rates can be determined from the daily production data. There were 407 major flow rate changes during the 26-month period. A total 168 flow rates were determined from the daily production data. Therefore, there are still 239 unknown flow rates remaining. The constraints for the regression in this case are both the determined flow rates and the cumulative production data. To simplify the analysis of this gas condensate reservoir (due to the lack of relative permeability data), the pressure data were converted to real gas pseudopressure assuming dry gas behaviors. An analysis of the reservoir and geologic information suggests that the well may be placed in a rectangular reservoir with three closed boundaries and a constant pressure boundary. A preliminary window width of 500 hours and translation length of 100 hours were chosen for the moving window analysis. As mentioned in the previous section, the window width and the translation length may be larger than the preliminary values to avoid beginning or ending a window in the middle of a transient. As in the previous example, the arithmetic weighting scheme was used in the moving window regression.

Regression matches to the pressure data for a few selected windows are shown in Figs. 5.44 - 5.47. Log-log plots of matches to long transients in windows 13 and 43 are

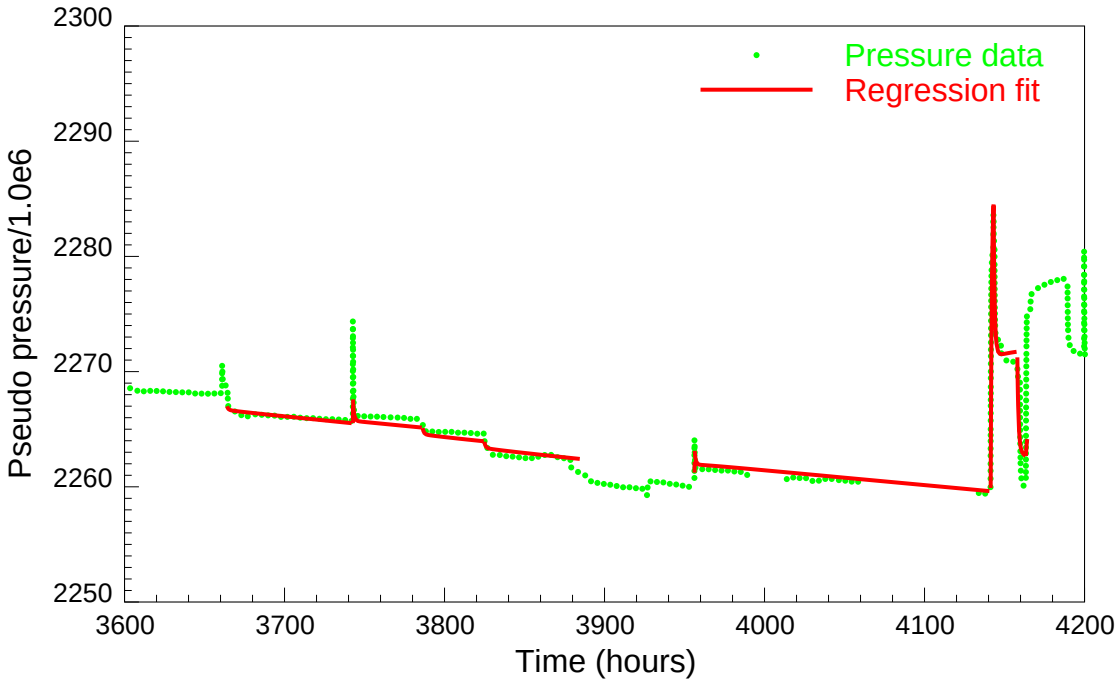

Figure 5.44: Regression match to window 10.

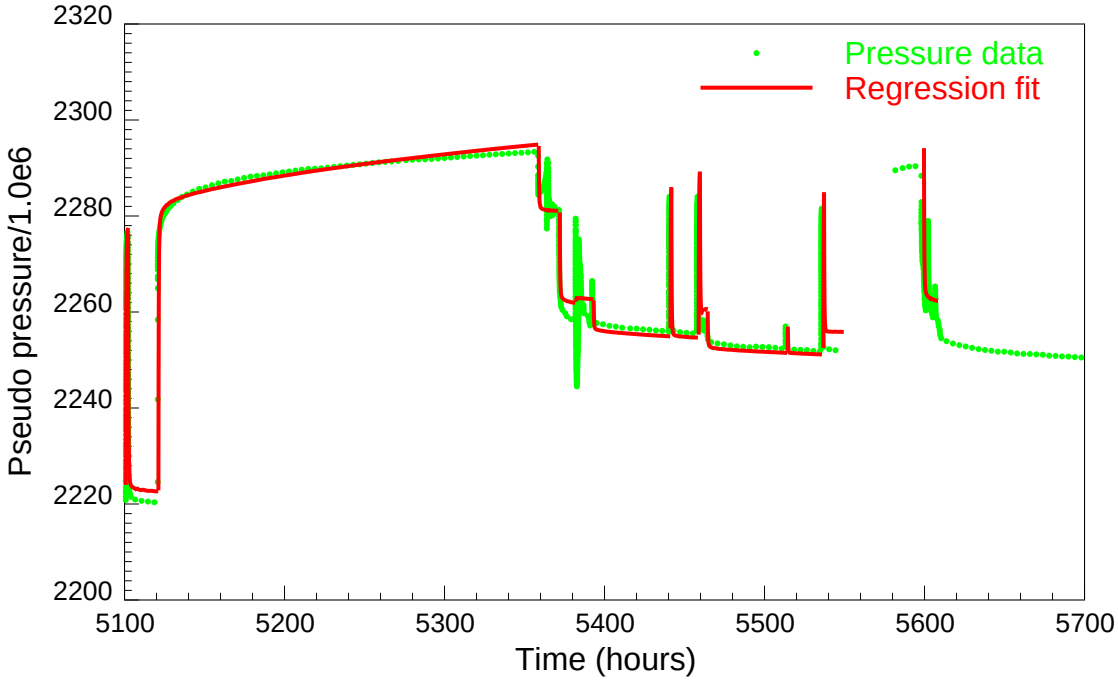

Figure 5.45: Regression match to window 20.

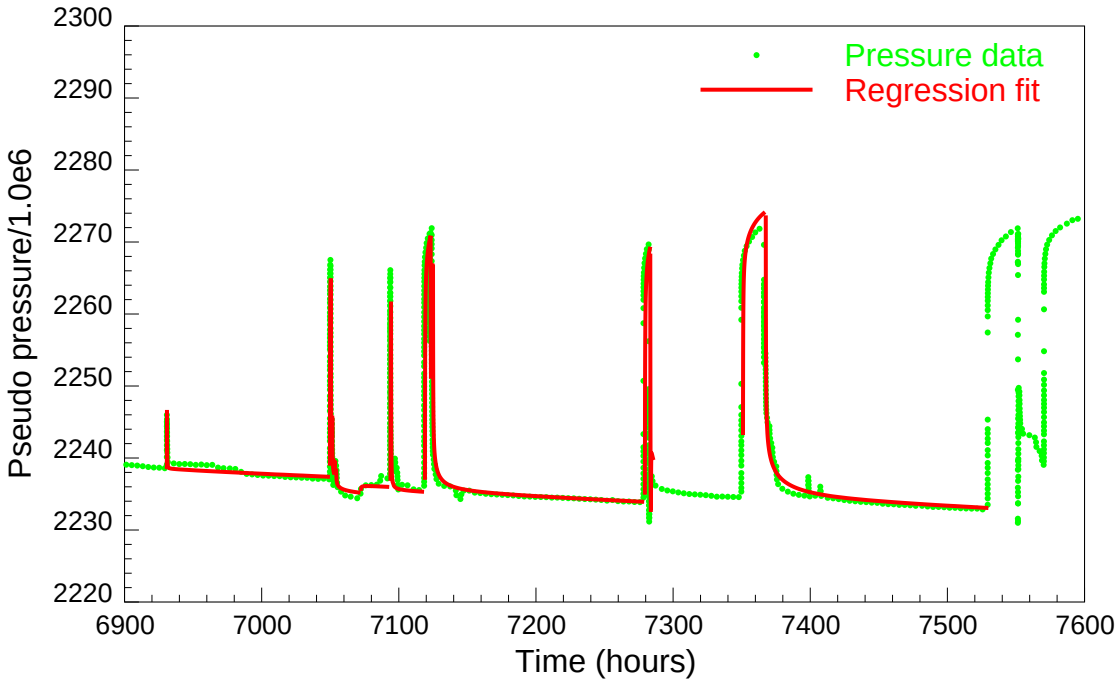

Figure 5.46: Regression match to window 30.

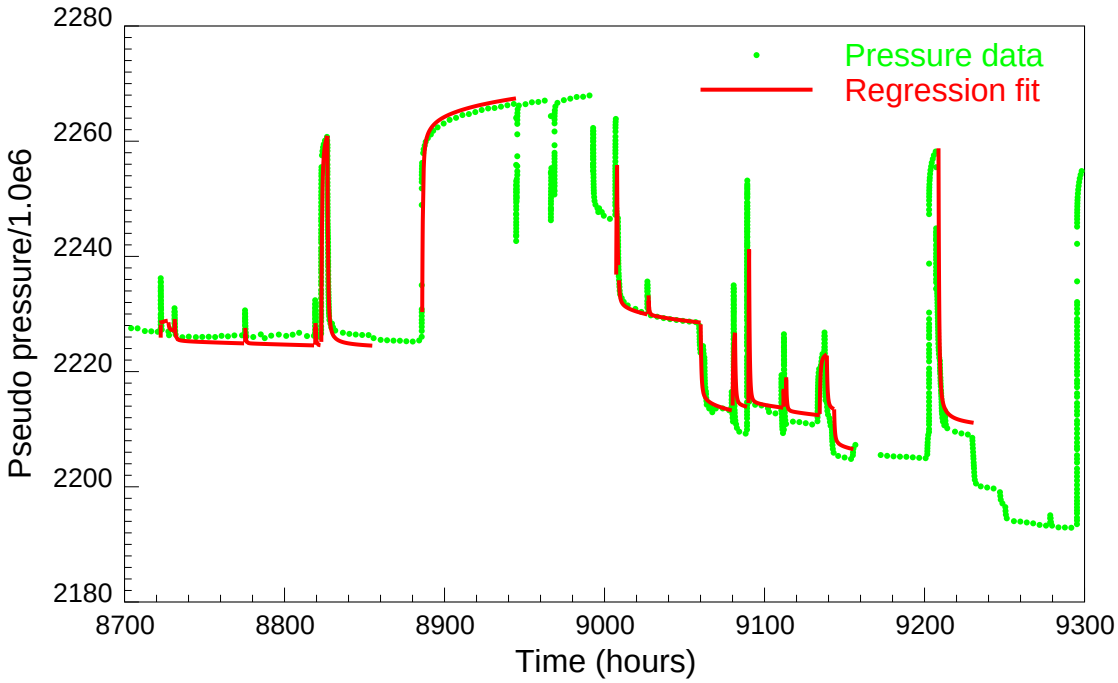

Figure 5.47: Regression match to window 40.

shown in Figs. 5.48 and 5.49, respectively. The middle-time and late-time matches to the pressure and derivatives confirm that the chosen model is an appropriate one. As mentioned in Section 5.3.1, the arithmetic weighting scheme weights each data point according to the time interval between the previous and the subsequent data points. Therefore, the early time data receive small weights due to their small spacings. As a result, the data are poorly matched at the early time. On the other hand, more weights are given to the middle-time and late-time data to force the regression to match the responses from the reservoir rather than the response occurred in the wellbore. The poor match during the early time period has the most effect on the estimation of storage coefficient. The estimation of other model parameters is minimally affected.

Fig. 5.50 plots the estimates of permeability, skin factor, and distances to rectangular boundaries as a function of time at the middle of each window. The east boundary is a constant pressure boundary while the rest of the boundaries are close boundaries. As in Field Example 2, the variations in the parameter estimates illustrate the uncertainties associated with the parameter estimation procedure. Fig. 5.51 shows the distributions of the parameter estimates along with their statistics. Only the estimates from windows in which the average error per measurement is less than 1.5 psi were included in these plots. As a result, the number of data in each of these distribution is 84 instead of the original number of 91 windows. The permeability distribution has an average value of 37.29 md and a standard deviation of 19.38. The skin is most likely to be in the range of -3.0 to 13 whereas its mean is estimated to be 5.44. The averages to the distances to the west, east, north, and south boundaries are 2,325, 21,429, 686, and 1,853, respectively.

In order to reduces the uncertainty due to the regression process, another run was made using limited search space as described in Section 5.3.2. The estimates of reservoir parameters using limited search space are shown in Fig. 5.52, and their distributions are plotted in Fig. 5.53. The estimate for each model parameter has less variation than the estimate obtained from the free search space in Fig. 5.50. All

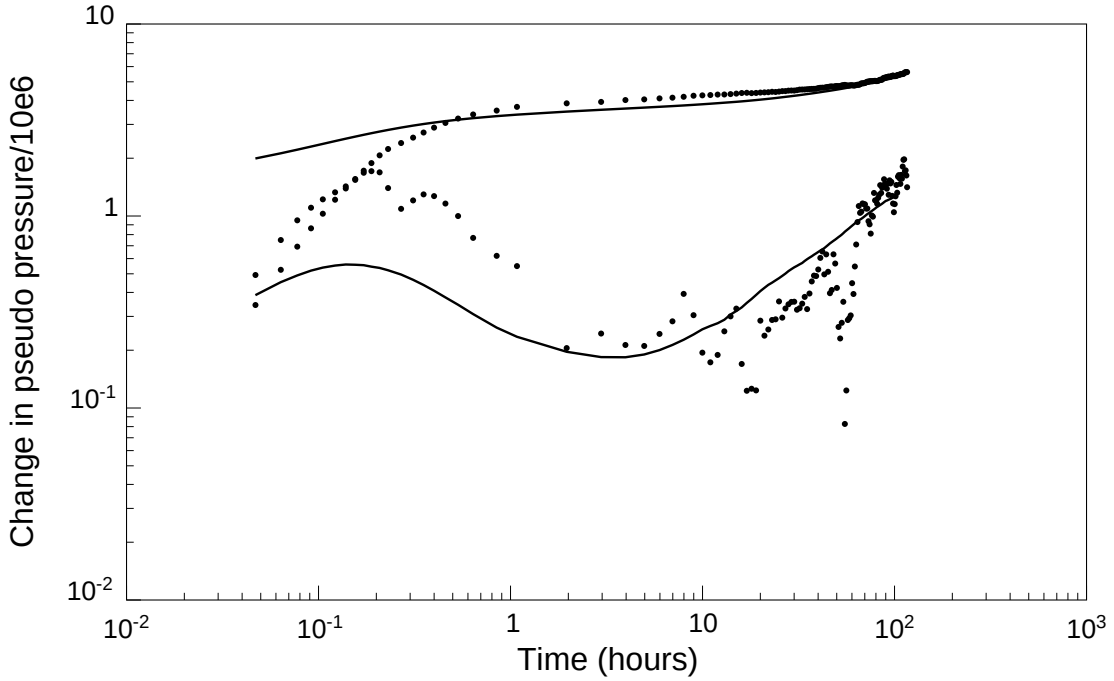

Figure 5.48: Log-log plot of regression match of a transient in window 13.

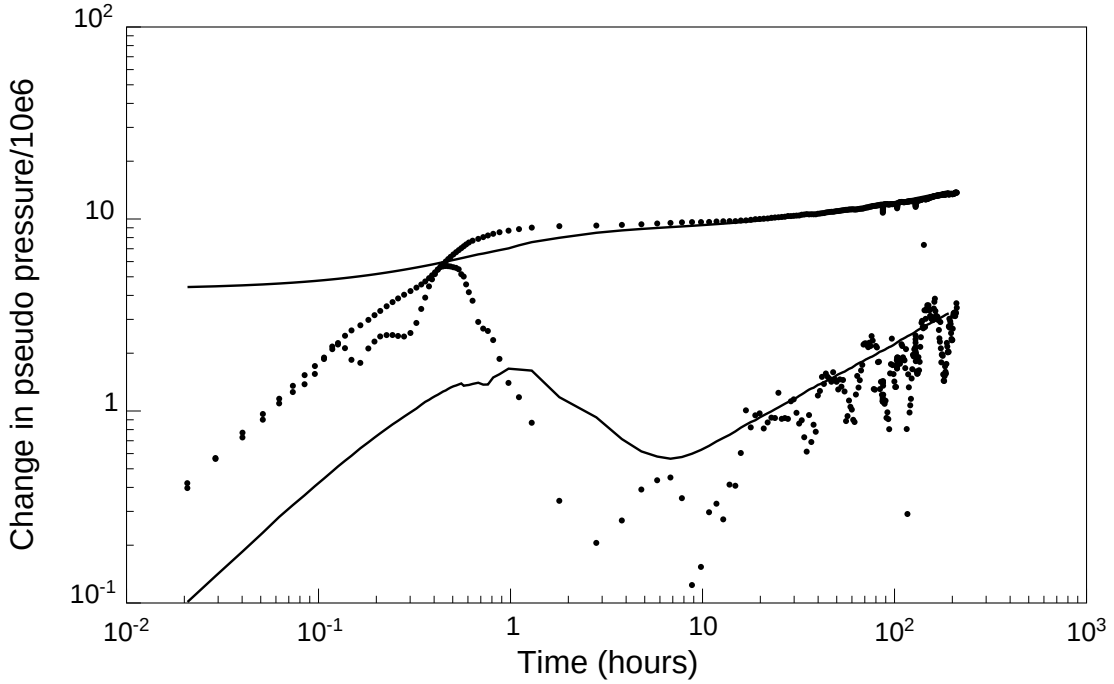

Figure 5.49: Log-log plot of regression match of a transient in window 43.

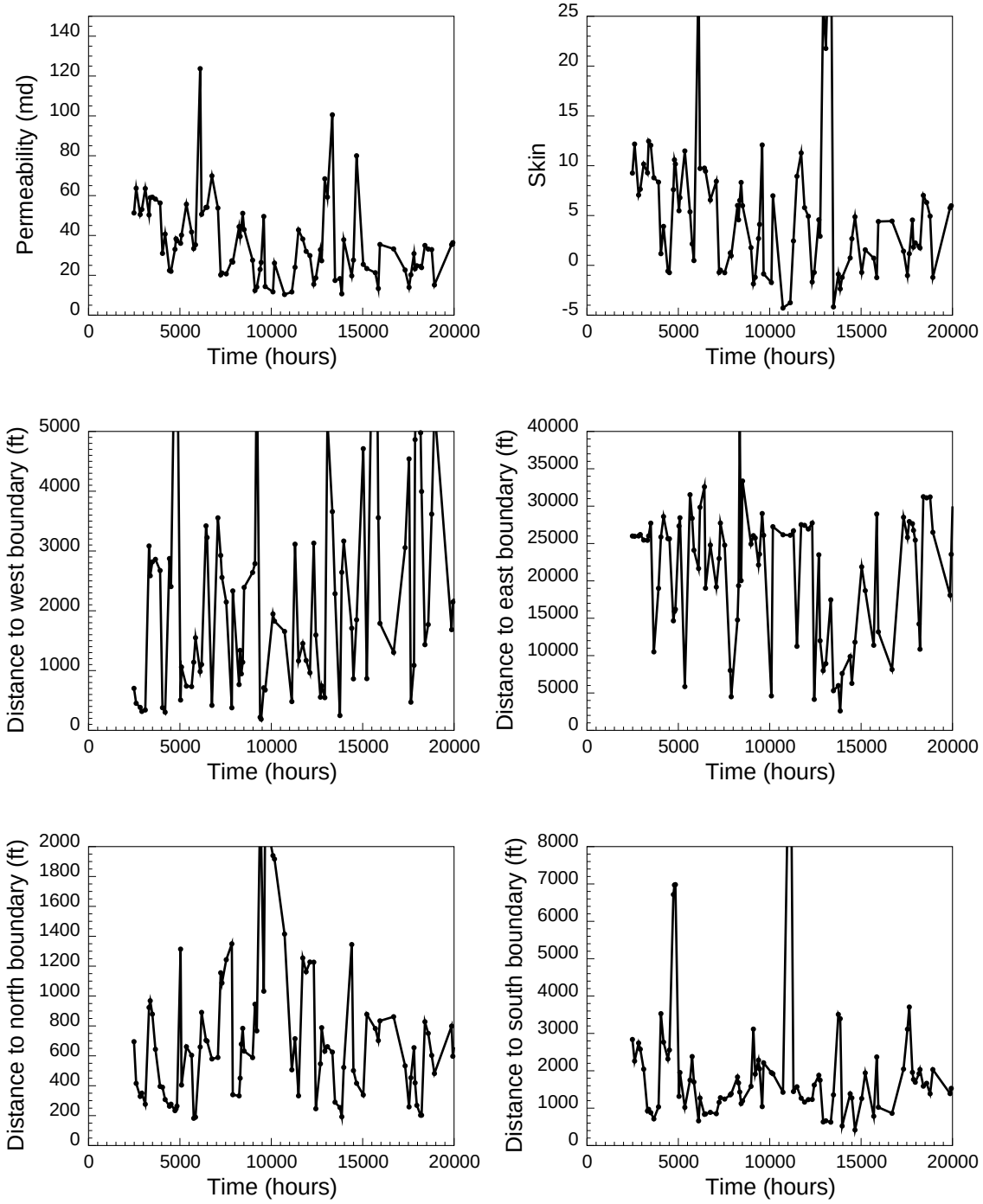

Figure 5.50: Estimates of model parameters using free search space (window width = 500 hours).

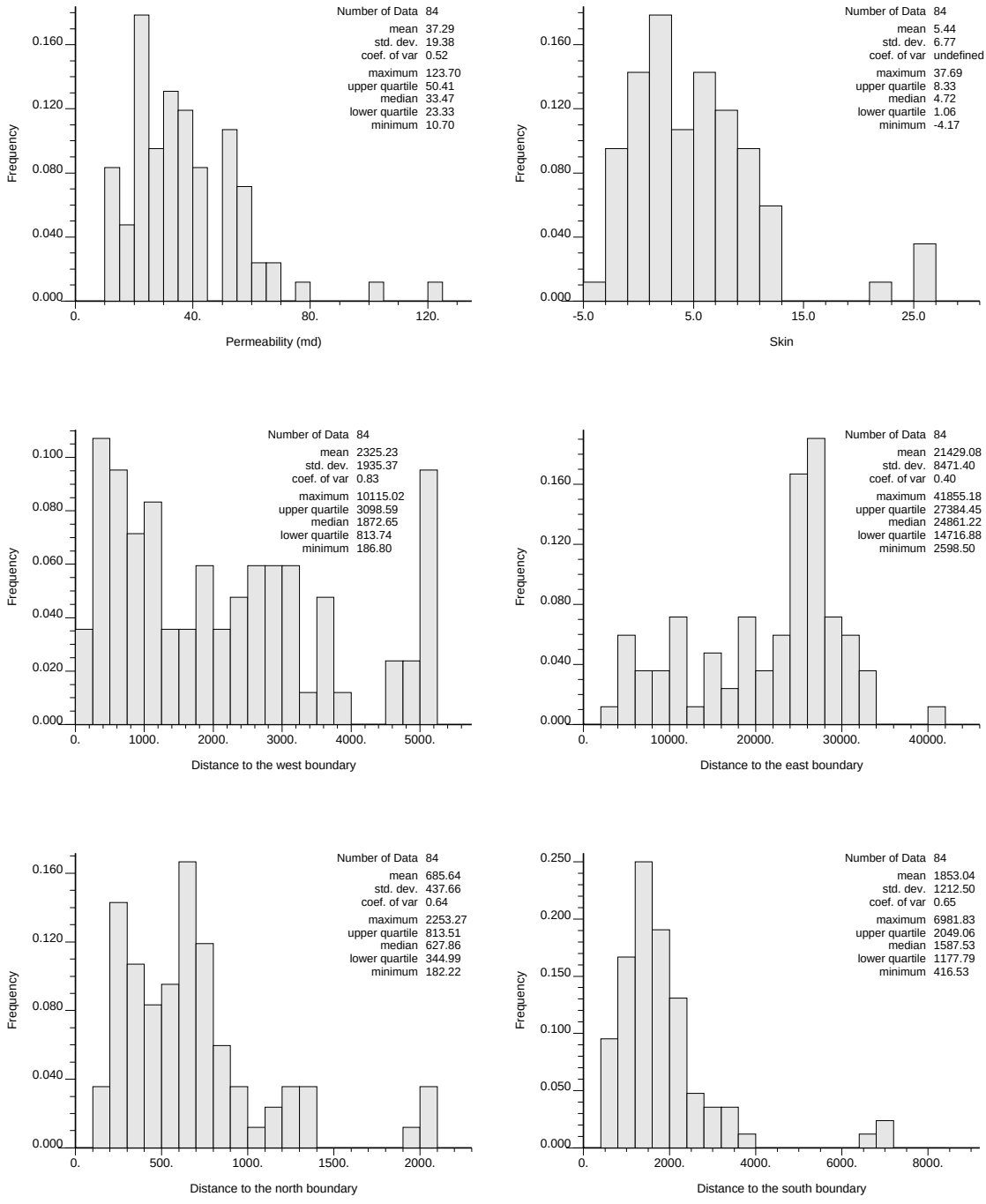

Figure 5.51: Distribution of estimates of model parameters using free search space (window width = 500 hours).

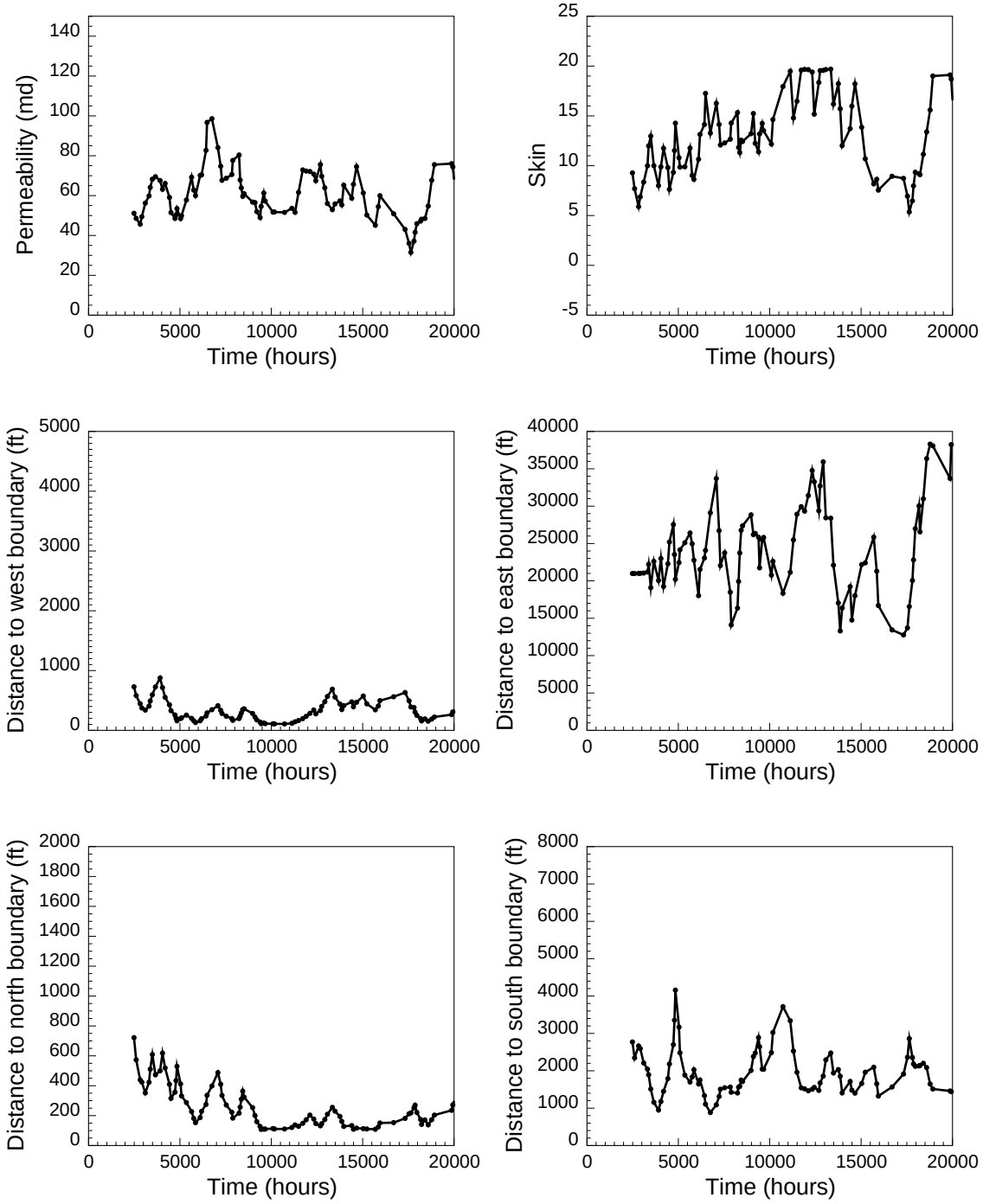

Figure 5.52: Estimates of model parameters using limited search space (window width = 500 hours).

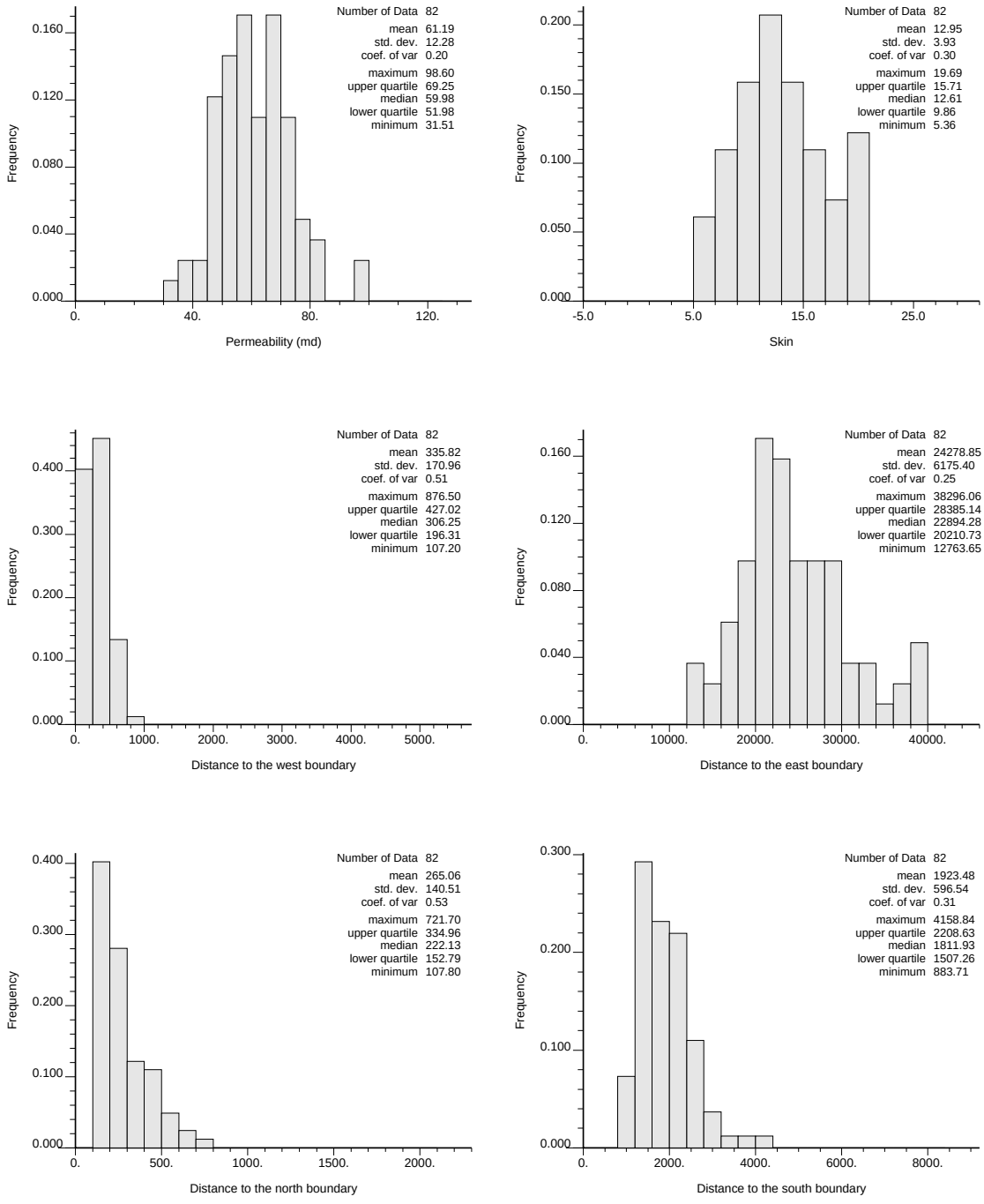

Figure 5.53: Distribution of estimates of model parameters using limited search space (window width = 500 hours).

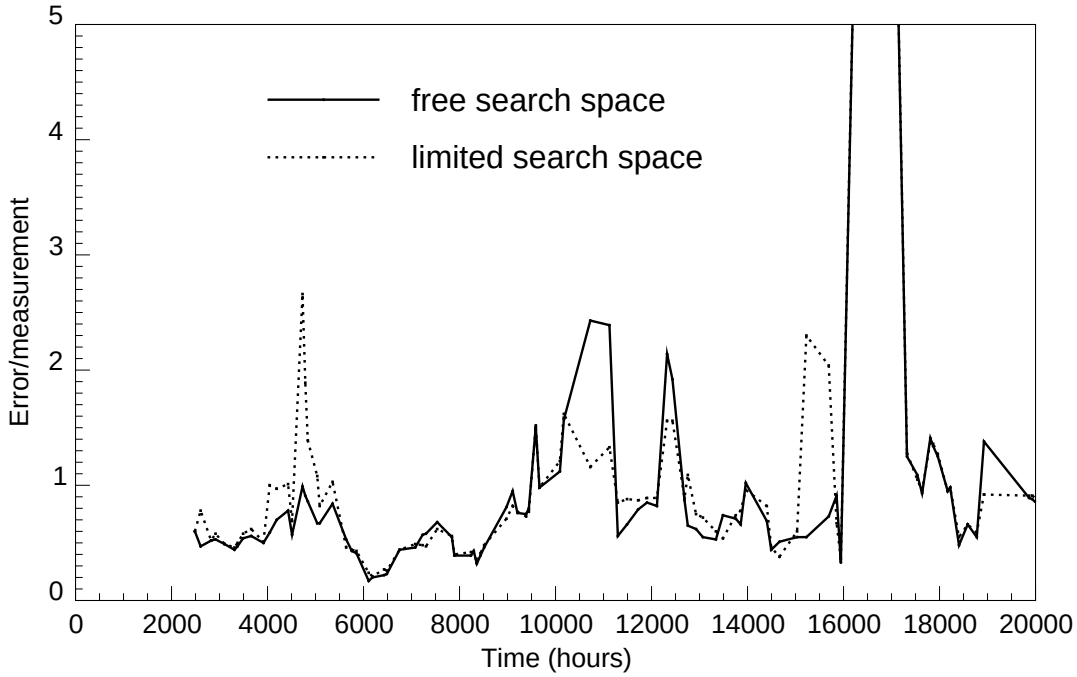

Figure 5.54: Comparison of errors obtained from regression with free search space and regression with limited search space.

distributions of the estimates in this case are narrower than those obtained from the regression with free search space. Fig. 5.54 compares the average errors in the regression with free search space and regression with limited search space. The small difference in the average errors between the two cases suggests that the results from both cases are equally good. The results from the limited search space implementation provide better representations of actual reservoir properties as they contain less variations.

Two additional analyses were conducted with a window size of 200 and 1,000 hours using limited search space in the regression. The estimates of the reservoir model parameters for the two cases are plotted in Figs. 5.55 and 5.57. Their corresponding distributions are shown in Figs. 5.56 and 5.58. Most parameter estimates appear to have more fluctuations as the window size increases. In general, the estimates to distances to rectangular boundaries may be poor due to the weak responses to the boundaries at late times. The response due to the closest boundary may dominate

Table 5.19: Comparison between the means of parameter estimates from moving analyses with different window sizes.

Window size	Permeability	Skin	r_{e1}	r_{e2}	r_{e2}	r_{e2}	Average error
200	30.93	3.57	1236	23,750	475	3158	0.59
500	61.19	12.95	336	24,279	265	1923	0.74
1000	39.60	6.00	3048	17,940	214	1870	0.77

the responses from other boundaries, thus making it difficult to estimate the further boundaries. Also, data that cover over a long time span may be subject to having high uncertainties due to changing reservoir conditions. The properties of gas condensate may change within a window of analysis since its properties are strong functions of pressure. Using shorter length of data in the analysis minimizes these variations of fluid properties. Therefore, the window should not be too large. Table 5.19 compares the means of the estimates of reservoir parameter using different window sizes. In this field example, the analysis with the window size of 200 hours provides the results with the least variations in the parameter estimates.

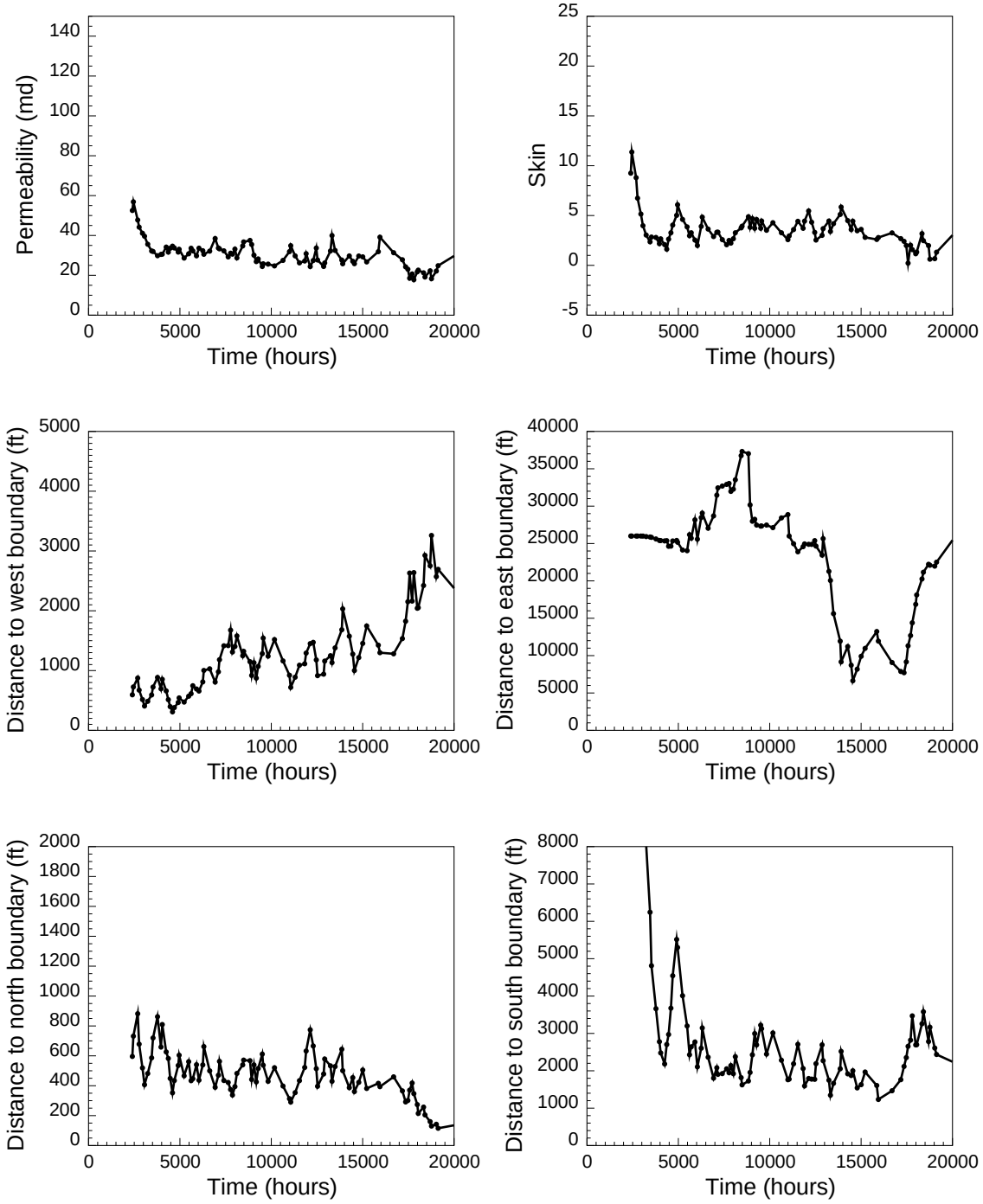

Figure 5.55: Estimates of model parameters using limited search space (window width = 200 hours).

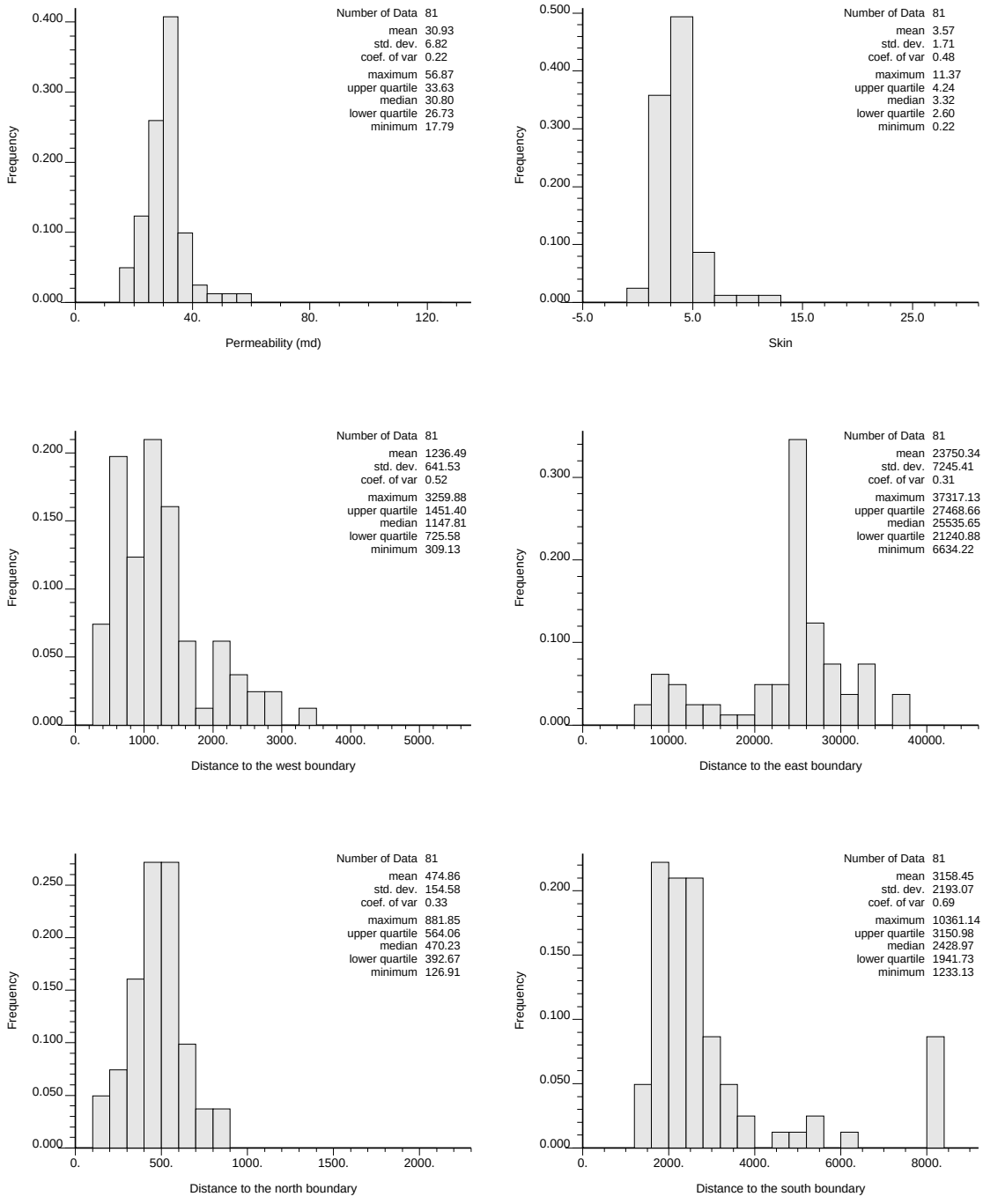

Figure 5.56: Distribution of estimates of model parameters using limited search space (window width = 200 hours).

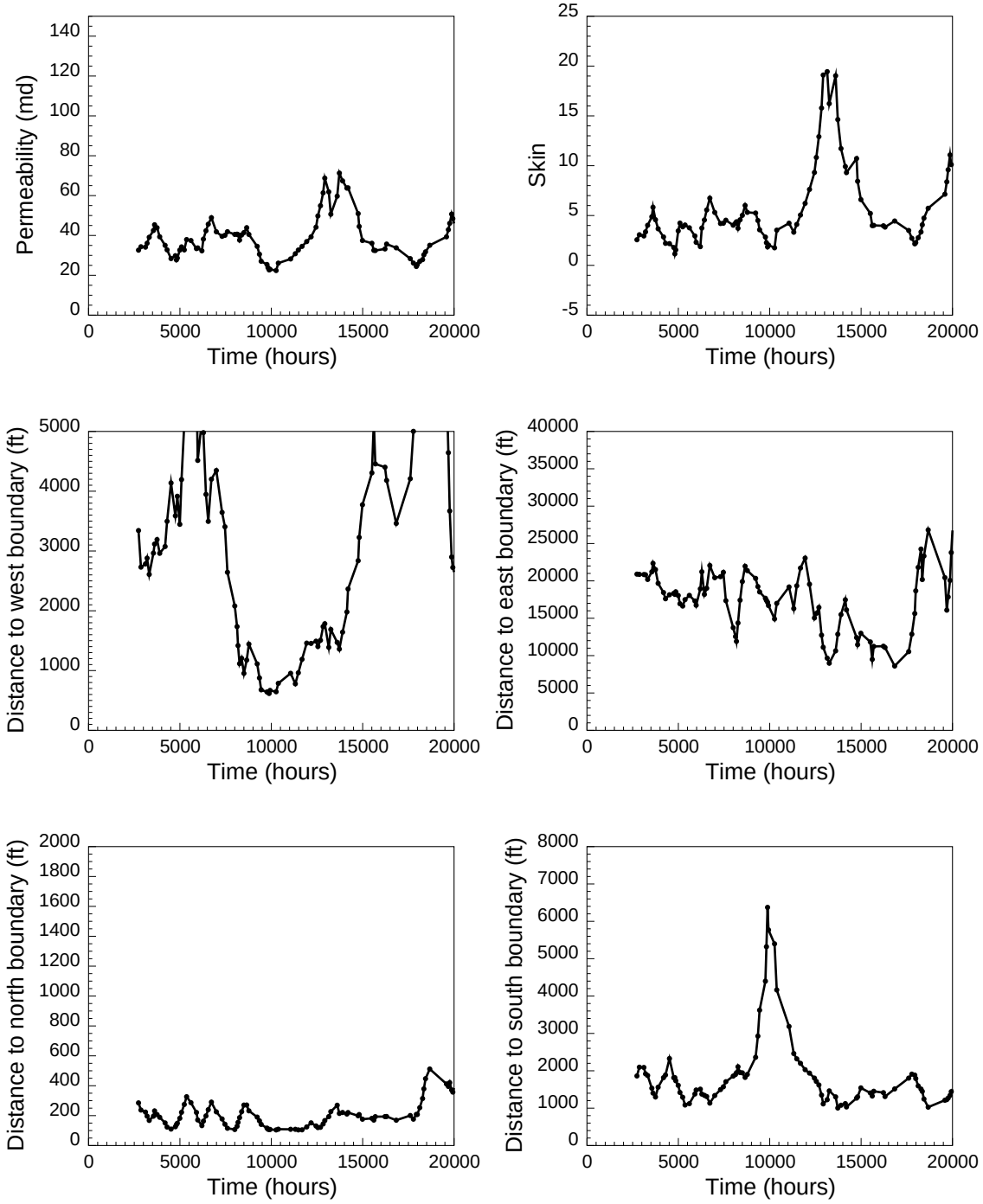

Figure 5.57: Estimates of model parameters using limited search space (window width = 1000 hours).

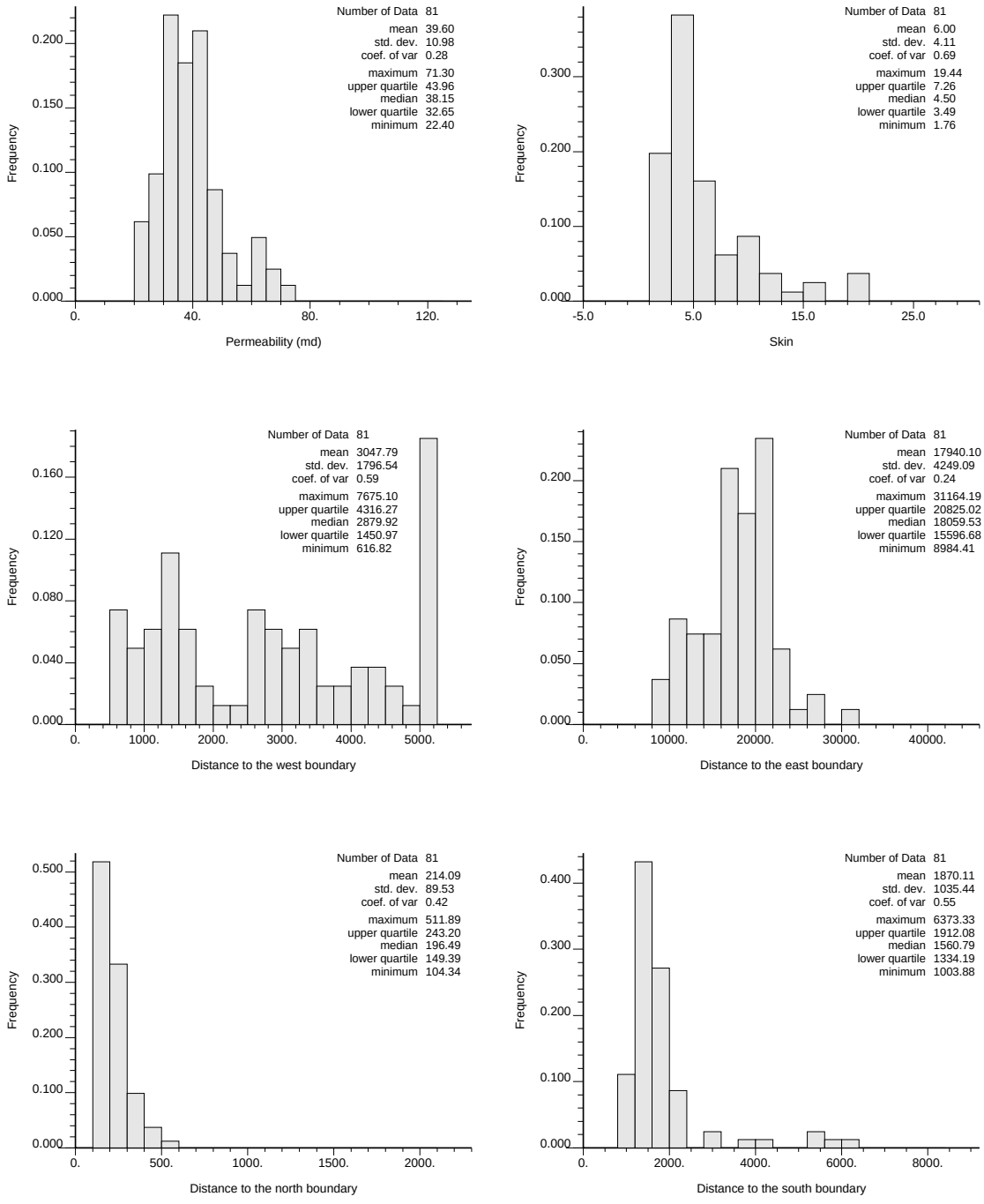

Figure 5.58: Distribution of estimates of model parameters using limited search space (window width = 1000 hours).

Chapter 6

Conclusions and Recommendations

A methodology to analyze data acquired with permanent downhole pressure gauges has been developed in this study and demonstrated on real field data. The approach involves a multistep procedure which may be grouped in three main categories: (1) data processing using wavelets, (2) data processing using nonlinear regression, and (3) data interpretation using moving window analysis. The analysis of the pressure data in the first category is based purely on signal analysis without any connection to the physical behavior of the reservoir. The pressure data are the only input in the data processing routines which include outlier removal, noise suppression, transient identification, and data reduction. The processing of data using nonlinear regression in the second category is associated with physical behaviors of the reservoir based on reservoir and fluid properties. The analysis procedures in this part includes (1) the reconstruction of incomplete flow rate history constrained by a few known flow rates and production data and (2) behavioral filtering of aberrant transients. These routines are intermediate steps between pure data processing and data interpretation. The third category, data interpretation, is the analysis of reservoir behavior in order to determine reservoir properties based on the moving window analysis.

Important remarks on the data processing by wavelet analysis can be summarized as follows:

1. Wavelet decomposition analysis can be used effectively to detect outliers in long-term data by identifying two consecutive singularities whose signs in the detailed signals are opposite. The uneven data spacings are all normalized to one, i.e., the time axis is replaced by the rank of data collected. An iterative thresholding method should be used to segregate the outliers from the rest of the data. Also, the data should be analyzed in a reversed order since the trends in late time behaviors are generally more established than the ones at the early times. The robustness of the outlier removal algorithm was demonstrated by two field examples.

2. A hybrid wavelet thresholding method was developed to denoise data. This new method has the capability to preserve most of the sharp features in the data while being able to smooth the noisy data at the same time. The hybrid method is superior to the standard hard and soft thresholding methods for this reason. In certain application where smoothness is desired, the soft thresholding method generally outperforms the hybrid thresholding method.

3. The transient identification algorithm developed in this study can be used effectively to allocate the starts of new transients by identifying the wavelet maxima corresponding to singularities in the pressure data. Although the accuracy of the identification is not perfect, the algorithm considerably reduces the amount of the task that is normally performed by hand.

4. Noisy data may need to be denoised before implementing the transient identification routine. Results from denoised data are more reliable than those from original noisy data.

5. Data collected at high frequency are more representative than lower frequency data. The transient identification algorithm may perform poorly when the spacings between data points are large. The interpolation between two points in the low frequency case generally creates a smooth transition between the two points thus concealing a possible abrupt change. Also, sharp data features are more subjective to being smeared out when data are collect at a low frequency.

Therefore, it is better to first collect data at a high sampling frequency and resample the data after denoising and transient identification to reduce the data size.

6. The data left from the reduction process is much smaller in number if the original data were denoised beforehand. The denoised data are more representative of signal characteristics since noise was suppressed, especially in high frequency cases. Therefore, it is more effective to remove the redundancy using the denoised data than using the original noisy data.

7. Since the wavelet decomposition routine requires uniform data sampling, the raw data are interpolated linearly. Except for the outlier removal application, all the data processing applications that utilize the wavelet decomposition algorithm in this study use linear interpolation.

The methods and results for the steps in nonlinear regression data processing can be summarized as follows:

1. Flow rate history can be reconstructed by parameterizing the unknown rates as unknown model parameters and matching the pressure response utilizing information on some known flow rates and production data.

2. Although the procedure for flow history reconstruction developed here was successful, it should be stressed that the continuous monitoring of flow rates downhole would be a much more desirable approach. Although downhole flow rate measurement is already feasible, it is not yet applied commonly.

3. The behavioral filtering process to eliminate aberrant transients from the rest of the data using the variance criterion is very effective in reducing the uncertainty in the solution obtained from nonlinear regression.

Conclusions from the moving window analysis used to interpret long-term pressure data can be drawn as follows:

1. The moving window analysis can account for changes in reservoir parameters given that the changes are gradual. If the changes are abrupt, the estimates of model parameters in that data region may not be as accurate. In any case, the estimates should improve in subsequent windows due to the diminishing effect of time-superposition.

2. The moving window analysis also provides distributions or ranges of estimates for reservoir parameters instead of a single set of estimates. These distributions may be useful to assess uncertainties in any type of subsequent analysis that uses the estimated reservoir properties as input information such as a reservoir study to forecast future reservoir performance.

3. The computational time in the moving window analysis is much less than the time needed to run regression on the entire data set. The reduction of the number of data and unknown flow rates in each window makes it possible to analyze the entire data sectionally with a modest computer resource.

Some of the procedures presented in this study could be expanded or applied to other types of problems. The following points are recommended for future study:

1. The transient identification algorithm may be improved to further increase the accuracy of the determination of new transients. By relaxing some of the rules imposed in this study and introducing more complex ones, this wavelet-based algorithm may be accurate enough to fully automate the task of discretizing pressure data into transients and eliminate human intervention.

2. The wavelet analysis has a lot of potential to be used in several applications in the petroleum industry and related fields. The outlier removal framework can be applied to any type of data to screen for outliers such as in geostatistical data. Besides detecting new transients, wavelet modulus maxima may be used to detect any type of discontinuities such as the layering behaviors of well log signals or it could be used to search for a departure from smooth trends such as high concentration of certain substances. Also, the denoising algorithm can

be used to smooth any type of data or fit the data nonparametrically. For the application of model recognition in well test analysis, it may be used to obtain smoother pressure derivatives to reveal certain characteristics hidden under the noise.

3. The principle of moving window analysis may be applied to reservoir characterization problems. Reservoir characterization alone provides a spatial description of the reservoir at one snapshot in time. Introducing the moving window analysis into reservoir characterization framework will give us either temporal changes or distributions of property fields. This should be useful in assessing the uncertainty of the outputs.

Nomenclature

a	=	Dilation parameter for wavelet transform
a	=	Discrete complementary wavelet transform
A	=	Approximation operator
b	=	Time at the center for windowed Fourier or wavelet transform, $hours$
B	=	Formation volume factor, bbl/STB
C	=	Wavelet complementary transform operator
C	=	Wellbore storage coefficient, STB/psi
d	=	Discrete wavelet transform
D	=	Detail operator
E	=	Objective function
E^*	=	Approximate objective function
$\hat{f}$	=	Fourier transform of f
F	=	Fourier transform operator
F	=	Model function
g	=	High-pass filter
$\tilde{g}$	=	High-pass dual filter
$\mathbf{g}$	=	Gradient vector
h	=	Formation thickness, ft
h	=	Low-pass filter
$\tilde{h}$	=	Low-pass dual filter
H	=	Hessian matrix
H^{-1}	=	Inverse of Hessian matrix

i	=	Imaginary unit
$I^2(\mathcal{Z})$	=	Vector space of square-summable integers
$L^2(\mathcal{R})$	=	Vector space of square-integrable one-dimensional function
k	=	Permeability, md
kq	=	Number of unknown flow rates
m	=	Number of unknown model parameters
n	=	Number of data
nq	=	Number of flow periods
nQ	=	Number of production data
p	=	Pressure, psi
p_D	=	Dimensionless pressure
Δp	=	Pressure change, psi
Δp_{max}	=	Maximum pressure change, psi
p_i	=	Initial pressure, psi
p_{wf}	=	Well flowing pressure, psi
q	=	Flow rate, STB/D
$\mathbf{q}$	=	Flow rate vector
Δq	=	Flow rate change, STB/D
Q	=	Fluid production function
$\mathcal{R}$	=	Set of real numbers
r_e	=	Distance to the outer boundary, ft
r_w	=	Wellbore radius, ft
S	=	Skin factor, dimensionless
t	=	Time, $hour$
Δt	=	Time difference, $hour$
Δt_{max}	=	Maximum time difference, $hour$
Δt_{min}	=	Minimum time difference, $hour$
t_D	=	Dimensionless time
u	=	Time when flow rate changes, $hour$

v	=	Time when fluid production is measured, *hour*
V	=	Vector space in $L^2(\mathcal{R})$
w	=	Observed fluid production, STB
W	=	Wavelet transform operator
W	=	Complementary vector space in $L^2(\mathcal{R})$
x	=	Dependent variable
y	=	Independent variable
$\mathcal{Z}$	=	Set of integers

GREEK LETTERS

ϵ_i	=	Error, *psi*
$\boldsymbol{\theta}$	=	Parameter vector
θ	=	Unknown parameter
θ^0	=	Initial guess for unknown parameter
λ	=	Wavelet denoising threshold
μ	=	Viscosity, *cp*
ϕ	=	Porosity, dimensionless
ϕ	=	Scaling function
$\tilde{\phi}$	=	Dual scaling function
ψ	=	Wavelet
$\tilde{\psi}$	=	Dual wavelet
σ	=	Noise level
ω	=	Frequency, *hertz*

SUBSCRIPTS

D	=	Dimensionless
i, j, k, l	=	Integer indices

SUPERSCRIPTS

0	=	Initial guess
-1	=	Inverse
(n)	=	Number of data
T	=	Transpose
window	=	Window transform used in Eq. 2.3

Bibliography

[1] Abbaszadeh, M. and Kamal, M. M.: "Automatic Type-Curve Matching for Well-Test Analysis," *SPEFE* (September 1988) 567–577.

[2] Anraku, T.: *Discrimination Between Reservoir Models in Well Test Analysis*, PhD dissertation, Stanford University (December 1993).

[3] Anraku, T. and Horne, R. N.: "Discrimination Between Reservoir Models in Well Test Analysis," *SPEFE* (June 1995) 114–121.

[4] Baker, A., Gaskell, J., Jeffery, J., Thomas, A., Veneruso, T., and Unneland, T.: "Permanent Monitoring - Looking at Lifetime Reservoir Dynamics," *Oilfield Review* (Winter 1995) **7**, No. 4, 32–46.

[5] Bard, Y.: *Nonlinear Parameter Estimation*, Academic Press Inc. Ltd., New York City (1974).

[6] Barua, J., Horne, R. N., Greenstadt, J. L. and Lopez, L.: "Improved Estimation Algorithms for Automated Type-Curve Analysis of Well Tests," *SPEFE* (March 1988) 186–196.

[7] Battle, G.: "A Block Spin Construction of Ondelettes. Part I: Lemarié," *Communications in Mathematical Physics* (1987) **100**, 601–615.

[8] Botto, G. and de Ghetto, G.: "Five Years' Experience in Using Downhole Pressure Gauges in the Hostile, Deep Wells of Villafortuna-Trecate Field," paper SPE 26448 presented at the 1993 SPE Annual Technical Conference and Exhibition, Houston, TX, October.

[9] Bourdet, D., Whittle, T. M., Douglas, A. A., and Pirard, Y. M.: "A New Set of Type Curves Simplifies Well Test Analysis," *World Oil* (May 1983) 95–106.

[10] Bourdet, D., Ayoub, J. A. and Pirard, Y. M.: "Use of Pressure Derivative in Well-Test Interpretation," *SPEFE* (June 1989) 293–302.

[11] Calderón, C. A.: "Intermediate Spaces and Interpolation, the Complex Method," *Stud. Math.* (1964) **24**, 113–190.

[12] Camona, R., Hwang, W. L., and Torresani, B.: *Practical Time-Frequency Analysis*, Academic Press, San Diego (1998).

[13] Chalaturnyk, R. and Moffat, T.: "Permanent Instrumentation for Production Optimization and Reservoir Management," paper SPE 30274 presented at the 1995 International Heavy Oil Symposium, Calgary, Canada, June 19-21.

[14] Chang, J. and Ershaghi, I.: "An Improved Microcomputer Approach to Well Test Interpretation," paper SPE 15928 presented at the 1989 SPE Eastern Regional Meeting, Columbus, OH, Nov. 12-14.

[15] Chu, L., Schatzinger, R. A. and Tham, M. K.: "Application of Wavelet Analysis to Upscaling of Rock Properties," paper SPE 36517 presented at the 1996 SPE Annual Technical Conference and Exhibition, Denver, CO, October.

[16] Chui, C. K. and Wang, J. Z.: "A Cardinal Spline Approach to Wavelets," *Proceedings of the American Mathematical Society* (1991) **113**, 785–793.

[17] Cook, G. and Beale, G.: "Application of Least Square Parameter Identification with Fixed Length Data Window," *IEEE Transaction on Industrial Electronics* (1983) **30**, No. 4, 334–339.

[18] Daubechies, I.: "Orthonortexmal Bases of Compactly Supported Wavelets," *Communication on Pure and Applied Mathematics* (1988) **41**, 909–996.

[19] Dogru, A. H., Dixon, T. N., and Edgar, T. F.: "Confidence Limits on the Parameters and Predictions of Slightly Compressible, Single Phrase Reservoirs," *SPEJ* (February 1977) 42–56.

[20] Donoho, D. L. and Johnstone, I. M.: "Adapting to Unknown Smoothness Via Wavelet Shrinkage," *Journal of the American Statistical Association* (1994) **90**, No. 432, 1200–1224.

[21] Donoho, D. L., Johnstone, I. M., Kerkyacharian, G., and Picard, D.: "Wavelet Shrinkage: Asymptopia?," *Journal of the Royal Statistical Society, Series B* (1995) **57**, No. 2, 301–369.

[22] Duffin, R. J. and Schaeffer, A. C.: "A Class of Nonharmonic Fourier Series," *Transctions of the American Mathematical Society* (1952) **72**, 341–366.

[23] Earlougher, R. C. and Kersch, M. K.: "Field Examples of Automatic Transient Test Analysis," *Journal of Petroleum Technology* (October 1972) 1271–1277.

[24] Economides, M.J., Hill, A.D., and Ehlig-Economides, C.: *Petroleum Production Systems*, Prentice Hall (1994).

[25] Gabor, D.: "Theory of Communications," *Journal of the Institute of Electrical Engineering, London III* (1946) **93**, 429–457.

[26] Gallivan, J. D., Kilvington, L. J., and Shere, A. J.: "Experience With Permanent Bottomhole Pressure/Temperature Gauges in a North Sea Oil Field," paper SPE 13988 presented at the 1988 SPE Annual Technical Conference and Exhibition, Oct. 8-11.

[27] Gerritsen, M.: *Designing an Efficient Solution Strategy for Fluid Flows*, PhD dissertation, Stanford University (December 1996).

[28] Gill, P. E., Murray, W., and Wright, M. H.: *Practical Optimization*, Academic Press Inc. Ltd., New York City (1974).

[29] Greenstadt, J. L.: "On the Relative Efficiencies of Gradient Methods," *Mathematics of Computation* (1967) **21**, 360–367.

[30] Grossman, A. and Morlet, J.: "Decomposition of Hardy Functions into Square Integrable Wavelets of Constant Shape," *SIAM Journal of Mathematics* (1984) **15**, 723–736.

[31] Harr, A.: "Zur Theorie der Orthoganalen Funktionen-Systeme," *Annals of Mathematics* (1910) **69**, 331–371.

[32] Holschneider, M., Kronland-Martinet, R., Morlet, J., and Tchamitchian, P.: "A Real-Time Algorithm for Signal Analysis with the Help of the Wavelet Transform," *Wavelets, Time-Frequency Methods and Phase Space* (1989) 289–297.

[33] Horne, R. N.: "Advances in Computer-Aided Well Test Interpretation," *Journal of Petroleum Technology* (July 1994a) 559–606.

[34] Horne, R. N.: "Uncertainty in Well Test Interpretation," paper SPE 27972 presented at the 1994b University of Tulsa Centennial Petroleum Engineering Symposium, Tulsa, OK, August.

[35] Horne, R. N.: *Modern Well Test Analysis: A Computer-Aided Approach*, Petroway, Inc., Palo Alto, 2nd edition (1995).

[36] Jansen, F. E. and Kelkar, M. G.: "Application of Wavelets to Production Data in Describing Inter-Well Relationships," paper SPE 38876 presented at the 1997 SPE Annual Technical Conference and Exhibition, San Antonio, TX, February.

[37] Jansen, F. E. and Kelkar, M. G.: "Upscaling of Reservoir Properties Using Wavelets," paper SPE 39495 presented at the 1998 SPE India Oil and Gas Conference and Exhibition, New Delhi, India, February.

[38] Kikani, J., Fair, P. S., and Hite, R. H.: "Pitfalls in Pressure Gauge Performance," *SPEFE* (December 1997) 241–246.

[39] Kikani, J. and He, M.: "Multi-Resolution Analysis of Pressure Transient Data Using Wavelet Methods," paper SPE 48966 presented at the 1998 SPE Annual Technical Conference and Exhibition, New Orleans, LA, September.

[40] Lamarié, P. G.: "Une Nouvelle Base D'ondelettes de $L^2(\mathcal{R}^n)$," *Journal de Mathematiques Pures et Appliquees* (1988) **67**, 227–236.

[41] Landa, J. L.: *Reservoir Parameter Estimation Constrained to Pressure Transients, Performance History and Distributed Saturation Data*, PhD dissertation, Stanford University (June 1997).

[42] Levenberg, K.: "A Method for the Solution of Certain Nonlinear Problems in Least Squares," *Quart. Appl. Math.* (1944) **2**, 164–168.

[43] Luo, W. and Billings, S. A.: "Adaptive Model Selection and Estimation for Nonlinear Systems Using A Sliding Data Window," *Signal Processing* (1995) **46**, 179–202.

[44] Mallat, S.: "A Theory for Multiresolution Signal Decomposition: The Wavelet Representation," *IEEE Transaction on Pattern Analysis and Machine Intelligence* (July 1989) **11**, No. 7, 674–693.

[45] Mallat, S.: "Multiresolution Approximations and Wavelet Orthonormal Bases of $L^2(\mathcal{R})$," *Transactions of the American Mathematical Society* (September 1989) **315**, No. 1, 69–87.

[46] Mallat, S.: "Multifrequency Channel Decompositions of Images and Wavelet Models," *IEEE Transaction on Acoustics, Speech, and Signal Processing* (December 1989) **17**, No. 12, 2091–2110.

[47] Mallat, S.: *A Wavelet Tour of Signal Processing*, Academic Press (1998).

[48] Mallat, S. and Hwang, W. L.: "Singularity Detection and Processing with Wavelets," *IEEE Transaction on Information Theory* (1992) **38**, No. 1, 617–643.

[49] Mallat, S. And Zhong, S.: "Characterization of Signals from Multiscale Edges," *IEEE Transaction on Pattern Analysis and Machine Intelligence* (July 1992) **14**, No. 7, 710–732.

[50] Marquardt, D. W.: "An Algorithm for Least-Squares Estimation of Nonlinear Parameters," *J. Soc. Ind. Appli. Math.* (June 1963) **11**, No. 2, 431–441.

[51] Meyer, Y.: "Principe d'Incertitude, Bases Hilbertiennes et Algèbres d'Opérateurs," Séminaire Bourbaki, 1985-1986, No. 662 (1985).

[52] Moridis, G. J., Nikolaou, M. and You, Y.: "The Use of Wavelet Transforms in the Solution of Two-Phase Flow Problems," *SPE Journal* (June 1996) 169–177.

[53] Nestlerode, W. A.: "The Use of Pressure Data from Permanently Installed Bottom Hole Pressure Gauges," paper SPE 590 presented at the 1963 Rocky Mountain Joint Regional Meeting, Denver, CO, May 27-28.

[54] Nilsen, S. and Espedal, M. S.: "Wavelet Upscaling Based on Piecewise Bilinear Approximation of the Permeability Field," *Transport in Porous Media* (May 1996) **23**, No. 2, 125–134.

[55] Ogden, R. T.: *Essential Wavelets for Statistical Applications and Data Analysis*, Birkhäuser, Boston (1997).

[56] Osman, M. S. and Stewart, G.: "Pressure Data Filtering and Horizontal Well Test Analysis Case Study," paper SPE 37802 presented at the 1997 Middle East Oil Show, Bahrain, March.

[57] Panda, M. N., Mosher, C., and Chopra, A. K.: "Application of Wavelet Transforms to Reservoir Data Analysis and Scaling," paper SPE 36516 presented at the 1996 SPE Annual Technical Conference and Exhibition, Denver, CO, October.

[58] Press, W., Teukolsky, S. A., Vetterling, W. T., and Flannery, B.: *Numerical Recipes in C*, Cambridge (1995).

[59] Rosa, A. J. and Horne, R. N.: "Automated Type-Curve Matching in Well Test Analysis Using Laplace Space Determination of Parameter Gradients," paper SPE 12131 presented at the 1983 SPE Annual Technical Conference and Exhibition, San Francisco, CA, October.

[60] Schmidt, L. Stright, D. H., and Forcade, K. C.: "Multiwell Data Acquisition and Analysis for Permanent Bottomhole Pressure Gauge Installations," paper SPE

16511 presented at the 1987 SPE Annual Technical Conference and Exhibition, Montgomery, TX, June 23-25.

[61] Shensa, M. J.: "The Discrete Wavelet Transform: Wedding the Á Trous and Mallat Algorithms," *IEEE Transaction on Signal Processing* (1992) **40**, No. 10, 2464–2482.

[62] Shepherd, C. E., Neve, P. and Wilson, D. C.: "Use and Application of Permanent Downhole Pressure Gauges in the Balmoral Field and Satellite Structures," *SPE Production Engineering* (August 1991) **6**, No. 3, 271–276.

[63] Stehfest, H.: "Algorithm 368: Numerical Inversion of Laplace Transforms," *Comm. ACM* (January 1970a) **13**, No. 1, 47–49.

[64] Stehfest, H.: "Remark on Algorithm 368: Numerical Inversion of Laplace Transforms," *Comm. ACM* (October 1970b) **13**, No. 10, 624.

[65] Sullera, M. M. and Horne, R. N.: "Inferring Injection Returns from Chloride Monitoring Data," *Proceedings, Twenty-Fouth Workshop on Geothermal Reservoir Engineering* (January 25-27 1999).

[66] Unneland, T. and Haugland, T.: "Permanent Downhole Gauges Used in Reservoir Management of Complex North Sea Oil Fields," *SPE Production and Facilities* (August 1994) 195–203.

[67] Unneland, T., Manin, Y. and Kuchuk, F.: "Permanent Gauge Pressure and Rate Measurements for Reservoir Description and Well Monitoring: Field Cases," paper SPE 38638 presented at the 1997 SPE Annual Technical Conference and Exhibition, San Antonio, TX, October.

[68] Weeks, S. G. and Farris, G. F.: "Peragauge - A Permanent Surface Recording Downhole Pressure Monitor - Through A Tube," paper SPE 5607 presented at the 1975 SPE Annual Technical Conference and Exhibition, Dallas, TX, September 28 - October 1.